DANMARKS OG GRØNLANDS GEOLOGISKE UNDERSØGELSE RAPPORT 2007/83

Geological setting of the Storø gold prospect, Godthåbsfjord region, southern West Greenland

Result of detailed mapping, structural analysis, geochronology and geochemistry

Jeroen A.M. van Gool, Anders Scherstén,
Claus Østergaard & Tomas Neraa

GEOLOGICAL SURVEY OF DENMARK AND GREENLAND
MINISTRY OF CLIMATE AND ENERGY

GEUS

DANMARKS OG GRØNLANDS GEOLOGISKE UNDERSØGELSE RAPPORT 2007/83

Geological setting of the Storø gold prospect, Godthåbsfjord region, southern West Greenland

Result of detailed mapping, structural analysis, geochronology and geochemistry

Jeroen A.M. van Gool, Anders Scherstén,
Claus Østergaard & Tomas Neraa

GEOLOGICAL SURVEY OF DENMARK AND GREENLAND
MINISTRY OF CLIMATE AND ENERGY

GEUS

Table of Contents

Table of Contents 3

Summary 5

Introduction 7

Logistical framework for the mapping and sampling 9
Map production 9

Geological background 13

Mineralisation 13

Rock types 16

Anorthosite – gabbro (an) 16
Dark layered amphibolite (ag) 18
Layered amphibolite and biotite gneiss (av) 18
Aluminous mica schist and mica-rich gneiss (ms) 19
Hornblende-biotite gneiss (ab) 19
Biotite gneiss (b) 19
Quartzitic gneiss (qmz) 22
Quartzite (q) 23
Garnet-rich gneiss (grt) 23
Amphibolite (a) 24
garnet calc-silicate gneiss (cs) 28
Ultrabasic rock (ub) 29
Hornblende garnetite (hb) 30
Garnetite and quartz-garnet-magnetite rock (if) 31
Pegmatites (P) 32
Metadolerite dykes (δ) 33
Breccia 34
Mesoarchaean quartzo-feldspathic biotite gneiss (gn) 34
Eoarchaean quartzo-feldspathic biotite gneiss (Agn) 34
Rocks on Schist Hill 35
Rocks in the Storø shear zone 36
Comparison of NunaMinerals rock type codes and map legend 36

Structure 39

Large-scale fold structures – thrust ramp setting 39
Storø shear zone 43
Upper (roof) thrust contact of the Storø supracrustal belt 46
Mesoscopic structures – main deformation phases 46
D1 – main foliation development 46
D2 early folding 47

D3 Storø shear zone and large-scale folds 48
Structural control on the gold mineralisation? 49

Petrography **51**

Metamorphism 51
Relative timing of mineralisation 53

Geochronology **57**

Sample description and analytical results 58
samples from the supracrustal sequence 58
Sample from the Archaean orthogneisses, overlying the supracrustal belt 74
Discussion of the geochronological results 75
Conclusions 77

Re-Os analyses of arsenopyrite in the gold-mineralised zones **79**

Analytical Procedure 79
Sample descriptions 80
Results 81
Discussion 81
Preliminary conclusions: 85

Geochemistry **86**

Sample collection and analytical procedure 87
Major elements: 88
Trace elements: 90
Testing the alteration hypothesis: 92
Chemistry of garnetites and garnet magnetite rocks 97
Main conclusions about alteration: 101
Petrogenesis: 101
Conclusions: 105

Discussion and conclusions **107**

References **109**

Appendix 1 petrographic descriptions and SEM backscatter images **112**

Petrographic descriptions 112

Appendix 2: Analytical methods for zircon geochronology **134**

Appendix 3: Tabulated geochronological data **135**

Appendix 4: Tabulated geochemical data **146**

Appendix 5: Bjørneøen geochemistry **157**

Summary

The gold prospects on Qingaaq and Aappalaartoq mountains on northern Storø are located in the strongly deformed and metamorphosed Storø supracrustal belt of Neoarchaean age. In a project co-financed by and carried out in cooperation with NunaMinerals A/S, the geological setting of gold prospects was re-investigated. The core of our project was the production of two detailed maps at 1:2 500 scale on a new accurate topographic base. The two maps cover the areas comprising the prospects on the two mountains. Furthermore, the project included a structural analysis, petrography, geochemistry and geochronology, all to refine the model for the geological setting of the gold mineralisation.

The Storø supracrustal belt is sandwiched in between Eoarchaean rocks of the overlying Færingehavn terrane, and the underlying Mesoarchaean gneisses of the Akia terrane. The latter is separated from the supracrustal belt by the *c.* 400m wide Storø shear zone that runs along the western edge of northern Storø. The supracrustal rocks are thrusted over the Akia terrane gneisses, and were folded in hanging wall anti- and synform pairs during thrusting.

The tectono-stratigraphy is rather consistent in the northern Storø area. A massive anorthosite at the base of the sequence is overlain by banded amphibolites, which in turn are overlain by interlayered quartzites and biotite gneisses. The latter comprises clastic metasediments and potentially also altered volcanic rocks. Overlying the metasediments is an aluminous garnet-rich gneiss that is the metamorphosed product of intense alteration of a rock type associated with amphibolites in the sequence. The highest part of the sequence is occupied by a thick amphibolite sequence, with compositions of tholeiitic basalt, and including metamorphosed volcaniclastic rocks. The amphibolites contain hydrothermal alteration zones, represented by garnet calc-silicate gneisses, garnet amphibolites and garnet-biotite-amphibole gneisses. The interpretation of the geochemistry of least altered amphibolites places them in an extensional environment, where the basalts were evolving from an original crustal or lithospheric source with an increasing asthenospheric mantle component towards the higher parts of the sequence. The preferred tectonic setting is in a continental rift basin or a back-arc basin.

All rocks in the area are affected by upper amphibolite facies metamorphism. Sillimanite is the dominant alumino-silicate, and minor partial melt veins occur in mica-rich rock types.

The structural setting of the Qingaaq and Aappalaartoq prospects is very similar, they both consist of a hanging wall synform-antiform pair in an oblique or lateral hanging wall ramp of the Storø shear zone. Movement of the Storø shear zone (*c.* 2630 Ma) is largely coeval with peak metamorphism. Gold remobilisation occurred presumably during folding and movement on the shear zone from previously mineralised zones into dilation sites within the fold structures.

Geochronological investigations confirmed previous work and resulted in a better resolution of the different zircon age populations. Most analysed samples contained a main zircon population at 2800–2850 Ma, as well as metamorphic populations at *c.* 2635 Ma and *c.* 2600 Ma. The older of the two metamorphic populations dates the main metamorphism, and this was likely the first metamorphic event to affect the supracrustal rocks. The population at 2800–2850 Ma consists mainly of zircons with igneous zonation, but the data can in most cases not distinguish whether these represent an igneous rock type or whether they were reworked material in a metasediment. Two quartzites with the same population were

interpreted to be of metasedimentary origin and contain Eoarchaean detrital material, derived from ancient shields. Overall the data suggest a Neoarchaean age for the supracrustal sequence. However, the anorthosite and the lower banded amphibolite are intruded by *c.* 3050 Ma orthogneisses and are therefore *c.* 250 Ma older than the Neoarchaean upper part of the supracrustal sequence.

Gold mineralisation on Storø occurs commonly together with arsenopyrite. The two most promising occurrences are on the north slopes of Qingaaq. One is referred to as Main Zone (NunaMinerals A/S terminology) and is situated in hydrothermally altered rocks of the upper amphibolite sequence in an antiformal fold core. Here the gold occurs mainly in quartz veined rocks, commonly rich in garnet and biotite. The other occurrence is on the contact between the biotite gneisses and the upper amphibolites, and is called the BD zone (NunaMinerals A/S terminology). BD zone mineralisation lies in quartz-veined, arsenopyrite-bearing zones on either side of the contact. The rocks immediately below this contact are extremely garnet rich (± sillimanite) and poor in quartz, and their trace element geochemistry is more reminiscent of the overlying amphibolites than of the (presumably) metasedimentary biotite gneisses below. The data are consistent with the interpretation that this is a pre-metamorphic (syn-volcanic?) altered mafic rock (or associated rock type).

Re-Os analyses on arsenopyrite sampled in these two gold mineralised zones show that two periods of mineralisation occurred. Arsenopyrite in the BD zone has a poorly constrained Re-Os age of 2714 ± 53 Ma, while the age of mineralisation in Main Zone is better constrained at 2636 ± 23 Ma, coinciding with the timing of peak metamorphism. Initial ratios from the two samples allow the interpretation that the mineralisation in Main Zone is a result of remobilisation of gold of the first mineralisation.

Introduction

The central part of Storø in the Godthåbsfjord region (Fig. 1) is known to have elevated gold concentrations in Archaean supracrustal rocks. The rocks around Qingaaq and Aappalaartoq mountains in the NunaMinerals A/S concession area have been exploration targets for many years and especially gold occurrences in the north face of “little Qingaaq” are well established. Saw channel profiles exist of large parts of the Qingaaq area and the surface traces of mineralised zones are fairly well-known. Drilling campaigns were undertaken in 1995, 1996, 2005, 2006 and 2007 and have added to the understanding of the three-dimensional geometry of the complex geology. Exploration activity around Aappalaartoq has not been so extensive and although isolated high gold values were reported, the surface geometry of gold mineralised zones is not well established and based mainly on individual samples. Only limited systematic saw channel sampling has been carried out, while only three drill holes existed from the 1995/6 drilling campaign, two holes were drilled while mapping took place in 2006. For a review of the gold mineralisation on Storø we refer to Østergaard & van Gool (2007).

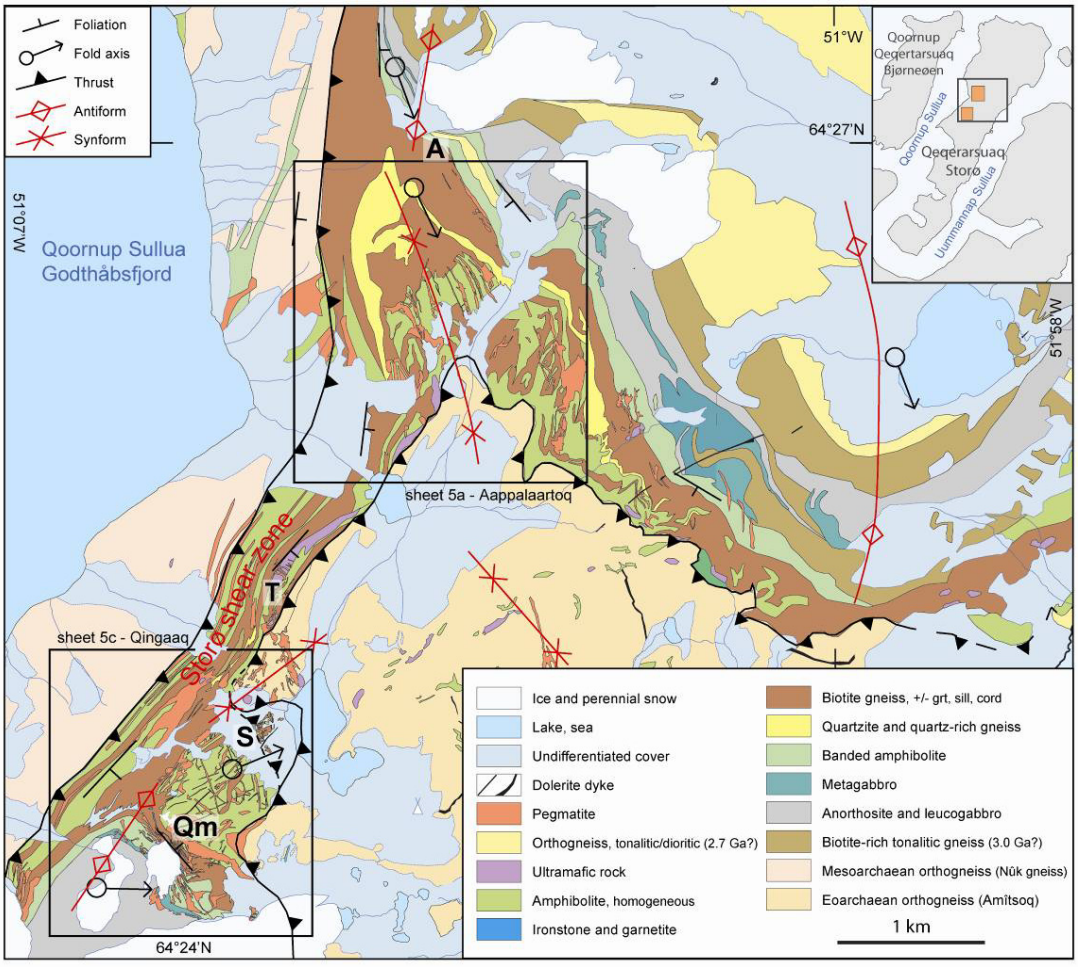

Figure 1. *Overview geological map of central Storø, showing the location of the two detailed map areas on northern Storø (see inset map). Mountain tops: A = Aappalaartoq, Qm = little Qingaaq, S = Schist Hill, T = 580 m top. Modified from Østergaard and van Gool unpublished 1:10 000 geological map, parts of sheets 5 and 6.*

The main objective of the project described here, is to improve the understanding of the geological framework in which the gold prospects occur. The project is carried out in cooperation with – and co-financed by – NunaMinerals A/S. One main objective was a set of new detailed maps of the prospects and surrounding geology at Qingaaq and Aappalaartoq mountains at 1:2 500 (Fig. 1). Furthermore, the structural setting of the area was investigated, while samples were collected for geochemistry, geochronology and petrography, in order to investigate the protoliths of the present rocks, their genesis, age, alteration processes, metamorphism and structural development, and to a minor extent the mineralisation. Here we report the main results of the mapping project and the subsequent analytical work. The mineralisation is mainly addressed by investigations in the Qingaaq prospect, since the mineralisation here is much better known.

Fairly detailed geological maps exist of Qingaaq and Aappalaartoq Mountains in NunaOil company reports. D. Coller produced a number of thematic maps at 1:1000 scale of “little Qingaaq” north face (Era Maptec 1995), while a geological map of a larger part of little Qingaaq was compiled by G. Smith at 1:2000 scale together with a number of thematic maps (in Skyseth 1997), in part based on 1:1000 scale maps of Pedersen (1996). J.S. Petersen compiled a geological map of Aappalaartoq mountain and surroundings at 1:5000 scale (in Grahl-Madsen 1994). The main alterations and mineralisations at main zone (the first mineralised area to be recognised, see below) at the foot of “little Qingaaq” north face was mapped in variable detail (e.g. Skyseth 1997, 1998; Pedersen 1996). Further maps of small areas (top 850m and area east of Aappalaartoq) exist (Skyseth 1997). All of the aforementioned maps were made in 1995 and 1996, based on a grid topographic maps which turned out to be inaccurate. They could not be used directly in combination with the drill core data to produce a three-dimensional model of the sub-surface geology.
New high quality aerial photographs that were taken in 2003 and topographic maps as well as orthophotograph mosaics produced in GEUS’ aerial photography laboratory are now available. These form a much more accurate base for mapping. Furthermore, GPS receivers generally can be used for detailed positioning, although the steep slopes in the map area can cause deterioration of the satellite signals. In several instances the location of an outcrop as measured by GPS needed to be relocated to conform with the aerial photograph. The new topography and aerial photographs were used by Østergaard and van Gool to compile a new set of accurate 1:10 000 scale geological maps, drawn digitally at GEUS laboratory for aerial photography (unpublished map 2005).

The aim of the mapping project was to produce a detailed and accurate geological map that can be used in combination with the saw channel and drill core data to produce a three dimensional model of the geological framework in which the gold mineralisations occur. Furthermore, a large number of samples was collected for geochemistry and petrography to characterise the different rock types and investigate the alteration processes that have been active in the rocks and may have played a role in the gold mineralisation.
In this report (and in literature on Storø in general), the name Qingaaq is informally used for the lower slopes north of the mountain in the southwest of Fig. 1, which has its peak (1610 m) south of the map. The top at 1086 m near the centre of the Qingaaq map sheet 5c is informally referred to as little Qingaaq (or Qingaaq minor). Schist Hill is the informal name of the knoll, *c.* 200 m NE of the foot of the main slopes of little Qingaaq. Map sheet 5a occupies the southern slopes of Aappalaartoq mountain, that has its top (1428 m) just

north of the map sheet (Fig. 1). The lower hill in between these two is informally referred to as “580 m top”.

Logistical framework for the mapping and sampling

The mapping was carried out from July 19th to August 23rd by Jeroen van Gool, assisted by Kristoffer Szilas during the whole period and Thomas Krog during the last two weeks of the project. The two assistants are experienced mountaineers as well as graduate students of geology, and their main role was to access the steeper parts of the mountainous area. The mapping was carried out from NunaMinerals A/S base camp on Storø, with limited helicopter support. Observations from few traverses during the 2007 field season are included.
The first half of the 2006 summer was concentrated on Qingaaq, the latter on Aappalaartoq, following activity of NunaMinerals A/S geologists and thus reducing helicopter time.
During the field work period, most of Aappalaartoq was free of snow, while the north face and, to a larger extent, the northwest side of little Qingaaq had extensive snow patches. While the snow enhances accessibility in the steeper parts of the slopes, it also hides part of the geology, and is both an advantage and disadvantage.

Map production

As a base for the mapping in the field we used to a limited extend 1:2 500 scale orthophotographic mosaics that were made from the *c.* 1:35 000 scale colour aerial photographs. Although these are of a high quality, they do not represent the steep slopes well, because of the oblique view and the existence of dark shadows on parts of the slopes. For most of the mapping we made use of oblique-view digital photographs that were taken from a helicopter at the beginning of the field season, and which could be printed as required at base camp. These turned out to be of high quality and very detailed, and therefore extremely useful (although not at all water resistant). Map data were subsequently transferred from the digital photographs to an overlay over the orthophotos, partly with the help of GPS data. For compilation of a field map, the orthophotos were used extensively for correlation through the parts of the map area that were not visited on the ground.
It should be noted that the central northern part of orthophoto 5a, the steep slopes south and southeast of the top of Aappalaartoq, shows a large distortion compared to the digital terrane model. Deviations increase slowly to about 150m along the northern edge of the orthophoto. This is due to the extremely steep slopes around the top of Aappalaartoq occurring at the edge of the orthophoto. The topographic maps, on which the geological maps are drawn, are generally correct within an error of about 5 m, with slightly larger errors on steep slopes and shadow-rich parts of the aerial photographs.
The final versions of the geological maps were drawn on the digital workstation at the aerial photography laboratory at GEUS. This allowed for the drawing of the maps in three dimensions. The 3D data were subsequently transferred to a cartography programme for 2D map production. For the drawing of the maps in 3D, the aerial photographs were complemented with oblique photographs with stereo overlap. These were corrected to fit with the terrane model based on the standard aerial photographs and viewable in three dimensions in the

aerial photography workstation. In this way also the most important of the steep slopes could be viewed in 3D.

Figures 2 and 3 are reduced copies of the two new detailed geological maps 5a Aappalaartoq and 5c Qingaaq, respectively. In both maps the rocks of the Storø supracrustal belt merge into the Storø shear zone to the west, which again overlies Mesoarchaean orthogneisses. To the southeast (map 5a) and the east (map 5c) the rocks are overlain by Eoarchaean orthogneisses by a tectonic contact. To the northeast in map 5a and to the southwest in map 5c the supracrustal belt overlies massive anorthosites. In both cases, but most visible in the map pattern of the Qingaaq map, the anorthosite bodies form the core of a kilometre-scale antiform around which the supracrustal rocks fold. In both mountains, the supracrustal rocks are intruded by a dense swarm of pegmatites.

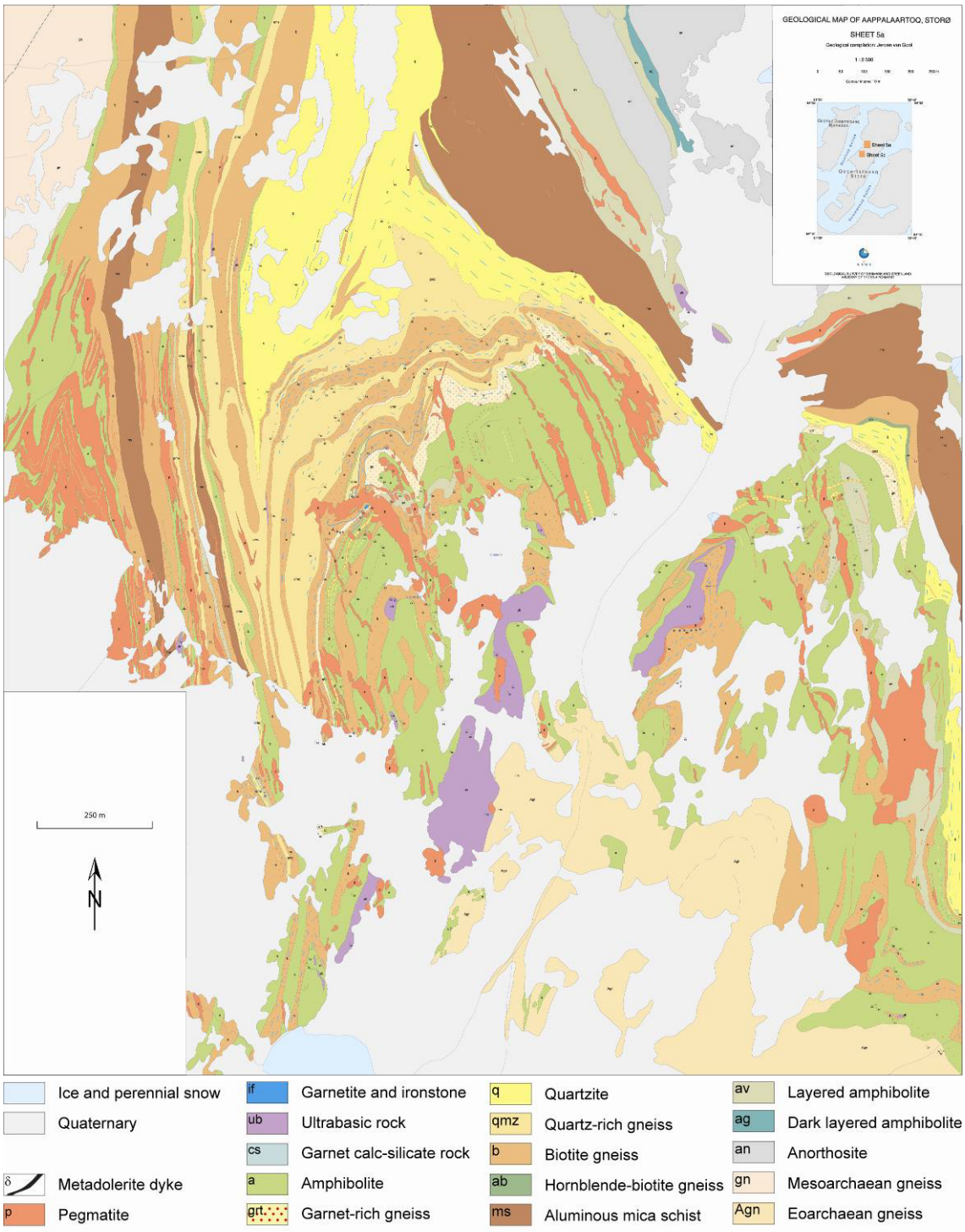

Figure 2. *Geological map sheet 5a of Aappalaartoq, strongly reduced from the 2 500 scale map. Location of the map area is indicated in Fig. 1.*

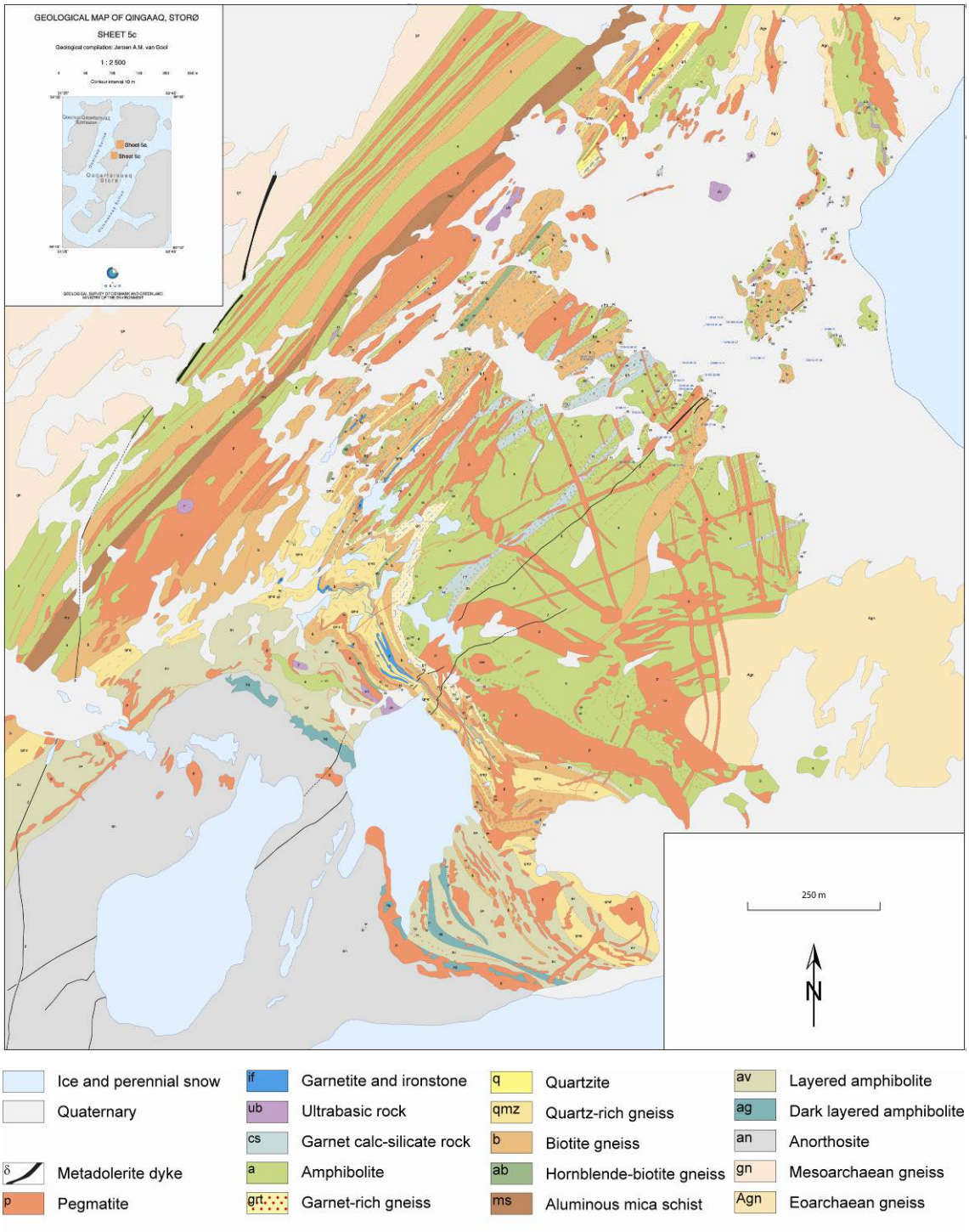

Figure 3. *Geological map sheet 5c of Qingaaq, strongly reduced from the 2 500 scale map. Location of the map area is indicated in Fig. 1.*

Geological background

Gold occurrences on Storø occur in a sequence of Archaean mafic and intermediate supracrustal rocks, here referred to as the Storø supracrustal belt, (cf. Storø greenstone belt in Hollis *et al.* 2004) sandwiched between Archaean orthogneisses. The Storø supracrustal belt is overlain by a grey biotite-bearing orthogneiss, mapped as Early Archaean Amîtsoq gneiss (McGregor, 1993), which contains inclusions of amphibolite and ultramafic rocks, especially close to the contact with the underlying Storø Supracrustal belt. The supracrustal belt is folded, together with the overlying orthogneisses, in a map scale fold pattern. To the north-west the supracrustal belt is truncated by the Storø shear zone, which emplaced rocks of the Storø supracrustal belt on top of *c.* 3050 Ma grey biotite orthogneisses (Nuuk gneisses) of the Akia terrane (Hollis 2005). The supracrustal rocks occur on Qingaaq and Aappalaartoq in respectively north-east- and south-plunging fold structures. The age of the rocks of the supracrustal belt is Neoarchaean with the youngest detrital zircons at *c.* 2800 Ma (Hollis 2005; Rink 2006).
The tectono-stratigraphy of the supracrustal rocks is fairly consistent throughout central Storø: The base of the supracrustal rocks (s.s.) is formed by a sequence of banded mafic to felsic amphibolites, overlain by biotite gneisses of variable composition including garnet and sillimanite- rich bands, as well as quartzite. These rocks are again overlain by amphibolites that include layers of more felsic/intermediate composition and are locally altered and now consist of garnet-rich or diopside-rich rocks. The highest exposed tectono stratigraphic level consists of biotite schists and gneisses, ± garnet and sillimanite, interlayered with amphibolite. Ultramafic rocks occur at all levels, but most commonly in the lower biotite gneiss unit of the supracrustal sequence. Anorthosite in antiformal fold cores on Qingaaq and Aappalaartoq forms the lowest lithology common to the whole map area. The anorthosite grades upward into (leuco-) gabbro and is overlain by the felsic/mafic layered amphibolite. Pegmatites occur both as deformed bodies apparently parallel with the foliation, as well as late dykes that cut all structures. Palaeoproterozoic dolerite dykes cut all other rock types.

Lately, more investigations have been directed towards the hydrothermal alteration in the area. It has become more obvious that some of the aluminous rock types, previously mapped as metapelites (e.g. Polat 2005), are the metamorphosed result of hydrothermal alteration (A. Garde *pers. com.* 2005: Eilu *et al.* 2006; Knudsen *et al.* 2007). Felsic diopside-rich veins ± garnet are an obvious metamorphosed product of calc-silicate alteration, as are alterations of amphibolite to biotite-rich schist along pegmatites and other felsic veins. More questionable are proposed more wholesale alterations of amphibolites to garnet- and sillimanite-rich biotite gneisses.

Mineralisation

At least four gold mineralised zones are exposed in the north face and near the summit of little Qingaaq (Fig. 4). These are from east to west (nomenclature as in NunaMinerals A/S company reports, see also Østergaard & van Gool 2007): Hanging wall zone, main zone, new main zone, and BD zone. The highest gold concentrations are linked to zones of

quartz veins and arsenopyrite mineralisation. In the first three zones, sulphide mineralisation occurs in an antiformal fold hinge, while the BD zone is associated with the contact between garnet-rich gneisses and amphibolite.

Gold mineralisation on Aappalaartoq is not mapped out or sampled systematically. Elevated gold concentrations occur in rust zones with sulphide mineralisation, some in association with quartz vein systems. The same lithological contact that hosts the BD zone mineralisation at Qingaaq shows similar mineralisation on Aappalaartoq, although gold values found to date are not as high as at Qingaaq. Assay analyses of some boulders returned high gold concentrations (up to 50 ppm Au), but these were not reproduced from samples in situ.

These mineralisations themselves are not the main topic of this report. For a more extensive description we refer to Østergaard & van Gool (2007) and a number of company reports referred to therein. Recently, Juul-Pedersen *et al.* (2007) published a petrographic study of the sulphide and gold mineralisations, and recognised different stages in the mineralisation.

Figure 4. *photo of the north face of little Qingaaq, with different rock types and gold mineralisation zones. The main structures are the main zone antiform (MZA), outlined by the lithological contacts, and the Qingaaq shear zone (QS, blue line), presumably truncating the supracrustal rocks. Most of this face consists of the upper amphibolite unit, but outlined in light green is a zone of altered amphibolites, within which most of the gold mineralised zones (outlined in yellow) are located. The thrust contact with the overlying Eoarchaean orthogneisses is exposed in the left side of the photo, and tentatively connected with the shear zone at the top of schist hill. Rock type labels: a = homogeneous amphibolite; aa = altered amphibolite (including mainly garnet-calc-silicate gneisses, garnet- biotite amphibolite, quartz veined amphibolite, calc-silicate-veined amphibolite); ac = calc-silicate veined amphibolite; Agn = Eoarchaean gneiss (Amîtsoq); an = anorthosite on Qingaaq in the background; a + b = tightly interlayered garnet-biotite gneisses and amphibolite on Schist Hill; b = biotite gneiss; grt = garnet ± sillimanite gneiss; ub = ultrabasic rock. SH = schist hill; LQ = little Qingaaq. Gold mineralisation zones in yellow labels: BDZ = BD zone; HWZ = Hanging Wall Zone; MZ = Main Zone: MZW = Main Zone West; NMZ = New Main Zone. Little Qingaaq is 600 m above schist hill.*

Rock types

Figures 2 and 3 are the two new maps reduced to page size and show the distribution of the different rock types in the area. The sequence comprising garnet-biotite gneisses, quartzites, amphibolites and ultramafic rocks are part of the Storø supracrustal belt (Hollis *et al.* 2004). The rock types are common to both Aappalaartoq and Qingaaq and on the large scale the tectono-stratigraphic sequence is fairly consistent. On both mountains anorthosite is structurally the lowest unit, the main amphibolite is the highest within the supracrustal belt. True top-bottom criteria were not found, therefore the upward or downward directions referred to in this report are with respect to the present structural reference frame, no original way up is inferred. The anorthosites that are the lowest in the tectono-stratigraphy, actually form the highest parts of both mountains and one walks down-hill to the higher tectonic units.

The tectono-stratigraphic sequence exists from bottom to top of a gabbro-anorthosite complex, a lower banded (leuco-) amphibolite, garnet-biotite gneiss (± sillimanite, cordierite) containing quartz-rich gneiss layers (± fuchsite-sillimanite-garnet) as well as garnetite and iron stone layers, and on top an upper more mafic amphibolite with (garnet-) biotite schist and garnet-diopside gneiss layers. Ultramafic lenses are common and the rocks are cut by abundant thick pegmatite dykes. Few metadolerite dykes occur. As far as possible, the rocks are described in the tectono-stratigraphic sequence from bottom to top. This sequence is reversed northwest and north of the top of Aappalaartoq, where the anorthosite is exposed as the highest unit in the overturned limb of the hanging wall antiform of the Storø shear zone. It should be noted that the lower tectono-stratigraphic units in the area do not occur in the NunaMinerals A/S drill cores of Qingaaq.

Anorthosite – gabbro (an)

A complex of massive, medium-coarse-grained rocks that range from leucocratic anorthosite in the core, and towards the margins of the complex with increasing content of mafic minerals grading into medium–coarse-grained leuco-gabbro and gabbro, dark green to black with minor feldspar phenocrysts and porphyroclasts.

The main body of the anorthosite is homogeneous and massive, consisting of calcic plagioclase with minor hornblende in stringers and along foliation planes. The foliation strengthens with decreasing grain size and increasing hornblende towards the margins. The most mafic gabbros consist of a dark hornblende-plagioclase gneiss, strongly foliated on Qingaaq, variably foliated around Aappalaartoq. In the highest strain zones these rocks consist of alternating white and black stringers (zebra-striped amphibolite). On the east and northeast side of Aappalaartoq remnants of igneous textures are preserved in the gabbroic rocks (Fig. 5).

Massive anorthosite forms the cores of the two main antiformal structures in the map area at Qingaaq and Aappalaartoq (see structural section). At Aappalaartoq the anorthosite is up to 400 m thick, and interleaved with (intruded by) grey orthogneisses (Fig. 6). Intrusive relationships are well preserved and exposed in the area east of Aappalaartoq mountain, just outside the mapping area (van Gool, unpublished field report 2004). High strain at Qingaaq prevents the recognition of intrusive relationships there, and the rocks are preserved as

dark, banded amphibolites (**ag**, see below). The anorthosite body at Qingaaq, has a maximum exposed width of 2 km south of the map area. This is a folded body, and the true thickness may well be considerably less.

The grey, tonalitic biotite gneiss that intrudes the gabbro-anorthosite east of Aappalaartoq (Fig. 6), was dated at 3053 ± 3.4 Ma (Hollis 2005). Intrusive sheets of the anorthosite are also found in the lower part of the supracrustal sequence. This makes the gabbro-anorthosite and the lower part of the sequence significantly older than the highest supracrustal rocks.

Figure 5. *Leuco gabbro exposed east of Aappalaartoq. (photo p2004jvg1495)*

Figure 6. *Lenses of deformed gabbro in a 3050 Ma orthogneiss, exposed east of Aappalaartoq. (photo p2004jvg1488).*

Dark layered amphibolite (ag)

Amphibolite gneiss and schist occurs as distinct 10–30 m wide dark layers near the contact between the anorthosite and the overlying supracrustal units. This unit is medium-grained, heterogeneous on a small scale, but overall uniform. The rocks are commonly very well foliated and variable proportions of hornblende and plagioclase in the rock gives a mm-to cm scale layering (locally black and white “zebra-striping”, see above). Garnet, biotite and quartz are less common. Plagioclase porphyroclasts occur locally with diameters up to 2 cm. In the lower strain area east of Aappalaartoq a similar mafic schistose layered amphibolite is observed grading with decreasing strain into a well-preserved gabbro. This is interpreted as the marginal phase of the gabbro-anorthosite suite. Although the protolith at Qingaaq and Aappalaartoq are not clearly recognised, these rocks occur as meta-gabbro on several previous maps, by correlation with a less deformed outcrop east of Aappalaartoq.

Layered amphibolite and biotite gneiss (av)

A heterogeneous amphibolite of intermediate composition and containing felsic layers overlies the anorthosite. Parts of this unit are compositionally layered on mm–cm-scale (Fig. 7) with variable proportions of hornblende, feldspar, quartz and biotite, commonly with titanite. Garnet is common in some layers, mostly in the more felsic parts. Distinct concordant felsic layers (predominantly quartz and plagioclase, with minor biotite) are 10 cm to 3 m wide. It is not clear whether these are an original part of a layered protolith, or intrusive felsic sheets into the amphibolite. Locally, this rock type is very highly strained (Fig. 7). One of these sheets was dated (U-Pb on zircon) and preliminary results indicate that the rock contains igneous zircons of *c.* 3.07 Ga, and a metamorphic zircon population of *c.* 2.59 Ga (see geochronology section).

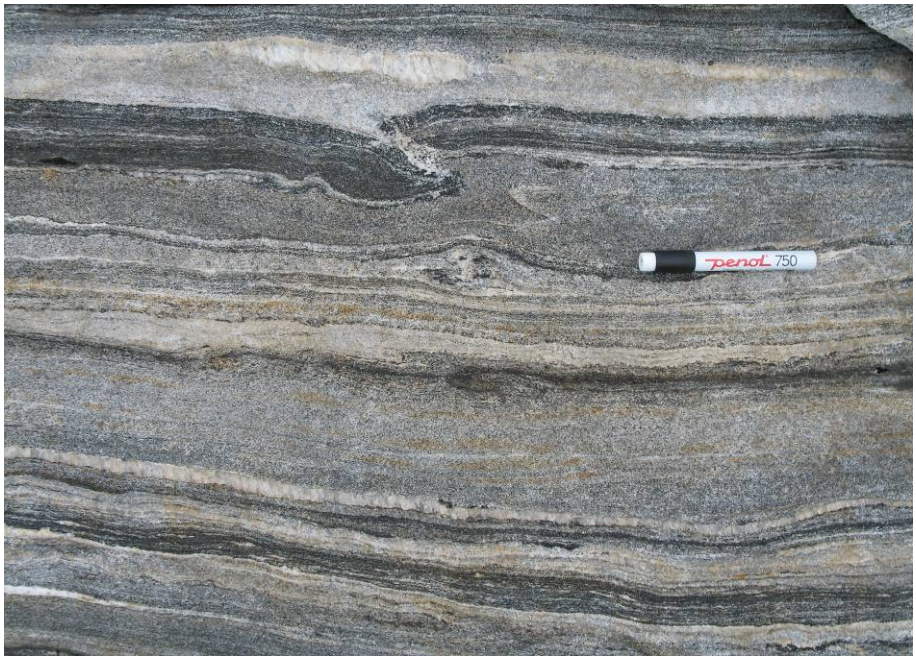

Figure 7. *Banded gneiss of the lower amphibolite sequence. The intra-folial fold and the asymmetric lens (sinistral asymmetry, top to west) to the left of the marker pen suggest that this is a high strain rock. (photo p2006jvg0319)*

Aluminous mica schist and mica-rich gneiss (ms)

Dark-brown weathering, coarse-grained, mica-rich rocks occur in a distinct and consistent band within the Storø shear zone, and in a large unit on the north-eastern slopes of Aappalaartoq. This aluminous unit is distinguished from other biotite-bearing gneisses and schists by its rather homogeneous character. The matrix of these schists and gneisses is coarser-grained and more schistose than the biotite gneiss unit (**b**) described below. It contains biotite, garnet and sillimanite throughout, in addition to quartz, plagioclase and locally muscovite. Cordierite occurs locally, most commonly associated with felsic veins. The rocks weather dark brown. Although similar rocks are common in the remainder of the supracrustal sequence, those tend to be more heterogeneous and comprise narrower layers alternating with less mica-rich gneisses within the same rock unit.
Zircons from a sample of this rock type collected from the main occurrence east of Aappalaartoq yielded LAM-ICP-MS U-Pb ages between 2940–2800 Ma, with few older zircons up to 3083 Ma, and slightly younger metamorphic grains (Hollis 2005). The older grains and the main population are interpreted to be of detrital origin, placing a depositional age after *c.* 2.8 Ga.

Hornblende-biotite gneiss (ab)

A light–medium grey, homogeneous gneiss of intermediate composition, with a poorly foliated, fine–medium-grained matrix. Garnet is rare and the rocks commonly lack large porphyroblasts. Commonly the mafic minerals comprise both hornblende and biotite, evenly dispersed, but locally biotite appears to be lacking (not yet confirmed by microscopy). These rocks are poor in quartz, and contain commonly minor titanite. They grade into biotite gneiss (**b**) which locally includes lenses and layers of the hornblende-biotite gneiss on a metre-scale. The gradual change to biotite gneisses can be explained by one or more of the following processes: a change to more felsic compositions, a metamorphic gradation (prograde or retrograde) or a variation in alteration of a hornblende gneiss to more potassic rocks. Field observations could not distinguish between these. Only few occurrences of this gneiss were found, mainly in the western slopes of little Qingaaq, where they grade into biotite gneiss (b). Minor layers, no more than a few metres wide, occur also within the amphibolites (a), but are not indicated on the map.

Biotite gneiss (b)

The biotite gneiss unit comprises a wide variety of rock types, all characterised by a biotite-rich matrix with plagioclase and quartz. They vary gradationally without clear contacts from massive, grey biotite gneiss to mica-rich aluminous sillimanite-garnet-biotite gneisses and schists. Compositional layering occurs on the scale of decimetres to tens of metres, but individual layers are commonly very homogeneous..
The most common lithology in this unit is a light–medium grey garnet-biotite gneiss with 10-20 % garnets up to 5mm (Fig. 8). It is homogeneous on a smaller scale with a fine-medium-grained matrix, and a granoblastic texture. Outside the Storø shear zone these rocks often display a weak foliation, in spite of the high biotite content, and their occurrence within

highly deformed gneisses. Sillimanite can occur in small amounts, often in small lenses (<5 cm long). Up to 20 cm wide layers and lenses of quartz-garnetite (up to 80 % garnet) can occur (Fig. 9). Otherwise, a subtle layering is locally present, but it is rarely distinct. Garnet-free biotite gneisses have similar characteristics as the garnet-bearing version. All biotite gneisses can weather in rusty colours.

Figure 8. *Well foliated light brown weathering garnet-biotite gneiss. (photo p2006jvg0072)*

Figure 9. *Light grey, poorly foliated garnet-biotite gneiss with thin, boudinaged garnetite layers. (photo p2006jvg0313)*

Sillimanite is common and occurs as fibrolite, in thin lenses and layers, or as cm-sized square pods, possibly pseudomorphs after andalusite. Leucocratic veins occur locally and cordierite was observed in them in few locations, locally with porphyroblasts of several cm. The matrix comprises rarely hornblende, but amphibolite lenses and layers occur locally. Only locally, most commonly in the Storø shear zone and in the most mica-rich parts, this rock type has a well developed foliation. Biotite-rich rocks (schists) are included in this map unit and include commonly garnet and sillimanite.

Together with quartz-rich gneisses, which are intensely interleaved with the biotite gneisses, these rocks occupy much of the central part of the lithotectonic stratigraphy, in between the lower and upper amphibolite.

Two layers of garnetiferous biotite gneiss, on either side of main zone on the northern slope of Qingaaq and on schist hill, are slightly distinct. These rocks are more biotite-rich, overall coarser-grained and more heterogeneous than the more common biotite gneisses. Centimetre-sized quartzo-feldspathic blebs (predominantly plagioclase) occur in part of this unit (Fig. 10).

A biotite-rich part of this unit on the ridge east of Aappalaartoq, situated between an ultramafic body and garnet sillimanite-gneisses, contains corundum instead of sillimanite, with minor garnet.

It should be noted that the occurrence of sillimanite and garnet in this rock type is indicated in the map with symbols. Lack of such symbols generally indicates a lack of garnet and sillimanite. However, exposures of the biotite gneisses that were not visited in the field, but rather mapped from interpretation of aerial photographs and extrapolation of visited outcrops, do not have these symbols in the map, but may contain garnet or sillimanite.

Figure 10. *Garnet-biotite gneiss west of Main Zone, containing distributed quartzo-feldspathic blebs, indicating the onset of partial melting. (photo p2006jvg0028)*

Quartzitic gneiss (qmz)

White–light grey-coloured, weathering light brown to ochre, mica-bearing, quartz-rich gneisses occur interleaved with the biotite gneisses on the scale of cm to tens of metres. They have a coarse fabric, often with regular, 5-10 mm spaced mica-rich partings (Fig. 11). Beside quartz (50-70%), these rocks contain biotite, muscovite and plagioclase. Garnet and sillimanite occur locally, and can be several cm in size, especially on the upper, south-facing slopes of Aappalaartoq. Minor amounts of fuchsite are common. The tight interleaving with biotite gneisses prohibited a precise mapping of the occurrences of these gneisses, and generally they are over-represented in the map.

Thin layers (few cm to 0.5 m wide) of more massive, poorly foliated quartzitic gneiss occur locally on the contacts between amphibolite and the upper biotite gneiss unit. Fuchsite and clinopyroxene are common in these layers, feldspar occurs as well. Outside the map areas, east of Aappalaartoq, these layers are up to 10 m wide, commonly layered and locally micaceous. Zircons from one of these layers were dated at 2.85–3.2 Ga (detrital ages) and *c.* 2.59 Ga (metamorphic ages; U-Pb LA-ICPMS, GEUS sample 481283, Rink 2006).

Figure 11. *Quartzitic gneiss with mica-rich partings and typical brown weathering colour. (photo P2006jvg0448)*

Quartzite (q)

Massive quartzite forms the upper part of Aappalaartoq mountain on the southern and western slopes. The fresh rock is medium grey, but it weathers orange to light brown (Fig. 12), giving Aappalaartoq its characteristic red colour. It is medium-grained, and beside quartz, the rocks contain minor muscovite, and variable small amounts of sillimanite and fuchsite, all fairly homogeneously distributed through the rock. Locally, fuchsite can form up to 20% of the rock. Garnet is rare, but garnet-rich layers contain commonly sillimanite in elongate, square pods, potentially pseudomorphs after kyanite. The contact with quartzitic gneiss (**qmz**) is gradual. No quartzite is indicated on the map of little Qingaaq (with the exception of the northwestern corner), but smaller parts of the quartzitic gneisses (**qmz**) are more massive and indistinguishable from the quartzite unit.

Figure 12. *Fuchsite-bearing massive quartzite (q), with greenish-grey-coloured fresh surface containing weathering spots with a typical rusty brown colour. (photo P2006jvg0451)*

Garnet-rich gneiss (grt)

A garnet-rich gneiss, with a light grey to white, felsic, biotite-bearing matrix (Fig. 13), commonly sillimanite-rich. Garnet forms often up to 40% of the rock, in *c.* 5mm-sized grains that are evenly distributed through the rock. The grey to white matrix is fine-medium grained, and consists predominantly of plagioclase, less quartz and minor biotite. Sillimanite-rich layers are common, and occurs either dispersed in these layers (intergrown with biotite) or as square lumps up to 1 cm wide, which may be pseudomorphs after andalusite. In thin section these are obvious intergrowths of fibrolite and quartz with minor garnet, biotite and opaque minerals. Thin sections show that they are poor in quartz, and contain minor rem-

nants of staurolite, both in the matrix and as inclusions in garnet. The rocks are locally layered, but they have a poor foliation. In few locations undeformed inclusions of amphibolite occur, which have a gradual transition to the garnet gneiss. The garnet-sill-bt assemblage has previous led to the interpretation of these rocks as metapelites, but their trace element chemistry suggests that these are altered mafic rocks (A.A. Garde pers. com. 2006; Knudsen *et. al.* 2007; see geochemistry section).
The garnet gneisses occur with few exceptions only at the lower contact of the main upper amphibolite unit (a) on both little Qingaaq (BD zone) and Aappalaartoq. It is typically about 50 m wide.

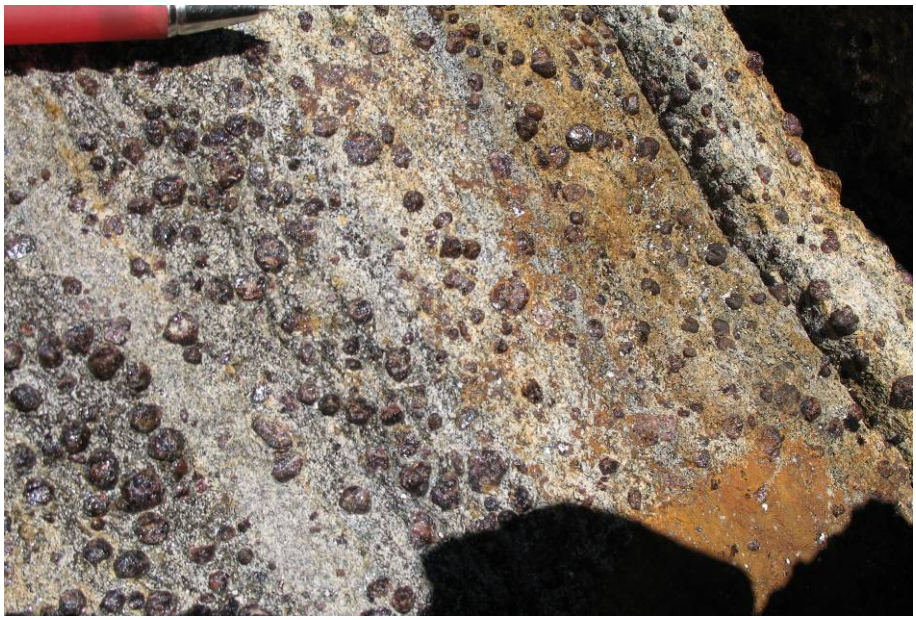

Figure 13. *Layered garnet-rich gneiss with regularly spaced garnets, that have overgrown a weak foliation. (Photo p2006jvg0157)*

Amphibolite (a)

This lithological unit is referred to as the main amphibolite or upper amphibolite, and includes beside a “fresh” amphibolite the variations garnet amphibolite, diopside-veined amphibolite and garnet-biotite amphibolite (as referred to in field data spreadsheet). The latter are assumed to be metamorphosed altered rocks, derived from the unaltered amphibolite. Occurrences of diopside veins and garnet are indicated on the map, but these are not outlined as map units (i.e. no boundaries were mapped out). Fig. 4 shows the north face of little Qingaaq where the zone of paler grey/green colours of the altered amphibolite clearly stand out from the black, unaltered amphibolite, occurring to the east of the altered zone and in the core of the large-scale fold exposed on the slope (Main Zone antiform).
The main (unaltered) rock type is a homogeneous to subtly layered dark amphibolite, medium grained and well foliated (Fig. 14). It consists of 40—60% hornblende, with plagioclase and *c.* 10% titanite. locally titanite has overgrown a core of ilmenite. The rocks have a well equilibrated texture with slightly elongate amphibole, plagioclase and titanite grains, all are well aligned. Opaque phases (sulphides) are rare in the least altered amphibolites.
The amphibolites on the north face of little Qingaaq and the south-eastern slopes of Aappalaartoq grade locally into a number of different, but associated rock types. These vary

considerable, but have been grouped in four rock types, garnet amphibolite, diopside-veined amphibolite, garnet-biotite amphibolite and garnet calc-silicate gneiss.

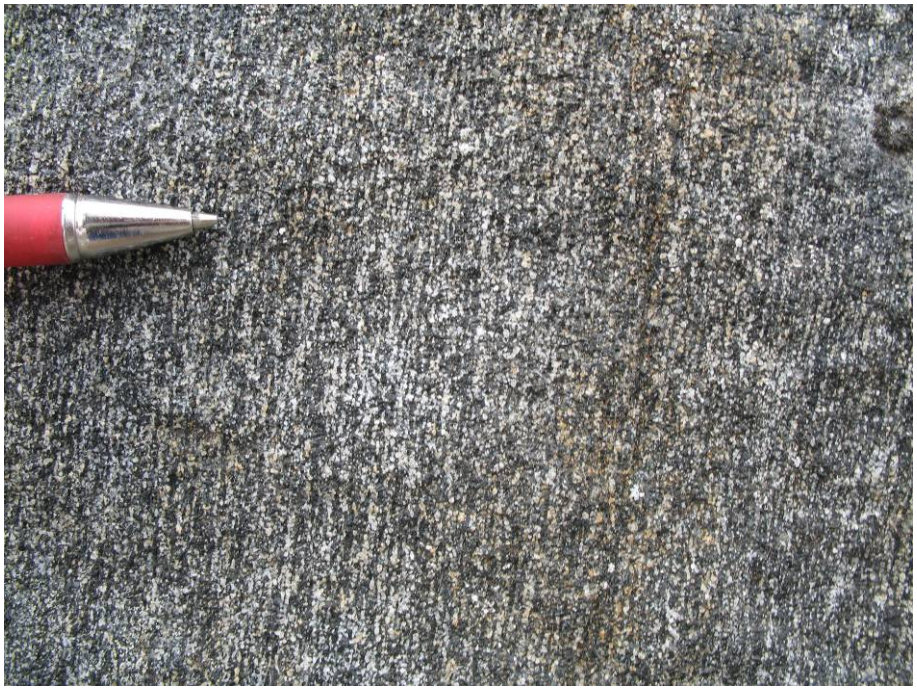

Figure 14. *Least altered amphibolite, consisting mainly of plagioclase and hornblende, on the northern slope of little Qingaaq. (photo p2006jvg0080)*

Only the latter forms mappable units and is described below. The three former rock types have irregular outlines and grade into each other, and are described together.

Garnet amphibolite occurs in two forms, distinguished mainly on the basis of petrography. One type of garnet amphibolite has sub- to euhedral crystals several mm to > 1cm in a regular, homogeneous amphibolite matrix (Fig. 15). These rocks display an equilibrium texture in thin section. The second type has clusters of sub-mm sized garnets in a matrix containing commonly plagioclase, diopside, epidote, sulphides and quartz veins, in some cases also cummingtonite/actinolite, biotite, calcite and chlorite (Fig. 16). These minerals commonly show disequilibrium textures, e.g. symplectites of diopside and quartz, or sericitisation of plagioclase. Garnet biotite amphibolites occur associated with vein systems, where biotite occurs both as an early phase, included in garnet and part of the matrix, defining an S1 foliation, and a late phase overgrowing hornblende. Diopside ± garnet-bearing quartz and quartzo-feldspathic veins are common throughout the amphibolite unit, but most abundant in the alteration zone in the amphibolites. They form generally 1-5 cm wide felsic veins with light greyish green diopside and commonly also garnet (Fig. 17). The veins have dark hornblende-rich selvages and are isoclinally folded. Variations of garnet-, diopside-, epidote-, actinolite-bearing, veined amphibolites occur within the alteration zone.

In 2007 two locations were found where the main amphibolite sequence contains pyroclastic rocks, consisting of cm-sized intermediate to felsic clasts in an intermediate to mafic matrix (Fig. 18). The best exposure of these rocks is just above main zone (see sample description 484652, geochronology section), but this exposure can be covered by snow a large part of the year.

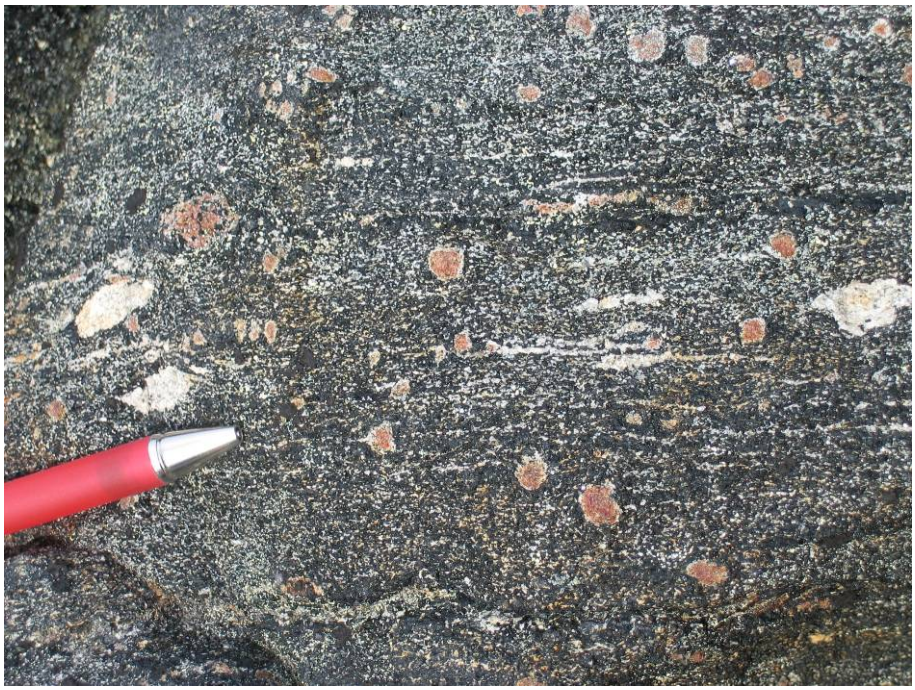

Figure 15. *Example of a garnet amphibolite exposed on Qingaaq. Garnet has plagioclase rims and overgrows the foliation. (photo p2004jvg0373)*

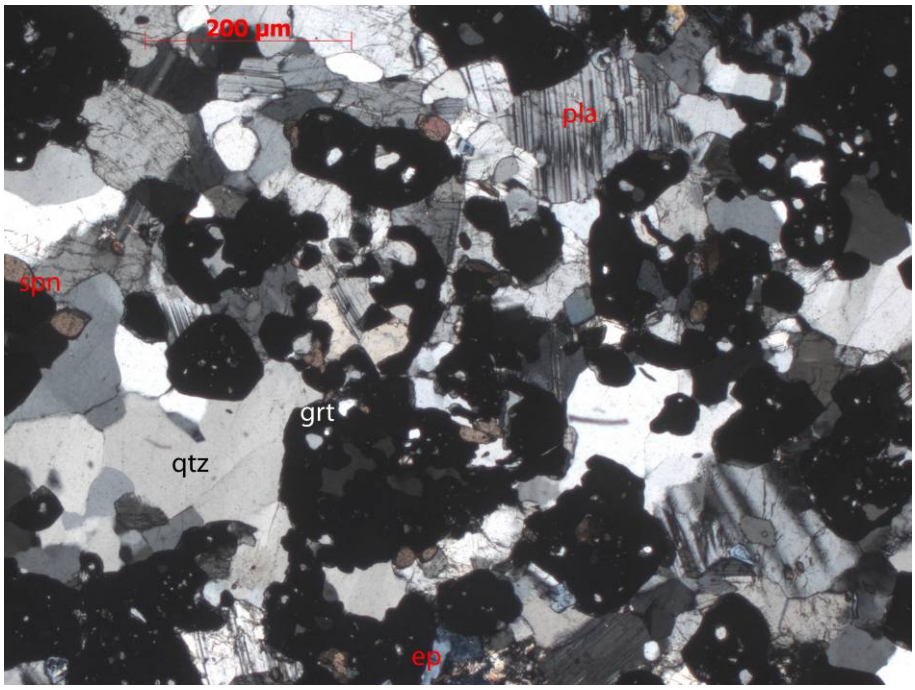

Figure 16. *Cluster of small euhedral garnets in a quartz-veined garnet amphibolite. ep = epidote, grt = garnet, pla = plagioclase, qtz = quartz, spn = sphene. Crossed polarised light, sample 487910.*

Figure 17. *Calc-silicate veins in amphibolite at Qingaaq. (photo p2006jvg0039)*

Figure 18. *Pyroclastic rock in the main amphibolite few tens of metres up-slope from main zone.*

garnet calc-silicate gneiss (cs)

The rocks in this unit are a variety of intermediate composition gneisses, of which most contain diopside and/or pale green amphibole, ± diopside, ± hornblende. They are commonly layered (referred to as banded leuco-amphibolite on the map compiled by G. Smith (in Skyseth 1997) and medium-grained, locally with cm-sized garnets, and always well foliated (Fig. 19). The rocks are mostly rich in plagioclase and commonly comprise garnet and minor epidote. Calcite is less common and occurs mainly in microfractures. Quartz forms commonly less then a few percent of the rock, but it can occur as veins. Hornblende-rich schlieren with gradational contacts to the gneissic host may well be remnants of the original less altered amphibolite rock type (Fig. 20). Locally this gneiss is gradational to a calc-silicate veined amphibolite with garnet and an unaltered amphibolite. The gradational contacts to the main amphibolite and to calc-silicate veined amphibolite, as well as the geochemistry of these rocks suggest that this is a calc-silicate altered amphibolite, or associated rock.

These gneisses have a light brown weathering colour, and are greenish, light grey in fresh surface. They occur interleaved with various types of amphibolite both on the north face of Qingaaq and within the amphibolites of Aappalaartoq. However, on the latter they form only narrow bands and not mappable units.

Figure 19. *Garnet calc-silicate gneiss, containing garnet, pale green amphibole, plagioclase and minor epidote. (photo p2006jvg0092)*

Figure 20. *Garnet calc-silicate gneiss with amphibolite schlieren, which are interpreted to represent domains of less altered amphibolite. (photo p2006jvg0093)*

Ultrabasic rock (ub)

Ultrabasic rocks do not occur within a consistent stratigraphic level. The largest bodies occur in the top (present-day reference frame) of the sequence on Aappalaartoq and 580 m top. In these locations discontinuous outcrop reveals elongate lenses up to 200 m wide, and the longest being more than 800 m long. More commonly they occur as slightly elongate boudins or lenses that are between few metres and several tens of metres long and wide. Thin but laterally extensive layers of ultramafic schist occur west and south of 580 m top, in the upper part of the Storø shear zone.

The ultrabasic rocks have metamorphic mineral assemblages, most commonly consisting of brown amphibole (tremolite) and phlogopite. In massive cores olivine and pyroxene may occur, together with hornblende and actinolite. Schistose margins are locally rich in phlogopite and chlorite. Pseudomorphosed remnants of an orthopyroxene cumulate texture are locally preserved in the massive parts (Fig. 21). In the large ultramafic lens south of Qingaaq high camp, an unusual texture was observed of aggregates consisting of 10-20 cm long blades of intergrown chlorite and olivine, which have overgrown a foliation at a high angle (see Knudsen *et al.* 2007). Serpentine and talc are common in late fractures.

Lenses of ultrabasic rocks occur also in the orthogneisses (both gn and Agn), most commonly in the vicinity of the contact with the supracrustal belt. It is not uncommon to find a foliation in the ultramafic rocks that is at a high angle to the foliation in the host rocks. This may suggest that some of the lenses represent isoclinal fold hinges.

Figure 21. *Orthopyroxene pseudomorphs in an ultramafic rock at Aappalaartoq. (photo p2006jvg0488)*

Hornblende garnetite (hb)

Equivalents of the quartz-biotite garnetite occur also in the amphibolites, but contain predominantly actinolite, grunerite or hornblende, in stead of biotite (Fig. 22). Garnet forms commonly up to 50—60% of the rock and is less abundant than in the garnetites within the biotite gneisses. One example from the east side of Main zone is transitional to garnet amphibolite, with abundant hornblende, diopside, titanite and epidote, and virtually no quartz. Garnet hornblendite may locally be a more appropriate name. This rock type occurs together with or within felsic vein systems.

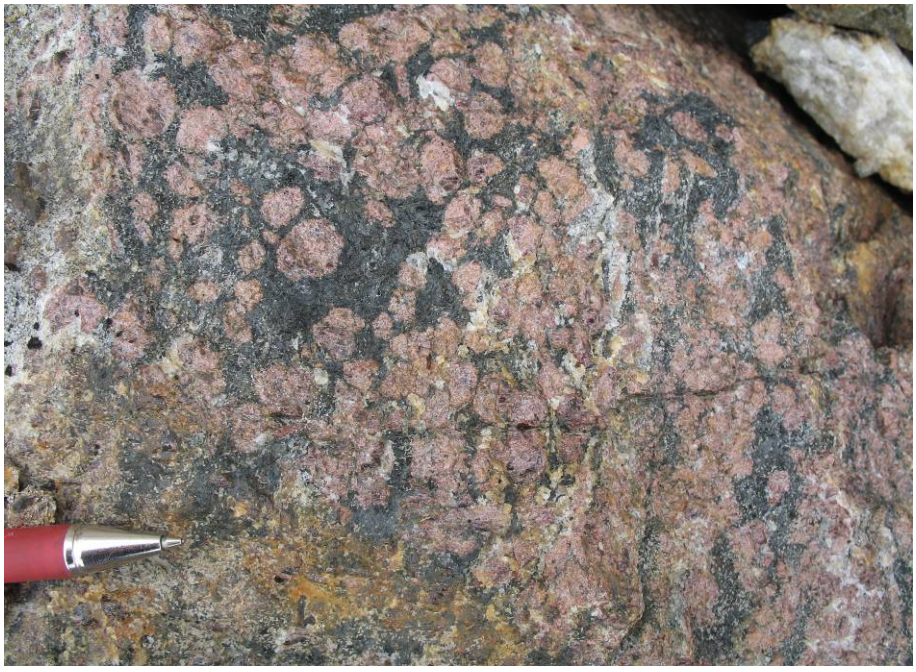

Figure 22. *Hornblende garnetite on the northern slope of little Qingaaq. (photo p2006jvg0050)*

Garnetite and quartz-garnet-magnetite rock (if)

These two rock types occur commonly together, often interlayered, or as a thin layer of the one on the margin of the other. Although these two rock types can easily be distinguished in the field, they occur commonly so closely interlayered, that they could not be mapped individually on the scale of the map. However, this distinction was made in field notes. The garnetite consists up to 80% of garnet, together with quartz and biotite, with minor magnetite and sulphides (Fig. 23). The rocks are commonly massive and locally have a subtle layering. They are medium-grained, with garnet being subhedral and fairly constant in grains size, also forming garnet networks where they form more than 70% of the rock.

The magnetite-rich rocks (ironstones) are generally finely layered on cm- to mm scale (Fig. 24), consisting of alternating layers dominated by respectively quartz, magnetite, or garnet. This may give the rocks the appearance of a banded iron formation. The ironstones are commonly very dark brown weathering, but in fresh surface have alternating steel grey and white layers, red where garnet-rich. Grunerite and cummingtonite occur in garnetite layers together with magnetite rocks. The magnetite rocks rarely occur without garnetite layers, but magnetite rocks do not always accompany garnetite.

Garnetite and the magnetite rocks occurs commonly as 1—3 m wide layers, up to 10 m locally, typically *c.* 50 m structurally below the lower contact of the main amphibolite. These rocks are found commonly on the contact between two other rock types. Single bands occur as well as braided networks of magnetite or garnetite rocks. The latter suggest that instead of a stratigraphic layer, these rocks are formed by hydrothermal fluids. Thin (mainly 2—30 cm wide) garnet-rich layers occur also within the biotite gneiss (Fig. 9), less commonly in the other rock types. Similar garnetite rocks occur within the amphibolites, but here they commonly contain actinolite, hornblende ± biotite and little quartz (**hb**).

Figure 23. *Quartz garnetite on western slope of Qingaaq. (photo p2007jvg0074)*

Figure 24. *Banded garnet-quartz-magnetite rock (ironstone)overlain by a quartz-veined biotite gneiss. (photo p2006jvg0189).*

Pegmatites (P)

The pegmatites are a characteristic part of the well-known northern slope of little Qingaaq, where they form 10—20 percent of the rock volume(Fig. 4). Several generations of pegmatite exist in various states of deformation. Most are undeformed, coarse-grained leucocratic quartz-feldspar pegmatites, locally with minor biotite or garnet, rarely magnetite or sulphides. Few are intensely sheared, medium or fine-grained and can contain biotite and muscovite. The oldest pegmatites observed are smaller boudinaged layers (sub-)parallel with the foliation. These are deformed in areas where the only structure is the S1 foliation. These pegmatites occur throughout the sequence. The later generations of pegmatites occur predominantly within the amphibolites, and in the Storø shear zone. These can form bodies that are up to *c.* 80 m wide and several hundreds of metres long. Typically, the pegmatites are most abundant in the amphibolites, the mica-rich rock types did not fracture in the same way to provide space for the pegmatites to intrude. On Qingaaq a conjugate set consists of one steep system of pegmatites, dipping NE—SE, approximately parallel to the Storø shear zone, but somewhat steeper, and a shallower system dipping moderately to the W—WNW. These two offset each other and are largely of the same age. An apparently shallower set appears to be deformed by the Storø shear zone and associated folds. Intensely sheared pegmatites occur both in the Storø shear zone and on the north slope of Qingaaq.

On Aappalaartoq occurs a fairly consistent set of pegmatites, which all have an orientation that is parallel with, or somewhat steeper than the Storø shear zone. Some of them are clearly axial planar to F3 folds. They occur predominantly within the amphibolites, and in the hinge of the dominant synform in the south and southeast slopes of Aappalaartoq, the pegmatites stop abruptly at the contact between amphibolite and biotite gneisses. The

largest pegmatite on Aappalaartoq occurs on the corner between the western and south-western slopes in the footwall of Storø shear zone and is folded in a large north-closing fold structure.

One pegmatite sampled *c.* 10 km south of Qingaaq in the supracrustal belt was dated at 2745 Ma., while three pegmatites sampled near Qingaaq yield U-Pb zircon ages around 2630 Ma (Hollis 2005). The latter include a slightly irregular discontinuous pegmatite with pinch and swell structures, that cuts through the lower part of Qingaaq (sample 465054, Hollis 2005). However, a straight-walled, undeformed pegmatite running almost parallel with this one but *c.* 25 m higher up the slope, was dated at *c.* 2550 Ma (Nutman *et al.* 2007). This is near the imprecise age of the thick pegmatite near the top of little Qingaaq (2523 Ma) and a straight-walled pegmatite east of Aappalaartoq (*c.* 2570 Ma; Hollis 2005). The geochronological data confirm that several generations of pegmatites occur in the Storø supracrustal belt. The youngest of these (*c.* 2550 Ma) are assumed to be the set of straight, undeformed dykes that form a conjugate set on the north face of little Qingaaq.

Metadolerite dykes (δ)

Dark green, straight-walled metadolerite dykes in the map area are commonly 2—5 m wide, but both thinner and thicker examples exist (Fig. 25). They are steeply dipping and most have a north-easterly trend. They are massive, and most are totally recrystallised, consisting of hornblende, clinopyroxene and plagioclase. Locally, remnants of an igneous fabric are preserved. Many of the dykes show fracture sets. Based on the recrystallisation of the dykes, their age is assumed to be Palaeoproterozoic.

Figure 25. *Metadolerite dyke at little Qingaaq, cutting both garnet-rich gneiss and pegmatite. The dyke is broken along fractures perpendicular to the dyke wall. Hammer handle c. 40 cm. (photo p2004jvg410)*

Breccia

On the northern slope of Qingaaq, in the western part of Main Zone, a series of small outcrops is underlain by a poorly consolidated, rusty polymict breccia, containing clasts of several of the surrounding rock types (Fig. 26). Grain sizes vary from few mm to 10 cm. Petrographic observation of broken, angular clasts in a hematite matrix suggests that this is a post-metamorphic fault breccia. No consistent structural pattern was observed in outcrop, mainly as a result of the overall crumbly nature of the rock. This rock type was not indicated in the map

Figure 26. *Rusty polymict breccia from the eastern side of Main Zone. Scale in centimetres.*

Mesoarchaean quartzo-feldspathic biotite gneiss (gn)

A light grey, medium-to coarse-grained quartzo-feldspathic biotite gneiss, overall homogeneous. These gneisses are of tonalitic to granodioritic composition (quartz, plagioclase, biotite and minor K-feldspar). Their fabric is variable, locally with a weak linear fabric and a granoblastic texture, but especially in the vicinity of the Storø shear zone, the rocks have a gneissic fabric. Large inclusions of amphibolite and ultramafic rock occur, but the host gneisses are fairly homogeneous. In the published 1:100 000 scale geological map (McGregor, 1993), these rocks were mapped as Nûk gneisses, and geochronological analyses of samples collected at sea level just west of the Aappalaartoq map were dated at *c.* 3.1 Ga (Hollis 2005), in accordance with the age of the Nûk gneisses. These gneisses occur in the footwall of the Storø shear zone.

Eoarchaean quartzo-feldspathic biotite gneiss (Agn)

These light grey to white gneisses are similar to the ones described above in terms of composition and overall appearance, but are more heterogeneous, locally with several melt phases and more complex deformation patterns. Large inclusions of amphibolite and ultramafic rocks are common and especially abundant in the area closest to the contact with the supracrustal rocks. Deformed and undeformed Ameralik dykes occur in several locations, some with spectacular large and well-preserved phenocrysts, e.g. in the lowest exposures in the southeast corner of map sheet 5c. Discordant amphibolites within some of the

larger amphibolite inclusions may also be remnants of Ameralik dykes (C.L.R. Friend and A.P. Nutman, *pers. com.* 2007). Some of the amphibolites at the contact between the Storø Supracrustal belt and the Eoarchaean gneisses, which were mapped as part of the supracrustal belt, may well be part of the Eoarchaean terrane.
These rocks are overlying the supracrustal belt and were mapped as Amîtsoq gneiss by McGregor (1993). The contact is interpreted to be tectonic, but obvious high strain fabrics were not observed. The Eoarchaean age of these gneisses (at least near the NunaMinerals camp) is confirmed by the geochronological analyses described below (sample 487918).

Rocks on Schist Hill

The structural analysis carried out for this project and interpretation of the drill core data by NunaMinerals A/S made it obvious that the rocks on schist Hill are separated from the northern slopes of little Qingaaq by a tectonic break (Figs 1, 4). Field observations in 2007 led A.P. Nutman and C.R.L. Friend (*pers. comm.* 2007) to the conclusion that the rocks on schist hill and to the northeast at the lake shore could well be Eoarchaean and part of the Færingehavn terrane. The rocks of schist hill consist of tightly interlayered and complexly folded amphibolite, locally garnet-bearing, garnet-sillimanite biotite gneiss and schist, small lenses of ultramafic rocks, and a 5–30 cm wide layer of rather coarse-grained, homogeneous quartzite, locally diopside-bearing, which separates the amphibolites from the biotite gneisses (Fig. 27). A small outcrop of amphibolite at the lake shore to the northeast, is layered on a cm- to mm scale, is intensely folded and contains homogeneous amphibolite layers that truncate some of the folded layering, and which are less intensely folded themselves. These may represent Ameralik dykes (Nutman and Friend *pers. com.*). This interpretation could be valid, since the Eoarchaean gneisses on Storø contain abundant lenses of amphibolite and ultramafic rock. But further geochronological data are required in order to substantiate this hypothesis, and analysis are in preparation to test this.
The detailed (1:2 500) maps do not distinguish the rocks on Schist Hill as different from the others in the Neoarchaean supracrustal belt, and do not portray this new interpretation.

Figure 27. *Tightly folded amphibolite and biotite gneiss, separated by 10—20 cm of diopside-bearing quartzite.*

Rocks in the Storø shear zone

The shear zone comprises predominantly interleaved amphibolites and garnet-biotite gneisses (± sillimanite) with minor fuchsite-bearing quartzites and intruded by abundant pegmatites, which all resemble similar rock types in the main, folded supracrustal sequence. However, there is a structural discontinuity between the rocks in the shear zone and the folded supracrustal rocks in the hanging wall. Based on the similarities of the rock types in the shear zone and hanging wall, there is no obvious reason to assume that the rocks are of a different ages, and no age difference is indicated in the map. This can be tested with further geochronological analyses.

Comparison of NunaMinerals rock type codes and map legend

NunaMinerals geologists used a subdivision of rock types and code for the description of the drill core that is slightly different from the one used in the maps. Whereas the drill core is described in purely lithological sense, the map units are tectono-stratigraphic, and the occurrence of a lithology within this sequence plays a role in the distinction and naming of the units in the map. Furthermore, mineralisation is an important factor for the drill core description, but this was not used as a distinction in the map. Also the scale of observation is quite different: whereas drill core is described in units that can be as small as few tens of centimetres, the map rarely distinguishes units that are less than 5 m wide. For example, within the biotite gneisses (**b**) the garnetite and ironstone bands are so closely associated, that it is virtually impossible to draw them separately on the map, and therefore they are joined in the one "**if**" unit in the map. The lowermost units were not sampled by the drilling. Drill cores penetrated as far down as the central biotite gneisses (**b**) and quartzitic units (**qmz**), but never the lower layered amphibolite (**av**) or aluminous mica schist (**ms**). In spite of the differences, many parallels can be drawn between the map legend and the drill core codes, and the map units can fairly easily be recognised in the drill core. Table 1 shows a comparison of the two.

Table 1. *comparison between the coding of the rocks in the drill core and in the 1:2 500 maps of Qingaaq and Aappalaartoq. Characters in bold refer to labels in the map.*

tectono-stratigraphy	NunaMinerals A/S drill core coding and description				GEUS map labels and description	
	Rcode	Code	nr	description	map label	description or comment
Upper amphibolite	1	UA	1	unaltered to moderately altered amphibolite (grt-di-hbl-bi). minor sulphides dark grey to black, hbl-rich rock. Common minor calc-silicate veining	**a**	dark grey to black, hbl-rich rock, minor calc-silicate or quartz veining, up to 2 % garnet
	1	GNA	2	garnet amphibolite (>20% garnet, <15% qtz-veins, moderate-strong alteration and sulphides) often gradational to garnetite	**a** with garnet symbols	garnet amphibolite grading into hornblende garnetite
	1	CA	3	intense calc-silicate alteration and/or silicification. Minor sulphides grading from UA	**cs** or **a** with calc-silicate symbols	amphibolite with calc-silicate veining, or garnet calc-silicate gneiss
	4	QA	4	highly qtz-veined (> 15%) and/or intense alteration/mineralisation (grt-di-hbl-bt + sulphides) often coarse-grained and heterogeneous	**a** with quartz vein symbols	amphibolite with quartz veining, may locally include garnet-calc-silicate gneiss
	5	GA	5	garnetite, (>50% garnet, often with sulphides and di-bi). Course-grained phenoblasts (porphyroblasts?) of grt "matrix" of hbl-bi-po. often disrupted by quartz veins.	**if** or **hb**	within the upper amphibolite mainly a hornblende (or calcic amphibole) bearing garnetite (> 40% garnet) +/- diopside, epidote, biotite, quartz
Biotite gneiss within upper amphibolite	6	BG1	6	bi-(grt) gneiss (altered/leached amphibolite?) light, leached appearance. Rich in qtz-fsp. gradational to amphibolite.	**ab, b**	pale grey biotite gneiss, fine-grained, gradational to both amphibolite and biotite gneiss
	6	BG2	7	mineralised bi(-grt) gneiss. (altered amphibolite?). Main Zone type (po + asp). Light, leached appearance. rich in qtz-fsp. gradational to amphibolite	**ab, b**	mineralised equivalent of BG1, not distinguished from previous rock type in the map

Table 1. *continued*

tectono-stratigraphy	NunaMinerals A/S coding and description				GEUS map labels and description	
	Rcode	Code	nr	description	map label	description or comment
lower biotite gneiss unit	8	BGN1	8	qtz-rich massive bi(-sill) gneiss. No or minor grt lower BD zone	**b** with quartz veins	quartz veined homogeneous, felsic, pale grey biotite gneiss gradational to quartz-rich gneiss and grt-sill-bt gneiss
	8	BGN2	9	qtz-rich massive bi-grt(-sill) gneiss lower BD zone.	**b, grt,**	garnet-bearing biotite gneiss +/- sil, grt + sil-bearing quartzitic gneiss (mainly on Aappalaartoq)
	8	BGN3	10	mineralised bi-(gnt-sill) gneiss BD zone. (po+cp+asp)	**b, grt**	mineralised equivalent of BGN1+2 includes biotite gneiss and garnet-rich gneiss, not distinguished in the map
	8	BGN4	11	qtz-rich to quartzitic mu-bi-sill-fuch gneiss lower BD zone.	**qmz, q**	quartz-rich gneiss with ms and fuch, locally also bt and sill, rarely grt. Also quartzite
Upper biotite gneiss	12	UGN	12	upper bi-gnt-(sil) gneiss. common code for all biotite gneisses above the Main Zone	**b**	coarse-grained and heterogeneous garnet-biotite gneiss, not distinguished as separate rock type in the map.
Not associated with a tectono-stratigraphic level	13	PEG	13	pegmatite	**p**	coarse-grained pegmatite, both undeformed and deformed
	14	CAS	14	casing	---	
	15	DOL	15	dolerite dyke	δ	massive black metadolerite dyke
	16	IF	16	iron formation (oxide facies)	**if**	quartz-garnet-magnetite rock, locally fine-grained and banded, in the map not distinguished from quartz garnetite
	17	MIL	17	milled or strongly broken core	---	
	18	UM	18	ultramafite	**ub**	ultramafic rocks and schists, locally serpentinised

Structure

The supracrustal sequence of central Storø lies sandwiched between different gneiss terranes and is multiply folded. It is structurally overlain by a sheet of Eoarchaean orthogneisses (Færingehavn terrane of Friend *et al.* 2005) in a shallow east-plunging gentle synform between Qingaaq and Aappalaartoq mountains. To the north-west the sequence is bound by (and sheared into) the Storø shear zone, which separates the Storø belt from the underlying Mesoarchaean orthogneisses of the Akia terrane. To the north/northeast the supracrustal sequence is overlying a lower tectonic slice, consisting of c. 2.7 Ga and 2.8 Ga orthogneisses, presumably intruding into a complex of Early Archaean orthogneisses and anorthosites that occur in the hanging wall of the Storø shear zone (Fig. 1).

Large-scale fold structures – thrust ramp setting

The large-scale structure in the map is dominated by kilometre-size anti- and synforms overlying the Storø shear zone (Fig. 1). Although the map patterns of Qingaaq and Aappalaartoq mountains appear quite different, the basic structural setting of the two is quite similar, although in different orientations, plunging to the east at Qingaaq, plunging to the south at Aappalaartoq (Figs 1, 28). The overall structure on either mountain is that of a hanging wall antiform-synform pair over the Storø shear zone. The anorthosite-cored antiforms are overturned to the northwest, with the overturned limb being dragged into - and truncated by - the underlying shear zone (Figs 29a, b). This is quite clear in the map pattern of Qingaaq (Figs 1, 3), but the geometry of the Aappalaartoq antiform is not obvious in the map. In contrast, the Aappalaartoq synform is enhanced in the map pattern. The folds and the shear zone are of the same age, which is consistent with the observation that pegmatites that are approximately of the same age as the shear zone occur both deformed by, and cross-cutting through these large-scale folds. Furthermore, the axial planes of the F3 folds are approximately parallel with the shear zone foliation, and mesoscopic F3 folds get more abundant and tighter towards the shear zone.

The geometry of the large-scale fold at the two mountains is sketched in a NE-SW schematic section along the shear zone (Fig. 30). This section also shows that part of the supracrustal belt in the study area defines two triangular areas, or triple points from which the belt radiates in three directions (*c.f.* Fig. 1). This geometry has been an enigma, but can easily be explained by the thrust ramp geometry. The section in Fig. 30 shows the geometry of two mirrored hanging wall thrust ramps. The development of the fold structures at this thrust ramp is sketched in Fig. 31. The overriding thrust sheet consisting of anorthosite and supracrustal rocks moves up the thrust ramp and develops the hanging wall antiform-synform pair as a geometric necessity. Since the thrusting occurs at elevated or increasing metamorphic grade, the lower part of the thrust sheet folds as a result of drag on the thrust plane in a fold-nappe fashion. This results in the folding the lower part of the supracrustal sequence around the anorthosite core and being dragged into the shear zone. It is likely that the Storø shear zone was shallowly-dipping at this time and later rotated in a steep orientation. The alternate solution has the shear zone in a steep orientation during thrusting. Although this cannot be excluded, this is energetically less favourable and would require large vertical movements in the crust.

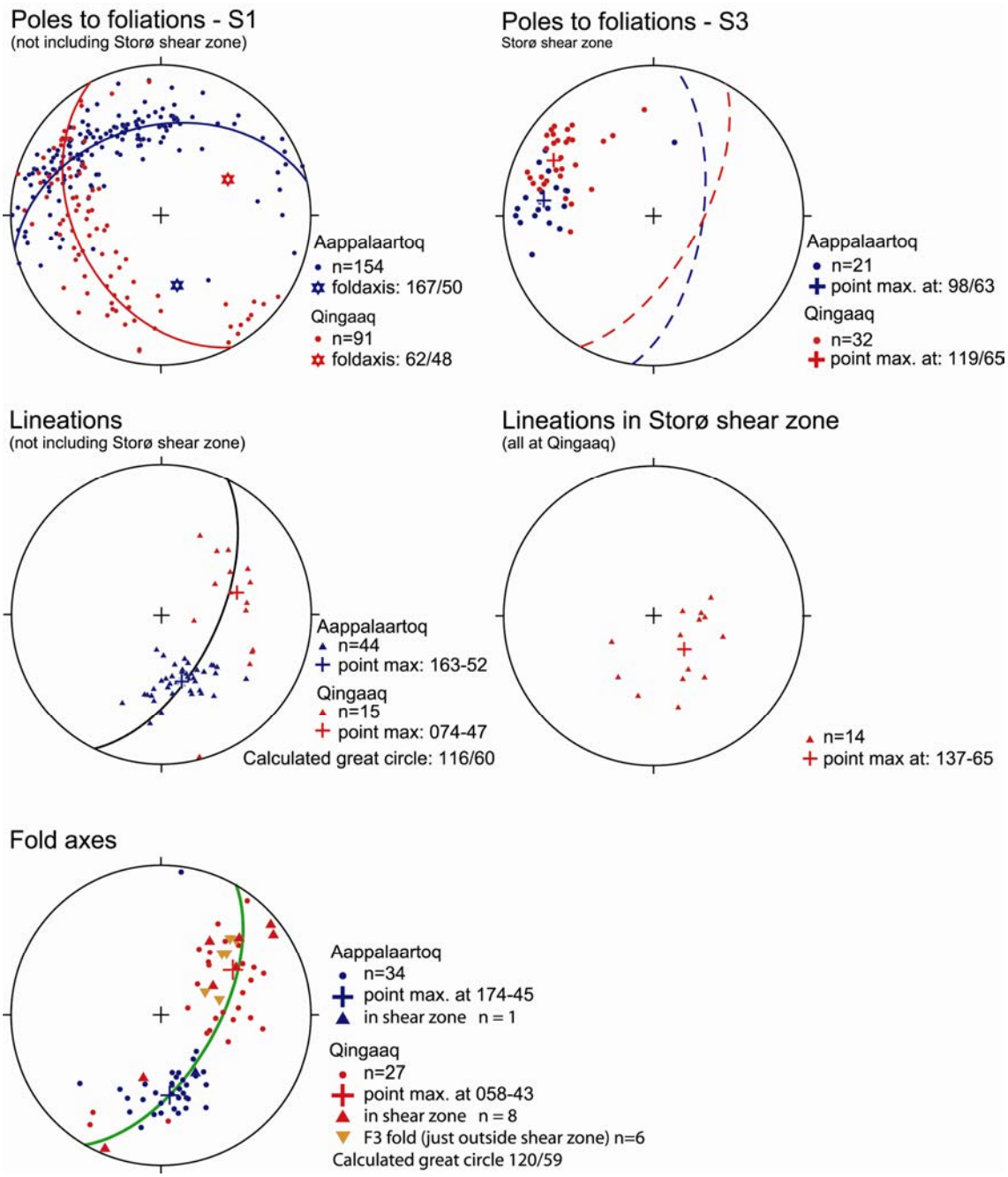

Figure 28. *Stereo plot of structural data from the two map areas on Storø. Data on the right hand side are from the Storø shear zone, on the left side from the remainder of the two map areas. Fold axis orientations in foliation plots and all point maxima are determined from eigen-value calculations. All plots in lower hemisphere, equal area projection.*

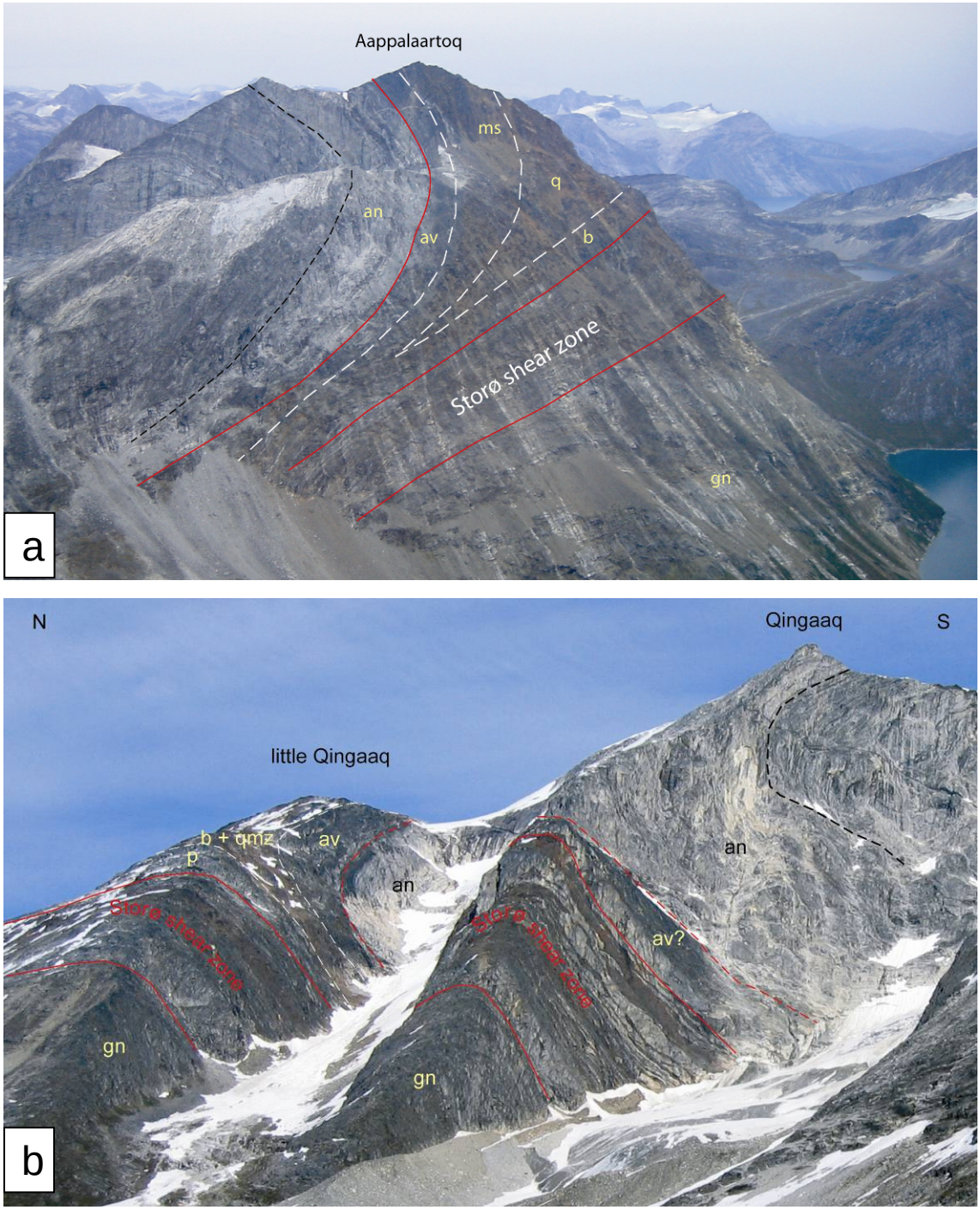

Figure 29. *Anorthosite-cored antiforms at Aappalaartoq and Qingaaq in the hanging wall of the Storø shear zone. The folds are visible both in the contact between anorthosite (an) and the lower banded amphibolite (av), and within the anorthosite. The Storø shear zone boundaries are marked with the red full lines. Rock type codes in yellow as in Fig. 3. a) South-east-plunging antiform at Aappalaartoq. The top of the mountain is 1428 m above sea level. Viewed from the north-north-west. b) North-east plunging antiform at Qingaaq. Viewed from sea level, towards the north-east. The top of Qingaaq (1610 m) is about 1400 m above the scree slopes in the foreground.*

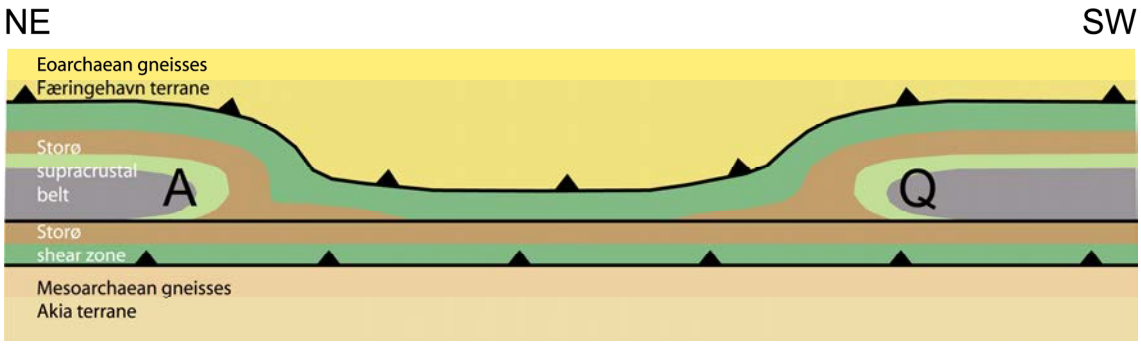

Figure 30. *Schematic cross section along the Storø shear zone at the western side of Storø showing the mirrored antiform-synform pairs at Aappalaartoq (A) and Qingaaq (Q). The section is tilted perpendicular to the shear zone. The two triple points near A and Q are outlined by the biotite gneisses in brown. Legend as in Fig. 1.*

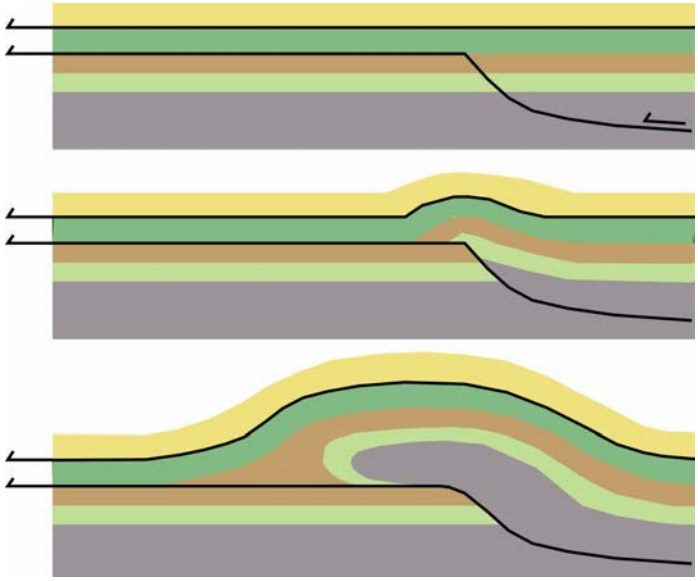

Figure 31. *Schematic model for the development of a hangingwall synform-antiform pair at a hangingwall ramp. This situation may represent a section through either Qingaaq or Aappalaartoq. Legend as in Fig. 1.*

One more item of discussion in this context is how the two mirror image fold pairs at Qingaaq and Aappalaartoq relate to each other. Since some of the gold mineralisation seems to be associated with these fold structures (see discussion below), it is important to evaluate whether they continue in the subsurface and meet, or whether they are two separate structures on either side of a thrust sheet (Fig. 32). Where exposed, the fold structures appear to plunge towards a common point about one km northeast of the lake at Qingaaq. They may form a single continuous structure if they were formed at an oblique/frontal thrust ramp, with hinge lines originating perpendicular to the NW-directed movement direction (Fig. 32a). These fold hinges were subsequently folded during (or after) thrust movement, since they plunge in different orientations at the two mountains. In the alternative solution, the two fold pairs formed at lateral/oblique ramps of the advancing thrust sheet (Fig. 32b) and do not connect in the sub-surface, in which case the similarity of the folds on the two mountains is coincidental. The fact that extension lineations are sub-parallel with the large-

scale fold axes may suggest that these folds originated at lateral ramps, parallel with the movement direction. Extension lineations would be expected at a high angle to the fold axes if the folds originated at a frontal thrust ramp. However, the similarity in shape and location makes it more likely that the folds exposed at the two mountains are part of the same structure. A test of these two hypotheses requires a thorough structural analysis of the area in between the mountains, both in the supracrustal rocks and the overlying orthogneisses.

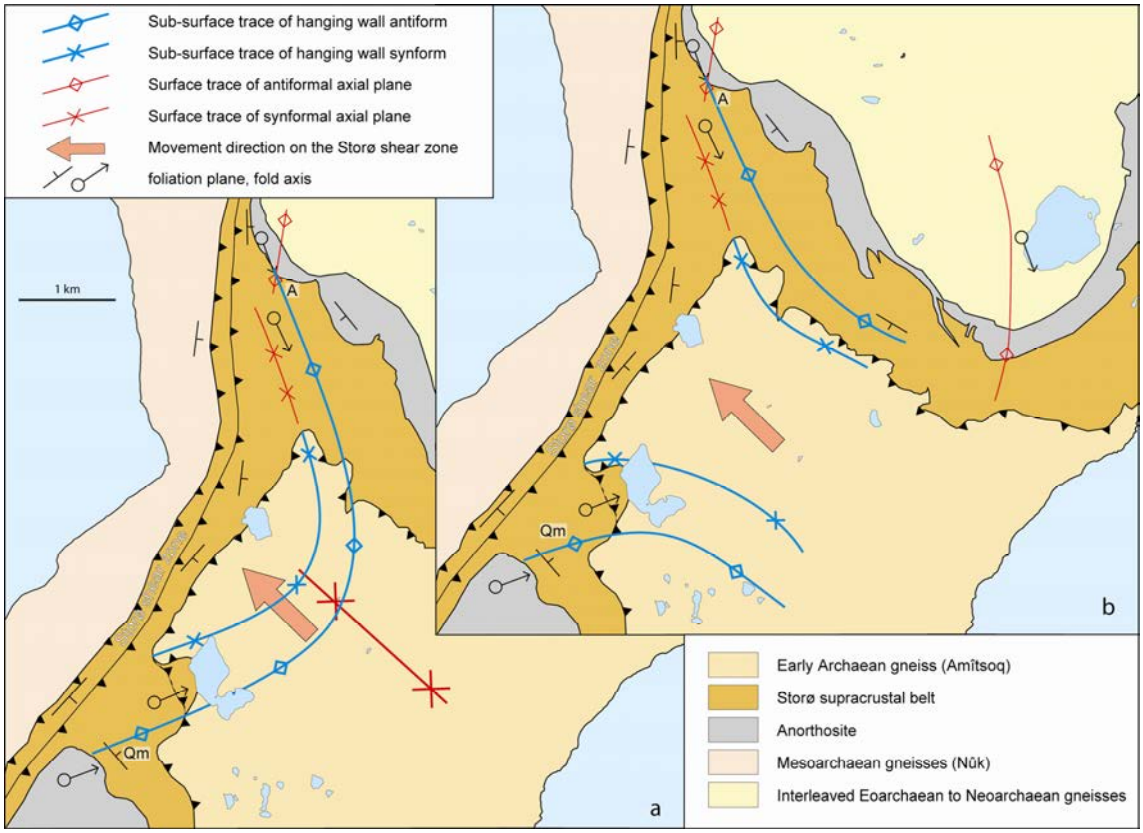

Figure 32. *Two different solutions for the relation between the large fold structures at Qingaaq and Aappalaartoq, showing tentative sub-surface traces of these structures. a) The folds formed at a common frontal ramp and are connected in the sub-surface. b) The folds formed at two lateral ramps and are not connected.*

Storø shear zone

The Storø shear zone is a *c.* 350 m wide shear zone that runs along the western side of northern Storø. It is well defined on the western flanks of Qingaaq and Aappalaartoq mountains (Figs 1, 29, 33, 34). It comprises supracrustal rocks, both mica schists and amphibolites, and abundant pegmatites, the latter predominantly in the amphibolites (Fig. 34). These rocks form straight gneisses with abundant deformed pegmatite remnants (Fig. 35), but clear mylonitic fabrics are scarce. The foliation dips fairly consistently to the south-east, with a *c.* 60° dip angle. However, there is at least 20° variation in the strike of the zone, as expressed by the difference in orientations of the foliation in the shear zone at Qingaaq and Aappalaartoq (Fig. 28). Elongation lineations are weak, and found mostly in the top of the

shear zone, where they plunge predominantly down-dip (Fig. 28). Overall, the strain increases downwards in the shear zone, as expressed in the straightness of the gneisses and the transposition of the pegmatites. Whereas pegmatites in the top of the zone occur both discordant and concordant, near the base all are parallel with the main foliation. Kinematic indicators do not give a clear and consistent indication of the sense of displacement, but antiforms in the hanging wall (exposed on both Qingaaq and Aappalaartoq, Fig. 29), asymmetric folds in footwall pegmatites (Fig. 34) and an asymmetric synform in the footwall (Hollis *et al.* 2004) suggest a thrust movement on the shear zone towards the west. The metamorphic grade in the zone as determined from field observations is similar to that outside the shear zone. The zone truncates structures both in the footwall and the hanging wall (Fig. 29). Both deformed and undeformed pegmatites in the shear zone were dated at *c.* 2630 Ma, which constrains the age of the shear zone (Hollis 2005).

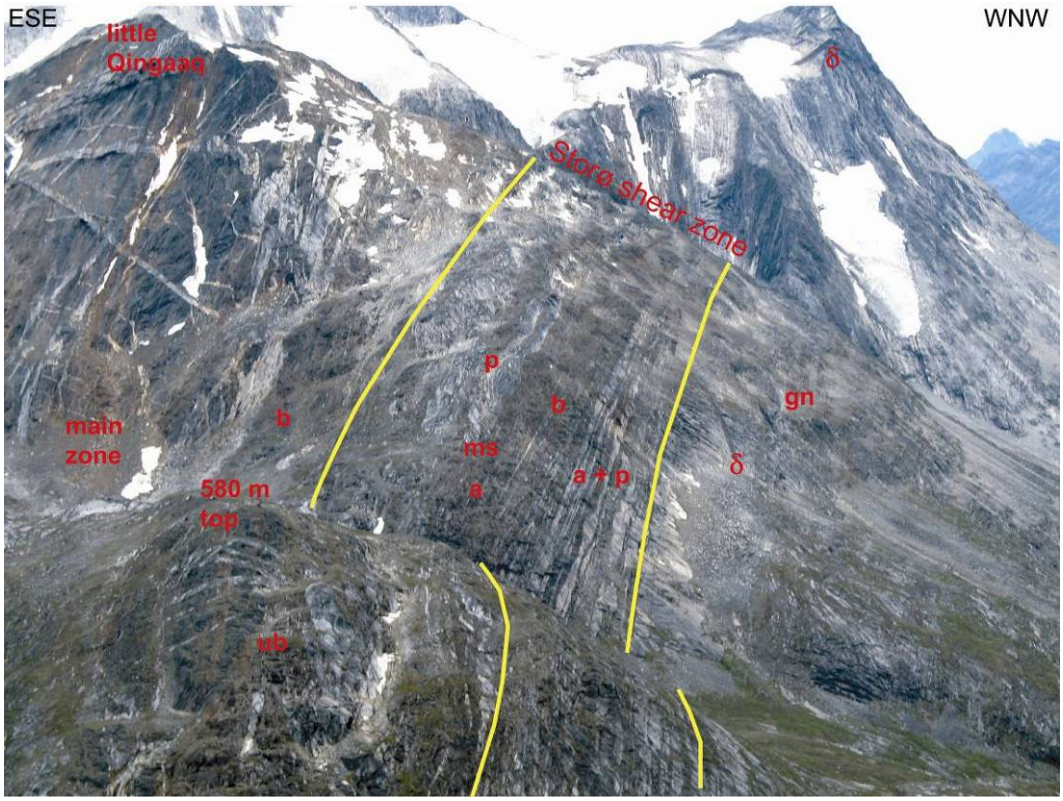

Figure 33. *Storø shear zone on the western slopes of Qingaaq. a=amphibolite, b=(garnet-) biotite gneiss, gn=Mesoarchaean orthogneiss, ms=garnet-biotite-sillimanite mica schist, p=pegmatite, ub=ultrabasic rock, δ=metadolerite. View to the southwest. The top of little Qingaaq is about 500 m above main zone.*

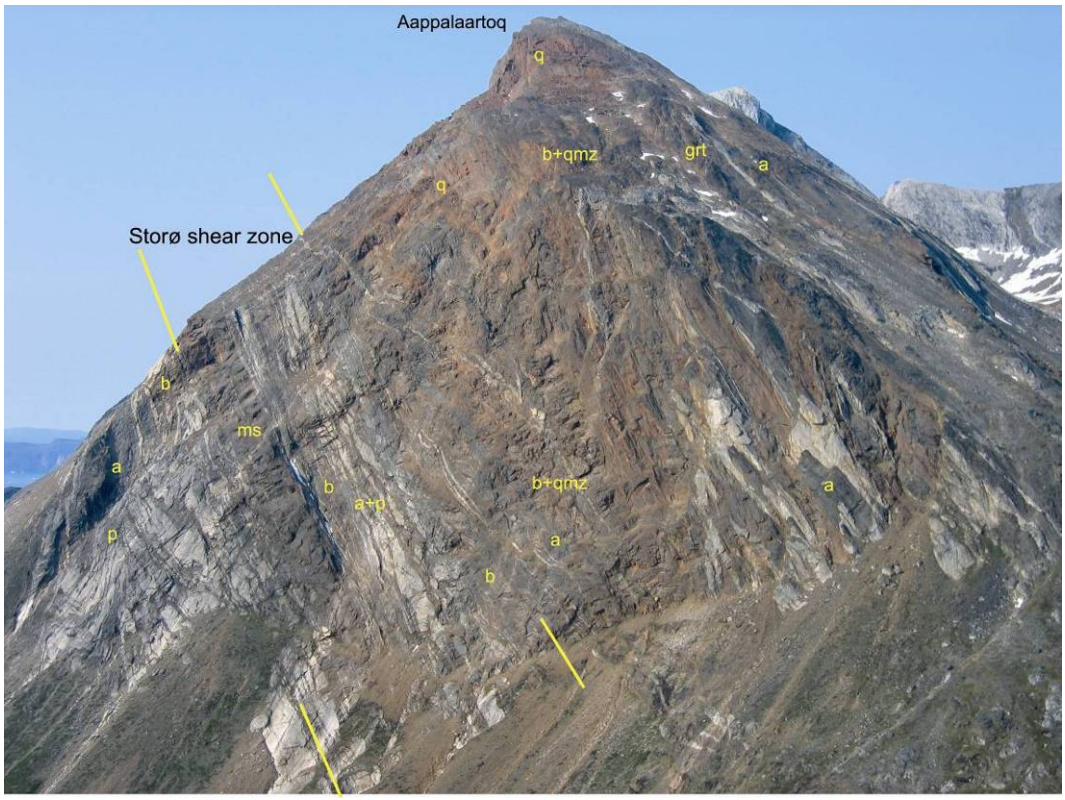

Figure 34. *Aappalaartoq south face with the Storø shear zone. Note the asymmetric footwall folds in the pegmatite in the left side of the photograph. a=amphibolite, b=(garnet-) biotite gneiss, grt=garnet-rich gneiss, ms=garnet-sillimanite mica schist, p=pegmatite, q=quartzite, qmz=quartzitic gneiss View towards the north (from 580 m top). From top of the scree to the top of the steep slope is about 500 m.*

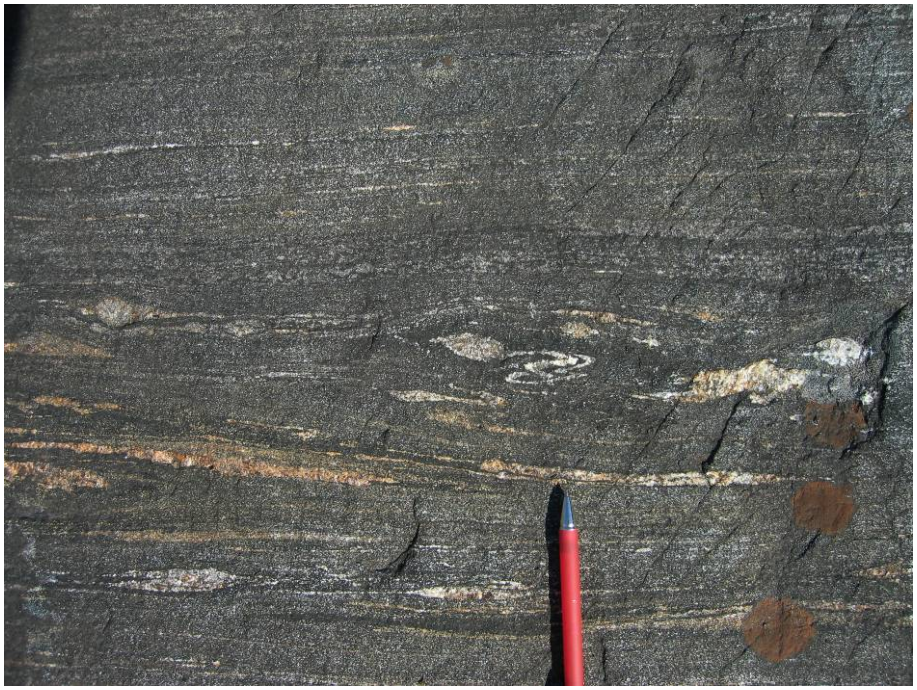

Figure 35. *High-strain fabric in amphibolite in the Storø shear zone. The rock contains intrafolial folds, pegmatite lenses and stringers and has overall a straight fabric. Viewing along the stretching direction. (photo p2004jvg1383)*

Upper (roof) thrust contact of the Storø supracrustal belt

The thrust contact that separates the supracrustal rocks from the overlying Eoarchaean gneisses is poorly exposed in the map area. Where exposed, it is marked by a straight foliation, but mylonitic fabrics have not been observed. Presumably, the position of the contact is also uncertain in several locations, where it separates rocks of the Storø supracrustal belt from amphibolite inclusions in the Eoarchaean orthogneisses. C.L.R. Friend and A.P. Nutman (*pers. com.* 2007) report a recrystallised shear zone fabric in the garnet-biotite gneiss that sits at the contact at the foot of the northern slopes of little Qingaaq (central eastern part of map sheet 5c). They also suggest that intense folding and interleaving of amphibolite and biotite gneisses at schist hill is a result of shearing on this thrust contact. Friend and Nutman (*pers. com.* 2007) propose that the main thrust contact between Eo- and Neoarchaean rocks is located at the top of schist hill (Fig. 4), and that the amphibolites and biotite gneisses on schist hill are part of an inclusion of supracrustal rocks in the Eoarchaean orthogneisses. The observation that the intense folding and fold interference on schist hill is not seen in the northern slopes of Qingaaq minor is in accord with a major structural break at the top of schist hill.
The roof thrust of the supracrustal belt is folded together with the large-scale F3 folds (which are largely contemporaneous with the Storø shear zone) and must therefore predate the Storø shear zone.

Mesoscopic structures – main deformation phases

Three main phases of deformation were recognised from overprinting structures in the supracrustal sequence. The Eoarchaean orthogneisses contain structures that predate those of the Neoarchaean supracrustal rocks, but these are not addressed here.

D1 – main foliation development

The oldest structure in the supracrustal rocks is the regionally dominant foliation S1. It is defined mainly by biotite, hornblende, and oblate quartz and feldspar. This foliation is present in most rocks, but variable in intensity in the different rock types. Generally the most mica-rich rock types are best foliated, but some of the intermediate composition gneisses with moderate biotite (map unit **b**) are poorly foliated, in spite of their elevated mica contents. S1 foliation is overgrown by garnets and thus predates peak metamorphism (Figs 13, 15). An extension lineation occurs on many S1 foliation planes, but is likely younger than the foliation (see below). Rare examples were found of isoclinal folds with S1 as axial planar cleavage. These folds are most obvious where a marker is folded, e.g. in quartz veins or the layers of garnet-magnetite rock. Large scale F1 folds occur on the southern slopes of Aappalaartoq, where they isoclinally fold and repeat the garnet-biotite gneiss and quartzitic gneiss.
In the lower part of the supracrustal sequence, in the layered amphibolites (**av**) above the anorthosite, the foliation is quite intense (Fig. 7), which may be the result of shearing along the contact between the anorthosite and structurally overlying amphibolites. Kinematic indicators are rare and not consistent. Part of these structures may actually predate the S1,

since the banded amphibolites are *c.* 250 Ma older than the overlying biotite gneisses and amphibolites, and may have undergone earlier deformation.

D2 early folding

Tight folds deform the S1 foliation in F2 folds (Fig. 36). Axial planes are overall sub-parallel with the S1 foliation, and a slight predominance of a west vergent asymmetry was noted, but all types of asymmetry occur. A weak axial planar fabric is common in the mica-rich rock types, but absent in the amphibolites. Outcrop scale F2 folds occur throughout the map areas, but are most intense west and southwest of the top of little Qingaaq where they are asymmetric, west-vergent and plunge to the east. The banded amphibolites in the lower part of the tectono-stratigraphic sequence show similar, but smaller, asymmetric folds in the same orientation, which are likely also F2 folds (Fig. 37). Also the folds in the ultramafic rocks on the ridge east of Aappalaartoq are F2. Fold axes are overall parallel with F3 hinges, and where clear overprinting criteria are lacking, the two cannot be distinguished.

Figure 36. *F2-F3 fold interference in the hanging wall of the Storø shear zone. Interlayered quartzitic gneiss and biotite gneiss. The red dashed line indicates the axial plane of the F2 folds, refolded in F3. (photo p2006jvg0440)*

Figure 37. *Asymmetric, west vergent F2 fold in banded amphibolites at Qingaaq. (photo p2006jvg0329)*

D3 Storø shear zone and large-scale folds

A new foliation formed in the Storø shear zone and the S1 foliation + F2 fold axes are refolded (Fig. 36). Approaching the shear zone from the hanging wall, F3 folds get progressively tighter and more abundant, while an axial planar cleavage (virtually absent outside the shear zone proper) increases in strength into the shear zone. Within the shear zone all older structures are transposed and the older foliation is only recognisable in D3 low strain domains (e.g. F3 fold hinges). Generally, the folds in the shear zone are isoclinal, rootless folds.

The maps and stereographic plots (Figs. 1, 28) show that the S1 is folded in SSE-plunging folds on Aappalaartoq, and in ENE-plunging folds at Qingaaq. Poles to the S1 foliation planes have a great-circle distribution in stereo plots in both areas. Fold axis orientations derived from these great circles coincide fairly well with the measured fold axes in the area (Fig. 28). There is also a tight fit between lineations and fold axes in the two map areas, suggesting a genetic link between the two. Fold axes and lineations all lie in a great circle dipping *c.* 120/60 (dip direction/dip) which is approximately the orientation of the Storø shear zone at Qingaaq, and close to the orientation of the Storø shear zone at Aappalaartoq.

The two anorthosite-cored antiforms at Aappalaartoq and Qingaaq both are hanging wall antiforms above the Storø shear zone, as discussed above. Their direct relationship to the shear zone implies that these are F3 structures. Similarly both mountains contain an F3 synform of the same magnitude, which is evident on the Aappalaartoq map, but less obvious on the Qingaaq map, where it is outlined by the lower contact of the upper amphibolite. The antiform exposed on the north face of little Qingaaq (Fig. 4), is here named the **main zone antiform**. It is a ENE-plunging fold, inclined to the east, with a steep western limb and

an eastern limb that dips 40–60° north-east. It is presumably continuous with the tight antiform in the lower contact of the upper amphibolite, *c.* 250 m NNW of the top of little Qingaaq, but this is difficult to confirm, because the central part of the slope is difficult to access. The hinge of the antiform changes from an open, rounded structure at the foot of the slope, to an angular, very tight fold at the base of the amphibolites near the top of the slope, and again to a more open rounded structure with abundant parasitic folds when approaching the anorthosite. The part of the fold that is exposed on the lower reaches of the slope is cut by several pegmatites. The youngest pegmatites (*c.* 2550 Ma, Nutman *et al.* 2007) are straight walled and undeformed, while the ones dated at *c.* 2630 Ma show pinch and swell geometry, but are not folded themselves. Other pegmatites in the upper western part of the slope are intensely deformed in the antiform and the Storø shear zone to the west. The western limb of the main zone antiform is significantly thinner than the eastern, and possibly truncated/offset by the Qingaaq shear zone (Qingat shear of D. Coller, ERA-Maptec 1995; Fig. 4). This shear zone is well exposed at the foot of the slope, west of the garnet biotite gneiss in the western limb. Higher up the slope it is difficult to trace in between the pegmatites and it is not continuing into the biotite gneisses on the northwestern slopes. Kinematic indicators are sparse and not always consistent but seem to indicate an oblique west side up movement, antithetic to the Storø shear zone.

Extension lineations (mineral lineations, aggregate aggregations and quartz rods) are very intense around the hinge of main zone antiform and are parallel with the F3 fold axes throughout the area (Fig. 28).

The association of the F3 folds with the shear zone, and the intrusion of a generation of pegmatites implies that the F3 folding occurred at *c.* 2630 Ma.

Structural control on the gold mineralisation?

There is no direct evidence that the gold mineralisation on Storø is structurally controlled. And it is likely that a first phase of mineralisation occurred during an early alteration event, potentially syn-genetically. Altered layers are isoclinally folded by D1 and deformed in zones with D1 deformation only, and the mineral assemblages in the alteration zones are metamorphic. Mineralisation of the BD zone is linked to the lithological contact between the garnet-rich gneiss – an intensely altered rock type (see geochemical section) - and the upper amphibolite. But in detail, the gold concentrations in the BD zone are highest around quartz veins that can be located several metres away from this contact. These veins predate the main foliation and are transposed, but locally their original geometry as a vein network can still be recognised (Fig. 38). The amphibolites in the immediate surroundings of the veins commonly show signs of alteration and contain garnet and biotite.

On the other hand, it is clear that the main gold prospects on Storø are located at fold hinges on both Aappalaartoq and Qingaaq, in the hanging wall of the Storø shear zone, and that many of the gold mineralisations occur in or near quartz veins. It is also important to emphasise that the structural setting of the two prospects (Qingaaq and Aappalaartoq) are virtually identical, although mirror images of each other, which makes it more likely that the structural setting plays an important role. Especially at Qingaaq, the highest gold concentrations of Main Zone occur in an F3 antiformal hinge. It is also clear, that somewhat elevated gold values occur in a large part of the Storø supracrustal belt (see various

NunaMinerals and NunaOil company reports), i.e. gold mineralisation is not restricted to the two mountains.

Figure 38. *Quartz vein system in amphibolite at the mineralised contact of the BD zone. (photo p2006jvg0288)*

Main Zone mineralisation occurs mainly in discontinuous zones, 5–10 m wide, that can be traced for tens of metres, most - but not all – marked by quartz veining and garnet-biotite assemblages in amphibolite. Some also occur within garnet calc-silicate gneisses. These discontinuous zones are most likely of a shape in between the two end members: 1) oblate and parallel with the axial plane of the F3 antiform, dipping steeply to the southeast, and 2) prolate and parallel with the F3 fold hinge, plunging *c.* 45° to 060°.
The preferred model for the gold mineralisation involves a first phase of mineralisation that predates early deformation and metamorphism, and a second phase of remobilisation and concentration of the gold that was originally present in the supracrustal belt. During D3 deformation at high grade metamorphism pathways were opened for fluids to concentrate the gold in the areas of largest dilation, near the F3 fold hinges. Potentially, the Storø shear zone might also have played a role in fluid transport over larger distances, but it may not have been necessary to transport over large distances, remobilisation of gold can have been restricted to the layers that were originally enriched. In this model, the mineralisation is not directly shear zone related (at least part of the gold in the area predated the shearing), but was remobilised in fold hinges in the hanging wall of the shear zone, during movement of the shear zone. This model is in accordance with petrographic observations and the Re-Os data reported below.

Petrography

Thirty eight thin sections were studied with the purpose of lithological descriptions, investigating the metamorphic grade, microstructures and occurrence of gold mineralisation. All rock types were sampled, and therefore only few samples of each rock type were available. All sections were studied by polarising light microscope, while 8 sections of sulphide mineralised or strongly altered rocks were imaged by scanning electron microscope (SEM), of which three were gold bearing. Brief petrographic descriptions of the samples are given in Appendix 1, as well as a selection of backscattered electron SEM images of samples from main zone. Similar studies were carried out previously (Pedersen 1996: Eilu *et al.* 2006, Juul Pedersen 2006; Juul Pedersen *et al.* 2007) and apart from a brief overview, only new results are reported.

Metamorphism

Metamorphic grade on Storø is amphibolite facies. Sillimanite is the dominant aluminosilicate and incipient melt veins occur locally in the mica-rich gneisses, suggesting peak metamorphic conditions at intermediate pressures and intermediate to high temperatures. P-T estimates of garnet-bearing thermo-barometric assemblages in both aluminous gneisses and intermediate composition amphibolites vary from 521–624°C and 4.5–6.1 kbar (Hollis & Persson 2005; Persson 2007). Indications exist that the region has undergone a complex metamorphic history (see also geochronology section). Zoned garnets (Fig. 39) occur commonly in the aluminous gneisses and suggest garnet has grown under changing conditions or during different events. Plagioclase rims around garnets in amphibolite and rocks of intermediate compositions are also common and might indicate a phase of decompression after garnet growth (Fig. 15). Amphibolites and biotite-rich rocks show commonly equilibrium textures, even in zones of high strain. This is a clear sign that the rocks have undergone a phase of static recrystallisation after deformation. Sericitisation and epidotisation occur on microscopic scale in areas of local retrogression, commonly associated with relatively late quartz veins.

Figure 39. *Zoned garnets in an aluminous biotite gneiss. The light core and dark rim in the left grain correspond to an inclusion-rich core and an inclusion-free rim observed in thin section.*

Garnet-diopside veins and garnet calc-silicate gneiss are common within the upper amphibolite. They are assumed to be metamorphosed alteration products of the amphibolite, or in few cases potentially alteration of a more felsic (leuco-) amphibolite. Generally, the calc-silicate veins within the upper amphibolite sequence are assumed to be early features associated with spillitisation of the rocks (Eilu *et al.* 2005) which were subsequently metamorphosed. Polat (2005) reported that some of the calc silicate veins cut the main foliation and textures were associated with retrograde metamorphism.
New field observations confirm that both early, isoclinally folded calc-silicate veins, and late transcurrent vein systems occur. Petrographic observations show that disequilibria textures after metamorphic reactions occur in some of these veins, postdating the prograde metamorphism in the host amphibolite. At the margins of one of the investigated veins, host-rock hornblende is partially replaced by clino-pyroxene, a prograde dehydration reaction. One of the garnet calc-silicate rocks shows several co-existing phases of clino-pyroxene and hornblende (Fig. 40). In another late quartz-garnet-calcic amphibole-epidote vein, garnet and epidote/zoisite have grown late and form large clusters of small crystals (Fig. 16). This vein truncates the metamorphic fabric and is not deformed itself, in spite of the fact that it sits on the limb of the F3 fold in main zone, where strain is rather high. This means that a late phase of garnet growth occurred, and that reports of timing of mineralisation with respect to garnet, must be scrutinised carefully, to determine if this is early or late garnet growth. Clearly, the metamorphic history of the different veins is rather complex, and requires a much more systematic study than what has been possible in this study. This can be especially important, because some of the vein systems may have been an important factor in the remobilisation of gold.

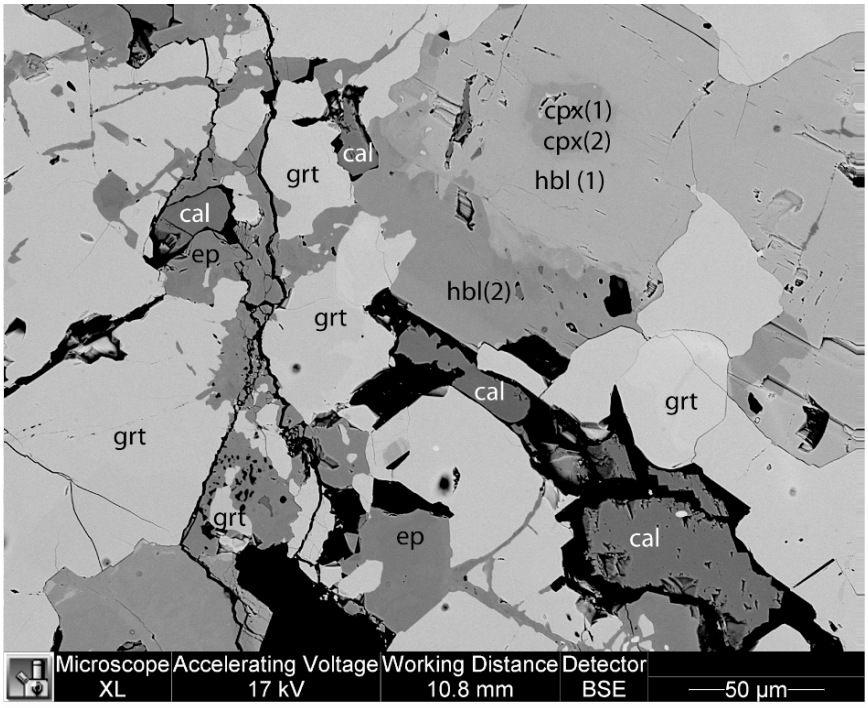

Figure 40. *Backscatter SEM image of a garnet calc-silicate rock containing two phases of hornblende and clinopyroxene. A core of diopside (cpx1) is replaced by a less calcic pyroxene (cpx2) and hornblende (hbl1), which forms rims on the less Fe-rich hornblende (hbl2). Besides garnet (grt) and epidote (ep) the rock also contains calcite (cal). The latter two occur commonly in fractures. Plagioclase (not visible in image) is common in the matrix.*

With respect to the metamorphism in the garnet-rich gneiss, it must be emphasized that, although this is an altered rock that has an affinity with the amphibolites (Knudsen *et al*. 2007; see also geochemistry section), the mineralogy of this rock is similar to that of an ordinary pelitic rock, with the exception of the low abundance of quartz. Garnet, sillimanite biotite appear to form a stable assemblage. Remnants of staurolite occur and are especially abundant as inclusions in garnet. Garnet zonation patterns resemble ordinary growth zoning in pelitic garnets (Persson 2007), suggesting that the changes in composition occurred prior to garnet growth, potentially prior to the start of prograde metamorphism.
The presence of unstable remnants of staurolite indicates that during peak metamorphism the staurolite breakdown reaction (to form garnet, biotite and alumino-silicate) was surpassed, which in the sillimanite field of P-T space lies at 600–700°C.

Relative timing of mineralisation

Petrographic investigations of gold-bearing rocks by Juul-Pedersen *et al.* (2007) showed that gold occurred mainly in assemblages with lollingite, arsenopyrite and pyrrhotite as well as inclusions in garnet, in quartz veins, and in sericitised plagioclase. In their preferred model for mineralisation, gold was included in early arsenopyrite, which during prograde metamorphism recrystallised to lollingite and pyrrhotite. During retrograde metamorphism lollingite broke down to form arsenopyrite, which cannot contain gold in its crystal lattice in the same way as lollingite, and gold precipitated on the grain boundaries, and was preserved as inclusions in arsenopyrite.
The present study involved only petrographic investigations of samples from Main Zone. Some of the microstructural relations reported by Juul-Pedersen *et al.* (2007) could be confirmed. Lollingite occurs predominantly as inclusions in arsenopyrite (Fig. 41). Arsenopyrite occurs in two different generations: 1) as deformed or recrystallised irregular grains, or as inclusions in garnet and is presumably older than the metamorphic peak, and 2) as euhedral grains that overgrow the matrix. Chalcopyrite occurs predominantly as inclusions in pyrrhotite. Pyrrhotite is anhedral, often filling interstitial spaces between hornblende grains (Fig. 42). In few samples pyrrhotite has rims of pyrite, suggesting a retrograde pyrite growth. These observations confirm that both early and late arsenopyrite exists, and that the latest generation of arsenopyrite is likely post deformation and major recrystallisation/metamorphism.

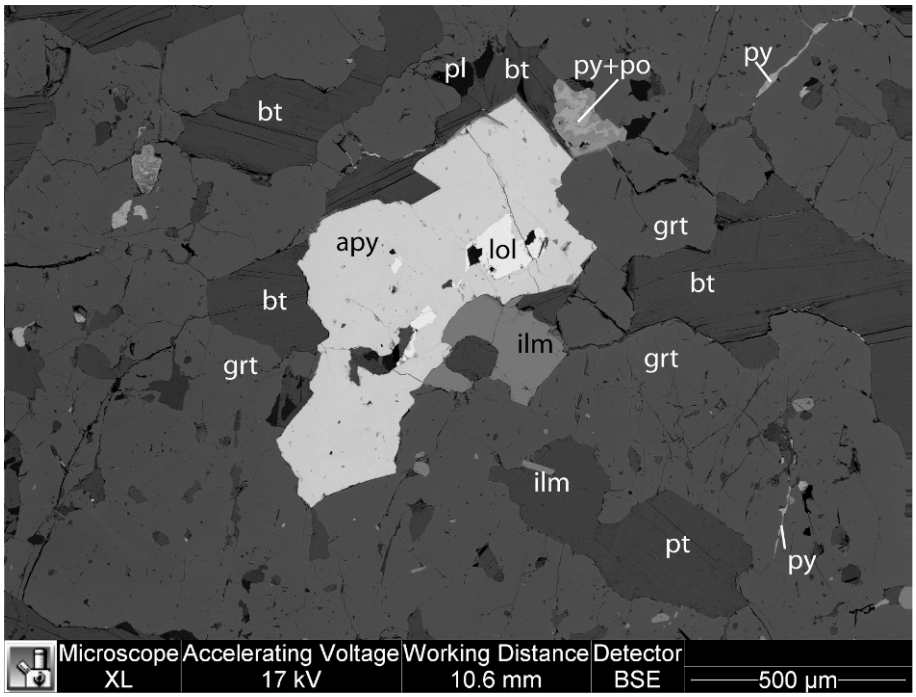

Figure 41. *SEM backscatter electron image of a large garnet grain (grt, filling the whole image) with abundant inclusions. The arsenopyrite (apy), has itself inclusions of lollingite (lol), that again include minute Bi-tellurides. Biotite (bt) is the most abundant included phase. Fractures in the garnet are filled with pyrite (py). ilm = ilmenite, po = pyrrhotite. (sample 487424)*

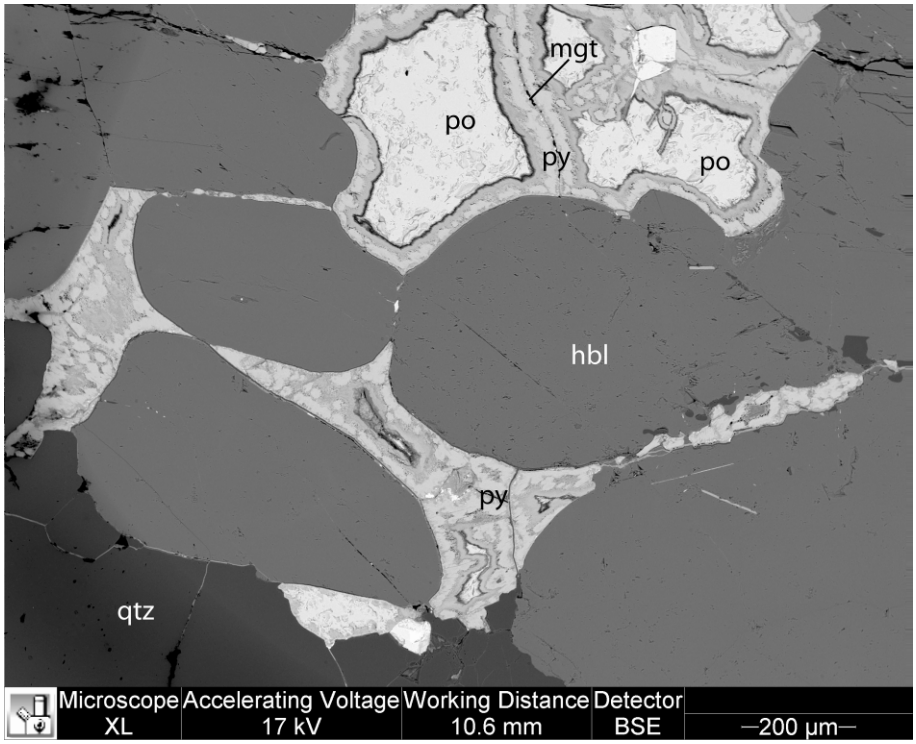

Figure 42. SEM backscatter electron image of a mineralised amphibolite. Pyrrhotite (po) is partially replaced by pyrite (py), which sits interstitially in between hornblende grains. At the bottom is a quartz vein (qtz). Note that the sulphides protrude into the vein. hbl = hornblende, mgt = magnetite. (sample 487424)

In the samples from Main Zone gold was encountered as inclusions in arsenopyrite (Fig. 43), which also contained lollingite inclusions, and in sericitised and epidotised plagioclase (Fig. 44). Epidote was found in the same sample as symplectite with quartz, on the grain boundary between plagioclase and hornblende, indicating that this is a retrograde reaction. Commonly, the gold-bearing amphibolites were altered and now contain garnet and amphibolite. or are intensely quartz veined. One of the investigated gold bearing samples showed intense calc-silicate alteration.

Assuming that the gold was in the system at an early stage, within prograde arsenopyrite and as inclusions in garnet, the gold associated with sericitisation and epidote shows that some of it is quite late, after peak metamorphism. It is uncertain whether this late gold was added to the system at a late stage, or whether it is a remobilisation of the gold that was already present. Present observation cannot determine the extent of such a remobilisation, whether it occurred on microscopic scale or kilometre-scale.

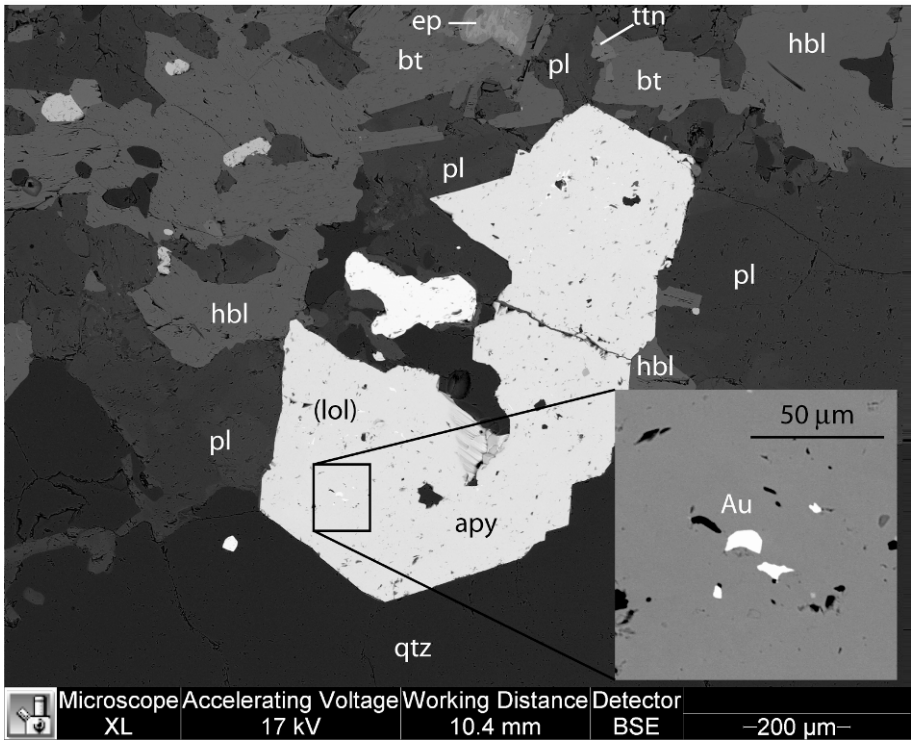

Figure 43. *Arsenopyrite (apy) with 5-10 µ gold grains and lollingite (lol) inclusions in a biotite-amphibole-plagioclase matrix. The arsenopyrite grain sits at the margin of a quartz (qtz) vein at the bottom of the image. (Sample 487425)*

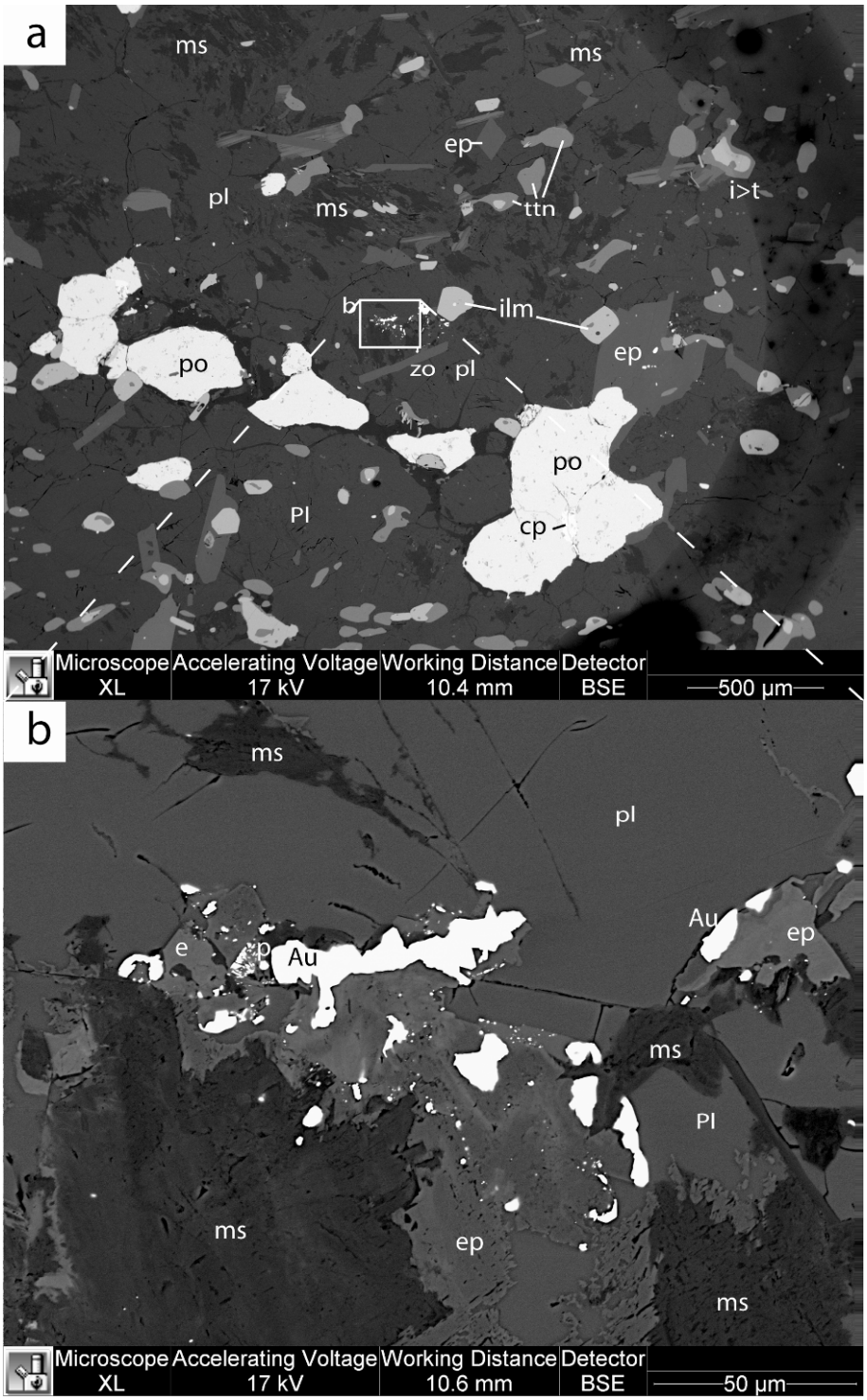

Figure 44. *Gold in a plagioclase-rich calc-silicate gneiss with pyrrhotite (po), epidote (ep), ilmenite (ilm) and titanite (ttn) in the matrix. Pyrrhotite contains chalcopyrite (cp) inclusions. Plagioclase (pl) is partially sericitised (ms) and epidotised. a. overview, b. close up of the area indicated in the middle of a. The gold grains are surrounded by heterogeneously zoned epidote. (sample 487429)*

Geochronology

A large number of samples was collected in the field for geochemistry and/or geochronology. Out of these samples, seven were suitable for zircon U-Pb age determinations. Two additional samples were collected in 2007 and dated subsequently. Four samples are of the upper part of the supracrustal sequence at the Qingaaq prospect, one is from the lower amphibolites of this sequence, three are from Aappalaartoq, one is an orthogneiss collected close to base camp on Storø. An original selection included three samples from Bjørneøen, as well as two more leucocratic amphibolites on Qingaaq, but mineral separates of none of these samples were suitable for analyses at the GEUS laboratory, because of the small size of the zircons. The analytical methods and data tables are presented in Appendix 2 and 3 respectively. Fig. 45 shows the sample locations of the nine analysed rocks.

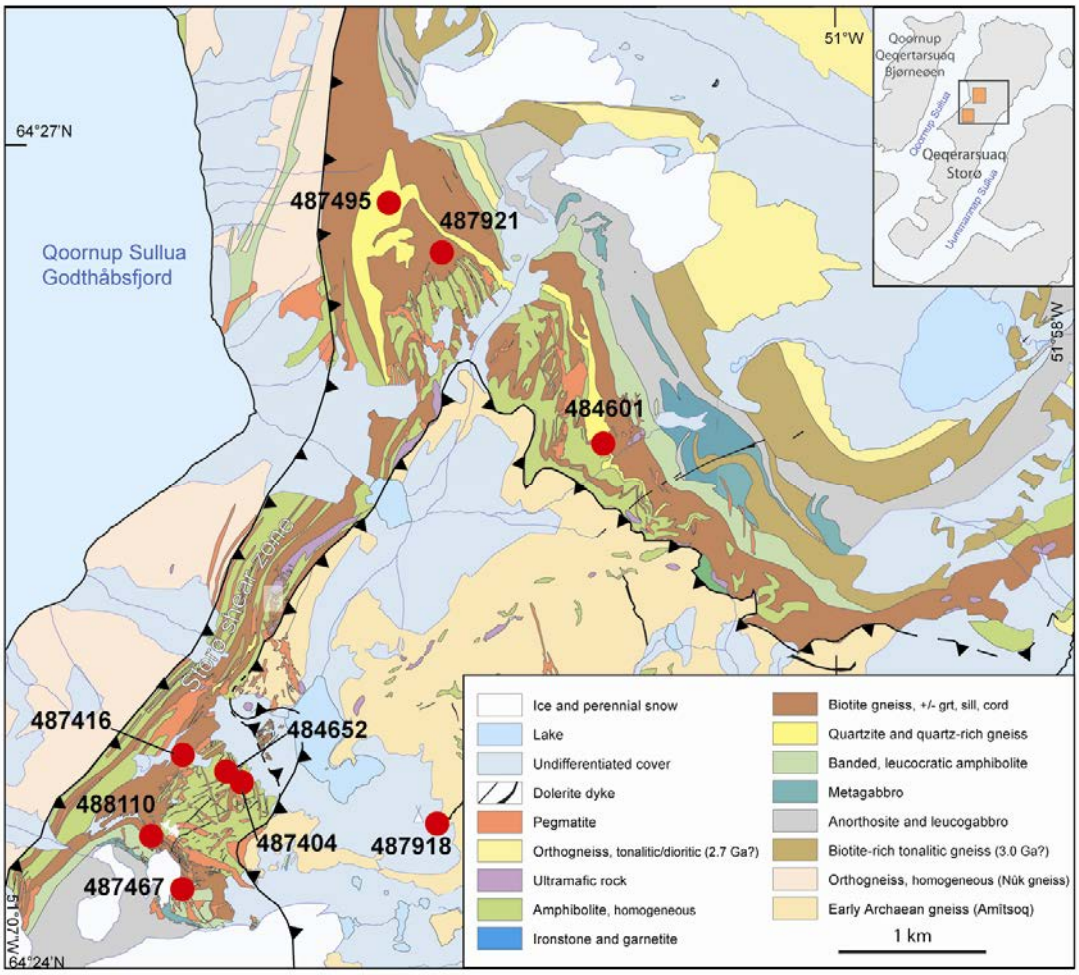

Figure 45. *Geochronology sample location map.*

Sample description and analytical results

Each of the analysed samples is described below. The zircons were separated and mounted in epoxy. They were imaged by SEM (BSE), and some representative examples of zircon grains are shown from each sample, together with the analytical results. Many of the original analyses were rejected as a result of a technical problem during the analyses. The sample stage moved slightly between the pre-programming of the points and actual analyses. As a result, and because many of the grains were rather small, a relatively large number of the points ended on rims, cracks or outside the grains. Where the resulting useable analyses were too few to give a meaningful result, the sample was re-analysed.

samples from the supracrustal sequence

Sample 484601

Fuchsite quartzite from the main quartzite sequence on Aappalaartoq, collected in 2007 100m east of the Aappalaartoq map sheet. This is a red-brown weathering, medium-grained, muscovite-sillimanite-fuchsite-bearing quartzite. It is well foliated and overall homogeneous. This is likely a clastic rock, collected for detrital zircon ages and can give a maximum depositional age, as well as a metamorphic age. This rock is part of the same tectono-stratigraphic level as sample 487495.

Zircon is brownish with a dull appearance in an ordinary light microscope; the grains have angular surfaces and a round to prismatic morphology (Fig. 46). The grains range in size from 100-250 µm. Many grains have oscillatory zoned cores and thin, homogeneous, bright rims. Most >3400 Ma grains have homogeneous to patchy zoned cores. The bright rims are equally present in zircons of different age.

Only grain cores were analysed in 45 grains (45 analyses) in order to focus on the detrital populations. The data span a wide range of ages, and several age groupings could be recognised, ranging in age between *c.* 2800 Ma and *c.* 3400 Ma (Fig. 47). Two main peaks in the probability density diagram have dates at respectively *c.* 2847 Ma and 2905 Ma (Fig. 48). Four smaller peaks occur at 3017 Ma, 3050 Ma, 3126 Ma and 3428 Ma, while individual grains have ages between *c.* 3177 Ma and 36237 Ma. Based on the quartz-rich nature of the rock type, and the range of ages in this quartzitic rock we assume this is indeed a metasedimentary rock, whereas the almost constant range of ages is assumed to reflect several detrital populations, which have undergone one or more phases of lead loss, and were deposited no earlier than *c.* 2840 Ma, the age of the youngest population.

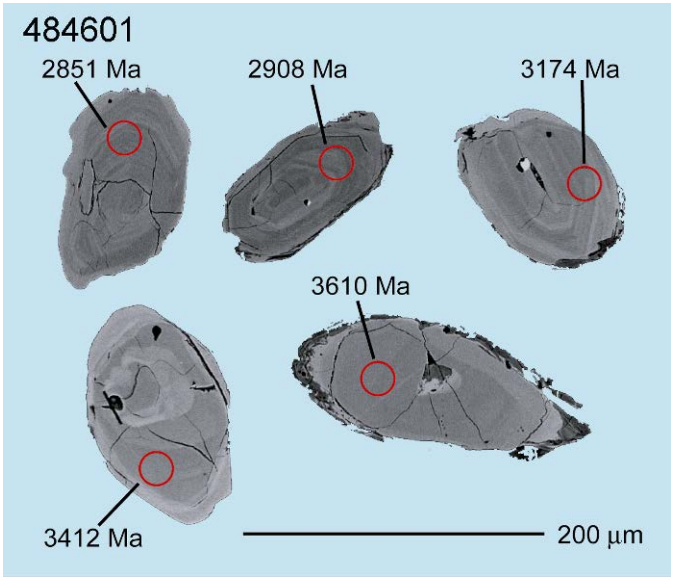

Figure 46…*SEM image of a selection of the zircon populations in sample 484601 with $^{207}Pb/^{206}Pb$ ages. These grains have well-preserved oscillatory zoning. Thin homogeneous (metamorphic) rims are common.*

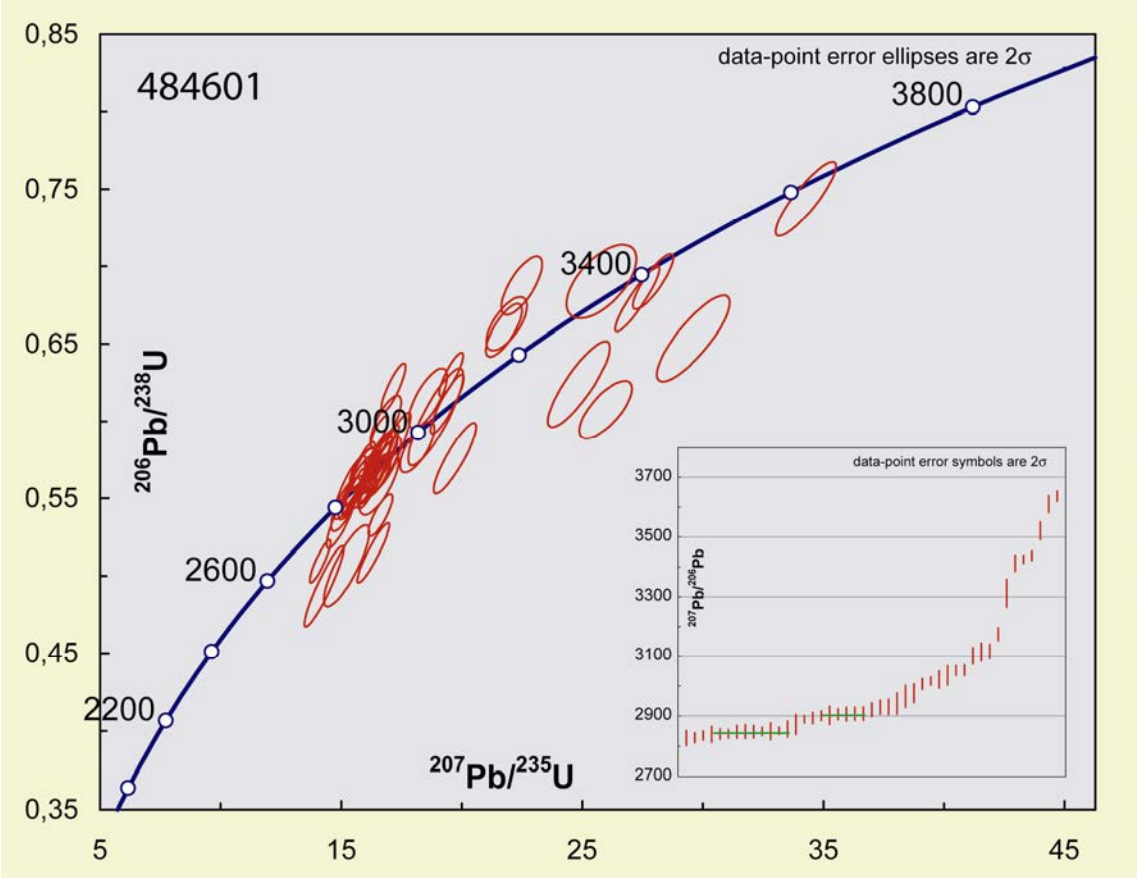

Figure 47. *Concordia diagram of sample 484601, including $^{207}Pb/^{206}Pb$ ages in the inset. The sample contains several zircon populations between 3400 and 2800 Ma.*

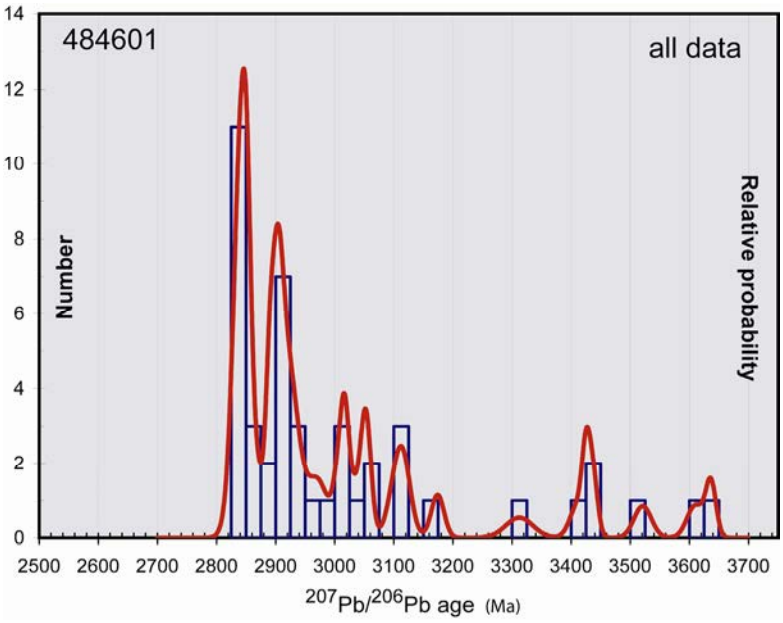

Figure 48. *Probability density diagram for sample 484601, showing a large number of peaks between 2847 Ma and 3637 Ma.*

Sample 484652

Volcaniclastic amphibolite from above main zone. This is a low-strain amphibolite (mafic to intermediate matrix) that contains slightly elongate intermediate to felsic clasts, up to *c.* 5 cm long, with fiamme textures (Fig. 18). This is a rock with a more felsic composition than the main amphibolites and is more likely to contain zircon yielding an igneous age.

Zircons have a pink pearly lustre in reflected light, and range in size from 50–100 μm (Fig. 49). Most grains are irregular, round to oblate, some with vague crystal faces. The grains have a homogeneous to patchy zoned internal texture, rarely with a vague concentric-cyclic zoning pattern, which usually is disturbed. No obvious core-rim relations were recognised.

Twenty six analyses were carried out in 26 grains. Regression of a concordia diagram shows a single population which has an upper intercept of 2632 ± 14 Ma, and an effective zero age lower intercept (Fig. 50). Therefore we assume only recent lead loss, and use the more precise $P^{207}Pb/^{206}Pb$ age of 2633 ± 5 Ma as the representative age for this rock. This age is interpreted as a metamorphic age. It may result from new growth of zircon during the recrystallisation of the original pyroxene to hornblende, in which case this metamorphic event would be the first phase of metamorphism affecting these rocks. The vague oscillatory zoning seen in a few of the grains might suggest that zircon grains existed prior to metamorphism, but lead loss resulted in a complete resetting of the isotope system.

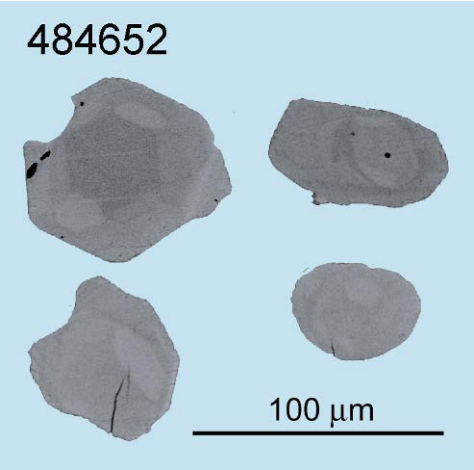

Figure 49. *SEM image of a selection of the zircon populations in sample 484652. Most grains are irregular, some with vague crystal faces. Most grains are internally zoned in an irregular pattern. Rarely, a concentric cyclic pattern can be recognised, but commonly with disturbances. No age connotation is given, since all grains give a similar metamorphic age.*

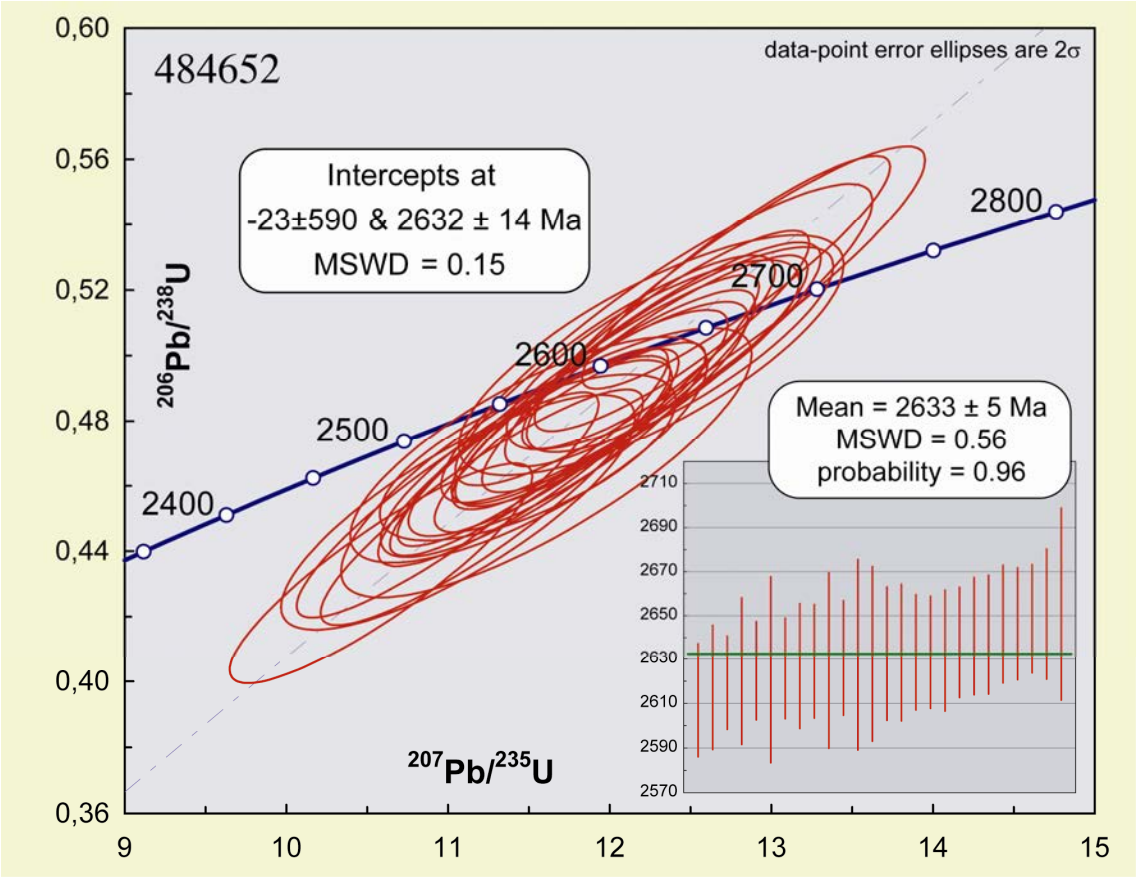

Figure 50. *Concordia diagram of sample 484652 showing a single zircon age population of 2632 ± 14 Ma, which is virtually identical to the average $^{207}Pb/^{206}Pb$ age.*

Sample 487404

Grt-bt gneiss collected in the *c.* 50m wide biotite gneiss layer within the amphibolites east of main zone, named the upper gneiss zone in the terminology of NunaMinerals. This is a coarse-grained grt-bt gneiss with large felsic blebs and <1% sillimanite (Fig. 10). Field observations suggest that this could well be true metasedimentary rock. The felsic blebs could be small initial local melt pockets. The sample was collected to investigate the provenance of the rock. Several zircon grains are visible in thin section, but they are small. The heavy mineral separate includes abundant sulphides.

Zircon is fine-grained (10–70 μm), elongate to prismatic and slightly rounded, also with irregular shapes (Fig. 51). Most grains are homogeneous, with few grains that are darker and slightly heterogeneous, in some cases with a lighter rim. Some grains have a metamict core.

Of all the analysed grains, only the homogeneous ones yielded meaningful data. The data show a spread of ages of over 100 my and do not yield a concordia age (Fig. 52). The probability density diagram shows that the $^{207}Pb/^{206}Pb$ ages have a peak at *c.* 2580 Ma (Fig. 53). The homogeneous character of the grains suggest that these are metamorphic zircons, which is confirmed by the age, which is overlapping with the metamorphism resulting from the intrusion of the Qôrqut granite (cf. Nutman *et al.* 2007). No zircons with obvious detrital (older) ages were found. However, some of the rejected data hinted the existence of an older component, but these were highly disturbed and very poorly constrained. This can be interpreted to suggest that older grains exist, which suffered lead loss. Typically, none of the grains with a core that is different from the rim gave good data, and some are clearly metamict. In conclusion, this is likely to be a metasediment with a component of detrital zircons, which were thoroughly disturbed at both *c.* 2635 Ma and later at *c.* 2550 Ma, the two known ages of metamorphism in the area. The peak in the probability density diagram (Fig. 53) has an asymmetry, due to the presence of several single $^{207}Pb/^{206}Pb$ ages that overlap with the *c.* 2635 Ma metamorphic age. It is likely that a zircon population already was formed at this age, but that it was affected by lead loss. However, there is no direct evidence in the zircon isotope system for the sedimentary origin of this rock.

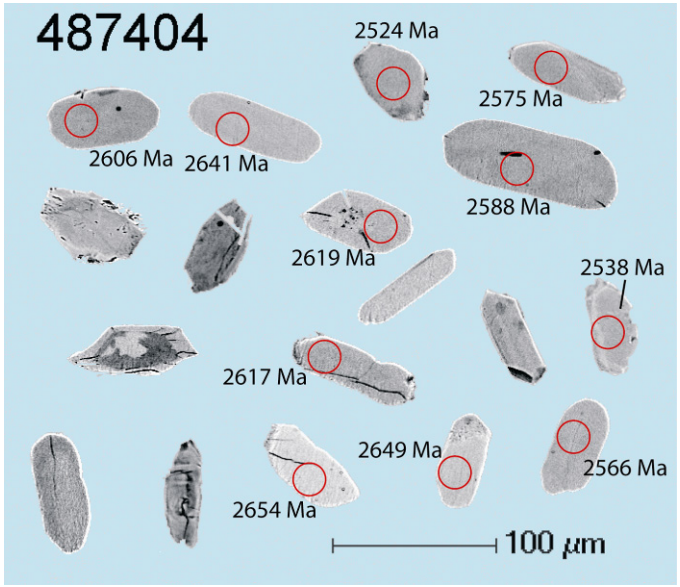

Figure 51. *SEM images of a selection of the zircons in sample 487404. The grains without age connotation gave no meaningful age (mainly the darker and heterogeneous ones on the left), or were not analysed (the prismatic grains on the centre-right hand side).*

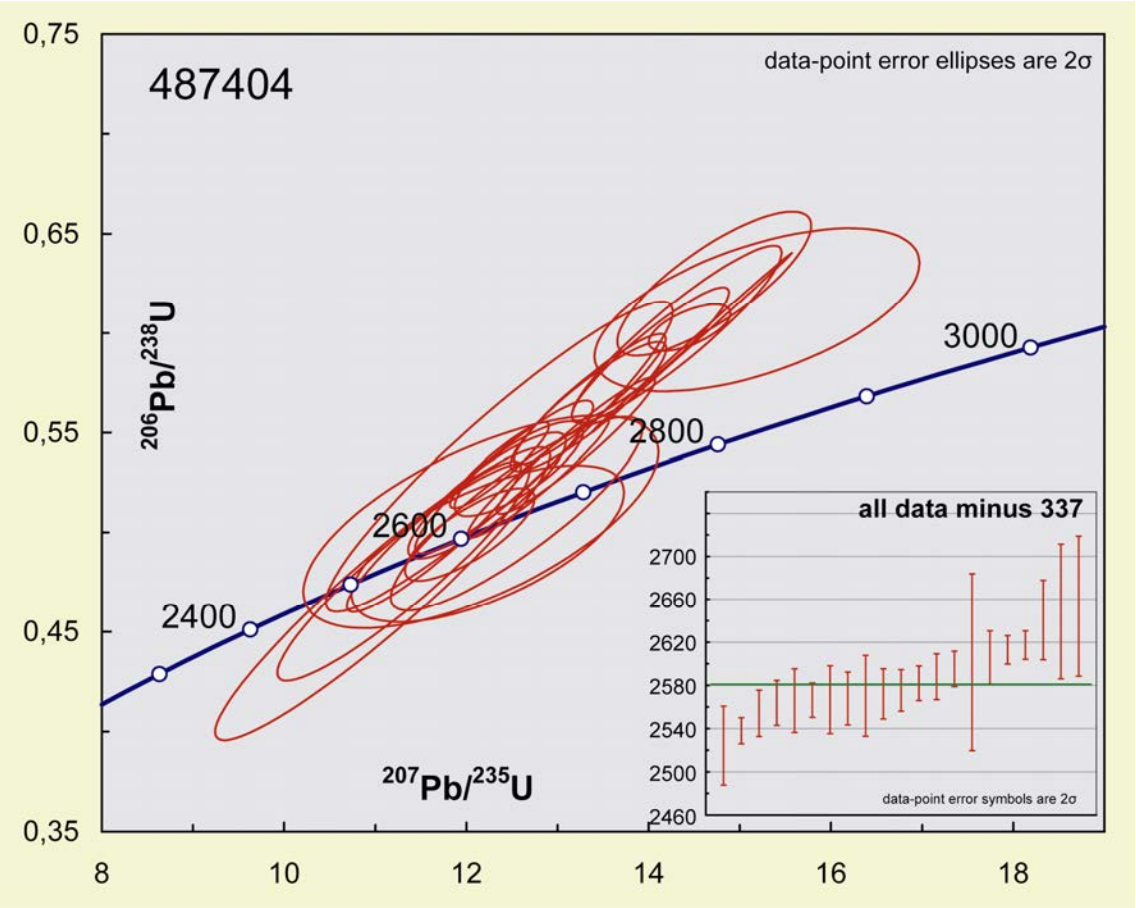

Figure 52. *Concordia diagram of the analyses of sample 487404. The dataset as a whole does not give a meaningful age, but the data plot around a $^{207}Pb/^{206}Pb$ age of c. 2580 Ma.*

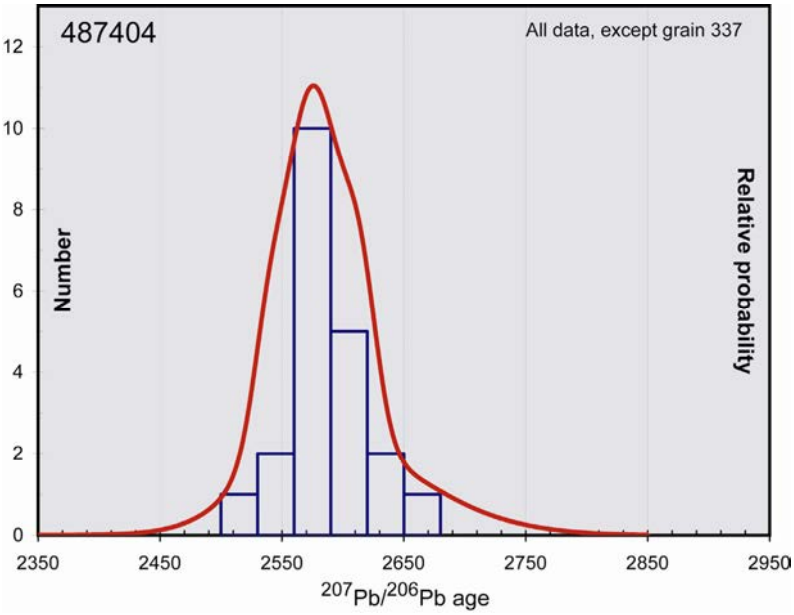

Figure 53. *Age probability density diagram showing age distribution of sample 487404 with one single peak at c. 2580 Ma.*

Sample 487416

This sample is a grt-bt gneiss with minor sillimanite sampled on the western slope of little Qingaaq, near the upper margin of the Storø shear zone. It is a homogeneous light brown foliated rock, grey in fresh surface (Fig. 8). It contains small (< 3 mm) garnets and abundant biotite. It remains uncertain whether this is a metasediment or an altered metamorphosed volcanic rock (cf. section on geochemistry). If it is a metasediment it might provide zircon provenance ages. If this is an altered volcanic rock, the zircons may provide an age for extrusion/deposition.

The zircons are medium-grained (50–120 μm) and most are slightly elongate and rounded (Fig. 54). Many grains have broad, homogeneous bright rims and dark cores with concentric oscillatory zonation that is truncated by the rims in some grains. The zonation is not always clear and sometimes irregular. The remainder of the grains are fairly homogeneous and bright.

Thirty one of the analyses gave meaningful results, although they are of fairly poor quality (Fig. 55). The data in the probability density diagram fall mainly in two groups representing analysis in cores and rims, respectively (Fig. 56). The majority of the core analyses give $^{207}Pb/^{206}Pb$ ages of *c.* 2850 Ma, with two slightly older grains. Fourteen rim analyses form a group that give an upper intercept age of 2628 +17/-22 Ma. The remainder of the data are from zircon cores that yield ages between the two peaks, mainly on the right hand side of the peak formed by the rim data in Fig. 56. These data may indicate ancient lead loss during *c.* 2635 Ma metamorphism. One slightly older grain of 2973 ± 84 Ma ($^{207}Pb/^{206}Pb$ age, see Figs 55, 56) may potentially represent an older population. The oscillatory zonation in the cores of the grains clearly indicates an igneous origin. However, the data cannot discriminate between an igneous (volcanic) and a sedimentary origin of the rock. The one older grain is not statistically significant to support the interpretation that this a detrital zircon population. The age of the younger population overlaps with error with the *c.* 2635 Ma metamorphic age known from the area.

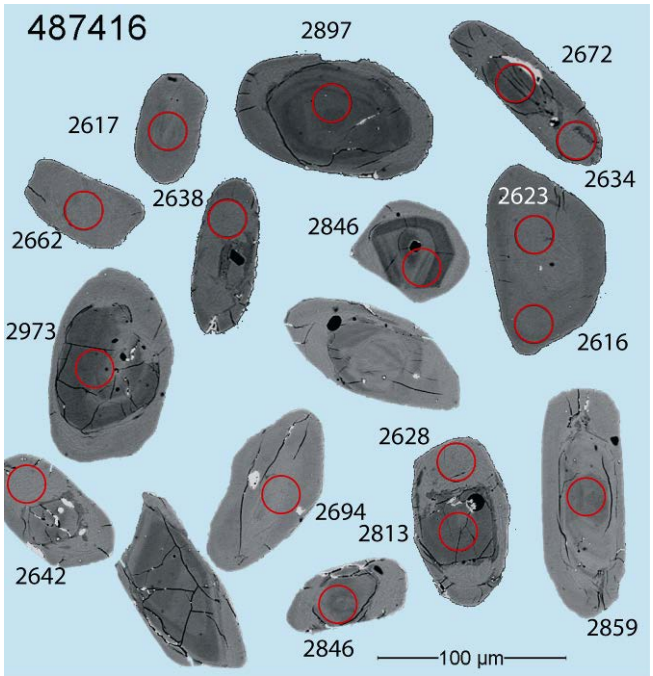

Figure 54. *SEM images of a selection of the zircon population in sample 487416, with $^{207}Pb/^{206}Pb$ ages of the analysed spots. Analysis of the grain in the centre gave no usable result, the grain in the bottom with the oscillatory zonation was not analysed. Many grains have obvious light rims around a darker core.*

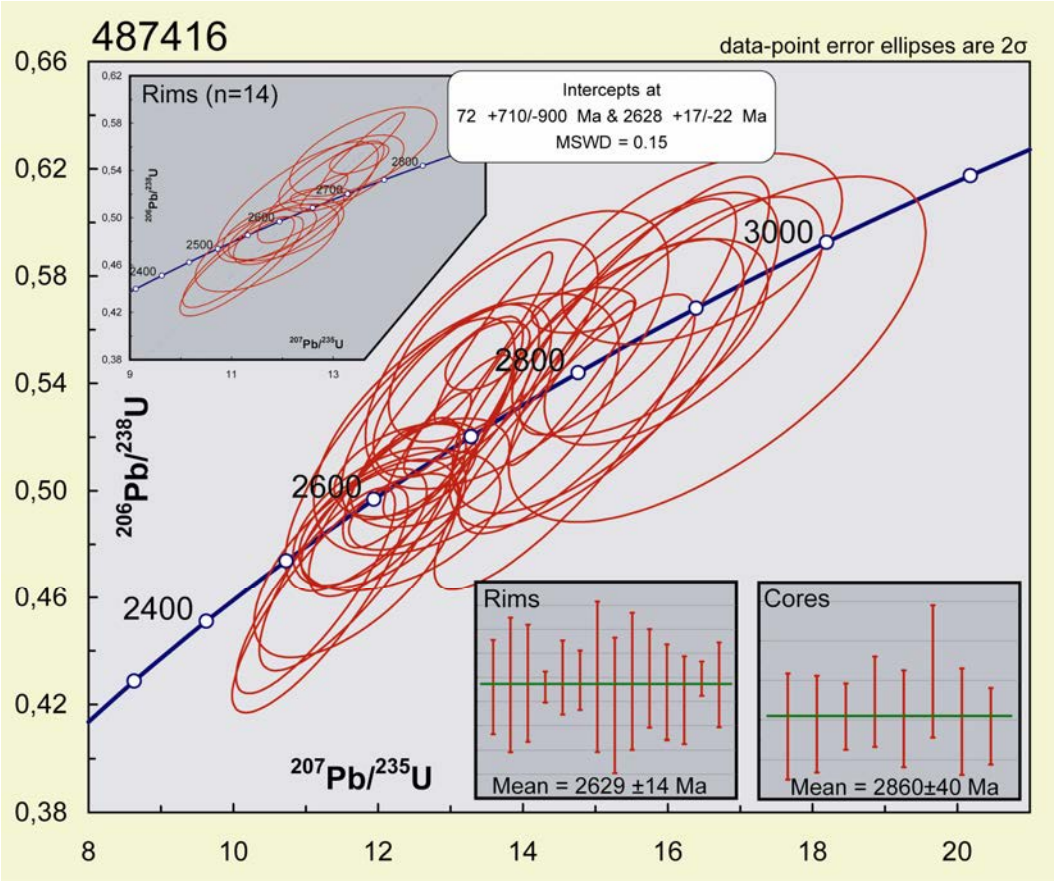

Figure 55. *Concordia diagram of sample 487416. The data have a wide range of ages, but can be divided in two groups, representing core and rim analyses.*

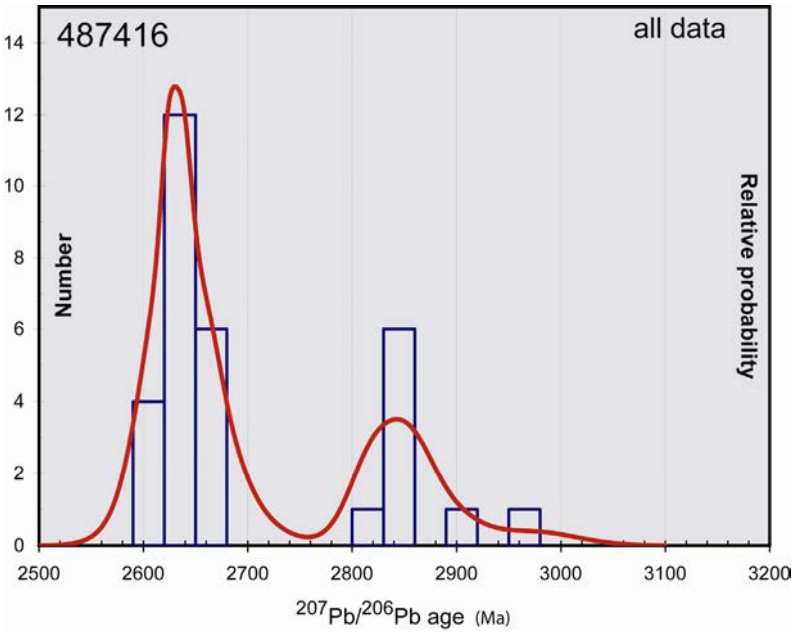

Figure 56. *Age probability density diagram showing the age distribution of sample 487416, with two main populations, representing broadly core and rim analyses, and two slightly older grains.*

Sample 487467

This is a sample from a felsic layer in a banded amphibolite (hbl-bt-bearing banded gneiss), consisting of interlayered mafic and felsic bands at 10–50 cm scale. Interpreted in the field as a felsic volcanic rock, but may be a felsic intrusive sheet in a mafic host rock. Collected in the lower layered amphibolite sequence, overlying the anorthosite, in order to determine the age of volcanic rocks southeast of small glacier at little Qingaaq, the basal part of the tectono stratigraphic supracrustal sequence. Alternatively it gives an intrusive age to the felsic layer and a minimum age for the supracrustal rocks it intruded in. The rock may contain metamorphic zircon.

Zircon grains are overall fine-grained (10-80 µm) with irregular shapes, many are fragmental with sharp corners (Fig. 57). Both homogeneous and heterogeneous grains occur. One grain fragment shows oscillatory zoning.

Fourteen analyses were carried out on 11 grains. One analysis was rejected. The majority of the grains form a population with an upper intercept age of 2591 ± 19 Ma (Fig. 58). Two grains yield a peak in the probability density diagram at *c.* 3060 Ma, and two grains (of which one very discordant) have $^{207}Pb/^{206}Pb$ ages around 2880 Ma (Fig. 59).

The youngest ages were all measured in homogeneous light grains, and are interpreted to represent the youngest metamorphic event. The age of 3060 Ma is close to the 3053 ± 4 Ma age of an intrusive gneiss sheet sampled in the lowest part of the tectono-stratigraphic sequence *c.* 3 km southeast of Aappalaartoq (Hollis *et al.* 2005) and an unpublished age of a tonalitic sheet at the same tectono-stratigraphic level as sample 487467, sampled 1 km to the northwest. Although no clear intrusive relationships were seen around the sample site, a tentative correlation with these other two intrusive rocks may well suggest that the lower part of the stratigraphic sequence is also here intruded by granitoids around 3060 Ma. Clearly, more work needs to be done on this sample in order to collect a statistically significant number of analyses to confirm this interpretation.

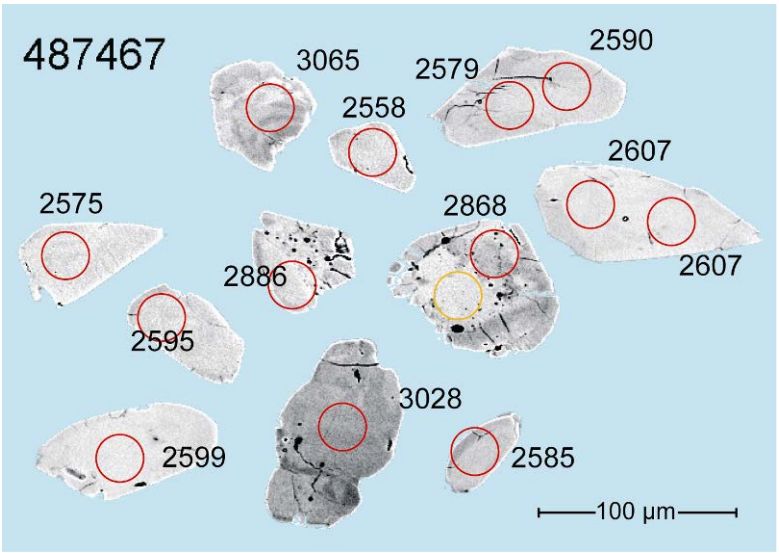

Figure 57. *All 11 analysed zircon grains of sample 487467, with $^{207}Pb/^{206}Pb$ ages in Ma. The analysis spot indicated in orange did not give a meaningful result.*

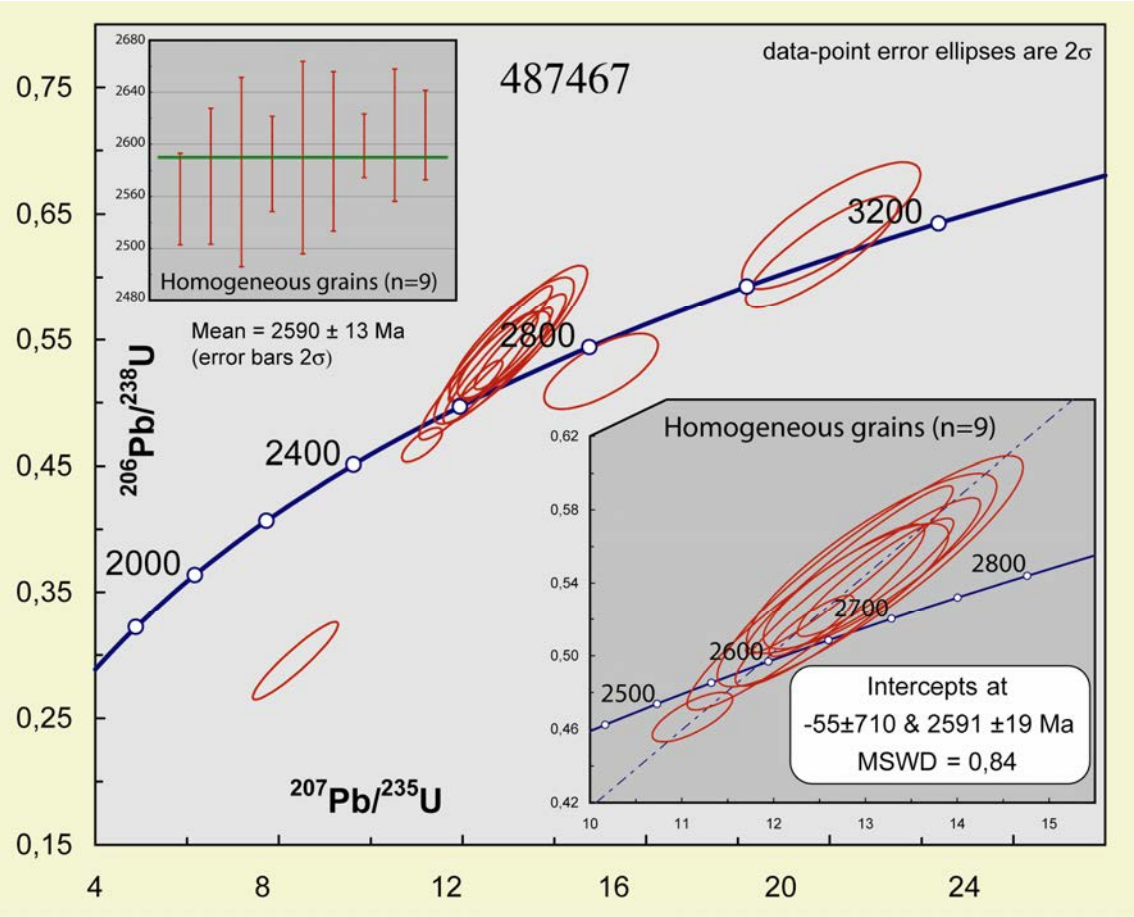

Figure 58. *Concordia diagram of sample 487467. The sample has one main population of metamorphic zircons (n=9), two older concordant grains (c. 3067 Ma) and two discordant grains that give a poorly constrained age of c. 2880 Ma.*

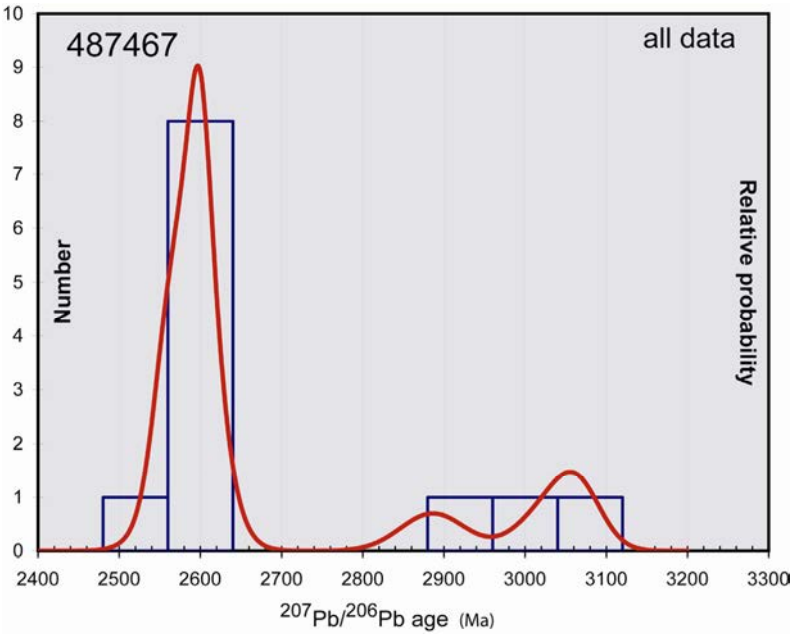

Figure 59. *Probability density diagram for sample 487467, showing one main peak at c. 2595 Ma and two minor peaks at c. 2880 and 3070 Ma.*

Sample 487495

Fuchsite quartzite sampled near the top of Aappalaartoq. It is a massive, homogeneous sillimanite-fuchsite quartzite, medium-grained and light grey (Fig. 12). It was interpreted in the field as a metasedimentary rock. If it contains a detrital zircon population, this can provide a maximum depositional age. Alternatively, if this is a heavily altered volcanic rock, the zircon data may yield the time of extrusion or alteration. This rock is part of the same tectono-stratigraphic level as sample 484601.

The rock contains many medium-grained zircons (100-200μm) that are slightly elongate or prismatic (Fig. 60). Cores with good oscillatory concentric zonation, and metamorphic (light and homogeneous in BSE) rims and tips. Metamorphic rims truncate oscillating zonation in the cores.

The data comprise 39 analyses in 24 grains in both cores and rims. Of the two main populations, the youngest was measured in the metamorphic rims and gave an upper intercept age of 2597 ± 10 Ma (n = 1; (Figs 61, 62). The diagrams show that this is a rather homogeneous population. The older main population has a wider spread and a main peak in Fig. 62 at 2880 Ma, with a subsidiary peak at *c.* 2825 Ma. These grains may include several populations and have presumably suffered lead loss during metamorphism. One grain yielded an Eoarchaean age of 3686 ± 34 Ma ($^{207}Pb/^{206}Pb$ n=2). The single Eoarchaean grain is statistically not very significant, but the data are consistent with the interpretation of this rock as a clastic metasediment. Especially the correlation with sample 484601 makes this interpretation likely.

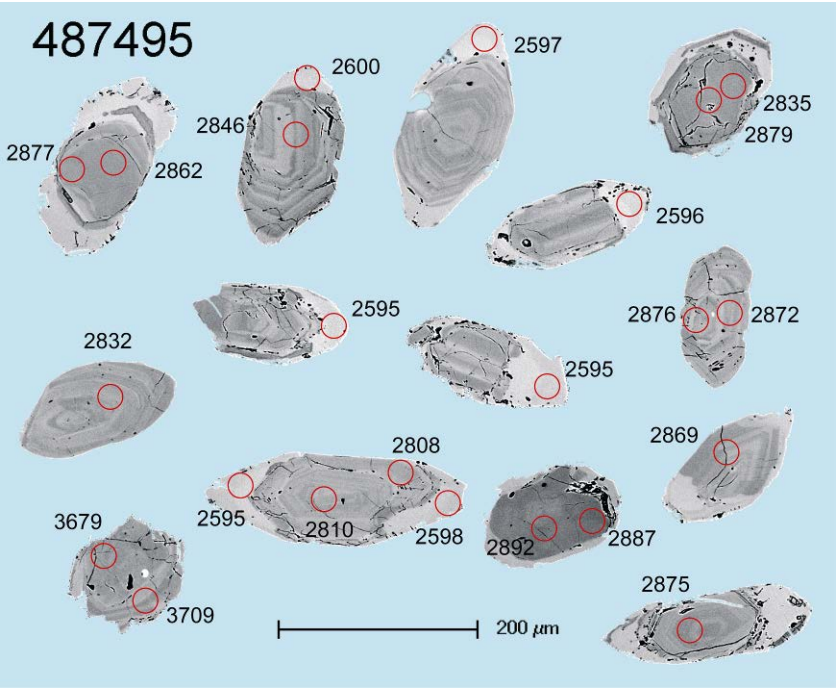

Figure 60. *Selection from zircon population of sample 487495, with $^{207}Pb/^{206}Pb$ ages. Most grains have a dark core with oscillatory zonation and a light homogeneous rim or tip, which truncates the zonation in the core. One Eoarchaean grain was analysed (bottom left).*

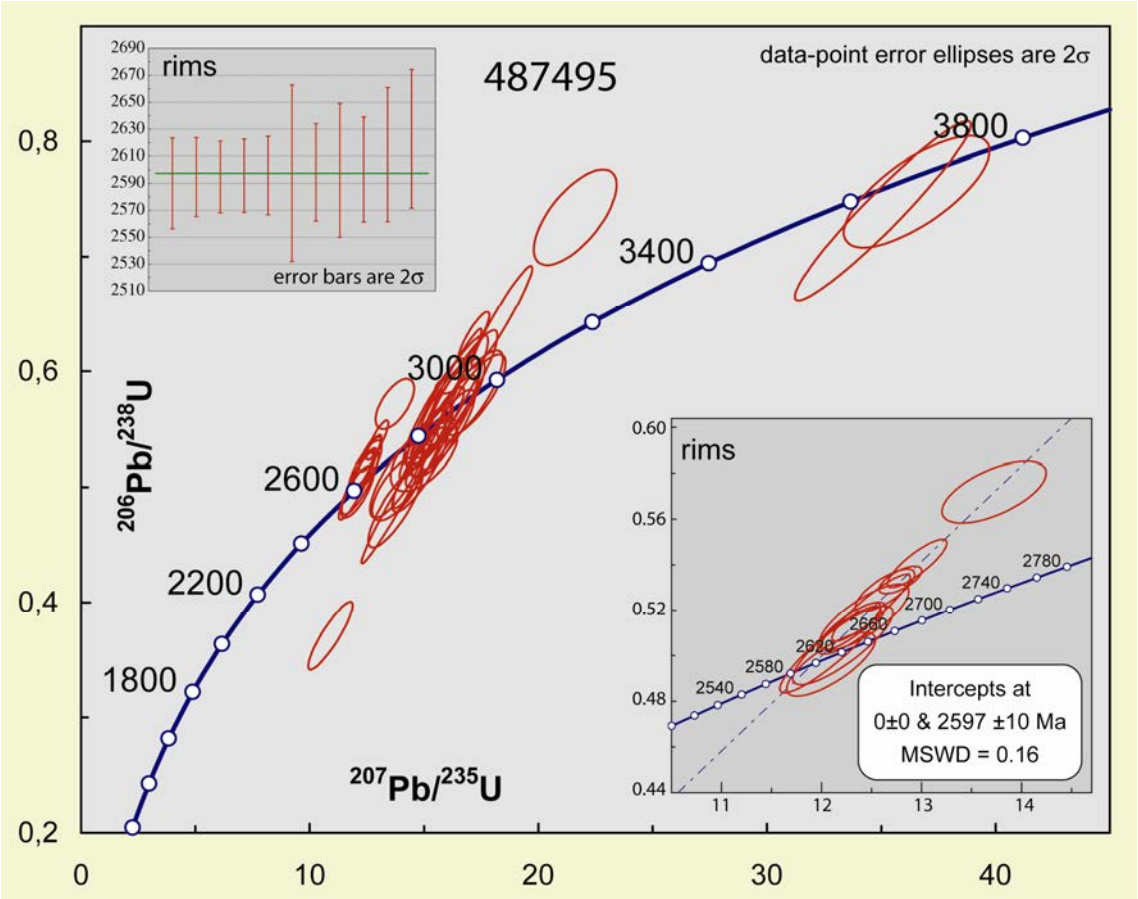

Figure 61. *Concordia diagram of sample 487495. The main population represents oscillatory cores. The upper intercept age of 2597 ± 10 Ma is from analyses of the bright metamorphic rims. Two analyses in one grain gave an average Eoarchaean age of 3686 ± 34 Ma ($^{207}Pb/^{206}Pb$).*

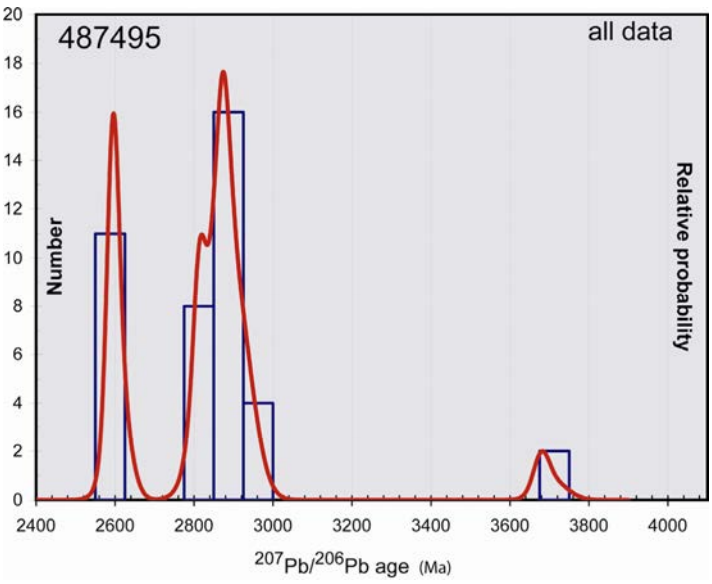

Figure 62. *Probability density diagram for sample 487495, showing two main peaks at 2597 Ma and 2875 Ma. Minor peaks occur at 2826 Ma, and 3689 Ma.*

Sample 487921

Grey homogeneous grt-bt gneiss, with a poor foliation, locally with minor sillimanite. It remains uncertain whether this rock is of magmatic origin, or if it is a metasediment. Due to this ambiguity, we treat the data as if either was true.

The zircon grains are fine to medium-grained (50-80μm), stubby to slightly elongate, with irregular grain boundaries (Fig. 63). Most grains are homogeneous (metamorphic?), or slightly heterogeneous (metamict?). Few have a core with concentric oscillatory zonation (igneous) and a narrow, light homogeneous rim (metamorphic). In all but two grains this rim was too narrow to be analysed.

Twenty one analyses were performed on 18 grains. Figs 64a and 65 show that many of the zircon data plot on concordia with a spread between two peaks. Two grains with distinct core and rim give dates of *c.* 2860 Ma and *c.* 2650 Ma respectively. Based on this information, and the probability density plot, two main groups were separated. Upper intercept ages of 2652 ± 29 Ma and 2833 ± 17 Ma (Figs 64b, c) are derived from respectively the grains (cores) with oscillatory zoning and light homogeneous grains (plus the two rim analyses). The range of ages between these two, measured in homogeneous light grains as well as heterogeneous (metamict?) resulted in a peak at *c.* 2750 Ma in Fig. 65. However, the inset in Fig. 64a suggests that the data do not form a platform, but form a constant range between the two higher peaks. This might be interpreted that these grains represent a phase of ancient lead loss (and recrystallisation?) during metamorphism around 2650 Ma. One younger grain and one discordant older grain were analysed. The age of 2584 ± 18 Ma ($^{207}Pb/^{206}Pb$) of the younger grain overlaps with the age of metamorphic overgrowths in other samples in the area. The age of the older grain, 3225 ± 13 Ma ($^{207}Pb/^{206}Pb$), is similar to that of a single grain in a quartzite from east of Aappalaartoq (Rink 2006), but does not occur in any of the other samples described here. Given the low number of analyses (n=21) and the number of significant age peaks in the probability density plot, perhaps a sedimentary origin is supported. Alternatively , this could be interpreted as an igneous rock with a large degree of inheritance.

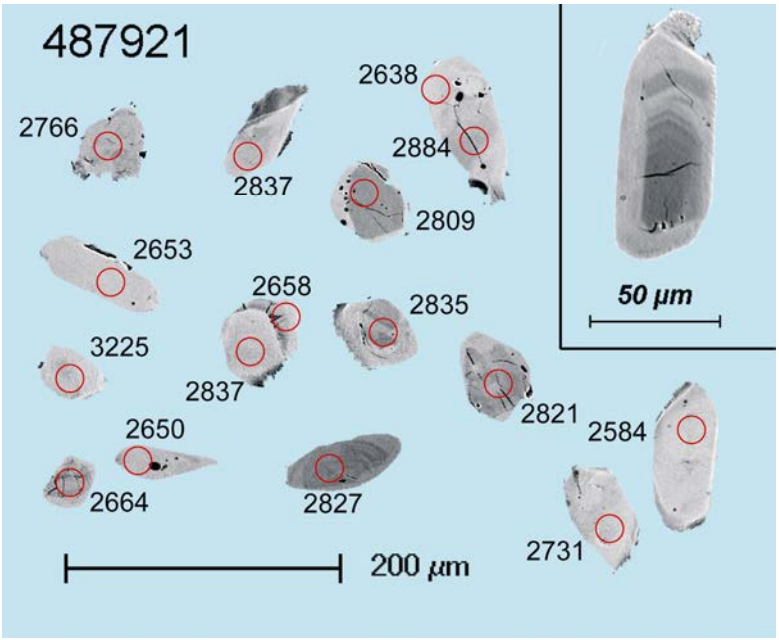

Figure 63. *SEM image of a selection of the zircons in sample 487921, with $^{207}Pb/^{206}Pb$ ages. The grain in the inset shows clearly how the oscillatory zoning in the core is truncated by the lighter homogeneous rim. The different zones in this grain are too narrow to analyse.*

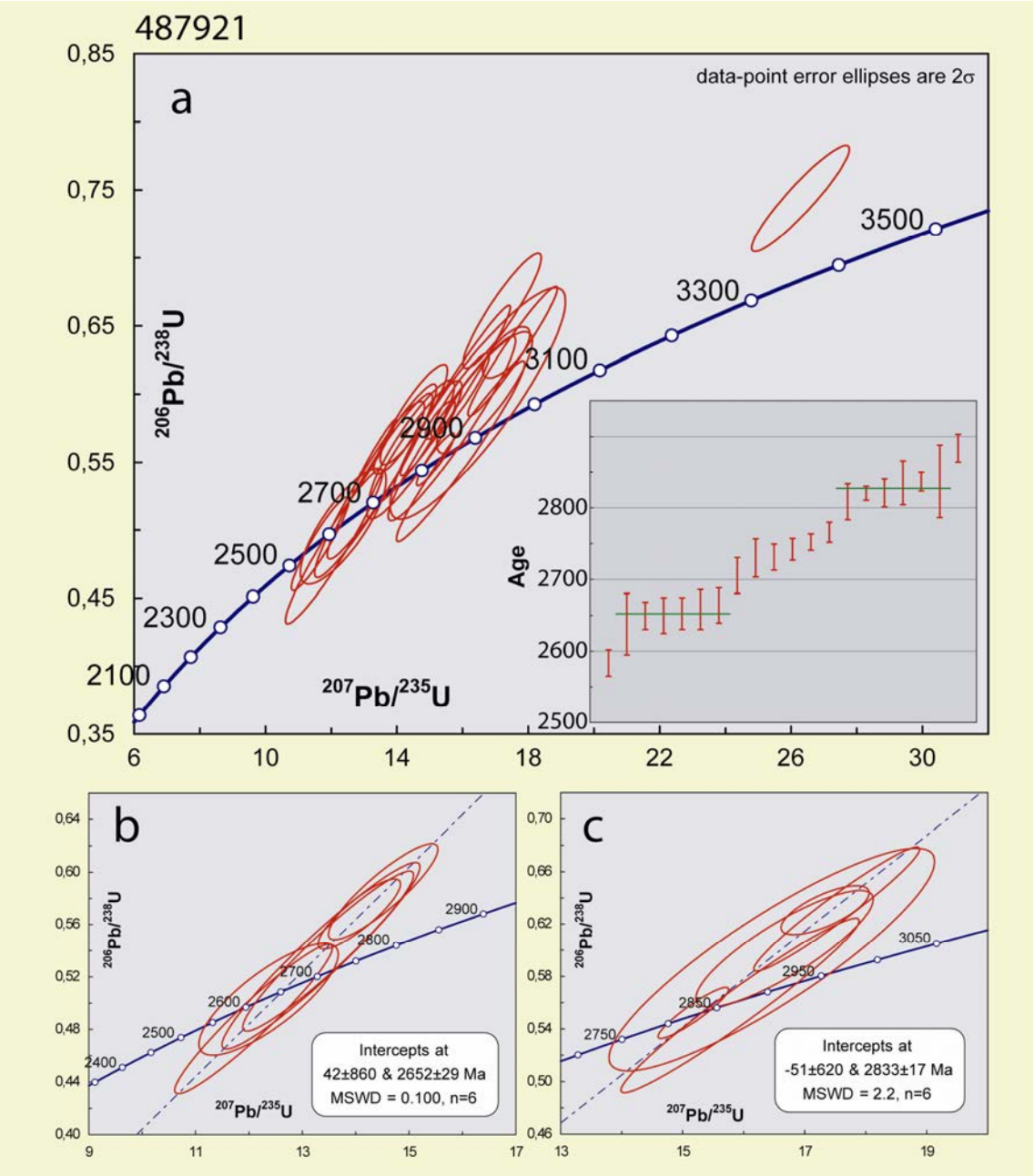

Figure 64. *Concordia diagram of sample 487921. The zircons comprise two main populations at 2833 ± 17 Ma and 2652 ± 29 Ma, plus a range of ages between these two. One reversely discordant Paleoarchaean grain was analysed.*

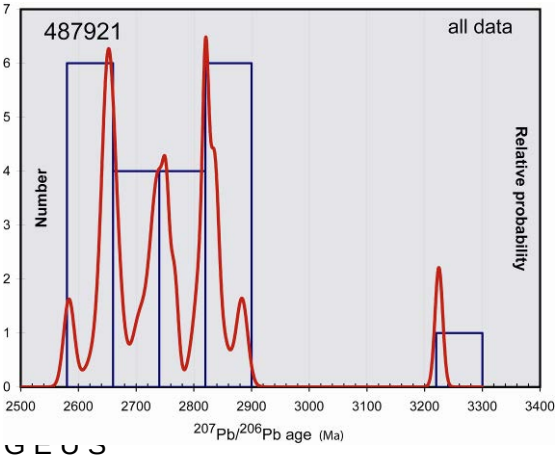

Figure 65. *Probability density diagram for sample 487921, The two main peaks at c. 2659 and 2820 Ma are within overlap with ages known from other samples (see text).*

Sample 488110

This is a fine-grained, homogeneous, grey bt-hbl gneiss with faint compositional layering, sampled at Qingaaq, near the base of the sequence with alternating biotite gneiss and quartzitic gneiss. This is potentially a meta-volcanic rock. Collected by Adam Garde and Claus Østergaard.
(UTM coordinates: 495375 – 7142428 @1035m)

The zircon grains are fine to medium-sized (30-100 μm), equidimensional and rounded, some are irregular in shape (Fig. 66). Most grains are homogeneous and bright in BSE images, but they include several metamict grains or grains in which a oscillatory zoning is overgrown by an irregular homogeneous phase. Two grains have clear igneous zonation.

29 analyses in 26 grains show two distinct groups that yield no good concordia age (Fig. 67). The analyses in the bright grains, the metamict grains and metamorphic rims yield $^{207}Pb/^{206}Pb$ ages that spread over *c.*100 my around an average 2609 ± 10 Ma (n=21). The remainder of the grains give an average age of 2846 ± 20 Ma (n=6).
The 2609 Ma date lies in between the two known metamorphic ages (*c.* 2550 and 2635 Ma; cf. Nutman *et al.* 2007)) and the data are spread widely. This may be the result of lead loss in metamorphic grains from the older metamorphic event during the younger event. However, a similarly aged peak was previously reported from Storø (Rink 2006).

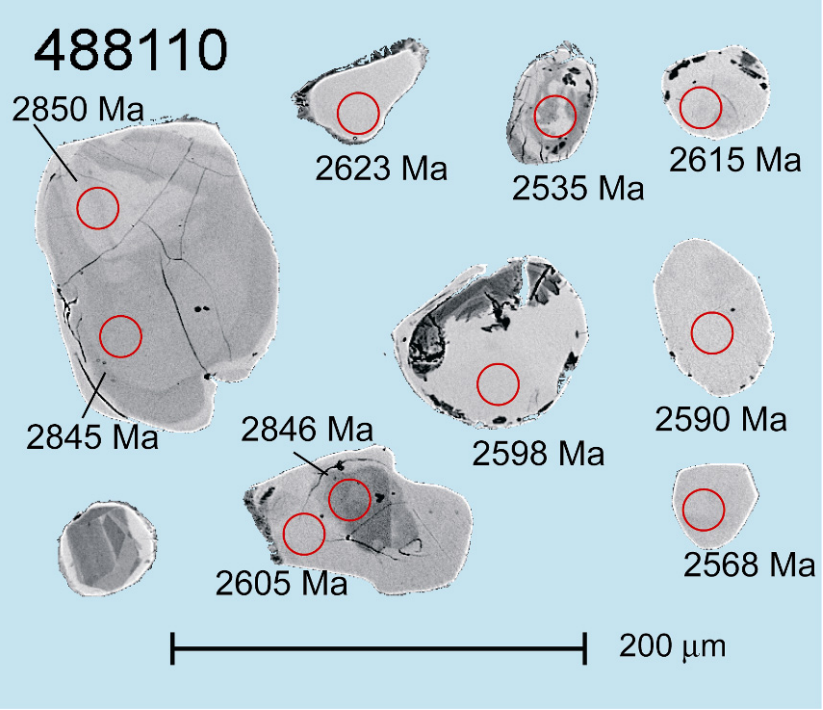

Figure 66. *SEM image of a selection of the zircons in sample 488110 with $^{207}Pb/^{206}Pb$ ages. Grains are rounded or irregular in shape and size. Many are homogeneous, light coloured, and give metamorphic ages. Many metamict grains exist (top row middle) or grains in which a oscillatory zoning is overgrown by an irregular homogeneous phase. Grains with dark core and narrow light rim (bottom right, analysis rejected) are scarce.*

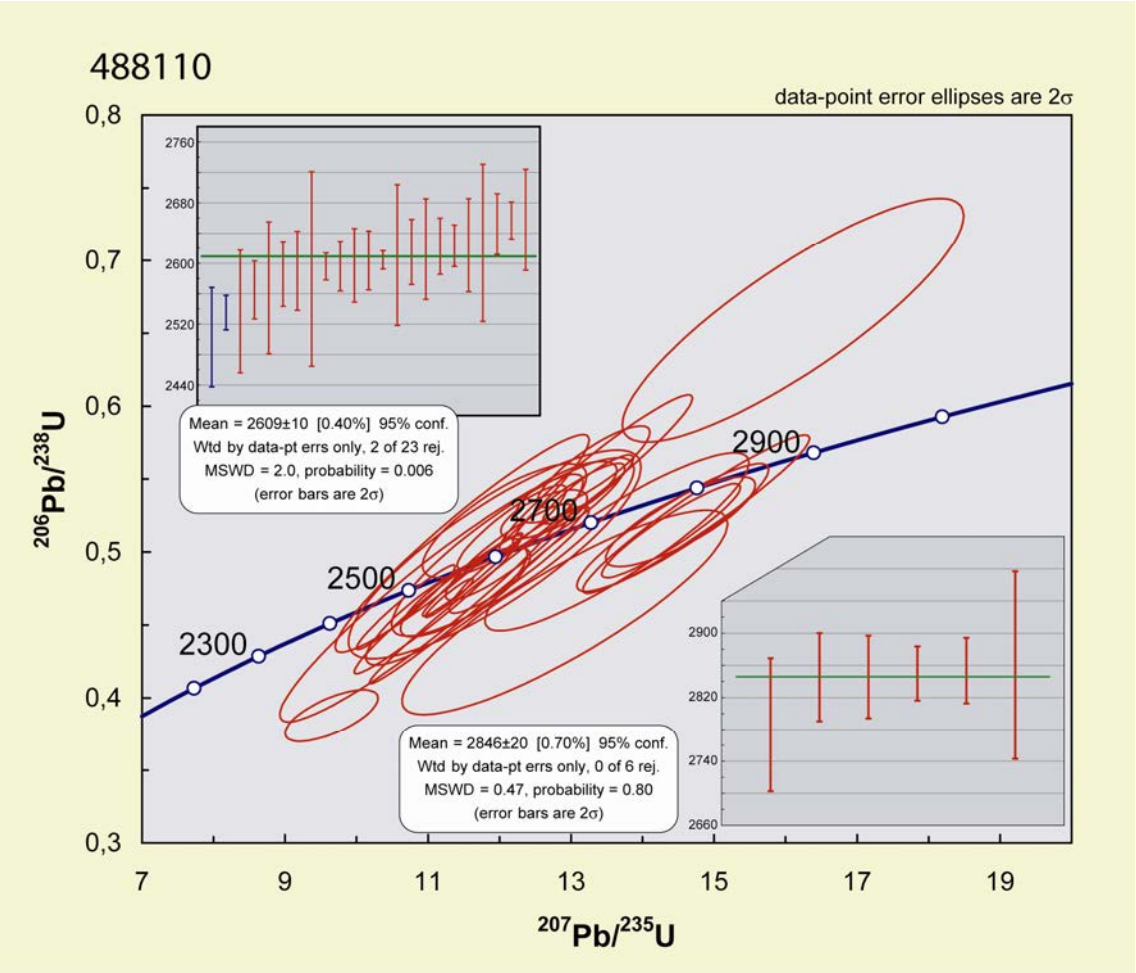

Figure 67. *Concordia diagram of sample 488110. The combined analyses gave no concordia ages, but the zircons comprise two main populations with average $^{207}Pb/^{206}Pb$ ages of 2846 Ma and 2609 Ma.*

Sample from the Archaean orthogneisses, overlying the supracrustal belt

Sample 487918

This is an orthogneiss sampled at NunaMinerals A/S base camp on Storø. The rock is a light grey, medium-grained banded orthogneiss with minor mafic layers. The sample was collected to test whether these gneisses, which have been mapped as Amîtsoq gneiss, indeed are early Archaean. This is relevant for the tectonic setting of the Storø supracrustal belt. Amîtsoq gneiss cannot have intruded the supracrustal belt, whereas a younger gneiss may well have an intrusive contact.

The zircon grains are medium to coarse-grained (mainly 70–200 μm), prismatic with slightly rounded tips (Fig. 68). Good oscillatory concentric zonation occurs in the cores of many grains, especially the most elongate ones. Brighter rims and bright homogeneous grains are metamorphic. Few very narrow rims have an even lighter colour, but could not be measured. Some of the grains have metamict cores.

The data confirm the Eoarchaean age of the rocks, but give a wide spread of ages from *c.* 3500–3800 Ma, which gives no meaningful concordia age (Fig. 69). The inset in the figure clearly shows the spread of the data. The oldest ages are measured in cores of larger grains with oscillatory zoning. The brighter, homogeneous grains and rims, as well as the metamict grains give the wide spread of younger ages, mainly from 3660 Ma and younger, with a peak at *c.* 3645 Ma.

These data are interpreted to indicate a minimum igneous age of the rocks at *c.* 3750 Ma with multiple metamorphic overprints (overgrowths and maybe lead loss?) at *c.* 3640 Ma and a younger, poorly defined time. There are no data at *c.* 2635 Ma, the metamorphic age of the underlying supracrustal rocks. Potentially, the very narrow bright rim on some of the grains represents a late Archaean metamorphic overgrowth.

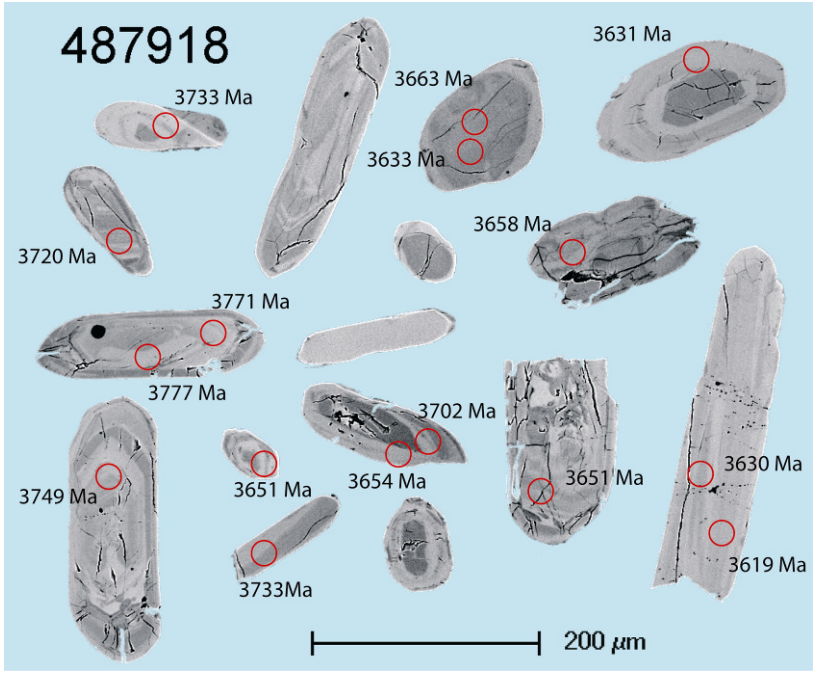

Figure 68. *Selection from zircon population of sample 487918, with 207Pb/206Pb ages.*

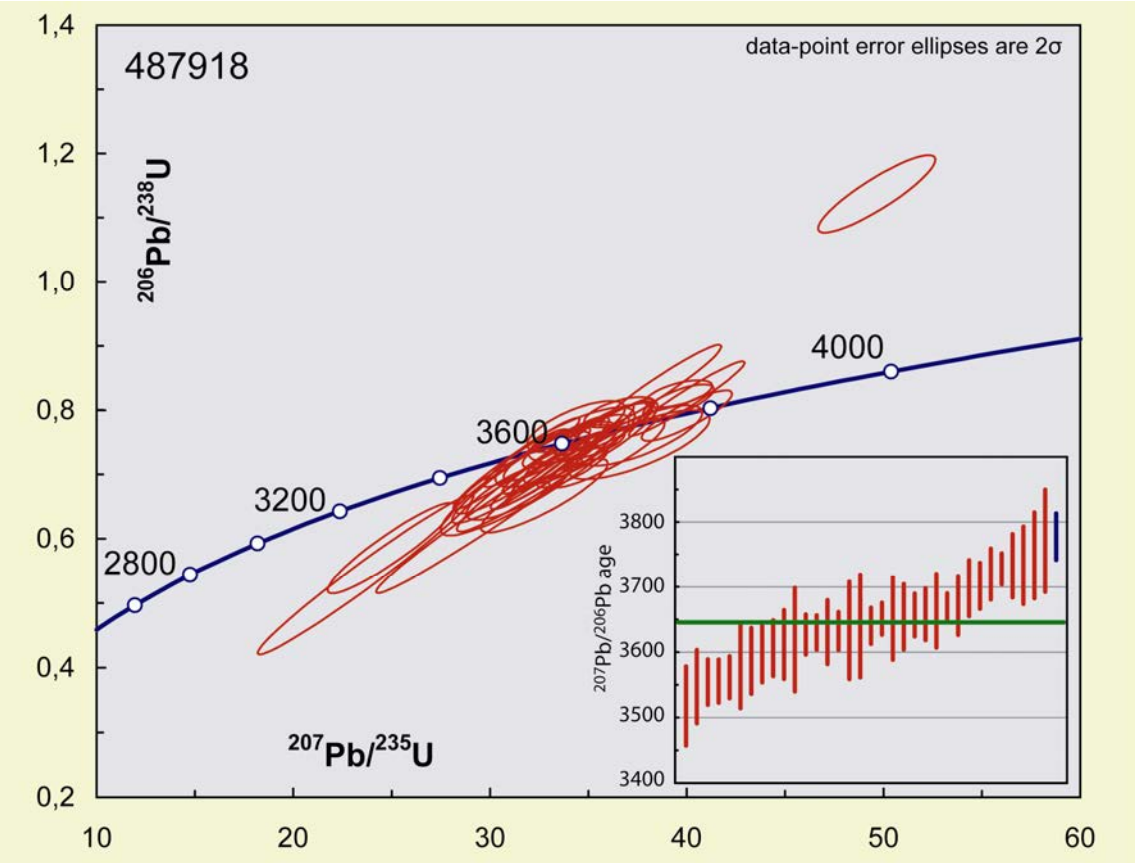

Figure 69. *Concordia diagram of sample 487918. The widely spread data give no concordia age or 207Pb/206Pb age average.*

Discussion of the geochronological results

In the probability density diagram of Fig. 70 all samples are plotted together and the recurring peaks stand out clearly. The eight samples from the Storø supracrustal belt include at least two metasediments – the quartzites – but potentially up to six can be interpreted as rocks with clastic protoliths. However, in most cases the geochronological data are not sufficient for a positive identification. With the exception of sample 487404, which has only a metamorphic zircon population, these six samples contain a main zircon population of around 2800-2850 Ma and most have a second slightly older peak, or a single wide peak around 2850 Ma (Fig. 70). Although many of these zircons have igneous internal textures, the rocks they occur in may well be metasediments. If one assumes that the supracrustal sequence is right way up in its present day orientation, and not internally disturbed or repeated, then the quartzites occur in the lowest part of the sequence. Since the youngest detrital zircons in the quartzites have an age of *c.* 2800 Ma, the overlying rocks must be younger, and zircon populations of the same age in these rocks must therefore also be detrital. Only sample 488110 occurs structurally below the quartzites. If the sequence is overturned, an igneous (volcanic) origin is still possible for three of the four rocks in question, but not 488110.

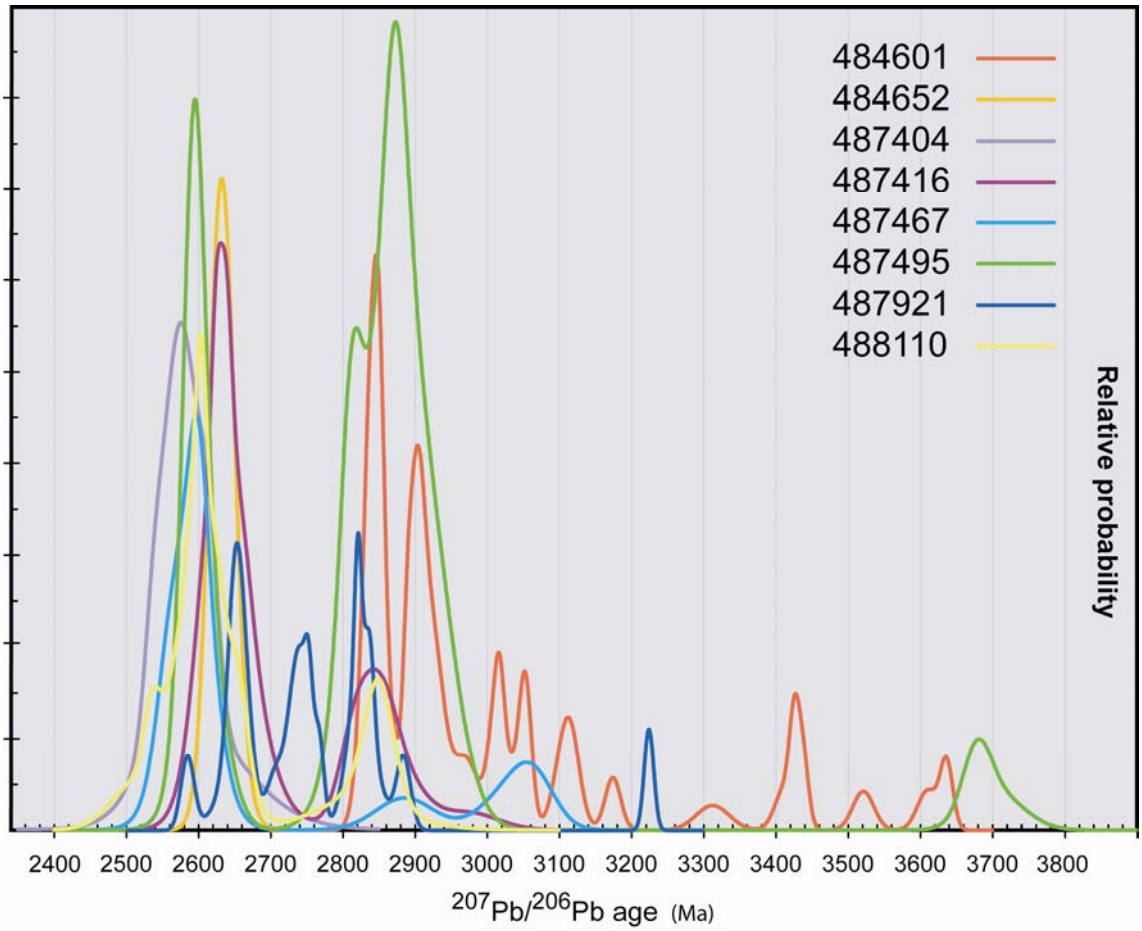

Figure 70. *Probability density plot of all samples combined, with exception of the early Archaean sample. The two main peaks at 2800–2950 Ma and 2650–2580 Ma are recurring in many samples. The absence of zircons with ages from 2700–2800 Ma (with one exception) is in stark contrast with the overlying Færringehavn terrane.*

With the exception of sample 484601, all samples from the supracrustal belt have a metamorphic zircon population of 2500–2700 Ma (Fig. 70). This is represented by new growth, lead loss or recrystallisation of zircon. Three samples yield a peak at the same date at *c.* 2635 Ma, while several somewhat more dispersed peaks occur at 2550–2605 Ma in the other samples. The former date is virtually identical to the timing of metamorphism reported by Hollis (2005) and Nutman *et al.* (2007; and references therein). Since it is unlikely that these rocks have different metamorphic histories, all must have been affected by the *c.* 2635 Ma metamorphic event. A possible interpretation for the younger peaks can be that their original metamorphic population of 2635 Ma suffered lead loss to varying intensities during a later metamorphic event, e.g. during intrusion of the Qôrqut granite (2560 Ma) in the lower levels of the crust, and the associated intrusion of pegmatites in the supracrustal belt (Nutman *et al.* 2007). This would explain the absence of a peak at 2635 Ma in these rocks, and the slight scatter in the younger peaks.

The zircon data constrain the time of deposition of the assumed clastic rocks between *c.* 2800 Ma (the youngest detrital zircons) and the metamorphic peak at 2635 Ma. The Re-Os age of the arsenopyrite in the BD Zone, 2714 ± 53 Ma, discussed elsewhere in this report, requires that the rocks in the supracrustal belt are equal or older than this date.

A large number of zircons have an age between 2950 Ma and 2800 Ma. The two quartzites have a major peak at *c.* 2890 Ma, close to the date of 2880 Ma that was reported by Hollis (2005) as recurring in samples from the Storø supracrustal belt. Ages around 2840 Ma are recurring in most samples. If the rocks with uncertain protoliths are interpreted as igneous, they could form part of an arc at this time. If they are clastic rocks, a source with zircons of this age must have been dominant in the supply of clastic material. The *c.* 2825 Ma intrusive rocks of the Tre Brødre terrane, which is presently near by, may have contributed to the zircon populations, although the peaks in the samples tend to be somewhat older. The Akia terrane seems not to have formed a significant source. This is in accord with the observation that the Storø shear zone has juxtaposed the supracrustal belt against rocks of the underlying Akia terrane at *c.* 2630 Ma (Hollis 2005) after deposition of these rocks. The quartzites clearly received input from older continental blocks.

Only sample 487921 shows dates between 2700 Ma and 2800 Ma, and these are likely to be pre-2800 Ma zircons with ancient lead loss and recrystallisation during 2635 Ma metamorphism, as argued above. This absence of zircons in this age range is in stark contrast with the abundant metamorphic ages in this range in the rocks of the overlying Færringehavn terrane, which itself is lacking the 2635 Ma metamorphic event (see discussion by Nutman *et al.* 2007). On the other hand, both Hollis (2005) and Persson (2007) report metamorphic zircons of *c.* 2700 Ma in the supracrustal rocks of Storø. Based on the presently available data, it is therefore not possible to conclude with certainty whether or not the rocks in the Storø supracrustal belt have experienced high grade metamorphism at the time that many of the terranes in the region were assembled at *c.* 2720 Ma (Nutman *et al.* 1989). Further investigations are required to resolve this.

The presence of two grains of *c.* 3060 Ma in sample 487467 from the lower banded amphibolites is consistent with the suggestion that the lower part of the tectono stratigraphic sequence is older than *c.* 3050 Ma (Hollis 2005). However, the data are not conclusive in this respect. This interpretation would require the presence of a structural break or an unconformity within the supracrustal sequence. Orthogneisses of *c.* 3050 Ma that intrude into Mesoarchaean mafic and intermediate supracrustal sequences are otherwise known from the Akia and Kapisillik terranes. The contact between Mesoarchaean and Neoarchaean gneisses is likely coincident with the contact between the lower banded amphibolites and the biotite gneisses, since the data from sample 488110 resemble the other samples from the central part of the sequence in rock type and zircon populations.

Conclusions

Our results are largely in agreement with previous work (Hollis *et al.* 2005; Nutman *et al.* 2007 and references therein). It shows the following main points:

- The orthogneisses overlying the supracrustal belt are confirmed to be of Eoarchaean age
- The lower part of the tectono-stratigraphic sequence may well be older than *c.* 3050 Ma.
- Quartzites include Eoarchaean detrital material as well as zircons at 2800–2900 Ma

- Many samples include zircons of 2800–2850 Ma, which is a major source for the rocks of the belt
- The earliest wide-spread evidence for metamorphism is at 2635 Ma
- Younger metamorphic zircon populations at *c.* 2600 Ma and later exist, but may be the result of lead loss in 2635 Ma metamorphic grains, potentially during the intrusion of the Qôrqut granite at *c.* 2560 Ma.

Further geochronological work will have to be directed to the proposed older age of the lower part of the sequence, the age of the anorthosite, and to unravel the multiple zircon populations between 2800–2950 Ma and the metamorphic age younger than 2610 Ma.

Re-Os analyses of arsenopyrite in the gold-mineralised zones

Anders Scherstén, Jeroen A.M. van Gool and Robert A. Creaser

Two samples from two gold mineralised zones on Storø, containing typically disseminated arsenopyrite, were selected for rhenium-osmium (Re-Os) isotopic analysis in order to determine the timing of sulphide mineralisation. The two samples, GGU# 487912 and GGU# 487931, were collected respectively from the contact between amphibolites and garnet-sillimanite gneisses near the top of "little Qingaaq" (BD zone) and from the foot of the northern slopes of this mountain (Main zone). The purpose was to constrain the timing of gold mineralisation, and to test if there is a difference in timing between the two mineralised zones as has been speculated.

Analytical Procedure

One isotope of Re (^{187}Re) decays to ^{187}Os at a known rate (λ=1.666×10^{-11} a^{-1}), and both elements show general chalcophile ('sulphide loving') behaviour, making the direct dating of many sulphide minerals possible. Recent journal articles describing the use of arsenopyrite include Arne *et al.* (2001), Morelli *et al.* (2005a,b), Stein (2006) and Morelli *et al.* (2007). Initially, one piece from each sample was used, and sulphide minerals concentrated by crushing, milling and gravity and magnetic methods. As pyrrhotite also appears to be present, this mineral has to be removed from the sulphide mineral concentrate by a Frantz magnetic separator – pyrrhotite is easily disturbed for the Re-Os isotope system. From the arsenopyrite-rich concentrate, a small amount (c. 10 mg) of material from each sample was analyzed for Re content only, to establish if full Re-Os analyses were warranted. These results showed Re levels of 30–40 parts per billion (ppb) Re characterized the samples, which given the expected Precambrian age of the samples, should readily yield enough radiogenic ^{187}Os to be able to determine the timing of formation. These values of Re are relatively high for arsenopyrite, which usually shows < 20 ppb Re. From these first samples, called "A", six complete Re-Os analyses were performed on sample 487912 and three complete analyses on sample 487931. However, a second piece of each sample had to be used to produce another sulphide mineral concentrate to yield enough sulphide minerals to produce isochrons for each sample, called "B". Subsequently, a total of nine complete Re-Os analyses were performed on sample 487912 and six complete analyses on sample 487931.

For each analysis, approximately 100 milligrams of arsenopyrite separate was accurately weighed and transferred to a thick-walled, borosilicate glass Carius tube. An accurately weighed amount of a mixed ^{185}Re + ^{190}Os spike was added to each sample and dissolved at 240°C for 48 hours, followed by chemical separation and purification of Os and Re using procedures described by Shirey & Walker (1995), Cohen & Waters (1996) and Birck *et al.* (1997), as described in detail by Morelli *et al.* (2005b). The total procedural blanks were measured to be less than 3 picograms Re and 0.5 picogram Os (< 0.01 picograms ^{187}Os). The decay constant used for ^{187}Re is that of Smoliar *et al.* (1996) of λ = 1.666×10^{-11} a^{-1}.

The analyses were carried out at the isotope laboratory of the department of earth and Atmospheric Sciences of the University of Alberta, Edmonton, Canada.

Sample descriptions

Sample 487912 is an arsenopyrite-rich garnet-amphibolite with abundant thin quartz veins and minor disseminated pyrrhotite. Seven pieces were collected within a short distance (*c.* 3 metres) from each other in a few metres wide mineralised zone at the contact between dark homogeneous amphibolites and felsic garnet-sillimanite gneiss (BD zone) near the top of little Qingaaq. Sample location is 2006jvg272 at 64.40896°N and 51.09451° W at 995 m altitude.

Sample 487931 is an arsenopyrite-rich biotite-hornblende schist from the main gold mineralised zone in the area (main zone). Five pieces with larger arsenopyrite crystals are collected from a less than one metre wide zone all within two metres from each other. Two pieces with smaller, disseminated arsenopyrite are from the same zone, but sampled *c.* 6 m further north. Sample location is 2006jvg400 at 64.41237°N and 51.08491°W at 584 m altitude.

Table 2. *Re-Os analytical results for arsenopyrite. Ppb = parts per billion, ppt = parts per trillion.*

Sample	Re ppb	±2σ	Os ppt	±2σ	^{188}Os ppt	$^{187}\underline{Re}$ ^{188}Os	±2σ	$^{187}\underline{Os}$ ^{188}Os	±2σ	ρ
487912A-1	22.8	0.1	828	18	21.8	661	13	30.62	0.59	0.95
487912A-2	23.3	0.1	831	20	20.4	720	14	33.39	0.70	0.92
487912A-3	23.5	0.1	829	21	20.0	741	16	34.08	0.73	0.96
487912A-4	23.7	0.1	859	18	22.9	654	12	30.15	0.55	0.96
487912A-5	23.7	0.1	852	18	21.9	683	13	31.44	0.61	0.92
487912B-1	50.8	0.2	1894	16	56.5	568	5	26.10	0.21	0.82
487912B-2	49.9	0.2	1831	19	52.5	600	6	27.45	0.26	0.81
487912B-3	51.3	0.2	1958	31	62.6	517	8	23.87	0.36	0.88
487931A-1	42.1	0.2	1542	16	44.1	602	6	27.57	0.27	0.87
487931A-2	42.3	0.2	1619	18	53.1	503	5	23.10	0.25	0.75
487931A-3	39.1	0.2	1491	14	47.8	517	5	23.79	0.22	0.88
487931B-1	24.5	0.1	1069	10	47.5	326	3	15.13	0.16	0.81
487931B-2	25.4	0.1	1138	9	52.3	307	3	14.38	0.13	0.81
487931B-3	24.5	0.1	1082	10	48.4	320	3	14.94	0.16	0.81

Results

All Re-Os analytical results are presented in Table 2. All samples show moderate $^{187}Re/^{188}Os$ ratios (300–700), and highly radiogenic Os, showing $^{187}Os/^{188}Os$ ratios of 15–34.

These results are plotted on a Re-Os isochron diagram in Fig. 71, Sample 487931 yields a well-fitted Model 1 isochron having an age of 2636 ± 23 Ma (2σ uncertainty, MSWD = 0.7) with a moderately constrained initial $^{187}Os/^{188}Os$ ratio of 0.56 ± 0.16. Sample 487912 yields a slightly less precise Model 1 regression (MSWD = 1.16) having an age of 2714 ± 53 Ma (2σ uncertainty) with an unconstrained initial ratio of -0.1 ± 0.6.

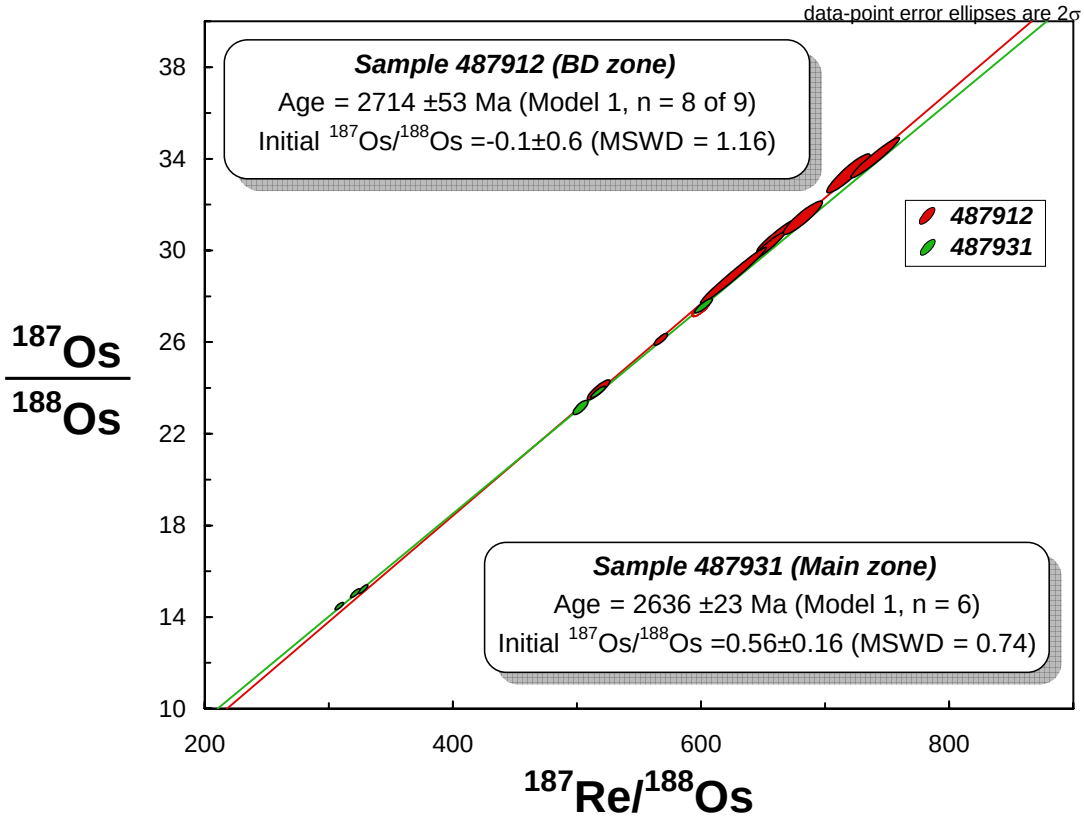

Figure 71. *Re-Os isochron plot for arsenopyrite samples.*

Discussion

The well constrained isochron for sample 487931 is most readily interpreted to date the sulphide crystallisation at 2636 ± 23 Ma in the Main zone. This age is in excellent agreement with a 2633 ± 8 Ma zircon population associated with (and partially included in) gold-bearing arsenopyrite from the same mineralised zone (Nutman *et al.* 2007) and overlaps with the *c.* 2635 Ma metamorphic age in the region. The initial $^{187}Os/^{188}Os$ ratio of 0.56 ± 0.16 indicates a crustally derived source of the Os, and by inference, the sulphide and associated gold. The current Re/Os ratios of the arsenopyrite imply a maximum possible age

of 2700 Ma if extracted directly from the mantle (Fig. 72). These mantle model ages assume that the mantle has chondritic Re/Os and an $^{187}Os/^{188}Os$ ratio, which is usually true (e.g. Shirey & Walker 1998). However, supra-subduction zone mantle may have elevated $^{187}Os/^{188}Os$ ratios, which would yield younger extraction model ages. The current model ages are thus maximum ages and any model invoking earlier mineralisation events might require contrived models to be reconciled with the present Re-Os results, which lends no support for events prior to 2700 Ma.

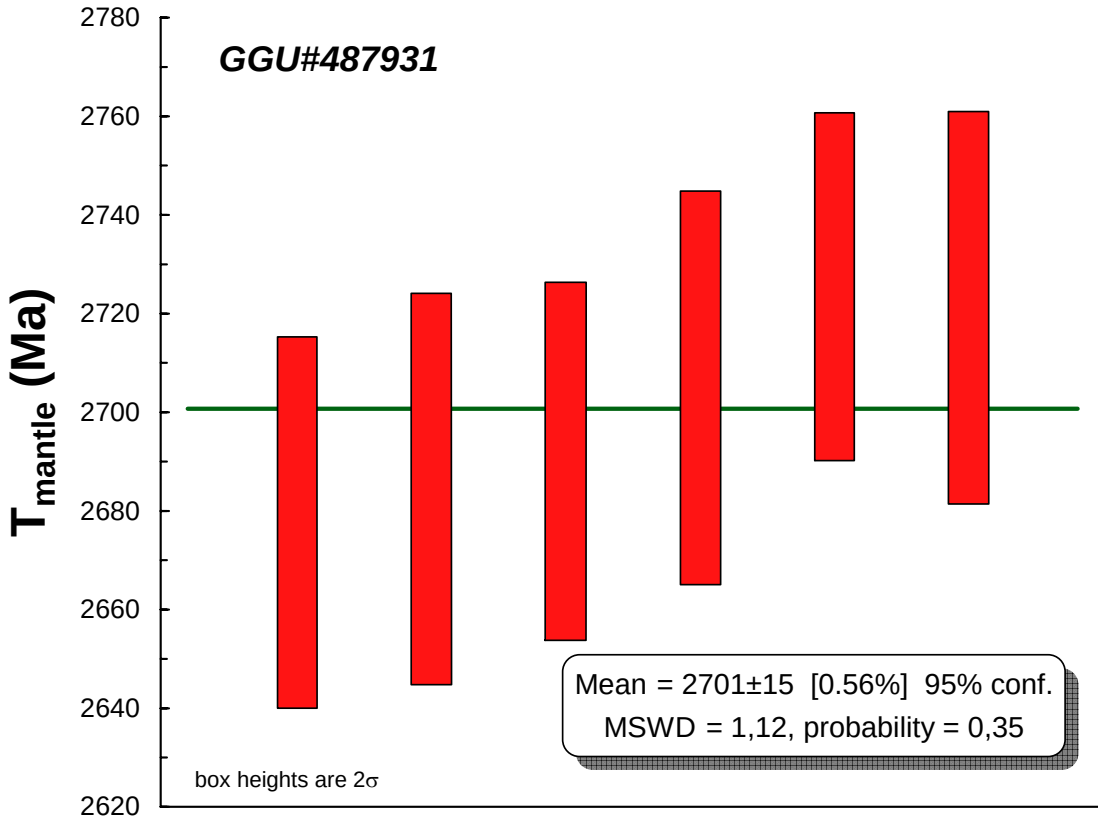

Figure 72. *Re-Os mantle extraction model ages for 487931.*

The isochron for sample 487912 is less well constrained at 2714 ± 53 Ma, but it remains significantly older than sample 487931, indicating that there are two distinct phases of sulphide mineralisation. The date coincides with general metamorphism in the region (e.g. Hollis 2005). However it remains unclear what the precise age of the host rocks is (see geochronology section). Current age constraints are limited to *c.* 2800 Ma of the youngest detrital zircons, which implies that these rocks cannot be older than 2800 Ma (Hollis 2005; Knudsen *et al.* 2007). The initial $^{187}Os/^{188}Os$ ratio of -0.1 ± 0.6 is poorly constrained due to the high Re/Os and $^{187}Os/^{188}Os$, which requires large corrections that yield greater uncertainty. Nevertheless, the current Re/Os of the sulphides does not allow long residence times in the continental crust prior to their current emplacement and the mantle extraction model ages are overlapping with the isochron age (Fig. 73).

The strata bound nature of the mineralisation in the BD zone (sample 487912) and the constraints from the mantle model ages are suggestive of a mineralisation process in the volcanic environment. If correct, it would imply that the mineralised volcanic host rock was

in fact emplaced within error of the 487912 sulphide isochron date of 2714 ± 53 Ma. Alternatively, the date is coinciding with regional metamorphism in e.g. the Færringehavn terrane around 2720 Ma (Friend *et al.* 1996; Hollis *et al.* 2006).

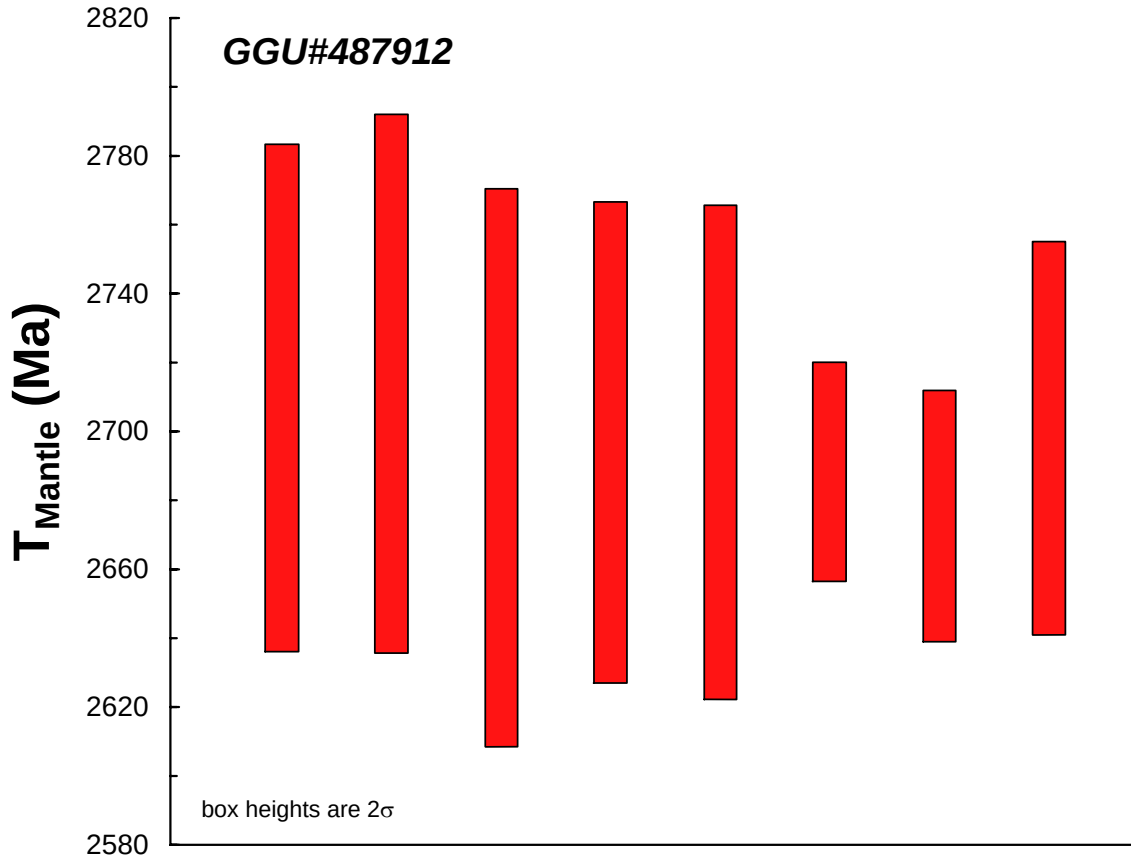

Figure 73. *Re-Os mantle extraction model ages for 487912.*

A two stage process for the Storø mineralisation is required to explain the two different isochron ages for the DB zone and the Main zone. We assume that the mineralisation in the Main zone is the result of remobilisation of an earlier mineralisation, which can well have been the one in the DB zone. This is consistent with their structural and relative age relationships, where the Main zone is located in a low-strain fold core, while the DB-zone appears to be associated with a tectono-stratigraphic contact. Also micro structural observations indicate that gold occurs both prior to garnet crystallisation, as well as post the metamorphic peak. It is notable that the sulphides from the Main zone (sample 487931) generally have higher common Os concentrations and lower Re/Os than the sulphides from the DB zone (Fig. 74). If the Main zone sulphides are derived through remobilisation of sulphides in the DB zone, there seems to have been a general increase in the Os concentrations coupled with a relative decrease in Re. The increase in common Os (expressed as ^{188}Os) is associated with enriched Au concentrations in the Main zone, and preferential mobility of Re could cause the decrease in average Re/Os. An important requirement for the Main zone sulphides to be derived from mobilised BD zone sulphides is that the $^{187}Os/^{188}Os$ at the time of Main zone mineralisation overlaps with that of the BD zone at 2635 Ma. As seen in Fig. 75, the individual and mean 487912 (BD zone) sulphides are overlapping the initial ratio of 487931 from the Main zone. A primary requirement is thus

fulfilled, and there is no evidence against the remobilisation hypothesis for the origin of the Main zone. It may thus be postulated that metamorphism around 2635 Ma acted to remobilise Re, Os and, by inference, Au, which were enriched along low strain zone in e.g. fold cores that formed the Main zone.

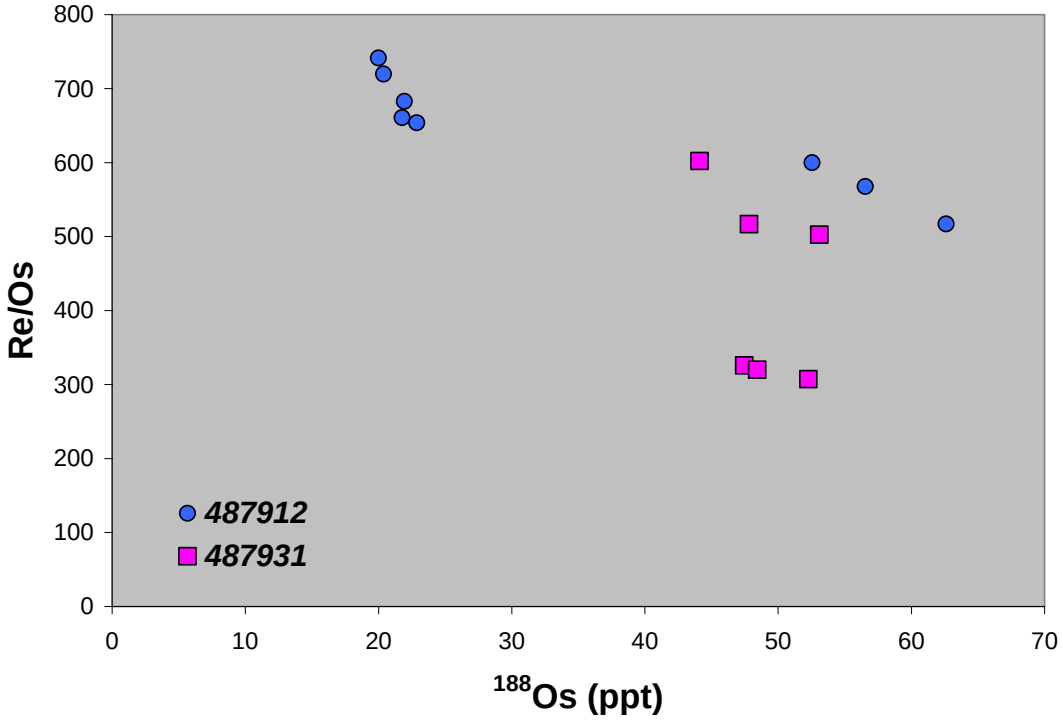

Figure 74. *Common Os expressed as ^{188}Os plotted against Re/Os ratios.*

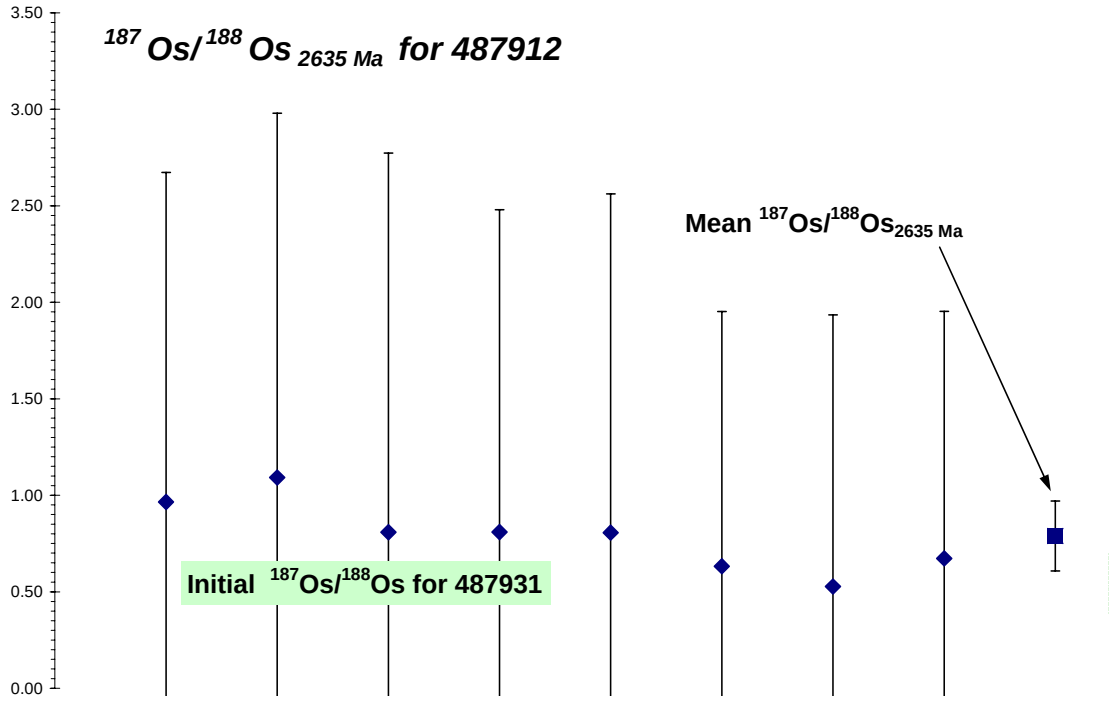

Figure 75. *^{187}Os/^{188}Os at 2635 Ma for 487912.*

Preliminary conclusions

The results from the two samples confirm the previous assumption that two phases of sulphide mineralisation occurred, implying that also the gold mineralisation occurred in two cycles. The younger mineralisation age clearly overlaps with the *c*. 2635 Ma metamorphic event, but the 2714 Ma age is not known as a main metamorphic event in the mineralised supracrustal rocks. However, regionally (e.g. in the rocks of the overlying Færringehavn terrane, this is known as time of coalescence of different terranes and high grade metamorphism. Alternatively, the formation of the first mineralisation in the BD zone, occurred in the volcanic environment, which must have occurred between *c.* 2800 Ma, which is the lower limit for detrital zircon ages in sediments associated with the amphibolites and 2714 ± 53 Ma, which is the date for the mineralisation for the BD zone. The BD zone mineralisation was likely remobilised to form the Main zone at 2636 ± 23 Ma, which seems closely associate with amphibolite metamorphism at Storø.

Geochemistry

Gold mineralisation on central Storø occurs predominantly in the upper, amphibolite-dominated part of the Storø supracrustal belt, in rocks that have been interpreted to have undergone extensive alteration. In order to understand the genesis of the gold, both the origin of the host rocks and the alteration events need to be investigated. The geochemical analyses described here address both of these aspects.

The mineralisation on Storø is mainly associated with arsenopyrite in amphibolite, both in the tectono stratigraphic base and middle of the upper amphibolite sequence. However, the highest gold concentrations are found in zones that contain rock types with mineral assemblages that diverge from the main homogeneous hornblende-plagioclase amphibolites ("a" in map legend). The rock types in the mineralised zone include garnet amphibolites, garnet-biotite amphibolite, calc-silicate-veined amphibolites, garnet-amphibole bearing felsic gneisses (cal-silicate gneisses) and garnet-rich felsic gneisses ± sillimanite. Many of the outcrops with these rock types have been interpreted as altered amphibolites, based on the field observations and preliminary geochemical analyses. Calc-silicate veining, containing diopside, garnet, feldspar, calcite, quartz and calcic amphibole in variable proportions, was interpreted as the metamorphosed result of spilitisation (Eilu *et al.* 2006). Especially the garnet-rich felsic gneisses (also referred to as sillimanite-garnet gneiss), which previously have been interpreted as pelitic paragneisses (e.g. Polat 2005), were shown to have chemical similarities to the amphibolite sequence (A.A. Garde, pers. com. 2005; Eilu *et al.* 2006; Knudsen *et al.* 2007) and interpreted as a product of intense alteration. However, Persson (2007) argued that these rocks were of sedimentary origin. Uncertainty exists to what extent any of the above rock types are 1) altered (and subsequently metamorphosed) equivalents of the main amphibolite, 2) genetically related, but different composition (often more felsic) phases of this sequence, or 3) different rock types (metasediments?) unrelated to the amphibolites. Some of these alternatives were discussed by Eilu *et al.* (2006) and Persson (2007).
Other rock types with questionable origin are the homogeneous garnet-biotite (± sillimanite) gneisses and the garnet-rich iron stones. Some of the garnet-biotite gneisses grade progressively into fine-grained amphibolites of intermediate composition (often biotite-bearing). Because some of the more felsic, biotite-bearing gneisses are apparently alteration products, these field relationships may suggest that also the wide-spread garnet biotite gneiss could be the result of alteration, and that the intermediate amphibolites are the unaltered – or less altered - equivalent. Garnet-rich iron stones and quartz garnetites occur in the middle part of the tectono-stratigraphic section, mainly inside the biotite gneisses, and are generally occurring in close vicinity, or are interlayered. The anastomosing pattern that these rocks display locally favours an interpretation that these rocks are the product of hydrothermal alteration. This hypothesis is tested.

The origin and tectonic setting of the supracrustal sequence is briefly discussed. Of special interest is the systematic variation in the geochemistry of the amphibolites, which might justify a division into two groups and reflect the evolution of the magma in a continental setting.

Here we discuss the major and trace element geochemistry of a collection of samples from Qingaaq and Aappalaartoq mountains to explore to which extent the different rock types might have been derived from a common precursor, presumably basaltic lava, through hydrothermal alteration and metamorphism. We will also briefly discuss a petrogenetic model for the amphibolites that seemingly preserve igneous compositions. The data will also be used in a Masters thesis at the geological institute of Copenhagen university, in which these matters will be investigated more extensively.

Sample collection and analytical procedure

Three sample sets are included in the data presentation and discussion. The larger set was collected during mapping of the Qingaaq and Aappalaartoq sheets in 2006 as part of the GEUS-NunaMinerals A/S contract. In order to improve the statistical relevance of the analytical results, they are supplemented with data from Persson (2007) from samples collected in 2004 for his M.Sc. thesis and data from Polat (2005), which include samples collected east of the map area, but in the same supracrustal belt. The grouping of the samples of Polat (2005) was re-interpreted (see Table 4.3 in Appendix 4), based on his descriptions (field data in GEUS database) and on the sample locations plotted in the map. The analytical data and sample locations are presented in Appendix 4. The samples cover a wide range of rock types, which are grouped as follows:

- HPT amphibolite = main amphibolite (**a**) least altered, high phosphorous-titanium group, lower part of the amphibolite sequence, includes CB and LQ amphibolites of Persson (2007)
- LPT amphibolite = main amphibolite (a) least altered, low phosphorous-titanium group, upper part of the amphibolite sequence
- grt amphibolite = presumably altered, garnet bearing equivalent of the main amphibolite (**a**), some with minor sulphide mineralisation. This group includes two garnetiferous Main Zone (MZ) amphibolites of Persson (2007)
- grt-rich gneiss = silica poor garnet-rich gneiss (**grt**) ± sillimanite and biotite, from top of biotite gneiss sequence (= BD zone gneiss), in contact with the HPT amphibolites.
- grt-calc-silicate gneiss = calc-silicate gneiss with garnet, calcic amphibole, diopside, plagioclase and epidote, commonly banded (**cs**). Occurs within the upper part of the amphibolite sequence.
- biotite gneiss = includes all rock types within the supracrustal sequence of which biotite, quartz and feldspar form the main components. These rocks commonly contain garnet, locally with sillimanite, more rarely cordierite or hornblende. This includes the biotite gneisses (**b**) and hornblende-biotite gneisses (**ab**) as defined in the map legends.
- garnetite-magnetite rock = quartz garnetite and garnet magnetite rock (**if**) forming narrow bands (mainly 1-2m, up to 5 m wide) within the biotite gneisses
- felsic band = A felsic band from the layered amphibolite in the lower part of the tectono stratigraphy (**av**)
- quartzite = quartzite and quartzitic gneiss (**q** and **qmz**)

Abbreviations in brackets refer to labels in the map legend. The last three groups are not plotted in the diagrams. Any amphibolite containing garnet was included in the grt amphibo-

lite group, independent of the percentage of garnet, and includes both “fresh” amphibolite with < 5% garnet, and amphibolites with > 30% garnet and abundant quartz and biotite. All samples from Polat (2005) are marked “(P)” in the diagrams.

All samples collected in the 2006 field season, as well as Persson’s (2007) samples were analysed at the Rock Geochemical Laboratory at GEUS for major and trace elements. Major element oxide compositions were obtained using X-ray fluorescence spectrometry (XRF) on glass discs (sodium borate flux) and atomic absorption spectrometry (AAS) for Na. The samples were analysed for trace elements by inductively coupled plasma mass spectrometry (ICPMS) upon dissolution of fused discs. See Polat (2005) for analytical procedure of his analyses.

Major elements

The different rock types show distinct compositional differences. All rock types, except the biotite gneisses are dominated by iron rich tholeiitic basalt and basaltic andesite compositions (Fig. 76). The biotite gneisses have the highest silica contents ranging between 53.5–64.4 wt% SiO2 and are strongly peraluminous (Figs 77,78). Garnet rich gneisses have low silica between 48.7–55.2 wt% SiO2, overlapping with the amphibolites, and are also peraluminous. This indicates that the current compositions of the rocks in the biotite gneisses and garnet rich gneisses formed through sedimentary or hydrothermal processes. The low silica content of the garnet rich gneisses is consistent with the petrographic observation that these rocks are very poor in free quartz.

There are some systematic differences between the amphibolites and the biotite gneisses and the two rock types form distinct groups in e.g. SiO2-TiO2 space. The biotite gneisses have higher SiO2 contents and tend to have higher Al2O3 and K2O and lower FeOt, MgO and CaO concentrations than the amphibolites (Fig.78). Alkali metals are showing considerable scatter in the SiO2 cross plots, but are well correlated with large ion lithophile elements (LILE) as is shown below, and tend to have higher concentrations in the garnet rich gneiss and garnet amphibolite. Al2O3 is inversely correlated with SiO2 for the biotite gneisses, while the amphibolites have a weakly correlated positive slope. A negative slope is commonly seen in sedimentary rocks, and reflects the decreasing feldspar content in more mature silica rich sediments. The garnet-calc-silicate gneisses have lower Ca than the amphibolites, which might be due to spilitisation of the amphibolites, as suggested by Eilu *et al.* (2006). To summarise, the garnet rich gneisses are generally showing considerable compositional overlap with the amphibolites, while the biotite gneisses have a distinctly different compositional range.

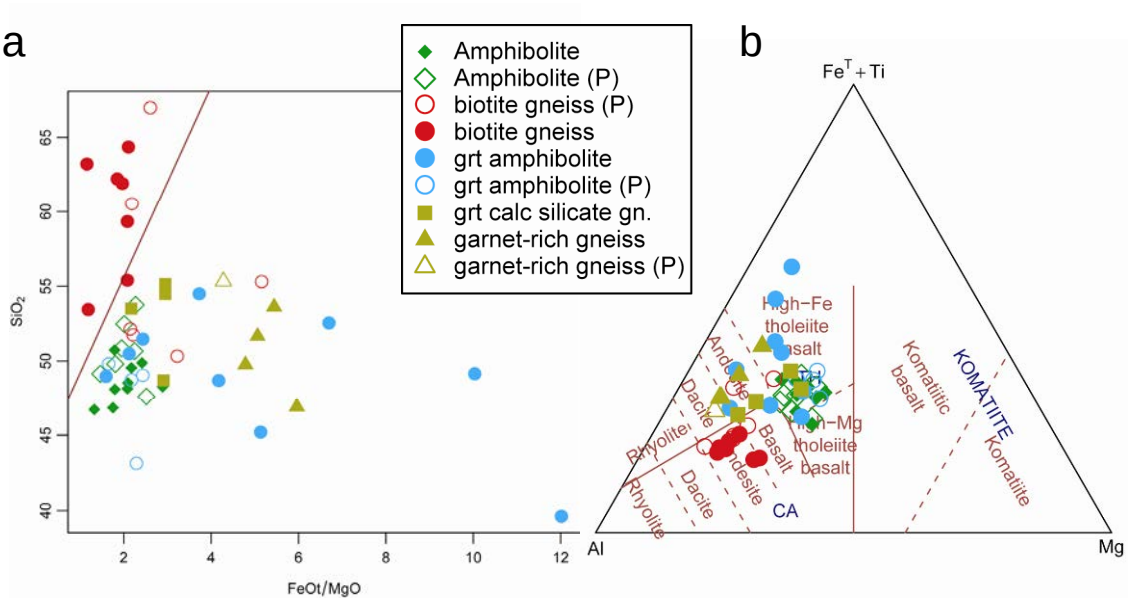

Figure 76. *Classification diagrams showing the composition of the different rock type groupings. a) FeOt/MgO versus SiO2 of Miyashiro (1974) shows a clear distinction between most of the biotite gneisses that plot along a calc-alkaline trend (i.e. steeper than the red reference line), while all others (including three biotite gneisses) plot along a tholeiitic trend. b) In the Jensen (1976) diagram the biotite gneisses plot predominantly in the andesite field, while the remainder plot in the andesitic and theoretic basalt fields. Open symbols marked with (P) are data from Polat (2005).*

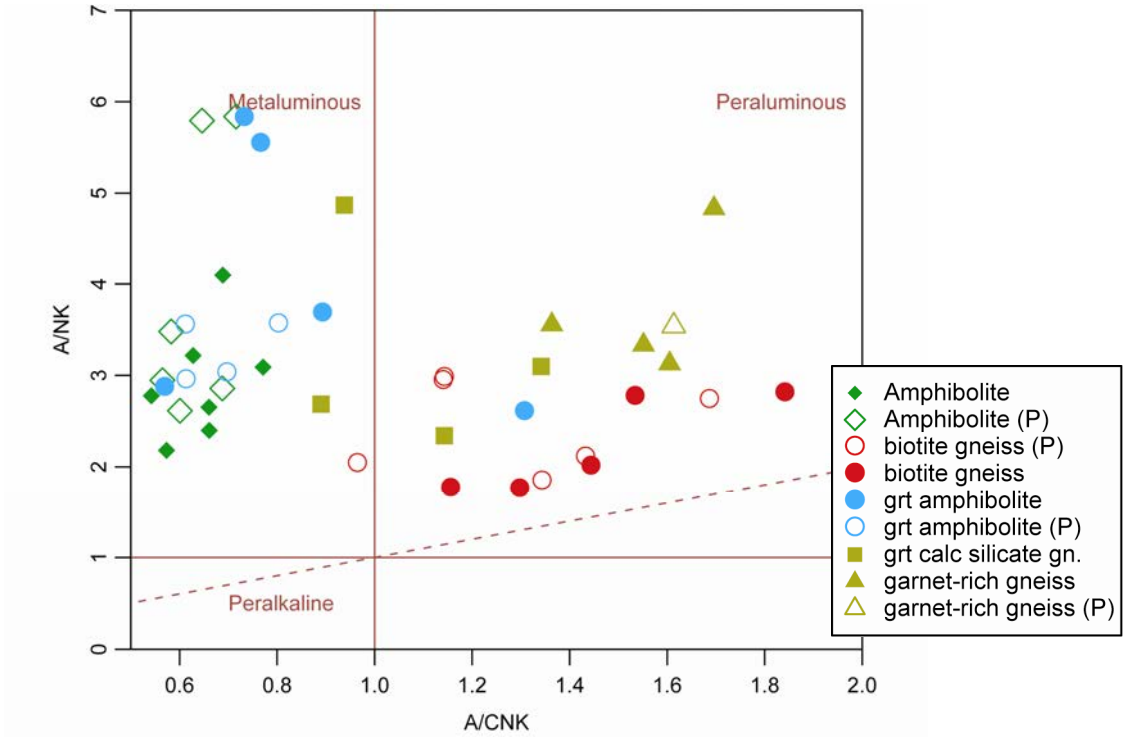

Figure 77. *Aluminium-alkali saturation diagram showing the overall peraluminous compositions of the biotite gneisses and garnet rich gneisses, while the amphibolites and garnet amphibolites plot in the metaluminous field, with the exception of one garnet amphibolite.*

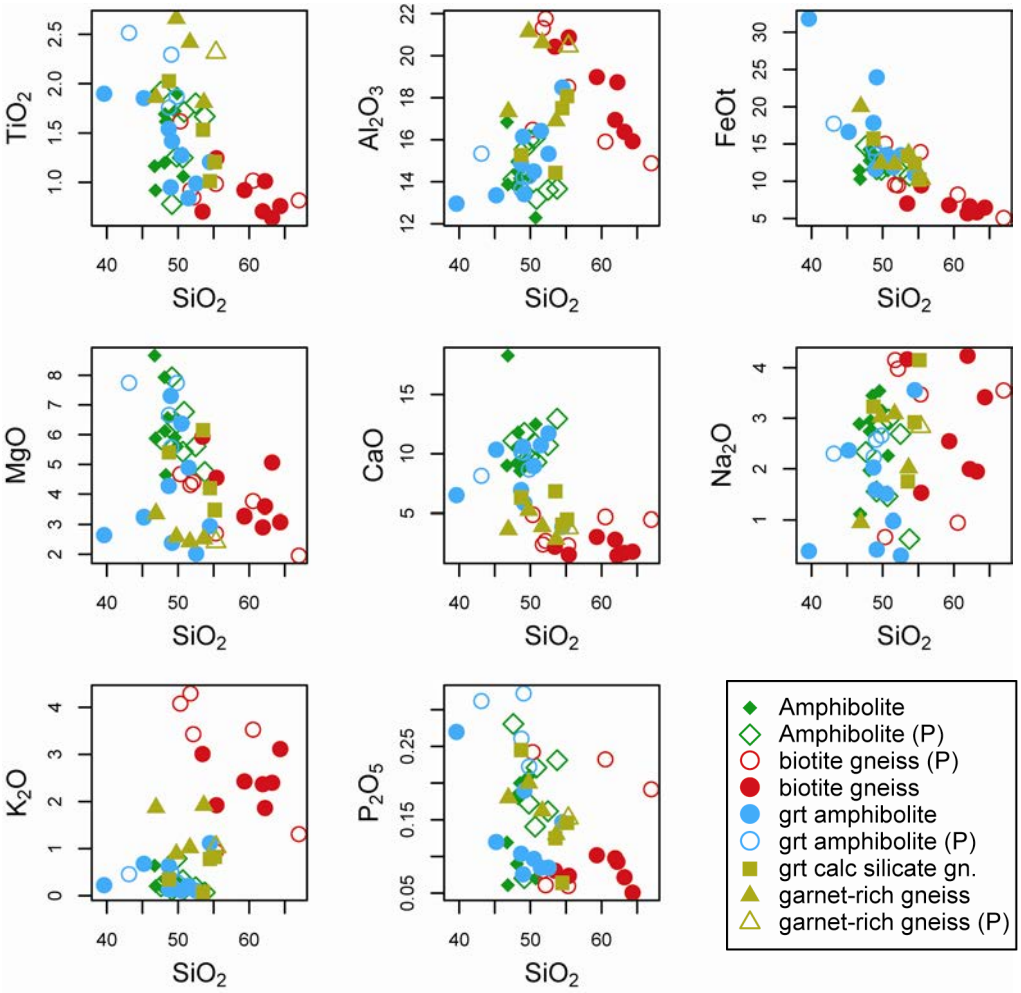

Figure 78. *Silica variation diagram for the major elements. Samples marked with (P) are from Polat (2005).*

Trace elements

There is considerable and systematic variation in the trace element abundances of the different rock types as seen in the mantle normalised variation diagram in Fig. 79. The large ion lithophile elements (LILE) display considerable scatter and range three orders of magnitude, where the biotite gneisses and garnet rich gneisses have systematically higher concentrations than the amphibolites. This is in good agreement with K2O, which is positively correlated with Rb and Ba (Fig. 80). However, the LILE are uncorrelated with immobile elements such as Zr, which are also enriched due to volume changes in the alteration hypothesis (Fig. 80).

The amphibolites display large scatter in the most incompatible elements (i.e. the left end of the diagram) but flatten out towards the less incompatible elements. Most samples have strongly positive U and Pb peaks. Three amphibolite samples have a divergent composition in that they have strongly enriched Rb, Ba and K, and lack a positive U peak, and in this way resemble some of the garnet rich gneisses. These three samples are inferred to have been affected by alteration during syn-volcanic hydrothermal activity and/or during metamorphism, and are omitted in the comparison to the other rock types in Figs 79b–d. The

different gneisses all have significantly higher light trace element concentrations than the amphibolites, with a clear negative slope for the biotite gneisses, with positive K and Pb peaks, and distinct negative Sr and Ti anomalies. In the right-hand side of the diagram, the garnet rich gneisses have slightly elevated compositions, with a marked negative Sr anomaly. Although similar to a large extent, the garnet rich gneisses have distinctly lower mid to heavy REE (Gd/YbN) ratios than the biotite gneisses. Garnet calc-silicate gneisses follow the amphibolites well in the heavy end, but show an increased scatter at the lighter trace elements. Garnet amphibolites overlap largely with the “unaltered” amphibolites, especially in the heavy end, with the main exception of a markedly higher Rb concentration.

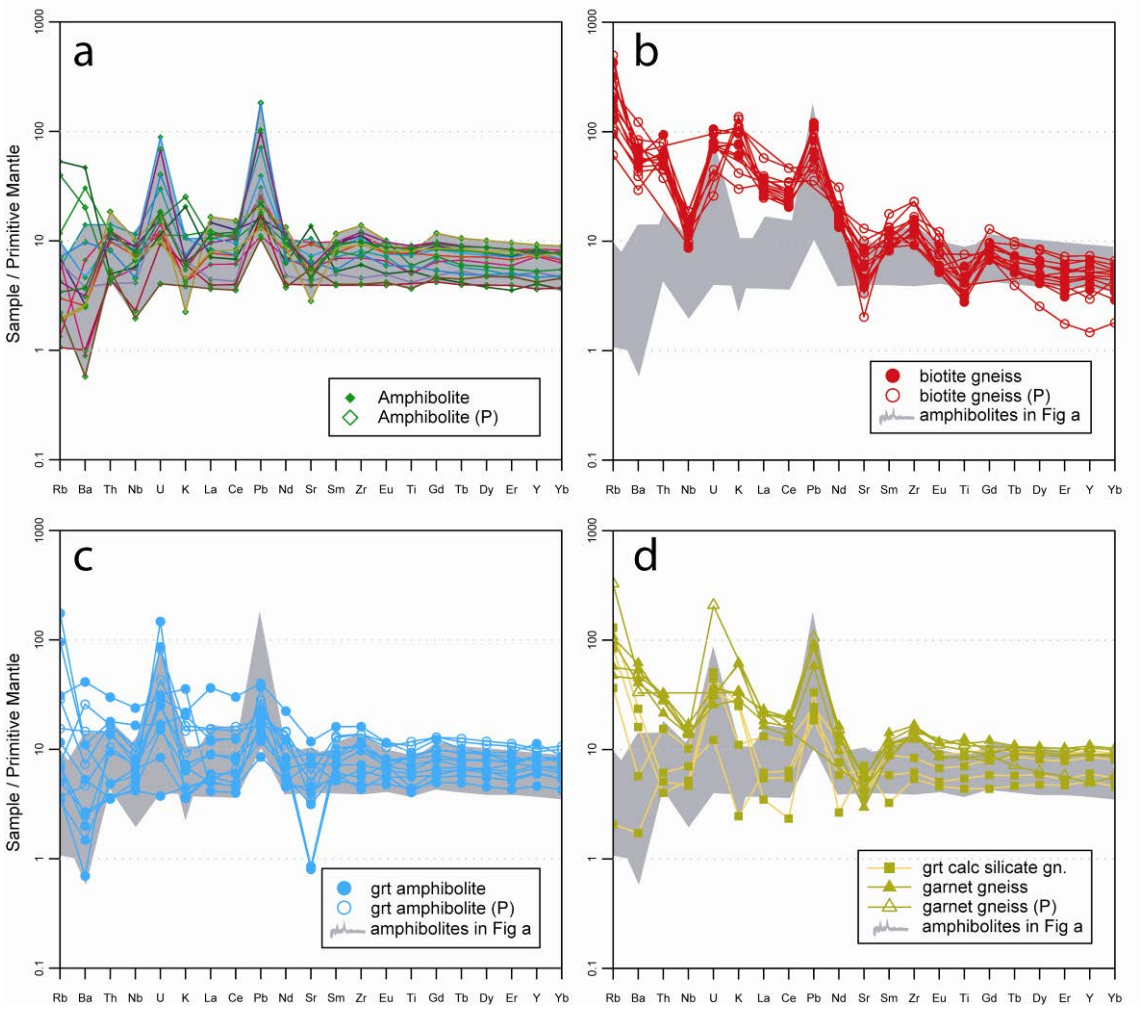

Figure 79. *Trace element variation diagrams normalized to primitive mantle of Palme and O’Neill (2003). Each of the main rock type groups is plotted separately, with the area covered by the amphibolites in a) indicated by the grey field. This amphibolite field in figures b–d does not include 3 samples, which have a distinctly different composition (see text). Element abundances for the biotite gneisses are greater than for the amphibolites for the most incompatible elements, while there is considerable overlap in the right-hand part of the diagram. The positive Pb-spikes are distinctive for the continental crust and arc related rocks, and might be a primary signal reflecting arc processes or continental crust contamination or due to Pb mobility during secondary metamorphic processes.*

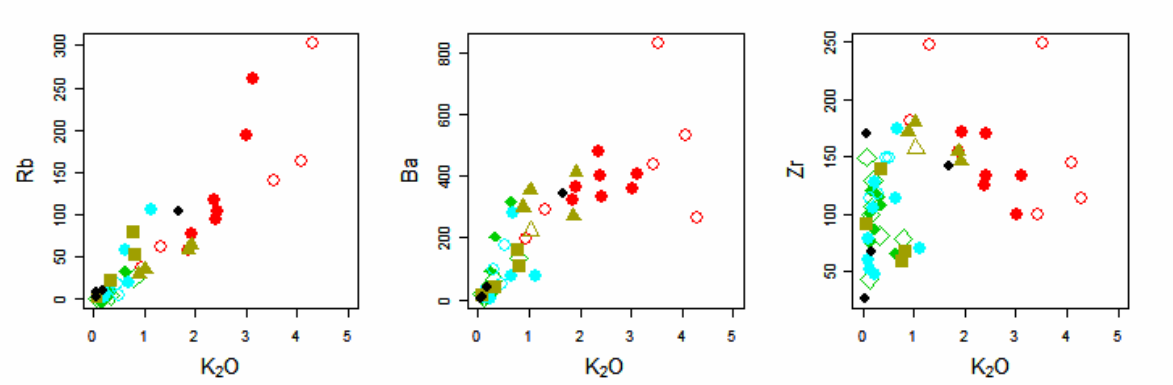

Figure 80. *K2O variation is well correlated with Ba and Rb, but not Zr. LILE enrichments and excessive scatter in mantle normalised trace element variation diagrams is likely due to element mobility during alteration or metamorphism, but not simply related to volume changes, which cause relative Zr enrichment.*

Rare earth element (REE) abundances provide important constraints on rock petrogenesis (Fig. 81). REE are generally incompatible and immobile elements and igneous crystallisation tends to fractionate them such that their relative abundances are moved in a parallel fashion. There is a clear distinction in slope between the amphibolites and the biotite gneisses. The garnet rich gneisses plot above the amphibolites with a slightly steeper slope. Grt-calc-sil gneisses and grt amphibolites scatter in the left side of the diagram, and lie within the amphibolite field in the heavy part. The amphibolites have flat relative REE abundances, while the biotite gneisses are enriched in the light REE (La to Sm), but not in the heavy REE (Dy to Lu). If the biotite gneisses were derived from the amphibolites, this would require a process that provides relative enrichment of the light REE.

Testing the alteration hypothesis

Persson (2007) extensively discussed the relationship between the garnet rich gneisses (referred to as biotite gneisses in his thesis) and the amphibolites. We will test the hypothesis that the biotite gneisses or garnet rich gneisses were derived from the amphibolites through alteration processes using a similar approach adding the data of Persson (2007) to our dataset. We make the assumption that volume change due to element mobility is the main process in changing the compositions of the altered rocks. Such a scenario implies that an immobile element will only be enriched or diluted through the addition or removal of other elements, and, importantly, the ratio of two incompatible immobile elements will remain constant (Fig. 82).

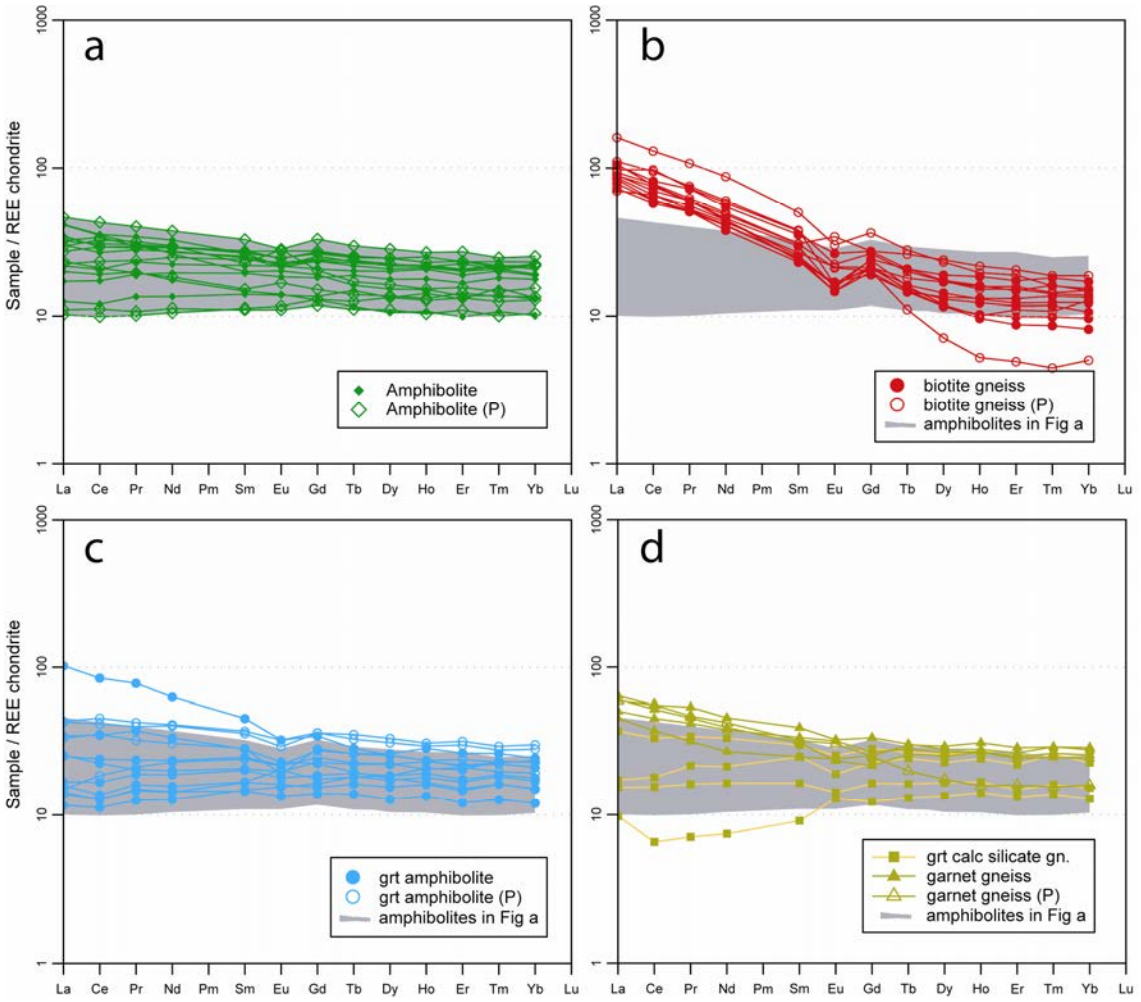

Figure 81. *Chondrite normalised (normalisation values from Palme & O'Neill, 2003) Rare earth element (REE) diagram for the samples from Storø. The amphibolites (a) have flat slopes, with the exception of one garnet amphibolite (c). The biotite gneisses (b) are enriched in the light REE, but are slightly depleted in the heavy REE, compared to the amphibolites. The garnet rich gneisses (d) follow the biotite gneisses in the LREE, but are the most enriched in the HREE. Garnet calc-silicate gneisses (d) are rather flat, with one exception with a negative slope, but have a wide scatter, especially in the LREE end.*

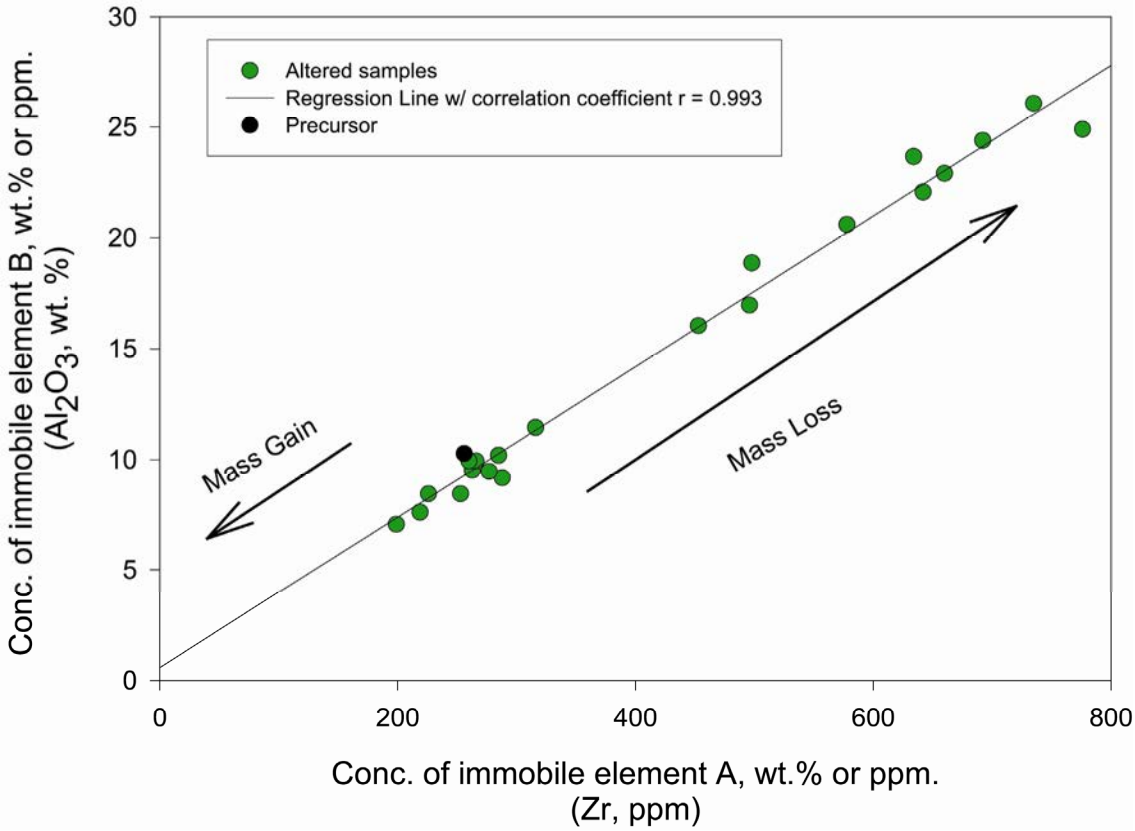

Figure 82. *An immobile – immobile element plot with a common regression line and a high correlation coefficient indicates a common precursor for the altered rocks. This diagram is from Persson (2007) and shows data of MacLean & Kranidiotis (1987).*

Zr is normally immobile during metamorphism, mainly because it is largely bound to the mineral zircon, which is extremely resilient to alteration, and which is preserved in these rocks. Zr is positively correlated with TiO2 and REE in most rock types which implies that these elements were more or less immobile during metamorphism and/or alteration (Fig. 83). The garnet rich gneisses show a clear enrichment compared to the other samples. The biotite gneisses plot along a parallel trend displaced from the corresponding amphibolite array and show overall more scatter. This emphasises the difference between the garnet rich gneisses and biotite gneisses and precludes a simple mass change to explain the origin of the biotite gneisses in terms of an altered amphibolite precursor. For instance, the rotation noted in the REE profiles (Fig. 81), requires loss of heavy REE and while, at the same time, light REE were added to the rock. Light REE enrichment can be achieved through the addition of e.g. a phosphate mineral, where apatite and monazite have strong light REE enrichment. This addition would have to work in concert with the removal of heavy REE, e.g. by the removal of a garnet component, which tend to have enriched heavy REE abundances. Following such a line of argument, it is predicted that P should be positively correlated with light REE and there should be a corresponding decrease in Al2O3 with decreasing heavy REE. None of the predicted trends are observed, however. La is positively correlated with P2O5 for the amphibolites, presumably reflecting igneous fractionation rather than alteration, while the biotite gneisses are uncorrelated (Fig. 83). Furthermore, high La is associated with relatively low P2O5, precluding simple mass loss or phase removal to explain the differences (Fig. 84). Similar decoupling is noted for Al2O3

and the REE (Fig.85), and the variations in the biotite gneisses are not readily explained by fluxing a garnet component.

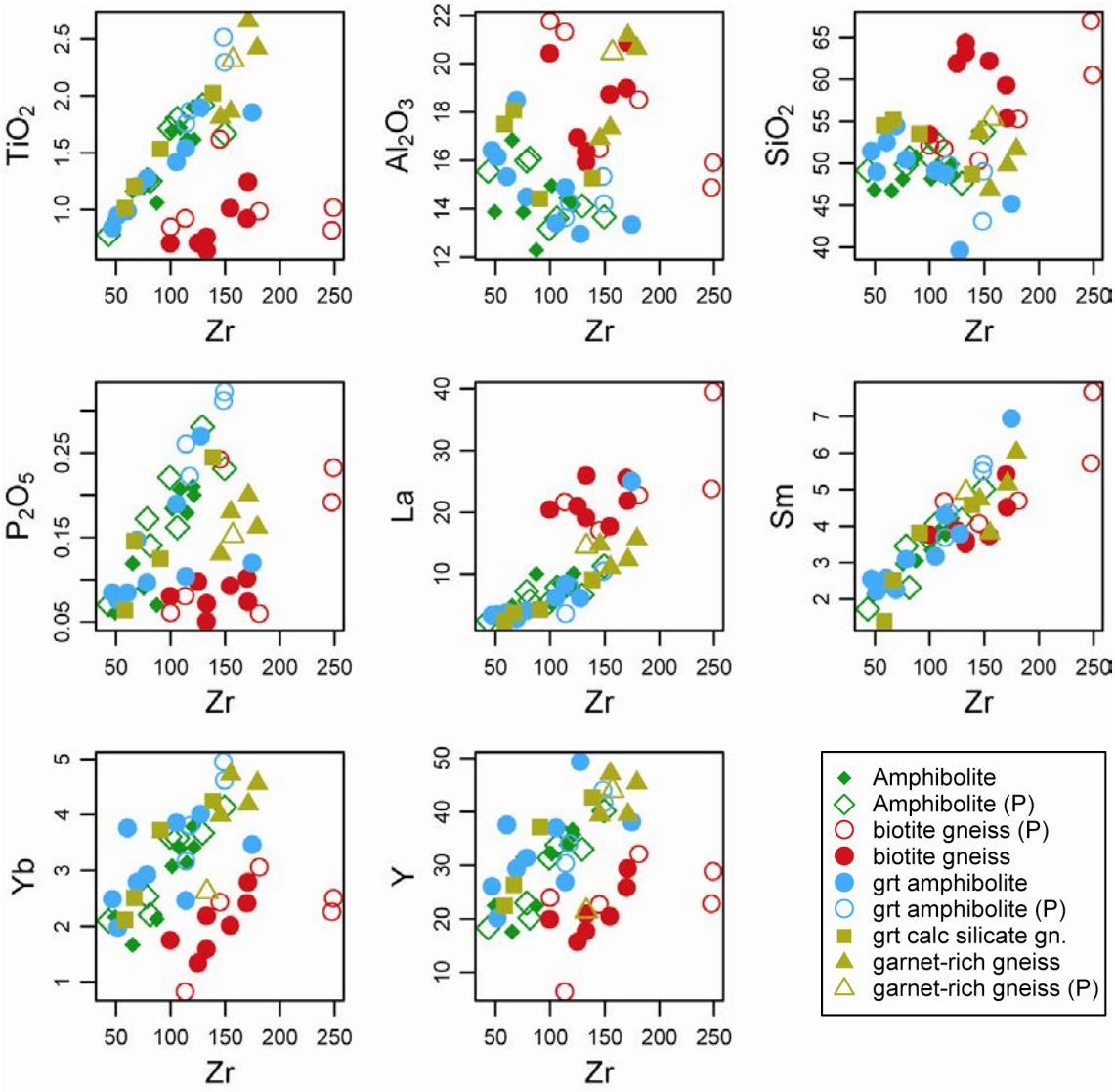

Figure 83. *Zr (immobile) –immobile element plots. The biotite gneisses scatter or form a separate trend, while all other rock types generally lie on a single fairly well-defined correlation line. The Garnet rich gneisses are enriched in the immobile elements.*

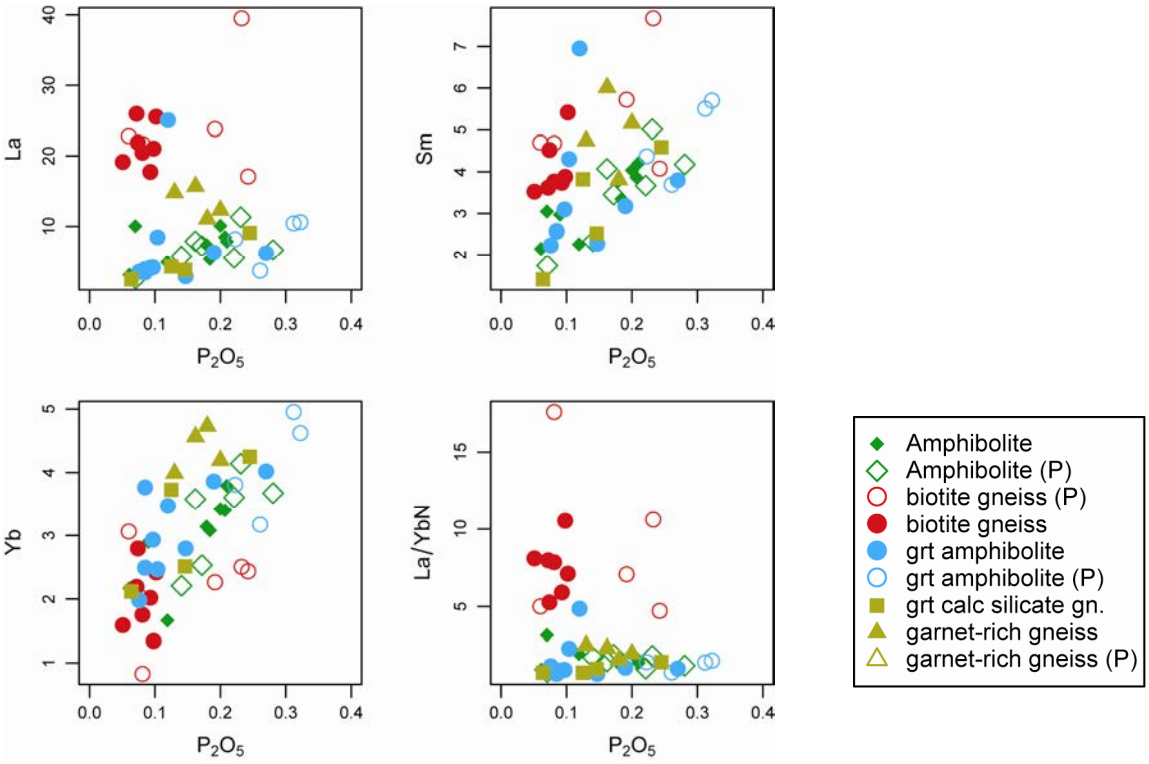

Figure 84. *P2O5 plotted against REE. The biotite gneiss inverse correlation for La and LaN/YbN is contrary to the prediction.*

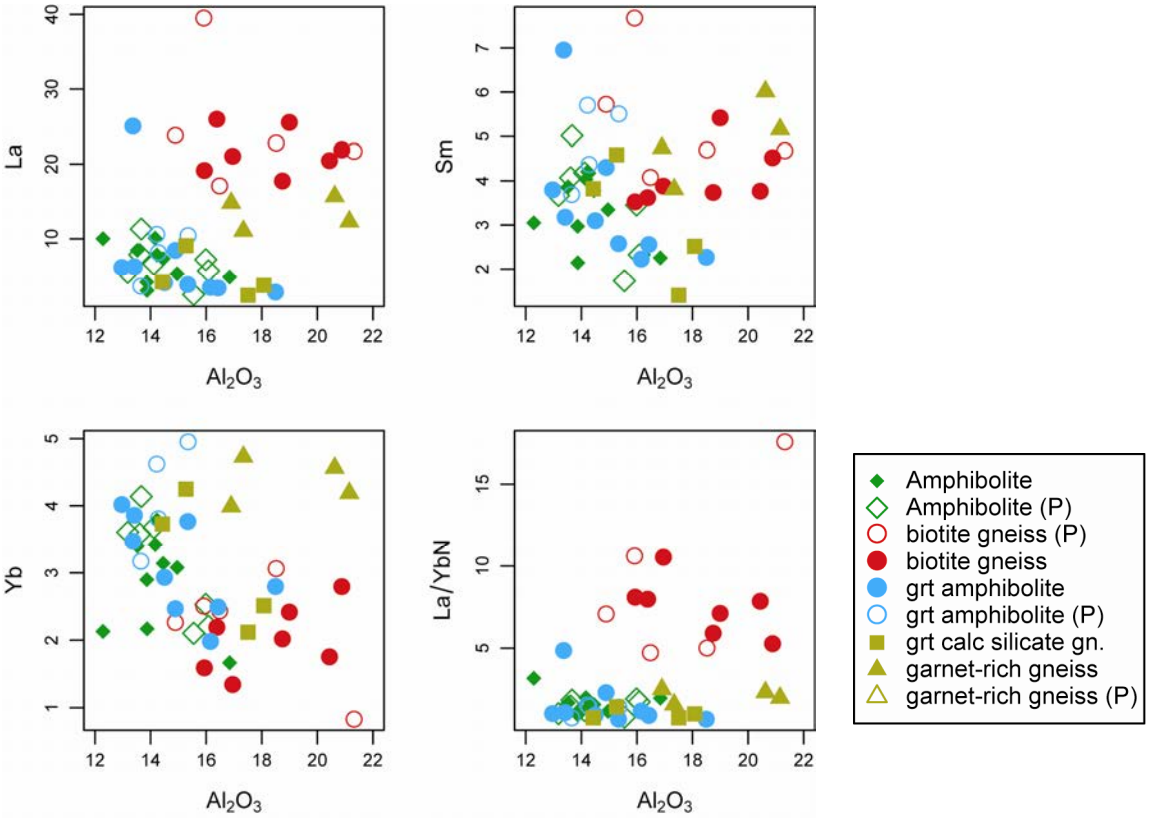

Figure 85. *Al2O3 plotted against REE. Correlations are generally poor for the biotite gneiss.*

Alkali metals and LILE are notoriously mobile and readily depleted or enriched during metamorphism. It might thus be anticipated that these elements will record alteration processes, and given the ubiquitous biotite in the biotite gneisses, we expect that K2O will be positively correlated with immobile elements that were enriched through volume changes (Fig. 86). Given the biotite enrichment in presumably altered rocks, K2O must have been added from the metamorphic fluids to the altering rock despite its mobile character, and K2O should be positively correlated with elements that were enriched through alteration. Conversely, K2O might be expected to be negatively correlated with elements that were removed from the altering rock. It may be concluded that heavy REE and TiO2 have been largely immobile in these systems, but their inverse correlation is contrary to our prediction. However, other elements that would have been preferentially enriched, e.g. La, are positively correlated with K2O.

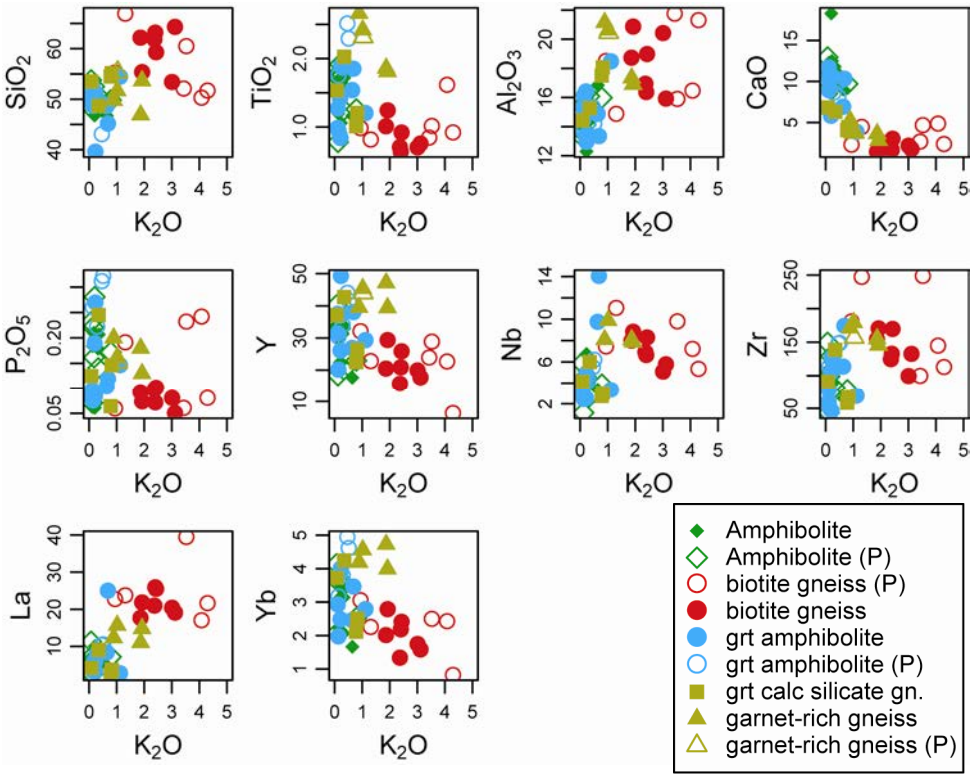

Figure 86. *K2O variation diagrams for major- and immobile trace elements.*

Chemistry of garnetites and garnet magnetite rocks

Five samples in the dataset are labelled similarly as garnet-magnetite rocks (Table 4.1 in Appendix 4) but consist of three distinct rock types: **quartz garnetites**, containing predominantly garnet, with minor quartz and magnetite ± biotite; **garnet magnetite rocks** (for brevity here referred to as ironstones), containing magnetite, quartz and garnet (almandine), often occurring in thin nearly monomineralic layers, resembling (but not to be confused with) banded iron formations. Minor grunerite occurs locally; **hornblende garnetite** occurs in a late, discordant quartz vein system in the garnet calc-silicate gneiss west of Main Zone

and contains beside garnet and hornblende (+ calcic amphibole) also minor diopside and epidote. These two former rock types (labelled together "**if**" in the map legend) are interlayered and occur as 1-5 m wide bands within the biotite gneisses interlayered, commonly with sharp internal contacts. The garnet-magnetite rocks occur rarely isolated. These bands are irregular and form an anastomosing pattern and are isoclinally folded (i.e. predate earliest deformation). The chemistry of these five very garnet-rich rocks is compared to that of the other rock types, in order to test whether these rocks are hydrothermal alteration products, as tentatively interpreted from field observations (cf. Eilu *et al.* 2006).

The three rock types have distinct compositions. They are variably enriched in Fe with contents of *c.* 15 wt %, 26–27 wt % and *c.* 43 wt % FeOt in the hornblende garnetite, quartz garnetite and ironstone respectively. Only SiO_2 is relatively constant at values between 43–45 wt%, while the other major elements are rather scattered (Fig. 87). Quartz garnetites and ironstones are low in Ca and Na. The hornblende garnetite plots together with the garnet calc-silicate rocks for most elements, but has considerably higher Ca and Mn than any other sample, presumable because the garnets are likely relatively grossular-spessartine-rich. The two ironstones have similar major element compositions, while the two garnetites are distinct with respect to some of the elements.
Zr-multi element plots (Fig. 88) show that one of the quartz garnetites plots in the biotite gneiss field, while the other quartz garnetite and the hornblende garnetite plot in the amphibolite field. The ironstones appear to lie on the amphibolite trend, but plot so close to the origin that this is uncertain. In a Zr-TiO2 plot of Eilu *et al.* (2006), the garnet magnetite rocks appear to plot closer to the trend of the biotite gneisses.

A possible origin for these rocks is by mass transfer during alteration, which is the working hypothesis. If correct, it follows that immobile elements are enriched during volume decrease (i.e. loss of mobile elements) and diluted during volume gain. This assumption requires these rocks to have formed by both volume gain and volume loss as they are more or less enveloping the observed concentration range. Rare earth element (REE) plots (Fig. 89) hint to different source rocks, where one of the garnetites has a pattern that is similar to that of the biotite gneisses (Fig. 81b). The other garnetite sample seems to be more conform the amphibolites, but has the Eu anomaly typical of the biotite gneisses. Although the hornblende garnetite lies within the amphibolite REE field (Fig. 89), its slope is opposite to that of the amphibolites, like some of the garnet calc-silicate gneisses (Fig. 81d) in which this rock occurs.

At present the number of data is too small to draw definite conclusions. It appears that the garnet magnetite rocks and the quartz garnetites, although interlayered, might have different origins. Only one of the garnetites has similarities to the biotite gneisses in which it occurs. The hornblende garnetite in the quartz vein system has a clear association with its host garnet calc-silicate gneisses.

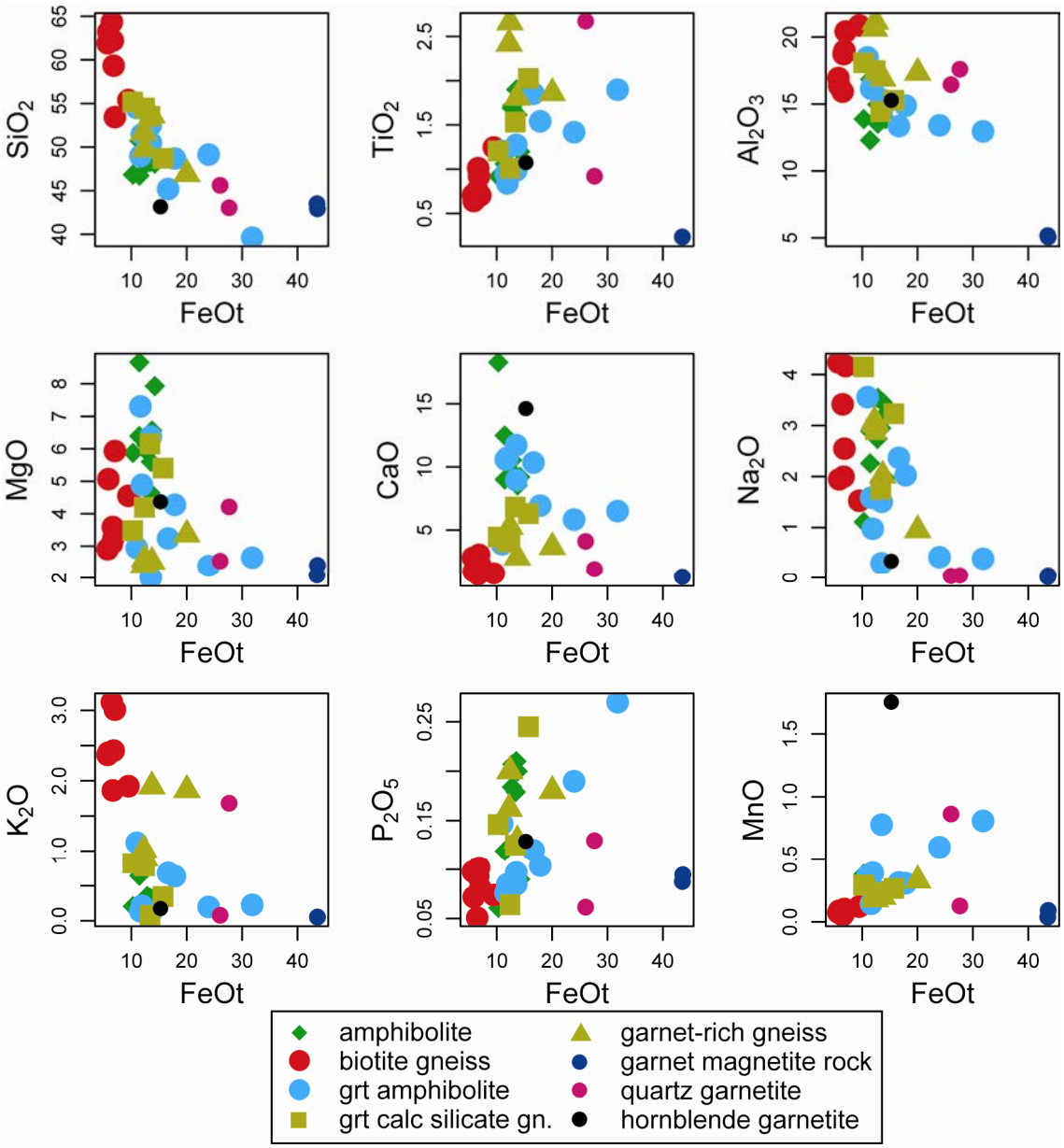

Figure 87. *Total iron oxide variation diagrams for major elements (all wt %).*

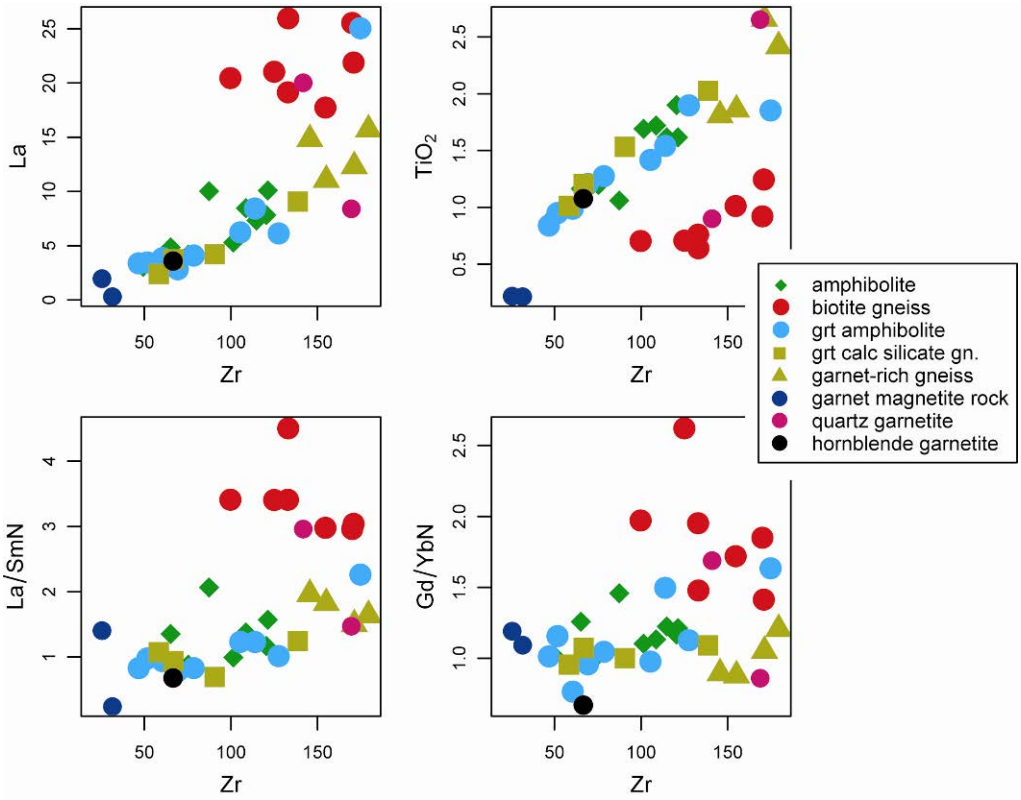

Figure 88. *Zr plotted against La, TiO2 and REE ratios. Note that one of the quartz magnetite rocks consistently plots in the field of the biotite gneisses, while the other garnet-rich lithologies plot in the amphibolite trend.*

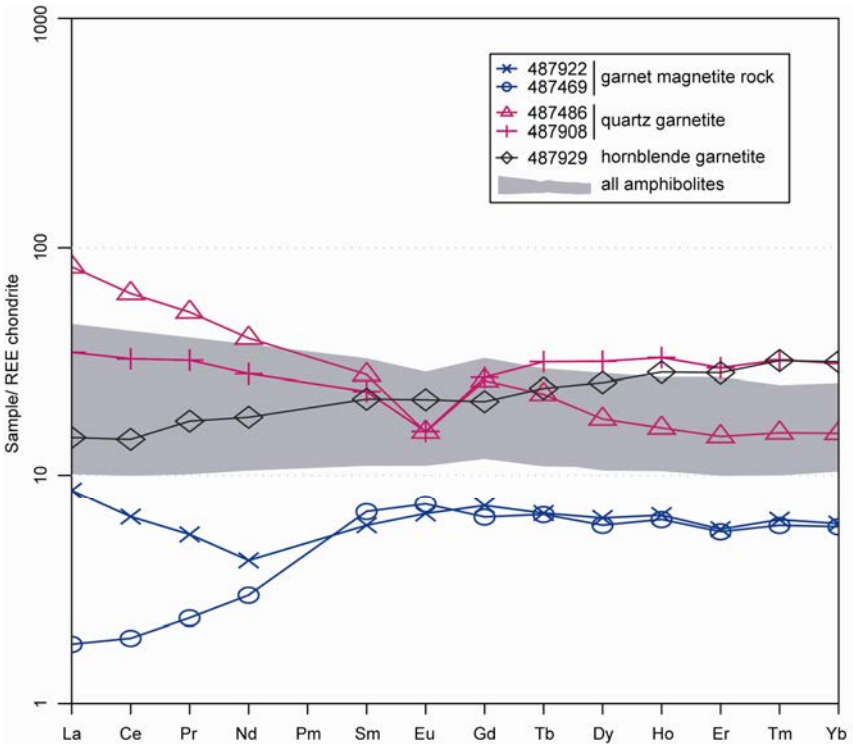

Figure 89. *Chondrite normalised Rare earth element (REE) diagram for the garnetites and ironstones (normalisation values from Palme & O'Neill, 2003).*

Main conclusions about alteration

the biotite gneisses plot with distinctly different trends and are not derived by alteration from the main amphibolite sequence. The data are in accord with an interpretation as metasediments. Although, in some of the plots (e.g. AFM and Jensen), 1-3 biotite gneisses plot on the amphibolite trend, and need to be investigated more carefully.
The garnet amphibolites, garnet calc-silicate gneisses and garnet rich gneisses all plot in the same fields/trends as the amphibolites and might be genetically related.
The garnet rich gneisses, which occur at the lower contact of the amphibolite sequence, plot closest to the HPT amphibolites (defined below). Their chemistry is consistent with the interpretation that they were derived from a rock type that is genetically linked to the amphibolites.
The garnet calc-silicate gneisses, which are exposed in the higher part of the sequence, plot closest to the LPT amphibolites (defined below).
The garnet amphibolites show a large spread but overlap with both groups of amphibolites, and are likely an altered variation of the amphibolites (which is in agreement with the fact that they were observed to grade into each other).

Petrogenesis

Despite the metamorphic and alteration history of the amphibolites from Storø, it is possible to make deductions about their origin. We only assess the least altered amphibolites as these are the only rocks that are of relatively unambiguous igneous origin. Garnet rich amphibolites, which might have disturbed element ratios, were excluded from the dataset. The rocks plot in the iron-rich tholeiitic basalt field and in the basaltic andesite field (Fig. 76). They can be divided into two groups, based on TiO2 and P2O5 for a given SiO2 (Fig. 90). The group with the higher TiO2 and P2O5 is called the HPT amphibolite (high TiO2-P2O5) and the group with the lower TiO2-P2O5 is the LPT amphibolite (low TiO2-P2O5). Furthermore, this subdivision seems justified on the basis of incompatible trace elements. The geochemical differences seem to be systematic with outcrop relationships and our inference is that the LPT amphibolites overlie the HPT amphibolites. Such a stratigraphic correlation implies a temporal change in the geochemistry of the amphibolites, which likely reflects an evolving or changing source rock.

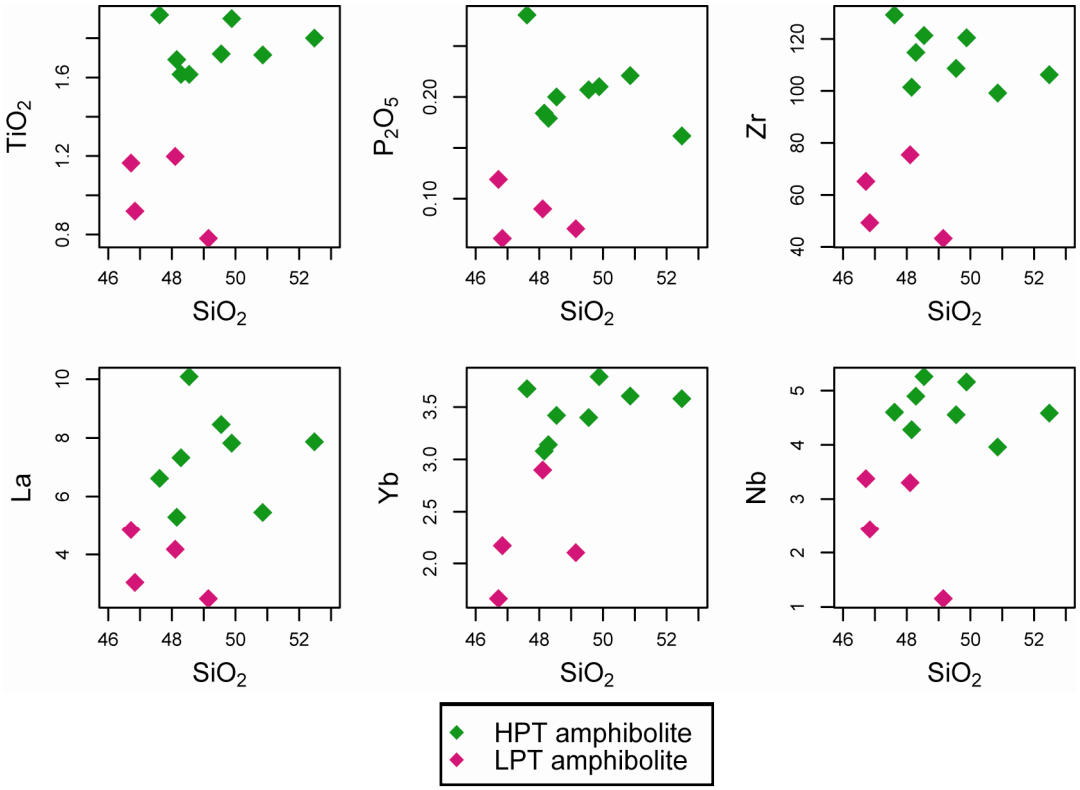

Figure 90. *Variation diagrams for TiO2, P2O5, and several elements against SiO2. The amphibolites plot along two trends, one with higher Ti and P for a given SiO2, the high phosphorous-titanium group (HPT), and the other called the low phosphorous-titanium group (LPT).*

The amphibolites are characterized by large scatter in the large ion lithophile elements (LILE), which is ascribed to metamorphic mobility, and it is assumed that Rb, Ba, U and K have no petrogenetic significance (Fig. 91). High field strength and immobile and incompatible elements such as REE and Nb are more likely to record important petrogenetic information as these element ratios are less likely to be disturbed during metamorphism. Multi element variation diagrams highlight the LILE mobility, which are not considered any further. Distinct positive Pb-anomalies and low Ce/Pb is indicative of subduction related volcanism and a typical signature of the continental crust, which prevails in all samples (Hofmann 1997). Ce/Pb of the Storø amphibolites are relatively constant and substantially lower than those found in modern oceanic volcanic rocks, they do not plot along any obvious mixing curve, and at face value, they might record a primary signal that is flagging arc processes (Fig. 92). However, as Pb-enrichment is a characteristic feature of the continental crust, this signature might be secondary due to Pb-mobility in the crust.

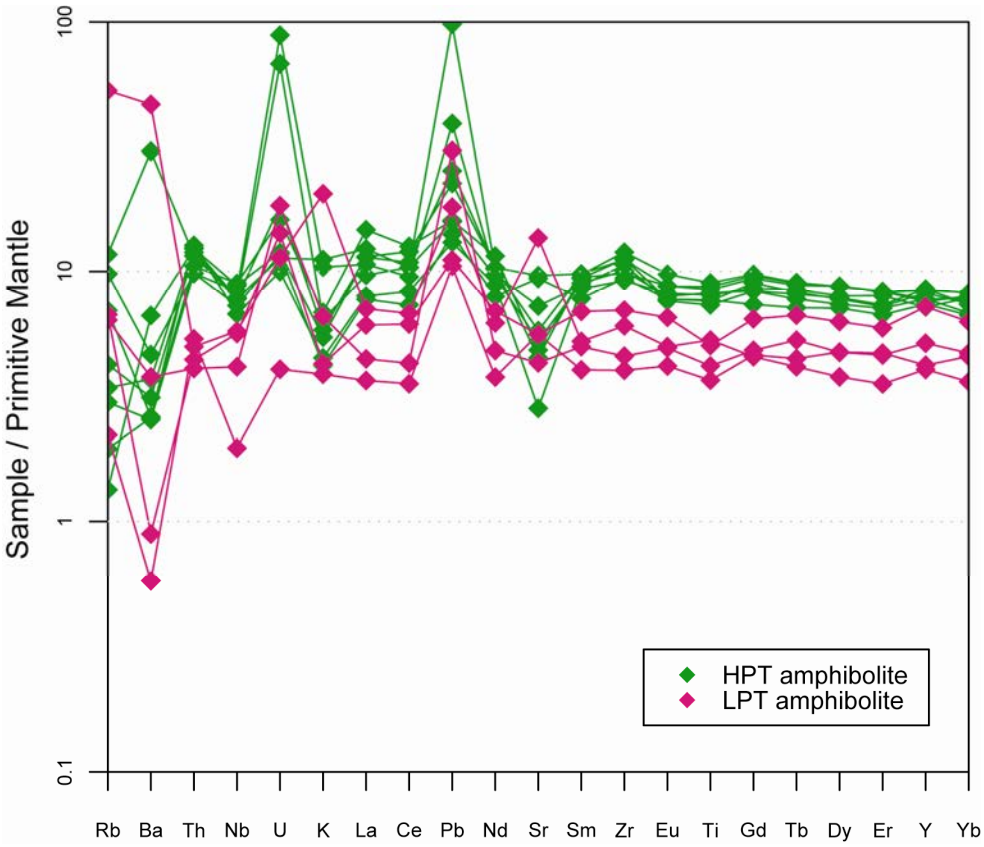

Figure 91. *Primitive mantle normalized multi element diagram (normalisation values from Palme and O'Neill, 2003) for the HPT and LPT amphibolites. Samples include those from Polat (2005) that could be identified as belonging to the upper or lower part of the tectono stratigraphic sequence, based on occurrence in the field.*

The LPT amphibolites are characterized by relatively flat overall REE patterns ((La/Yb)N =0.7-1.0; (La/Sm)N =0.7-0.9), while the HPT amphibolites are more enriched in the light REE (La/Yb)N =1.2-2.0; (La/Sm)N =1.0-1.6; Fig. 93). Furthermore, the inferred temporal decrease in the overall REE slopes (i.e. decreasing (La/Yb)N) is coupled with increasing Nb/La (Fig. 94). The higher Nb/La values are similar to modern MORB and OIB. This signals a transition towards an increasingly depleted mantle source for the LPT amphibolites, or that the magmas saw less lithospheric or crustal interaction over time. A plausible scenario for such a temporal change might be a rifting environment with an increasing relative amount of asthenospheric mantle in the basalt source. The rifting might be related to back-arc extension or continental break-up.

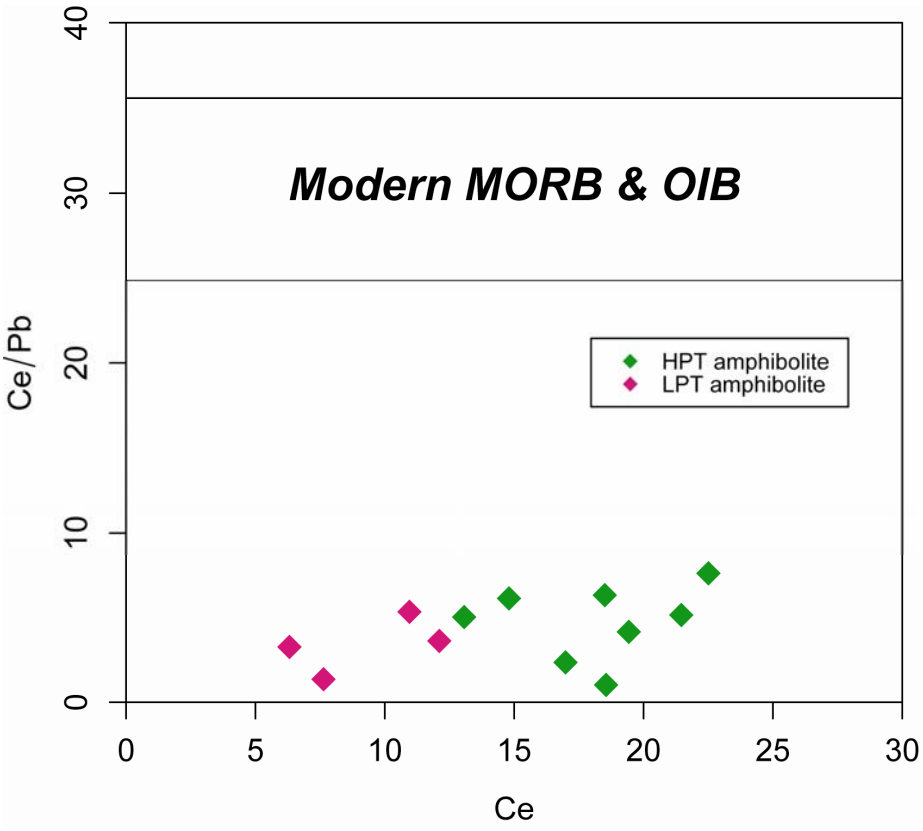

Figure 92. *Ce (ppm) plotted against Ce/Pb. The Storø amphibolites have low arc or continental crust like ratios, but this may be a contamination artefact. See text for discussion.*

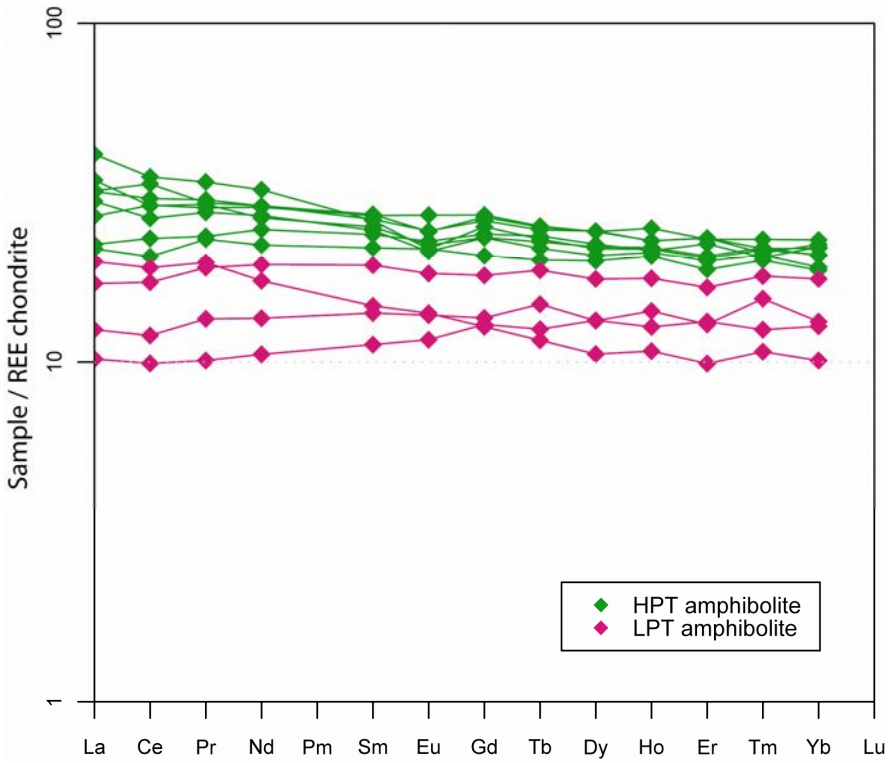

Figure 93. *Chondrite normalised rare earth element diagram for the Storø amphibolites. Normalisation values from Palme & O'Neill, 2003.*

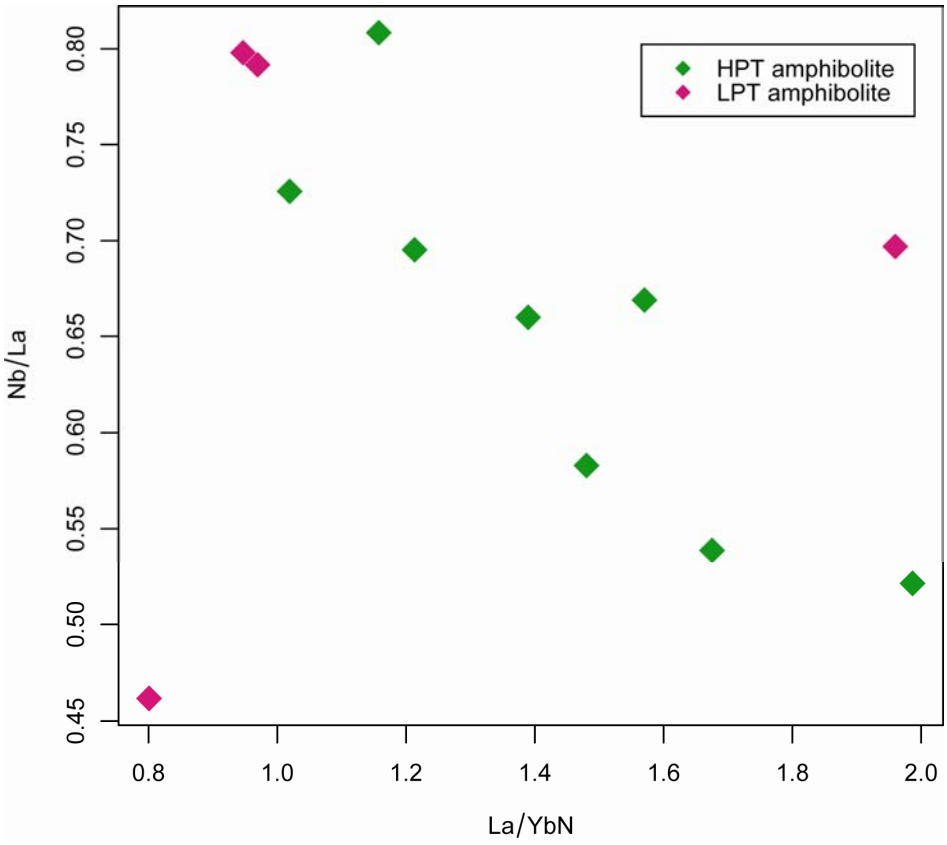

Figure 94. *Chondrite normalised (La/Yb)N plotted against Nb/La ratio for the amphibolites.*

Conclusions

The hypothesis that the biotite gneisses are derived from the amphibolites through alteration is not easily reconciled. The biotite gneisses rarely plot along predicted trends or mixing lines such that their element abundances can be explained in terms of simple volume loss or gain. Additional mineral phases would be required in order to decouple e.g. the light rare earth elements from the heavy. However, the data can not be fitted with likely such mineral phases, and we conclude that, although there may have been some level of alteration in the biotite gneisses, these are not derived from the amphibolites. Their origin remains unclear, and has not been addressed here, but a volcanic or sedimentary origin remains viable alternatives.
On the other hand, the garnet rich gneisses, garnet calc-silicate gneisses and garnet amphibolites, do plot along similar trends together with the least altered amphibolites, and there are no geochemical evidence against these rocks being amphibolite alteration products. Furthermore, field observations of transitional changes between different rock types is indeed suggestive of such an origin.

The amphibolites display systematic variations in their chemistry, and consist of tholeiitic basalt compositions. They form two subgroups with distinct differences, which we interpret as reflecting a gradational change in their source with time. In the current stratigraphic in-

terpretation, this implies a change towards lower TiO2, P2O5 and incompatible trace element concentrations for a given SiO2 value. Ce/Pb ratios are reminiscent of subduction processes, but these ratios have to be treated with caution as Pb may have been mobile in the crust, rendering these ratios only reflecting secondary processes. However, the secular changes in Nb/La ratios are suggestive of crustal or lithospheric involvement, and our preferred model is an extensional environment with an increasing component of asthenospheric mantle. This environment might be a back-arc system or an extensional basin in response to continent break-up.

Discussion and conclusions

The multitude of data presented in this report give a much improved overview of the geological framework around the gold mineralisations on northern Storø. Although improved, the understanding is not complete and many uncertainties remain. Here we discuss and summarize the main results of this cooperative project between GEUS and Nunaminerals A/S.

The Storø supracrustal belt comprises a sequence of metavolcanic and metasedimentary rocks, likely deposited in the early Neoarchaean, and affected by at least one early phase of hydrothermal alteration and a later phase of amphibolite facies metamorphism (Hollis *et al.* 2005; Knudsen *et al.* 2007). Amphibolites in the upper part of the sequence (present reference frame) contain volcaniclastic rocks and have iron-rich tholeiitic basalt and basaltic andesite compositions. None of the rocks sampled in this upper part of the sequence contained zircon that gave an indication of a protolith age, but Nutman *et al.* (2007) report that a rock sampled just west of main zone contained a zircon population of volcano-sedimentary origin ranging from 2800–2850 Ma, likely deposited shortly after 2800 Ma. This is also the most likely age for the biotite (± garnet, sillimanite, cordierite) gneiss and quartzite/quartzitic gneiss sequence underlying the upper amphibolite. Several samples of the biotite gneiss/quartzite sequence contain a zircon population with similar ages between 2800–2850 Ma. This makes this central and upper parts of the supracrustal belt Neoarchaean. East of Aappalaartoq amphibolite in the lower part of the supracrustal belt is intruded by anorthosite that itself again is intruded by a 3.05 Ga tonalite (Hollis *et al.* 2005) and therefore is at least 250 Ma older than the upper part of the sequence. Preliminary zircon U-Pb data of a felsic sheet within the lower amphibolite at the base of the sequence at Qingaaq are consistent with this older age of the lower amphibolites. Because dated samples on either side of the contact between the lower amphibolites and the biotite gneiss series were collected close to that contact, it is inferred that this lithological contact is the boundary between the two sequences with distinct ages. The nature of the contact is not known. The rocks at the contact are not obviously more highly strained than those on either side at a distance to the contact. But all rocks here have a strong foliation and are highly strained.

The geochemistry data indicate that the majority of the biotite gneisses of the supracrustal belt are not the altered equivalents of the upper amphibolites or rocks associated with the upper amphibolites. The geochronological data from the two quartzites within the biotite gneiss sequence from Storø, with zircon populations ranging from Eoarchaean to Neoarchaean, make it likely that these are metasedimentary rocks. However, the aluminous gneiss at the contact between the amphibolites and biotite gneisses – the garnet-rich gneiss – has a composition that is consistent with the interpretation that it is a hydrothermal altered amphibolite (or an associated rock), that was subsequently metamorphosed. Garnet amphibolites (± biotite) and garnet calc-silicate gneisses that occur within the upper amphibolite plot on the same geochemical trends as the freshest (mineralogically and texturally simplest) amphibolites and are likely metamorphosed alteration products of the amphibolite. This is particularly obvious in the field where garnet calc-silicates occur in veins in the amphibolite. Gradual transitions from leuco-amphibolite to garnet biotite gneiss that were

commonly observed within the upper part of the biotite gneiss sequence, can be explained as a gradual change in the source of the detrital material.
The geochemical data from the amphibolites suggest a continental source at the base, with increased mantle input near the top of the sequence, which is in accord with a rift or back arc setting. As suggested by Knudsen *et al.* (2007), the detrital zircon ages, including both rare Eo- and Mesoarchaean grains as well as dominant populations of grains between 2850 and 2800 Ma, can be explained by a back arc setting, where detrital input is derived from both a continental and an arc source.

The present data confirm a strong metamorphic imprint on the rocks at *c.* 2635 Ma, but an absence of metamorphic zircon of *c.* 2.7 Ga. Some of the samples contain metamorphic zircon with ages spread between 2600 and 2550 Ma. This is in stark contrast with the absence of the 2.6 metamorphism and a strong metamorphic imprint at *c.* 2.7 Ga in the Færingehavn terrane gneisses that overlie the Storø supracrustal belt (see discussion by Nutman *et al.* 2007). This could potentially reflect the fact that by 2.6 Ga the zircon populations in the Eoarchaean orthogneisses were robust and not affected by the increased metamorphic grade, or alternatively, this may indicate that the overthrusting of the Eoarchaean gneisses occurred at a relatively late stage, syn or post the 2.6 metamorphic event.
The structure of the region is dominated by the *c.* 2630 Ma Storø shear zone and the hanging wall antiform-synform pair. The shear zone placed the rocks of the Storø supracrustal belt on top of Mesoarchaean gneisses of the Akia terrane. But the occurrence of Eoarchaean gneisses in both the hangingwall and footwall of the shear zone suggests that this is not a fundamental crustal scale structure.
The similarity in the setting of Aappalaartoq and Qingaaq mountains is an important feature in the interpretation of the geometry of the mineralisation on the larger scale. Lithologically and structurally the two are very similar, and the two mountains expose mirror images of what potentially is the same antiform-synform pair. Furthermore, these structures comprise some of the most intense mineralised rocks. It is not unlikely that these fold pairs are linked in the subsurface. This can potentially be confirmed by careful structural analysis of the orthogneisses in the hanging wall of the Storø shear zone in between the two mountains.
Several lines of evidence suggest that gold mineralisation occurred in two stages. Both petrography and Re-Os geochronology indicate that two generations of arsenopyrite occur. Because the gold mineralisation in most cases occurs in rocks with arsenopyrite, the same can be inferred for the gold. Gold mineralisation occurs in or near hydrothermally altered rock types (both BD zone and Main Zone), and therefore it is likely that this alteration was responsible for the original mineralisation. Timing of this alteration is likely constrained by the Re-Os age of the prograde (pre-peak metamorphism) arsenopyrite at 2714 ± 53 Ma, derived from arsenopyrite in the BD zone. The younger arsenopyrite Re-Os age of 2636 ±23 Ma from rocks of main zone is identical to the metamorphic zircon age and is interpreted as a phase of syn-metamorphic remobilisation. Petrographic observations (gold in retrograde arsenopyrite and retrograde epidote) suggest it is likely that the gold was remobilised after peak metamorphism, during retrograde recrystallisation by which gold was released from lollingite and (partially?) remobilised into the Main Zone antiform and on the larger scale into the hanging wall antiform-synform pair. It is not clear to what extend the remobilisation occurred and both prograde and retrograde arsenopyrite occurs in the Main Zone. The data cannot discriminate whether this was a very local (microscopic or metre-scale) or a regional remobilisation.

References

Birck, J.L., Roy Barman, M., and Capmas, F. 1997: Re-Os isotopic measurements at the femtomole level in natural samples. Geostandards Newsletter **20**, 19–27.

Cohen, A.S., and Waters, F.G. 1996: Separation of osmium from geological materials by solvent extraction for analysis by thermal ionization mass spectrometry. Analytica Chimica Acta **332**, 269–275.

Eilu, P., Garofalo, P., Appel, P.W.U. & Heijlen, W. 2006: Alteration patterns in Au-mineralised zones of Storø, Nuuk region - West Greenland. Danmarks og Grønlands Geologiske Undersøgelse Rapport **2006/30**, 73 pp.

Friend, C.R.L., Nutman, A.P., Baadsgaard, H., Kinny , P.D. & McGregor, V.R. 1996: Timing of late Archaean terrane assembly, crustal thickening and granite emplacement in the Nuuk region, southern West Greenland. Earth and Planetary Science Letters **142**: 353–365.

Frei D., Hollis J.A., Gerdes A., Harlov D., Karlsson C., Vasquez P., Franz G., Johansson L., & Knudsen C. 2006: Advanced in-situ trace element and geochronological micro-analysis of geomaterials by laser ablation techniques. Geological Survey of Denmark and Greenland Bulletin **10**, 25–28.

Friend, C.R.L. & Nutman, A.P. 2005: New pieces to the Archaean terrane jigsaw puzzle in the Nuuk region, southern West Greenland: steps in transforming a simple insight into a complex regional tectonothermal model, Journal of the Geological Society of London **162**, 147–162.

Garde, A.A. 2007: A mid-Archaean island arc complex in the eastern Akia Terrane, Godthabsfjord, southern West Greenland. Journal of the Geological Society **164**, 565–579.

Gerdes, A., Zeh, A. 2006: Combined U-Pb and Hf isotope LA-(MC)-ICP-MS analyses of detrital zircons: Comparison with SHRIMP and new constraints for the provenance and age of an Armorican metasediment in Central Germany. Earth and Planetary Science Letters **249**: 47–61.

Grahl-Madsen, L. 1994: Storø gold project, Southwest Greenland 1994. Internal report, Nunaoil A/S, 20 pp., 7 app., 16 plates (in archives of the Geological Survey of Denmark and Greenland, GEUS Report file **21413**).

Hofmann, A.W. 1997: Mantle geochemistry: the message from oceanic volcanism. Nature **385**, 219–229.

Hollis J.A. (ed.) 2005: Greenstone belts in the central Godthåbsfjord region, southern West Greenland: geochemistry, geochronology and petrography arising from 2004 field work, and digital map data. Danmarks og Grønlands Geologiske Undersøgelse Rapport **2005/42**, 215 pp.

Hollis, J.A., & Persson, M.F.2005: Garnet amphibolites and garnet-mica schists: petrography, mineral chemistry and thermobarometry. In: Hollis, J.A. (ed.): Greenstone belts in the central Godthåbsfjord region, southern West Greenland. Danmarks og Grønlands Geologiske Undersøgelse Rapport **2005/42**, 126–139.

Hollis, J.A., van Gool, J.A.M., Steenfelt, A. & Garde, A.A. 2004: Greenstone belts in the central Godthåbsfjord region, southern West Greenland. Danmarks og Grønlands Geologiske Undersøgelse Rapport **2004/110**, 110 pp., 1 DVD.

Hollis, J.A., Frei, D., van Gool, J.A.M., Garde, A.A. & Persson, M., 2006: Using zircon geochronology to resolve the Archaean geology of southern West Greenland. Geological Survey of Denmark and Greenland Bulletin **10**, 49–52.

Jackson, S., Pearson, N.J., Griffin, W.L. & Belousova, E.A. 2004: The application of laser ablation – inductively coupled plasma – mass spectrometry to in situ U-Pb zircon geochronology. Chemical Geology **211**, 47-69.

Jensen, L.S. 1976: A new cation plot for classifying subalkalic volcanic rocks. Ontario Division of Mines, Miscellaneous Paper **66**, 22pp.

Juul-Pedersen, A., Frei, R., Appel, P.W.U., Persson, M.F. & Konnerup-Madsen, J. 2007: A shear zone related greenstone belt hosted gold mineralization in the Archean of West Greenland. A petrographic and combined Pb–Pb and Rb–Sr geochronological study. Ore Geology Reviews **32**, 20–36.

Knudsen, C., van Gool, J.A.M., Østergaard, C., Hollis, J.A., Rink-Jørgensen, M., Persson, M. & Szilas, K. 2007: Gold-hosting supracrustal rocks on Storø, southern West Greenland: lithologies and geological environment. Geological Survey of Denmark and Greenland Bulletin **13**, 41–44.

MacLean, W.H. & Kranidiotis P. 1987: Immobile Elements as Monitors of Mass Transfer in Hydrothermal Alteration: Phelps Dodge Massive Sulphide Deposit, Matagami, Quebec. Economic Geology **82**, 951–962.

McGregor, V.R. 1993: Geological map of Greenland 1:100 000. Descriptive text. Qôrqut 64 V.1 Syd. The regional geology of part of the Archaean block of southern West Greenland, including a segment of the late Archaean mobile belt through Godthåbsfjord. 40 pp. Copenhagen: Grønlands Geologiske Undersøgelse.

Miyashiro, A 1974: Volcanic rock series in island arcs and active continental margins. American Journal of Science **274**, 321–355.

Morelli, R.M., Creaser, R.A., & Bell, C. 2005a: Re-Os arsenopyrite geochronology of the Homestake gold deposit, Black Hills, South Dakota, and implications for chronometer closure temperature (abstract). Geological Society of America Annual Meeting, abstracts with programs **37**, no.7 (cd version).

Morelli, R.M., Creaser, R.A., Selby, D., Kontak. D.J., & Horne, R.J. 2005b: Rhenium-osmium geochronology of arsenopyrite in Meguma Group gold deposits, Meguma terrane, Nova Scotia, Canada: evidence for multiple gold mineralizing events. Economic Geology **100**, 1229–1242.

Morelli, R.M., Creaser, R.A., Seltmann, R., Stuart, F., Selby, D., & Graupner, T. 2007: Age and origin of the giant Muruntau gold deposit, Uzbekistan, from coupled Re-Os-He isotopes in arsenopyrite. Geology **35**, 795–798.

Nutman, A.P., Christiansen, O. & Friend, C.R.L. 2007: 2635 Ma amphibolite facies gold mineralisation near a terrane boundary (suture?) on Storø, Nuuk region, southern West Greenland. Precambrian Research **159**, 19–32.

Nutman,A.P., Friend,C.R.L., Baadsgaard,H. & McGregor,V.R. 1989b: Evolution and assembly of Archean gneiss terranes in the Godthåbsfjord region, southern West Greenland: structural, metamorphic, and isotopic evidence. Tectonics **8**, 573–589.

Østergaard, C. & van Gool, J.A.M. 2007: Assessment of the gold mineralisation on Storø, Godthåbsfjord, southern West Greenland: Mineral resource assessment of the Archaean Craton (66° to 63°30'N) SW Greenland, Contribution no. 5. Danmarks og Grønlands Geologiske Undersøgelse rapport **2007/78**, 20 pp..

Palme, H. & O'Neill, H.S.C. 2003: Cosmochemical Estimates of Mantle Composition. In: Holland, H.D. & Turekian, K.K. (eds.) Treatise on Geochemistry **Vol. 2**, The mantle and core, 1–38.

Pedersen, N.H. 1996: Guldmineraliseringer på Storø, Sydlige Vestgrønland. Progress report, forskeruddannelsens del A. Geologisk Instirur, Århus Universitet, 83 pp. (in archives of the Geological Survey of Denmark and Greenland, GEUS Report file **22029**)

Persson, M. 2007: Metamorphic and geochronological evolution of the Au-bearing rocks on central Storø, Nuuk region, West Greenland. Unpublished MSc thesis, Copenhagen University, 98 pp.

Polat, A. 2005: Geochemical and petrographic characteristics of the Ivisaartoq and Storø greenstone belts, southern West Greenland: progress report. In: Hollis, J.A. (ed.): Greenstone belts in the central Godthåbsfjord region, southern West Greenland. Danmarks og Grønlands Geologiske Undersøgelse Rapport **2005/42**, 215 pp., 1 DVD.

Rink, M. 2006: In situ U-Pb datering af zirkoner i teori og praksis til bestemmelse af alder og populationer af detritale zirkoner, med anvendelse på en prøve fra Nuuk regionen I det sydlige Vestgrønland. Unpublished Bachelor's thesis, Copenhagen University.

Shirey, S.B., & Walker, R.J. 1995: Carius tube digestion for low blank Re-Os analysis. Analytical Chemistry **67**, 213–2141.

Shirey, S.B. & Walker, R.J. 1998: The Re-Os isotope system in cosmochemistryand high temperature geochemistry. Annual reviews of Earth and Planetary Sciences **26**, 423–500.

Skyseth, T. 1997: Gold Exploration on Storø 1996 South West Greenland, Exploration License 13/97 (former 02/92). Internal report, Nunaoil A/S. 14 pp., 12 appendices, 3 plate. [21564 temporary report] (in archives of the Geological Survey of Denmark and Greenland, GEUS Report file **21565**).

Skyseth, T. 1998: Gold exploration on Storø 1997: South West Greenland. Internal report, Nunaoil A/S. 25 pp., 5 appendices, 3 plates (in archives of the Geological Survey of Denmark and Greenland, GEUS Report file **21601**).

Smith, G.M. 1998: Report on the structure and geometry of the gold mineralization at Qingaq Storø, Nuukfjord, South West Greenland. Internal report, Nunaoil A/S. 13 pp., 14 plates (in archives of the Geological Survey of Denmark and Greenland, GEUS Report file **21602**).

Stein, H. 2006: Commentary on Rhenium-osmium geochronology of arsenopyrite in Meguma Group gold deposits, Meguma terrane, Nova Scotia, Canada: evidence for multiple gold mineralizing events: SEG Newsletter **64**, p.24–25.

Appendix 1 petrographic descriptions and SEM backscatter images

The following are brief petrographic descriptions of the thin sections from rocks in the map areas. After each sample number follow a rock type and in parentheses the code from the map legend. All sections were studied in a polarizing light microscope, most of the samples with sulphide mineralisation also in reflected light. A few of the samples were imaged by SEM BSE. The descriptions are followed by a selection of the SEM backscatter images of a few of the rocks from main zone with sulphide mineralisation, some of which are carrying gold.

The following abbreviations are used:

acc	accessory phase	mag, mgt	magnetite
asp, aspy, apy	arsenopyrite	ms	muscovite
apa	apatite	opq	opaque
bt	biotite	pla, plag	plagioclase
cc, calc	calcite	po, pyrh	pyrrhotite
chlor	chlorite	py	pyrite
cp, cpy	chalcopyrite	qtz	quartz
cpx	clinopyroxene	sil	sillimanite
cum	cummingtonite	sp	sphalerite
di	diopside	spn	sphene
ep, epi	epidote	stt	staurolite
grt	garnet	ttn	titanite
hbl	hornblende	turm	turmaline
ilm	ilmenite	zois	zoisite
kfsp	K-feldspar		

Petrographic descriptions

487403 + 487404 garnet biotite gneiss (b)

Medium-grained garnet-biotite gneiss, with minor sillimanite. Rock contains small felsic blebs that have minimum melt composition of plag+qtz+kfsp.

Quartz – 25 % rather coarse-grained and well equilibrated in parts. Few larger elongate grains. Locally irregular grain boundaries, but no internal deformation textures.

Plagioclase – 25 % finer grained and more irregular grain shapes than quartz.

K-feldspar – 5 % rather fine-med gnd. Irregular grain shapes.

Biotite – 25 % define a coarse foliation, irregular.

Garnet – 15 % rounded grains, few inclusions of quartz, plagioclase, opaques, minor biotite and chlorite. No internal foliation.

Opaques – 5 % fine-grained and anhedral

Sillimanite – 5 % very fine-grained trails in the bt-rich layers.

487405 layered amphibolite with isoclinally folded quartz vein (a)

2 sections, one polished with layering., one regular with folded quartz vein

Rock consists of alternating bands of amphibolite and grt-bt gneiss. Sulphides: pyrrhotite and chalcopyrite are irregular and likely early metamorphic. Arsenopyrite occurs both as irregular grains and large euhedral grains, suggesting that two generations exist.

Amphibolite layers contain:

hbl- 40 %, m-gnd, anhedral grains with abundant inclusions

pla- 30 % m gnd, irregular grain shapes, smaller than hbl

spn- 15 % fine grained

opq 10 % f-m gnd, irregular grain shape, pyrrhotite and chalcopyrite (inclusions in pyrh)

arsenopyrite <5% euhedral, square grains.

qtz <5%

apatite acc

epidote acc

grt-bt gneiss layers contain:

quartz – 40 % irregular grain shapes but no internal deformation textures

biotite – 30 %

grt – 15 % anhedral, very irregular grain shapes. Locally partially replaced by arsenopyrite and biotite

pla – 10 %

accessory sphene and opaques (mainly pyrhotite and chalcopyrite, few large aspy grains)

folded quartz vein shows that quartz recrystallised after folding. Biotites follow fold outline, but are also recrystallised. Hornblende has no good preferred orientation around the fold nose, may also be recrystallised. i.e. this fold (collected in the field as F1) deforms a foliation, but is followed by a phase of intense static recrystallisation.

487407 biotite-amphibolite with minor garnet (a)

Amphibolite with a grt-biotite-rich lens. Strong foliation defined by hornblende.

Amphibolite layers contain:

hbl- 50 %, m-gnd, subhedral grains that have a good grain shape fabric

pla- 30 % m gnd, irregular grain shapes, smaller than hbl

opq 10 % f-m gnd, irregular grain shape, pyrrhotite often fills in gaps between hbl grains and on hbl grain boundaries

qtz 5%

apatite 5 %

biotite acc

epidote acc

grt-bt gneiss lens contains:

quartz – 40 % irregular grain shapes but no internal deformation textures

biotite – 30 %

grt – 15 % anhedral, one very irregular grain consists of a cluster of fragments, tightly intergrown with bt and quartz and fine opaques

pla – 10 %

pyrrhotite – 5 %

487411 quartz-cummingtonite-garnetite (if)

massive m-c gnd garnetite with qtz and cummingtonite (-grunerite) in the matrix
garnet 60-70% up to 8mm grains, larger grains are subhedral to anhedral, small grains are often euhedral. Inclusions mainly quartz, also chlorite and opaques, rarely biotite. quartz and opaques form internal foliation in cores of some of the larger grains, not in all. margins of large grains and small grains are inclusion free. locally grt grains are grown together to form networks
qtz 10–20 % equilibrium texture, ondulose extinction and some deformation bands
cum 10–20% colourless, twinned, not as inclusions in grt randomly oriented
opaque 5% mag(?) + ilm (?) + ?
chlorite and biotite only as inclusions in garnet, not in the matrix

487415 garnet biotite gneiss (b)

felsic biotite rich gneiss, homog and grey in outcrop, poorly foliated.
overall well-equilibrated texture, slightly preferred orientations of biotite and elongate feldspars define a foliation.
pla 30-40% twinned, elongate and irregular grains part of foliation defining fabric
bt30-40% euhedral to subhedral crystals.
qtz 20-25% minor undulatory extinction
grt 10% subhedral with minor quartz inclusions, locally also bt. probably also rutile.
accessory zircon, apatite and opaques (ilmanite)

487417 biotite-garnet gneiss (grt)

felsic biotite-garnet gneiss, vaguely banded, light grey to white matrix, foliated. commonly 30-40% garnet, evenly distributed. (but not in thin section)
overall well-equilibrated texture, preferred orientations of most biotite and elongate feldspars define a foliation.
pla 40% twinned, elongate and irregular grains part of foliation defining fabric
bt 20-30% euhedral to subhedral crystals, majority along foliation, but also many at random angles.
grt 20-30% subhedral with inclusions of qtz, bt, chlor, rutile and very fine sill. Most have good internal foliation, at an angle to the matrix foliation (but not in consistent orientation from grain to grain).
qtz 10% few mm-sized grains
rutile <5%
sill 1-2% few clusters, together with muscovite, also as inclusions in
accessory zircon, apatite, turmaline and opaques (ilmanite + ??)

487418 diopside-veined amphibolite (a)

amphibolite with felsic, di-bearing vein. No grt in section, but observed in the veins in the field
Matrix is regular amphibolite 50% hbl, 40% pla, 10% ttn, f-m-gnd, well foliated.
most plag is zoned
ttn forms rims on ilmenite cores
rare and tiny epi-qtz symplextites on pla-hbl contacts.
vein felsic with pla>qtz and hbl replaced by cpx
pla 30-40% equilibrium texture
cpx 20-30%
hbl 10-20% largely replaced by cpx
qtz 10%
spn 10%
epi 5-10% forms symplectites with qtz on the hbl-pla contacts
opaques, 5% likely po and/or mag. an-subhedral

The alteration of hornblende to cpx in and along the vein, should indicate that the rock was metamorphosed at the time that the vein intruded.

487424 grt-amphibolite with qtz vein (a)

heterogeneous

hbl 70% brownish colour with blue-green edges + small grt inclusions

pla 10%

grt 10% poikiloblastic with incl of bt, opq, hbl - no internal foliation

opq 10% often on grain boundaries of silicate phases

bt 1%

opaques: few aspy with good crystal shape, manily complex pyrh with cpy inclusions

487425 qtz-veined amphibolite with aspy, po and cp + gold (a) (upper part of south-eastern limb of main zone)

qtz vein, med gnd, with aspy inclusions and minor plagioclase.

The matrix is a med gnd biotite amphibolite and contains stringers rich in plagioclase, potentially representing recrystallised veins. The plagioclase is heterogeneous, zoned in an irregular pattern. minor sericitisation, and with exsolution of quartz.

Rock has a weak foliation, mainly defined by hbl and bt

hbl 25 % subhedral, matrix is overall hbl-rich

bt 20% occurs throughout the section, but mainly in zones rich in plagioclase

pla 20% concentrated in zones together with bt and minor hbl + po, with irregular contacts to the hbl-rich matrix. pla is sub-hedral, strongly zoned, and with exsolution of qtz. very minor sericitisation.

spn 10 % fine-gnd, forms rims on ilmenite. rounded, sometimes irregular forms.

aspy <5 %, euhedral, overall good straight and square-shaped crystal faces. contains 5-10 µm grains of lollingite and gold (see SEM image).

po 5% anhedral, probably prior to metamorphism.

cp <1% inclusions in po

qtz only in vein, and minor “drops” in plagioclase

minor Ag-tellurides in fractures in amphibole

487429 garnet calc-silicate gneiss (field name: grt-di gneiss) (CS) (main zone)

pla 20% sericitised, and epidotised. irregularly zoned. High anorthite percentage in most of section, but albitic near hornblende-ilmenite symplectite

qtz 20% equil texture, mainly in a zone in center of section

hbl 15% m gnd poikiloblastic. locally as rims on po(?). often blue margins, especially against po.

grt 10% c-gnd, poikiloblastic and subhedral, chlor inclusions + all matrix minerals. clusters of intergrown small grt grains.

spn 10% fine-grained. rims on ilmenite

opaques 15% very complex - symplectitic, forms main foliation, cp incl in po, large aspy, small ilmenite grains

zois/epi 10 % overall heterogeneously zoned, overall tiny grains within plagioclase

chlor 5% only as inclusions in grt

gold acc grains in zoned epidote and sericitic plag.

A symplectite of pargasitic hornblende and ilmenite occurs between grains of sphene and arsenopyrite

487430 garnet-diopside gneiss - 2 sections (cs)

di 30% both large, poikiloblastic, and small grains. poik grains contain both spots and inclusions of hbl/arfveds (blue-green amphibole)

pla 20% zoned, many with zoisite symplectite coronas

grt 20% anhedral, mainly small inclusion-free grains - form clusters

spn 10%epi/zoi swarms of small needles in plag rims

opq >1%mainly pyrh, w minor cpy

zoisite-quartz symplectites

microscopic calcite grains

The second section is more layered. Has more and larger epi. opaques mainly pyrh w cpy, but also others, locally complex symplectites

487432 bt-grt gneiss (grt)

Massive, garnet-rich gneiss, with abundant bt and little qtz. plag forms most of felsic component and has a fairly well developed equil texture. biotite reasonably alligned. OK foliation overall.

pla 30-40% granoblastic

grt 20% large subhedral (rounded) w small incl of qtz (?), pla, sil, stt, ilm, minor po, tiny inclusions of Co-pentlandite in po, minor rutile. No internal foliation, rims poor in inclusions – zoned.

bt 20%

opq 10% mainly ilmenite well alligned

qtz <5%

sil <5% well alligned

apatite < 5%

accessory rutile

487433 garnet -biotite-amphibole ironstone (if)

medium grained magnetite-rich rock containing quartz, garnet, blue amphibole (grunerite) and biotite

mag 25%– fine-med gnd, sub-hedral grains, evenly distributed

quartz 25%– med gnd, fairly well equilibrated texture. occurs predominantly in layers, alternating with biotite and garnet-rich layers.

bt 20 %– green, m gnd, fairly well alligned to form foliation parallel with layering.

garnet 15 % - elongate, irregular and poikiloblastic grains with good internal foliation. inclusions of qtz, bt and magnetite ocurs mainly in bt-rich bands.

amphibole10 % - blue-green amphibole, presumably grunerite grains are evenly distributed, and randomly oriented, may have grown after the other minerals.

487434 biotite-garnet quartzitic gneiss (qmz)

quartz-rich gneiss containing biotite and fine-grained grt. Well foliated

qtz 70% equigranular (1-2.mm diam.), but with serrated grain boundaries, locally subgrains. few smaller grains.

bt 10-20% sub-euhedral, defines a good foliation

grt 10%, clear sub hedral +/- 1 mm grains, few inclusions, relatively large, qtz and bt.

pla 5%

487465 Quartzitic gneiss (qmz)

quartz-rich gneiss, well foliated, containing bt and ms. Bt>ms in most of section, but a narrow ms-rich zone in the middle of the section, w finer-grained qtz, has ms >>bt, and little pla. This may well be a shear band.

qtz 70% equigranular, irregular shapes, serrated grain boundaries

bt 10-20% (only 5% in central zone)
plag 10%
ms 5% (but 30-40% in central zone)

487466 garnet-biotite gneiss (b)

homogeneous, garnet-biotite gneiss lacking a foliation. Granoblastic, equigranular fabric (well equilibrated).
plag 30-40%
bt 20 % euhedral randomly oriented
grt 20% +/- 3mm subhedral round grains, zoned. few and relatively large inclusions (pla, opq, qtz and bt) in the core, near the rim is a thin zone of tiny inclusions (same comp), and again an inclusion-poor outer rim. These inclusion rich zones outline good crystal shapes, and since parts are missing, they shows that parts of the grains have been resorbed.
qtz 10-20%

487467 felsic hbl-bt gneiss within banded amphibolite (av)

Well foliated quartzo-feldspathic rock, with biotite, blue-green amphibole (cummingtonite?) and minor garnet. not very good differentiation in felsic and melanocratic layers.
palgioclase 40 % m-gnd, sub hedral
quartz 30 % m gnd, irregular grain shapes, likely strongly deformed and slightly recovered
biotite 10 % f-m gnd, well alligned
amphibole <10 % – blue pleochronism, anhedral.
grt 5 %– f-m gnd, anhedral, with small qtz inclusions, slightly elongate along foliation
epi <5%– f-gnd, some with alanite cores
chlor <5% mainly growing on biotite
opaque acc
alanite acc – forms cores in some epidotes.
apatite acc
Uncertain whether this is an integral part of the banded amphibolite (metavolcanic rock?), or if it is an intrusive dioritic layer in a mafic rock.

487468 biotite gneiss with isoclinally folded quartz veins (b)

homog, well foliated biotite gneiss, with minor late ms, and very few tiny sil grains
total recrystallisation after isoclinal folding, micas show no sign of being folded.
pla 30% slightly zoned equigranular
qtz 20% (in matrix) undulose extinction
bt 20% well equil, subhedral, defines foliation
ms<10% locally overgrowing bt fabric
sil <1% few tiny laths
grt <1% few tiny grains
1% turm few large grains (1-2 mm)

487469 garnetite - grt-amphibole gneiss (hb)

anhedral - poikiloblastic garnet, with inclusions of opaques and minor qtz.
amphib - pale green - colourless with abundant twinning (cummingtonite?)
qtz
opaques mainly/only magnetite

487474 qtz vein in bt-grt amphibolite (a)

quartz vein is well equilibrated with good tripple point grain boundaries (metamorphic texture). Both crs. and fine-grained. irregular vein boundaries, > recrystallisation after veining.

Vein is 95 % quartz, overall c-gnd, but fine-gnd parts which may indicate some deformation syn-post recrystallisation.
few small hbl grains in the vein are very elongate and look strongly deformed.
The mafic part is very mafic (ultramafic) – no plag. Restite??
hbl 60% green, locally blue, subhedral to euhedral. m-gnd
grt 20% subhedral, fairly large grains with good internal foliation of qtz, bt and opaques in most of the grains.
bt 20%
opaques only as fine inclusions in grt
apa – accessory, and one larger grain

487476 amphibolite w cpx + grt (a)
amphib part - NO FOLIATION!:
hbl 90% - minor bluish edges
pla 5%
spn 5%
grt poikiloblastic
cpx, large grains w many hbl inclusions (poikiloblastic)
pla - large grains often with epi (+?) symplectite rims
minor opaques, often at grain boundaries of silicate phases, predom pyrh + cp + ?

487481 amphibolite with quartz vein (a)
Medium grained amphibolite with 1 cm quartz vein and a hornblende-rich selvage. Also two thinner plag veins/layers.
Qtz vein: coarse-gnd, with one cpx grain, and a cluster of zoned plag grains in one part. Hornblende-rim on quartz vein (mainly on one side). Hornblende has bluish rims, mainly along fractures, in vicinity of the quartz vein.
Plag layer med gnd, and almost monomineralic, with minor zoisite and chlorite. Irregular grain shapes.
Matrix/host rock is a m gnd amphibolite with equil texture and poor grain shape fabric
Hbl 50 % m gnd, sub hedral, blue rims in vicinity of quartz vein.
Plag 40 % - m gnd, sub hedral, minor sericitization, minor epidote
Opaque 5 % - f gnd, concentrated in layers in the host rock.
Bt <5%
Qtz acc, minor inclusions in hbl and plag.

487482 bt-grt-sill gneiss (grt)
cm-sized sillimanite clusters in grt-sil-bt-pla matrix, with distributed garnets. section cut perp to crenulation axis. abundant sulphides
Sillimanite occurs both in clusters and to a lesser extent in the matrix. contains remnants of stt both as inclusions in the garnets and in the matrix.
sill 30% fibrolite, intergrown in patches with quartz, opq and minor bt. Pseudomorph after and?? In matrix fibrolite intergrown with bt, few larger (sub-mm) grains overgrow fibrolite. locally tiny clusters of very fine grains (but not fibrolite) on pla grain boundaries
pla 20% in matrix clear (no sericite) equil texture, opq and sill locally on grain boundries
bt 20 % sub-hedral defines poor foliation

grt 10 % ≤ 5 mm. Few, relatively large inclusions of qtz, bt, stt, pla
qtz 10% predominantly in sill clusters (30-40%), fine grained, <2% in pla-bt matrix
opq 5-10 % partially ilmanite, but abundant squarish (asp?) and irregular (po?) grains, many on plag grain boundaries. few oval opaque grains.
turm 5%
stt 5% small euhedral, often rounded remnants, in matrix and as inclusions in grt.

487486 qtz-bt garnetite (if)

Massive, m-c gnd rock, dominated by grt. Beside dusty opaque inclusions in grt only one smallish opaque min
grt 80 % subhedral w few, small chlor and qtz incl and opaque dust + small grains. rims rather inclusion free no internal fabric. grain size *c.* 3-9 mm. Grt is heavily fractured and healed by qtz.
bt + qtz interstitial between grt grains bt relatively c-gnd (up to 5mm). qtz equil texture and undulose extinction
only one largish opaque, sheeth like, might be molly (graphite?)

487487 quartzitic gneiss (qmz)

Quartz-rich biotite gneiss with minor ms and sil.
qtz 60-70% irregular grain shapes and sizes
bt 20% defines good foliation.
pla 5-10%
ms 5-10% most common in mica-rich parting of the rock together with sil. ms locally overgrows bt foliation at odd angles.
sil 5% fine-grained, intergrown with muscovite. few (mm-sized) larger grains.

487490 foliated sillimanite quartzite (q)

foliated quartzite with sill and minor ms on foliation planes. may well be sheared, but apparent kin indic. point in opposite directions
qtz 80 % overall m-c gnd equil texture, but along foliation planes f-gnd and cerriate grain boundaries
sill 15% fine-grained (coarser than fibrolite) and well oriented. sits predom on foliation planes.
ms 5% m-gnd mainly on fol planes, but also in matrix
1% bt few anhedral grains
opaque only few small grains

487498 Layered amphibolite with arsenopyrite (a)

Center is regular amphibolite, both top and bottom are more felsic and cpx+epi-bearing
amphibolite core:
hbl 60 % with some pale bluish rims
pla 30% clean
spn 5%
opques 5% - commonly in connection with sphene
felsic top and bottom:
hbl 30% more intense alteration to blue-green amphibole at margins
plag 30%
cpx 20%

epi 10% mainly in symplectites on plagioclase margins
opaque 10%
spn <5 %

opaques in central part are mainly pyrhotite
opaques in felsic parts are mainly arsenopyrite

487901 bt-amphibolite boudin in qtz-vein system within amphibolite (a)

massive,c-gnd, heterogeneous mafic-ultramafic rock with disseminated po+apy+cp. No pla. Disequilibrium textures suggest late (post-metamorphic) alteration
hbl 30-40%: pale green, c-gnd, sub–euhedral, random orientation, overgrows bt.
bt 30%: smaller than hbl, random orientation, overgrown by chlorite and hbl
epi 10%: heterog anhedral masses, intergrown with chlorite.
chl 10-20%: overgrows bt and probably also hbl. intergrown with epidote. euhedral. (photo)
turm 5-10%: few large sub–euhedral grains, with irregular zonation
opaques 5-10%: probably po + mag. also apy?
ilm + spn <5%: rounded ilm grains, often with spn rims
very few fine-gnd garnets in one of the chl-epi clusters.

487904 qtz-veined garnet amphibolite (a)

part of layered rock with alternating dark and light amphibolite bands
deseuilibrium texture surrounding the qtz vein
cm-sized garnets with abundant inclusions, in an amphib matrix (hbl, pla, spn)
near veins the amphibolite contains epi and chlorite chlor mainly surrounding grt (euhedral) and as inclusions
qtz vein is very high strain, with subgrain boundaries parallel with the vein boundary (qtz ribbons), and contains thin stringers of plag + hbl + apa (10% of the stringer is apa), which locally are pulled apart and form asymmetric porphyroclasts.
surrounding the qtz vein is minor heterogeneous cpx with calcite and hbl inclusions. also epidote and sericite in plag occurs near the vein.
grt forms lare overall roundish grains, which may be formed by clusters of smaller grains or a late recrystallisation giving the grain boundaries a serrated form (but with short straight segments) as if there is a second phase of grt growth. Abundant inclusions of chlor, epi, calc, hbl + opq (po), but no internal foliation.
opaques, 5% in matrix, locally with epi rims.
plag - one plag vein, locally sericitised, with minor fine-gnd epi.
cpx - few grains along qtz vein, very heterogeneous, with blebs/inclusions of dark green hbl.

487905 layered garnet amphibolite (av)

2 thin sections – 1st homog pale amphibolite, 2nd is garnetiferous pale-amphibolite with hbl and cumm.
layered grt amphibolite - pale
layering mainly variable proportions of hbl-cum-pla. ¼th is bt-rich + cum, and only few hbl remnants
poor equil texture, recrystallised at sub-peak grade. also one layer hbl-free, consisting of cum+pla. cum is coarser-grained here.
main composition:
hbl 30-40% - subhedral defines foliation
cum 20-30% sub-euhedral, finer-gnd than hbl
pla 10-30% minor zonation and twinning, farther fine-gnd, but good equil texture
qtz 10%

grt 5-10% - few large grains that overgrow a layering defined by qtz and opq inclusions. bt along some of the grts.
opq 2% - very fine gnd.
bt-rich layer:
bt 10-30%
cum 20-30%
grt 30%
pla 20-30%
qtz 5-10%
turm 5% few anhedral grains, relatively large
opq 2% coarser than in hbl-rich layers.
One bt-rich layer has no/little amphibole and is more grt-rich.
pla/qtz proportion same as in other layers. grades to either side to layer in which cum>>hbl.
no epidote or sericitisation

487908 garnetite (if)
massive qtz garnetite. No foliation
grt 70-80 % subhedral grains in clusters, inclusions mainly chlor, qtz and opaques. opaque inclusions much finer grained than in matrix
qtz 20% equil texture, ondulose extinction
bt 5% few small grains in matrix, not as inclusions
opq 5-10% in matrix larger than in garnet often interstitial at grt and qtz grain boundaries mag + ?

487910 grt amphibolite (a)
heterogeneous grt-rich amphibolite with chemical desequilibrium textures. abundant epi and ttn, relatively qtz-rich: few qtz veins w di and minor epi.
grt 30% - anhedral, mainly clusters of small., subhedral grains, apparantly with some larger (older?) grains.
incl-rich, all matrix phases. Inclusions look very irregular, probably remnants of interstitial spaces between grt grains in the cluster while the individual grains in the cluster grew.
epi 20% - both small euhedral grains and irreg heterogeneous mosaics
hbl 20–30% bluish green, partly replaced by cpx to form an irreg pattern, spotty
cpx 5–10% few larger grains with hbl remnants, spotty.
pla 20% - to large extend replaced by epi and with minor sericite.
qtz 10% in veins, irregular grain shapes
apa < 5%

487917 amphibolite (a)
hbl 80% slightly blue-green on edges
pla 10% sericitised
spn 8% woth inclusions of ilmenite(?)
one cluster of di with minor qtz
opaques are complex, mainly pyrhotite (?) with cp and ?? inclusions
opaques occur mainly on grain boundaries of other phases

487922 garnet-cummingtonite-magnetite rock (hb - ironstone)

garnet porphyroblasts (up to 1 cm) in a med. gnd. qtz-mag-cum (grunerite) matrix. One isoclinally folded quartz vein.

poor foliation with irregular orientation, defined by quartz, magnetite and amphibole. Foliation is apparantly both parallel with and perpendicular to the quartz vein, wrapping weakly around the garnets. Isoclinally folded quartz vein is re-folded in very open folds.

cumm 30%, pale, greyish green, poor cleavage, but locally moderately cleaved. Cores locally messy, with abundant fractures or intense cleavage. Sub.hedral to anhedral, good twinning (simple Karlsbad, locally lamellar)

magnetite 30% - sub-anhedral

qtz 20% - f-gnd, overall equilibrium texture, straight to slightly serrated grain boundaries with triple point junctions, and minor subgrain formation

grt 20% coarse-grained, up to 1 cm. grains have a good internal foliation defined by trains of qtz inclusions, which themselves do not show a consistent orientation

blue amphibole few very small grains

bt, apa, epi, chlor are accessory

Potentially, a pale green pyroxene occurs besides the amphibole, very difficult to distinguish from each other. This suspicion is based on occurrence of 90° cleavage.

The rock had an equilibrium texture, i.e. it recrystallised statically during and after deformation at high metamorphic grade. Quartz texture shows that it was mildly deformed again at lower grades, during which the folded quartz vein got refolded and the foliation wrapped around the garnets.

487923 mylonitic bt gneiss (qf)

felsic biotite gneiss, with mylonitic S-C fabric. fine-grained, largely recrystallised matrix. abundant grt and pla porphyroclasts with asymmetrix pressure shadow indicate sinistral shear (in section, not oriented in field).

bt 40% overall fine-grained, partially recrystallised after shearing

qtz 30% both larger porphyroclasts, recrystallised qtz ribbons and fine-grained matrix. subgrain-size crystals.generally with equilibrium texture.

pla 20% mm-sized porphyroclasts and fine matrix grains (but coarser thab qtz).

grt 5% (sub-) clear, mm sized porphyroclasts with few inclusions of qtz, fsp, bt and opaques. No internal fol.

chlor <5% locally intergrown with bt, on shear planes.

487924 layered amphibolite (a)

mainly hbl (90%) and plag in amphibolite

lighter bands of qtz-fsp hbl-opq and tiny grt

biotite at one margin of section

one plag vein, c-gnd w mag (?) crystal

opaques pyrhotite complex,

487927 grt-sil gneiss (ms)

Coarse-gnd sil-rich grt-mica-gneiss/schist. Looks in every way like an ordinary metasediment. Same tectono-stratigraphic level as the cordierite-sillimanite-garnet-biotite gneiss dated by Julie Hollis (sample 481465, Hollis 2005) and interpreted as a metasediment.

bt 30-40% - large grains + intergrown with fibrolite and fine-gnd sil. Locally tiny inclusions of rutile (?) which occur both randomly oriented and oriented along the bt crystal planes.

Sil 20-30% - mostly fibrolite in pods and layers. To minor extend also fine-grained sil crystals. Mainly overgrowing biotite. Both folded and sheared.

qtz 20-30% - equilibrium texture, slightly deformed, with serrated grain boundaries.

Grt 10-20% - few, large, subhedral grains < 8mm. Locally rimmed by chlorite. mainly quartz and opaque inclusions, with minor bt, pla, rt
pla 10% - mainly surrounding garnet (decompression reaction?)
opq < 2%
stt - few minor remnants
chl – minor “beards” on grt
ms and alanite accessory

487929 hbl-grt-epi-di gneiss (cs)

very messy rock with all kinds of phases intergrown
grt 30% poik, subhedral, incl of chlor+hbl+epi+qtz. grt forms often clusters of small grains
amphib 15% large amphib with blueish green-green-yellow pleochroism. being replaced by cpx
cpx 10% symplectitic with amphib and epi, incl as well as rims on amphib
epi/zoi 15% mainly replacing di or plag
spn 10% both small and large grains
plag 5% mainly replaced by fine-grained epi/zoi clusters
calcite 5 % mainly tiny grains, but also some larger ones. also included in grt
Chlor 5 % few larger clusters, replacing amph/cpx
qtz <5% mainly inclusions in grt
bt <5% few small bright orange grains
opq some tiny shiny grains in grt, either po or aspy

487932 Garnet amphibolite with qtz-di vein and abundant aspy (a)

heterogeneous rock
hbl 80-90%
opaque 10%
in vein:
grt with lots of inclusions of plag and opq
plag zoned, minor sericite

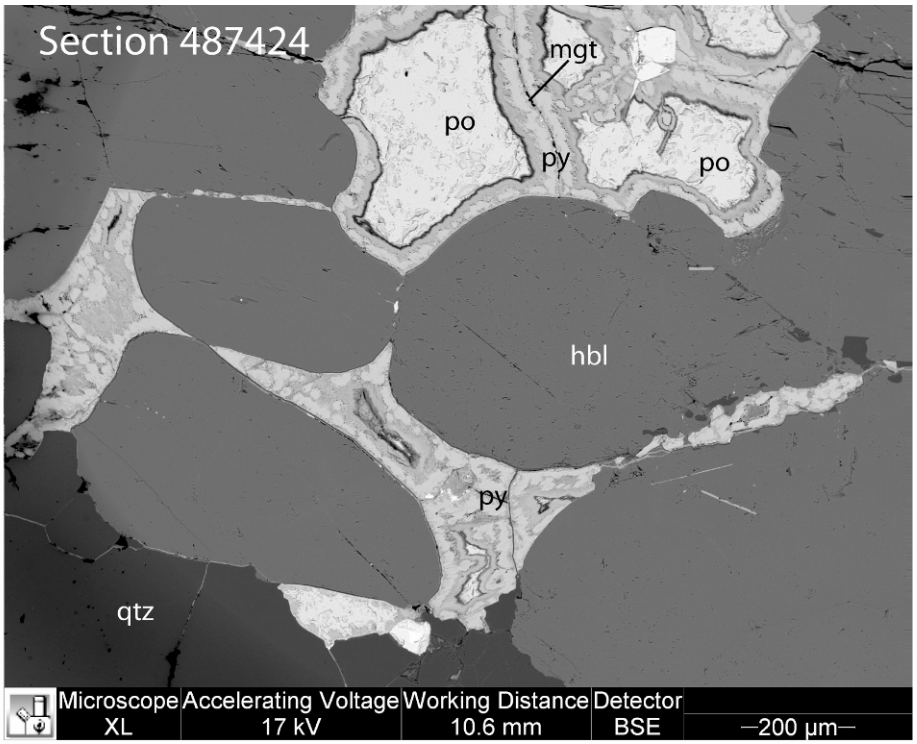

Section 487424 pyrrhotite (Po) with pyrite (Py) rims, with decreasing Fe content towards the rims, Pyrite(locally with Po cores) sits interstitially in between hornblende grains. Bottom left is a quartz vein, note that the po/py protrudes into the vein.

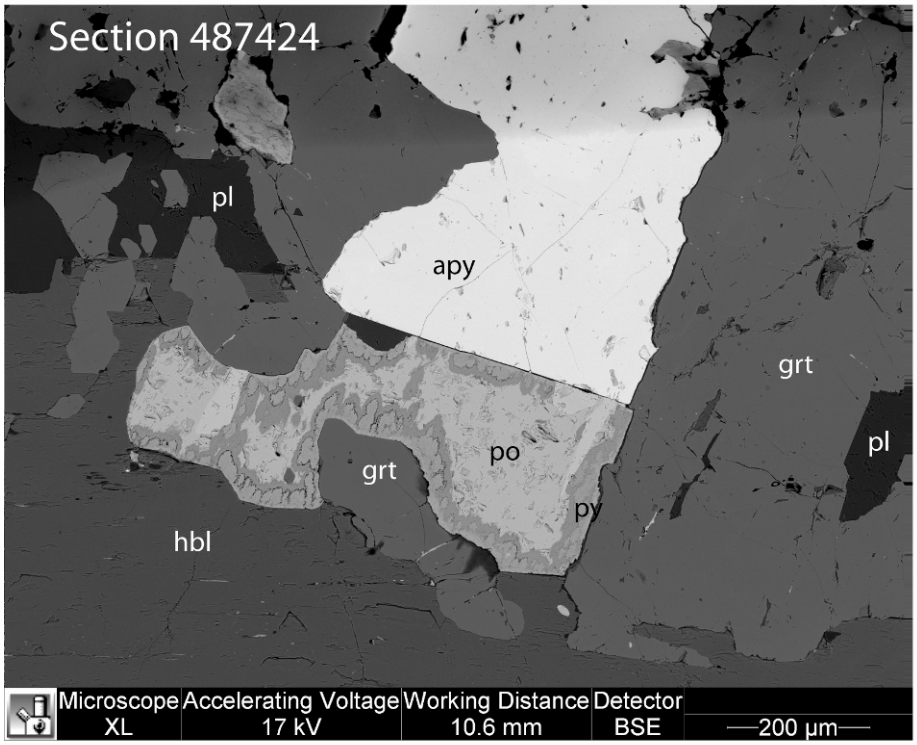

Section 487424 Arsenopyrite)Apy) grain within garnet (Grt) with straight contact against pyrrhotite (Po) with pyrite (Py) rim. shadow at the top of the image is a filt-tip pen mark on the section. The Arsenopyrite grain has 5-10 µ Bi-telluride inclusions (too small to be visible on the scale of the image).

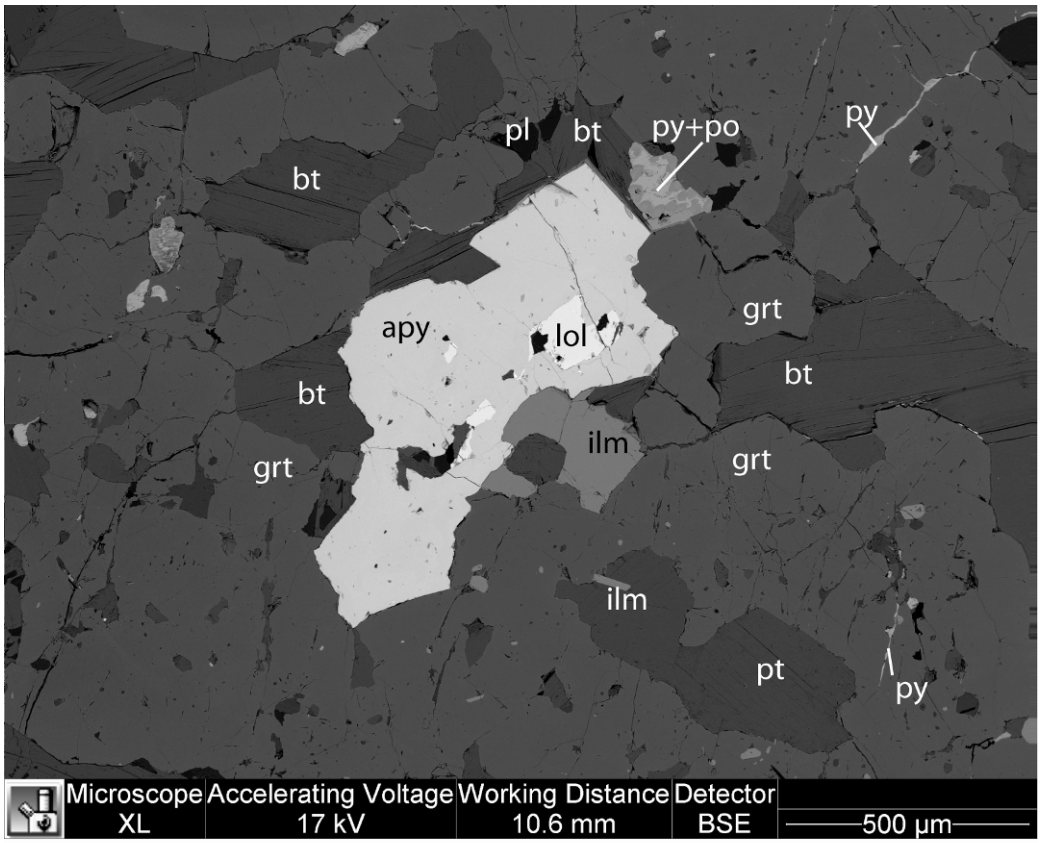

Section 487424 Bacscatter image. Large garnet grain (grt, filling whole image) with inclusion of arsenopyrite, which includes lollingite, that itself has inclusions of Bi-telluride. The latter also occur elsewhere within this garnet as rims on Ilmenite. Biotite is the most abundant inclusion. Fractures in the garnet are filled with pyrite.

sample 487425
spot 1

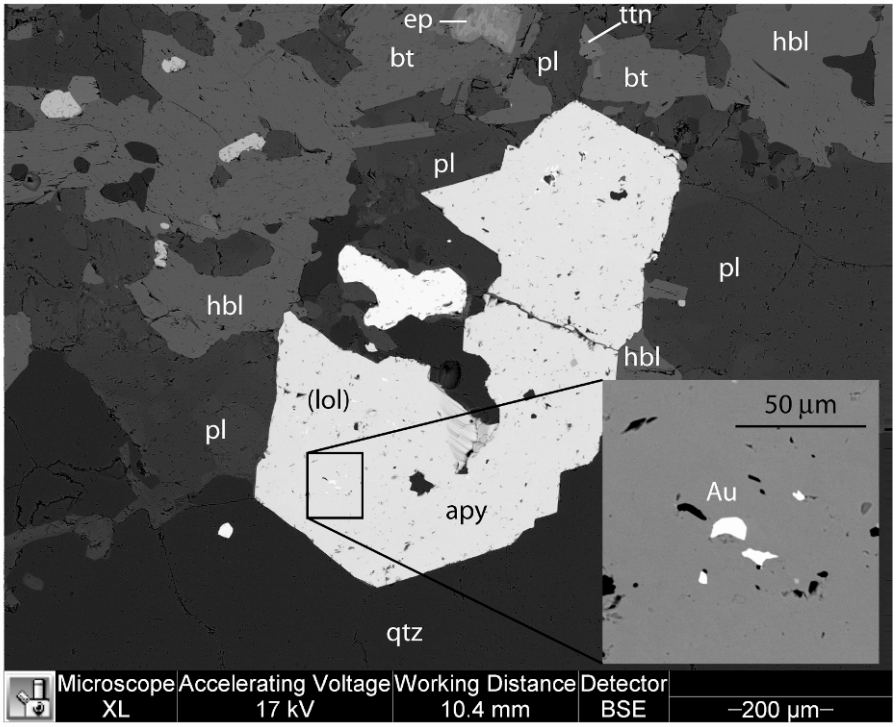

Arsenopyrite (apy) grain with 5-10 mm gold and lollingite (lol) inclusions in a biotite-amphibolite matrix. The grain sits at the margin of a quartz vein (bottom of image). Epidote is zoned, with an aluminous rim, and Fe-rich heterogeneous core.

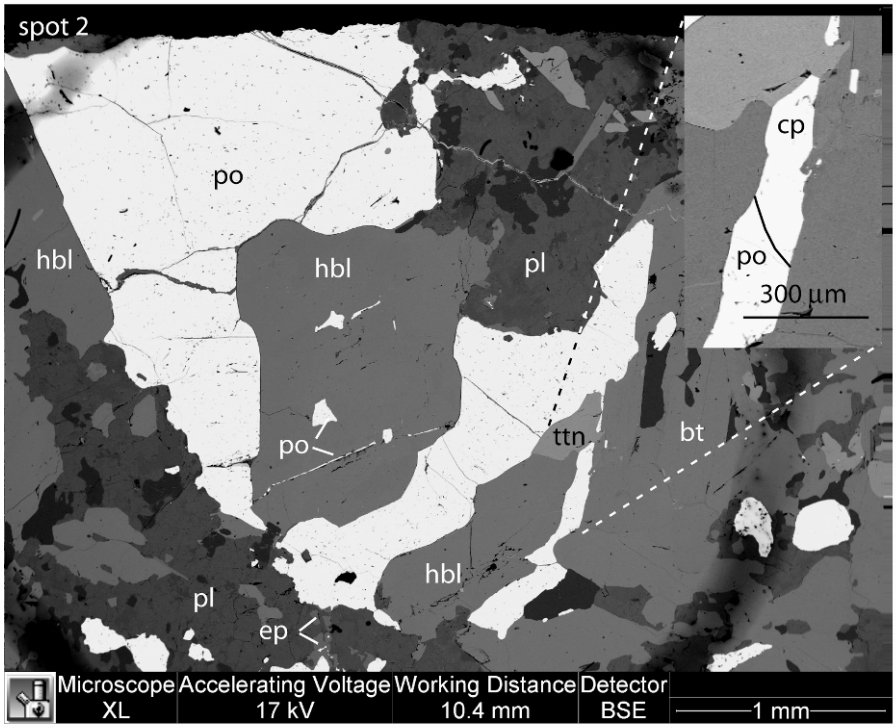

Section 487425. Anhedral pyrrhotite grain, intergrown with hornblende. contains a small chalcopyrite grain (cp). The pyrrhotite(po)-filled fracture contains 2-5 µm Ag-telluride crystals.

section 487425

spot 3

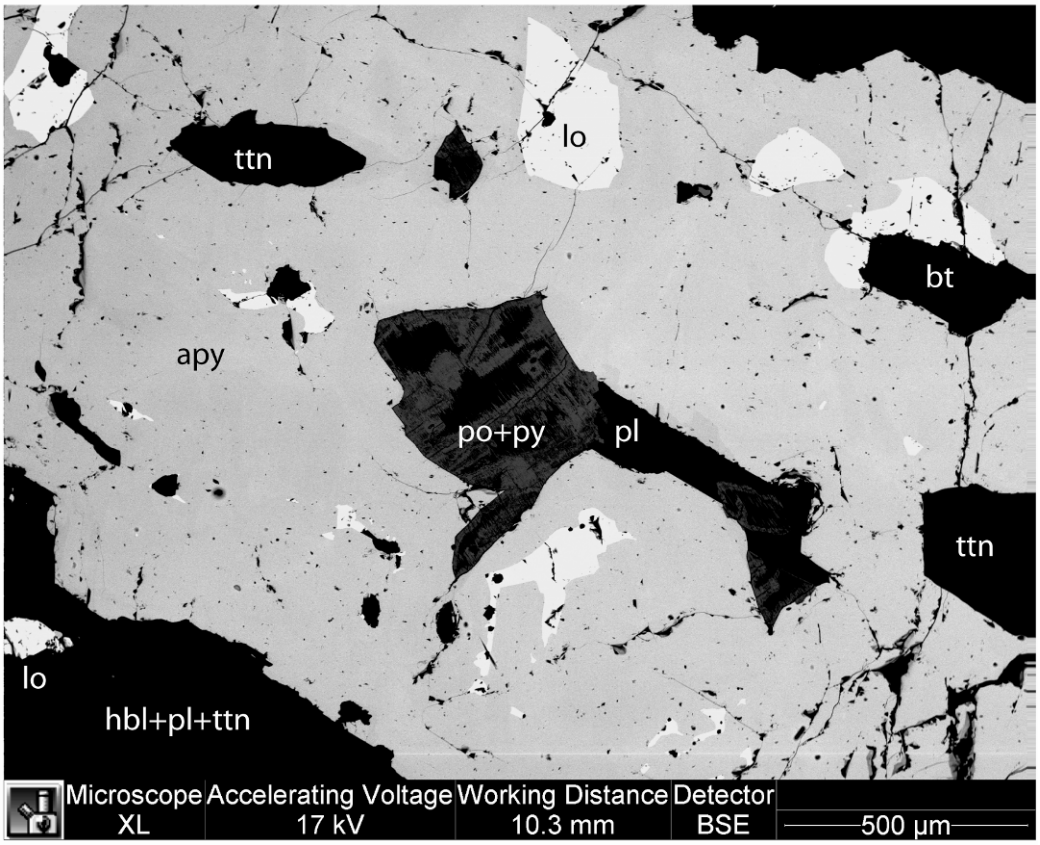

Arsenopyrite grain within titanite-bearing biotite-amphibolite. Inclusions of lollingite (lo) pyrrhotite (po), titanite (ttn), biotite (bt) and plagioclase (pl). Lollingite contains Ni and Co, especially in the matrix. Matrix arsenopyrite also contains Ni and Co. Note that the arsenopyrite is slightly heterogeneous.

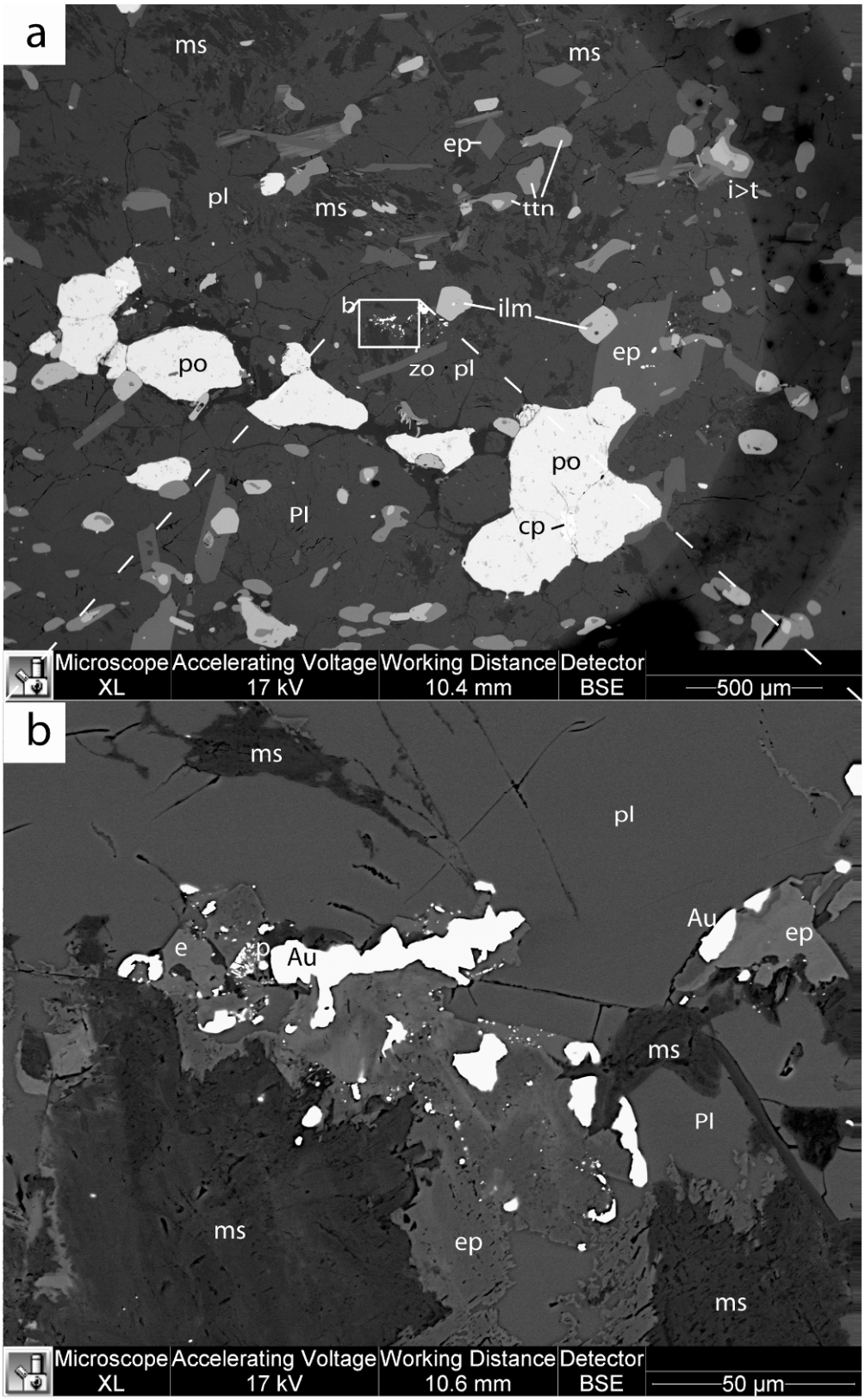

sample 487429, spot 1. Gold dust in plagioclase-rich calc-silicate gneiss with pyrrhotite (po), epidote (ep), ilmenite (ilm) and titanite (ttn)in the matrix. Po contains cp inclusion. The plagioclase grains are partially sericitised (ms). a: overview, b: close-up of the gold grains surrounded by heterogeneous epidote (box in a).

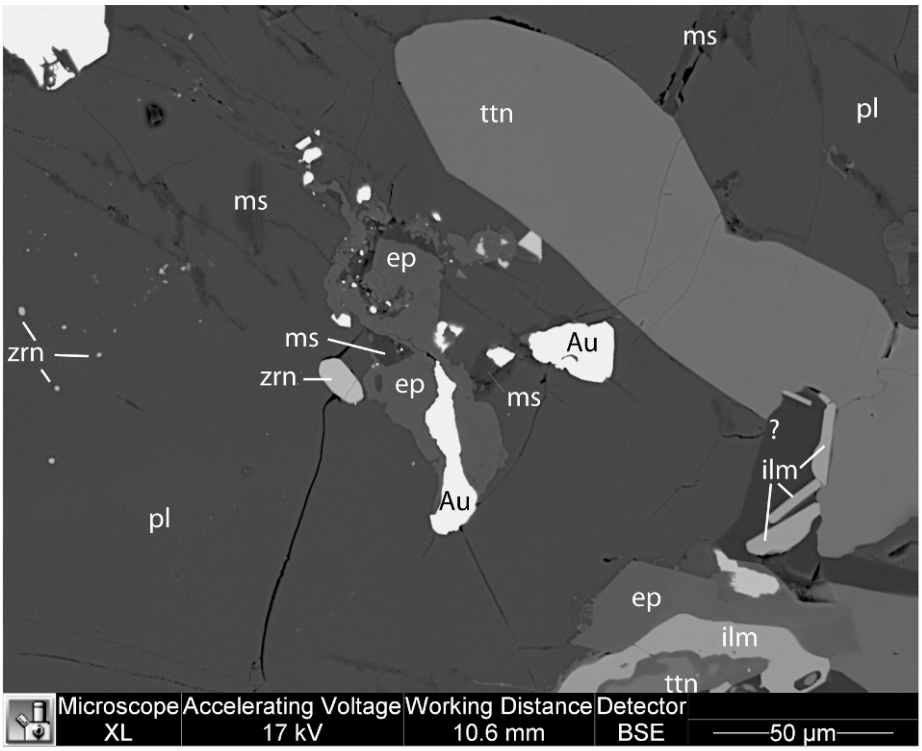

487429 gold grains up to 25 µm associated with retrograde sericite (ms) and epidote (ep) within plagioclase. Much of the sericite sits on plagioclase grain boundaries.

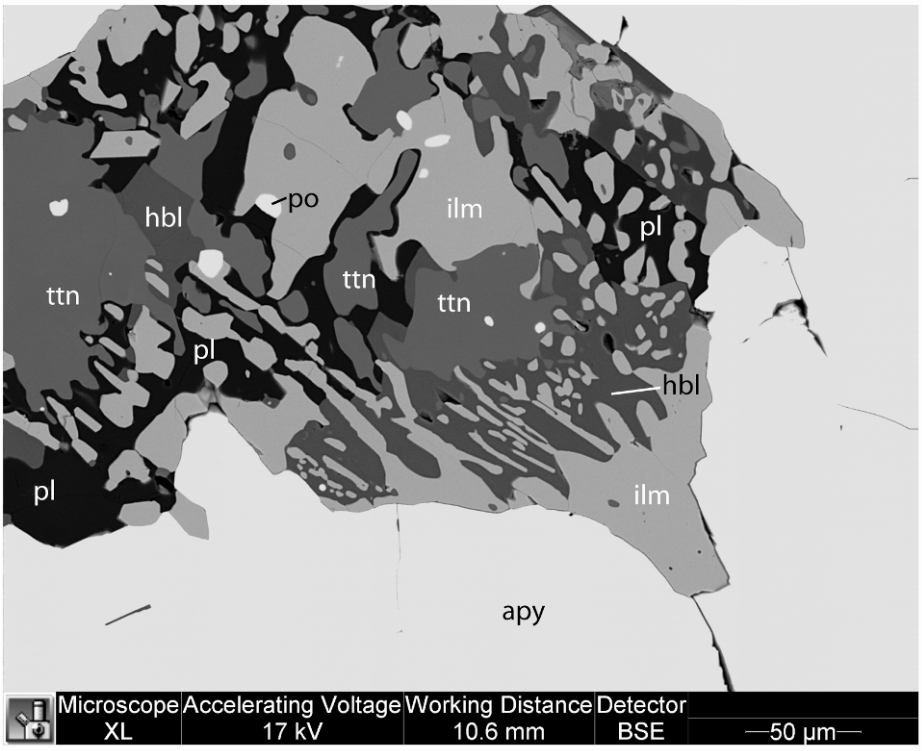

487429 spot 2 Symplectite of ilmenite (ilm) and pargasitic hornblende (hbl) in between titanite (ttn) and arsenopyrite (apy). Locally also a rim of sodic plagioclase separates ilmenite and titanite (which elsewhere are in contact.Plagioclase is calcic in most of section , but gets sodic in vicinity of the symplectite

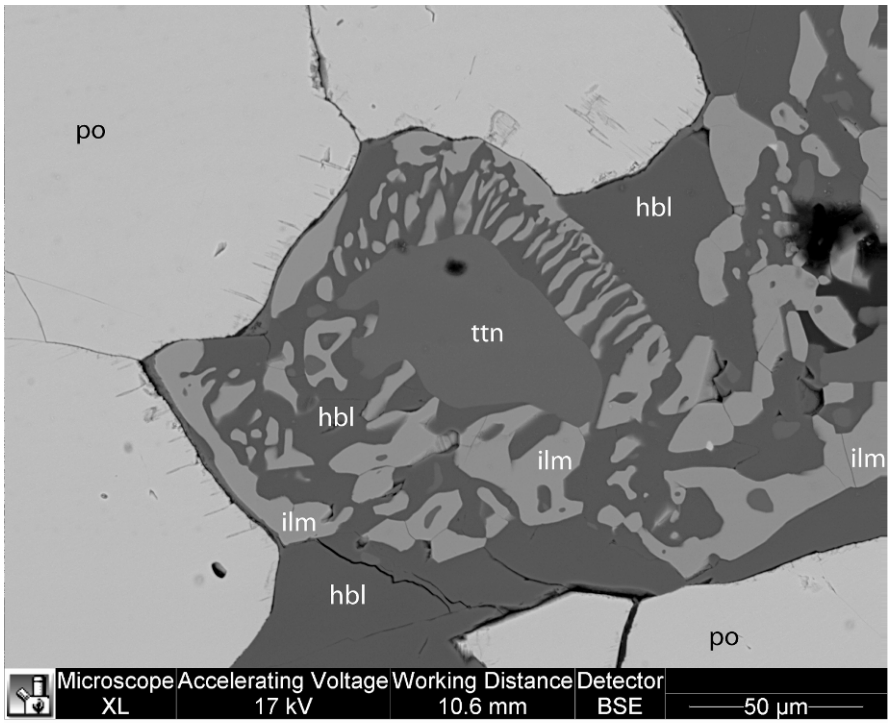

487429 spot 4 hornblende (ca amphibole/Fe hornblende?) symplctite with ilmenite (ilm). titanite in core seems to break down to ilmmenite + hornblende. Hornblende composition in symplectite is approx the same as adjoining matrix hornblende.

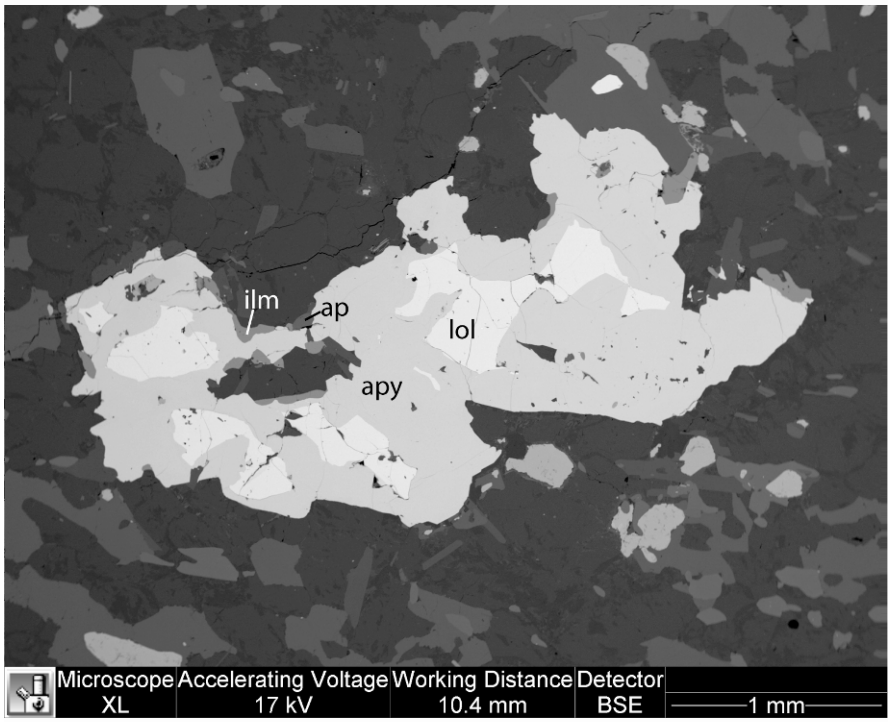

487429 spot 5 Arsenopyrite (apy) with lollingite (lol) inclusions. Also (invisible, 2-5 mm Au-Bi telluride inclusions. Matrix of sericitised plagioclase, hornblende, epidote, titanite and ilmenite.

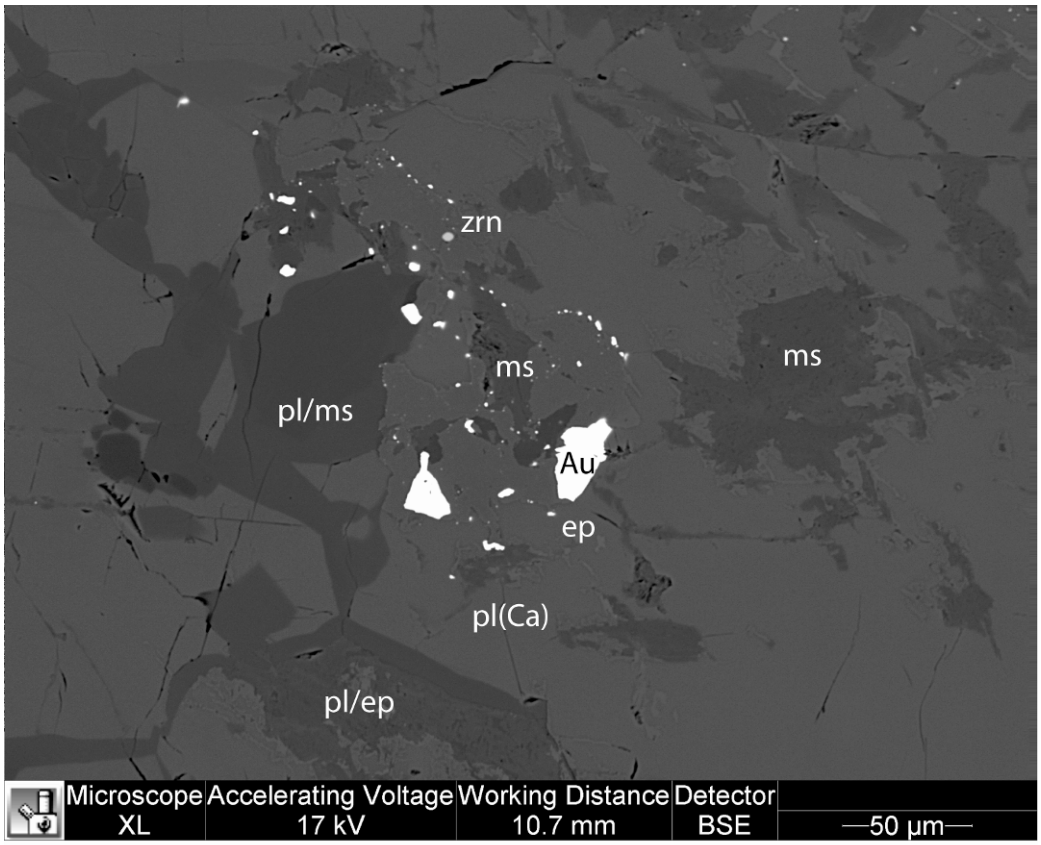

487429 spot 6 Gold in sericitised + epidotised plagioclase

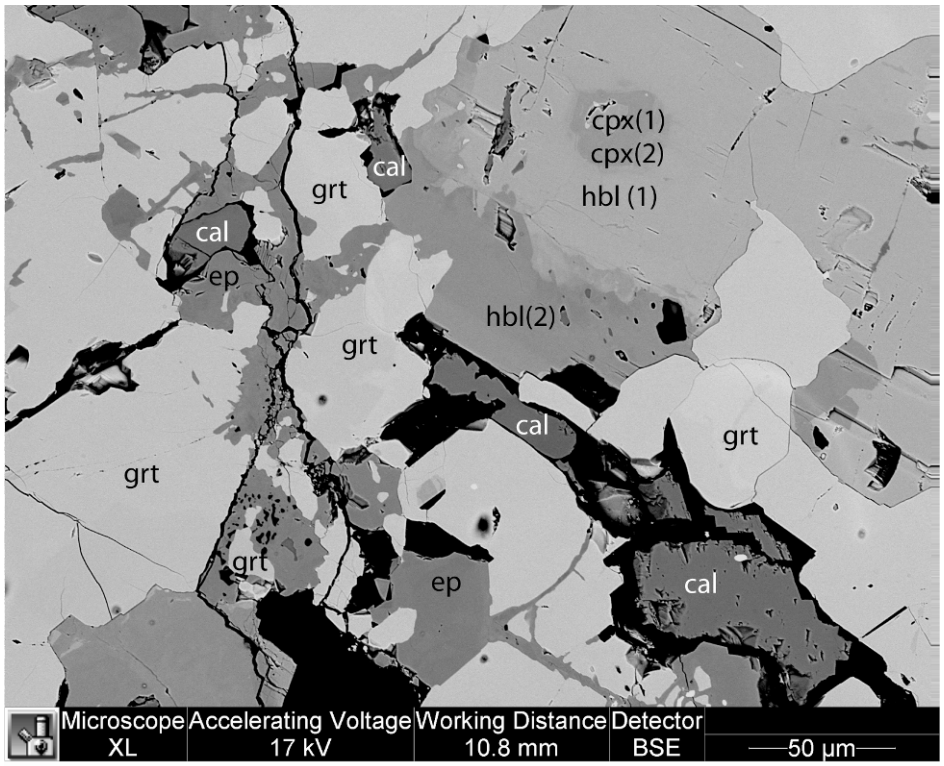

497430 spot 2 clinopyroxene (diopside-hedenbergite - cpx1) with rim of less calcic pyroxene regrogressing to amphiboles, (hbl1, and less Fe-rich hbl2). Black areas are holes in the section. Calcite sits mainly in fractures

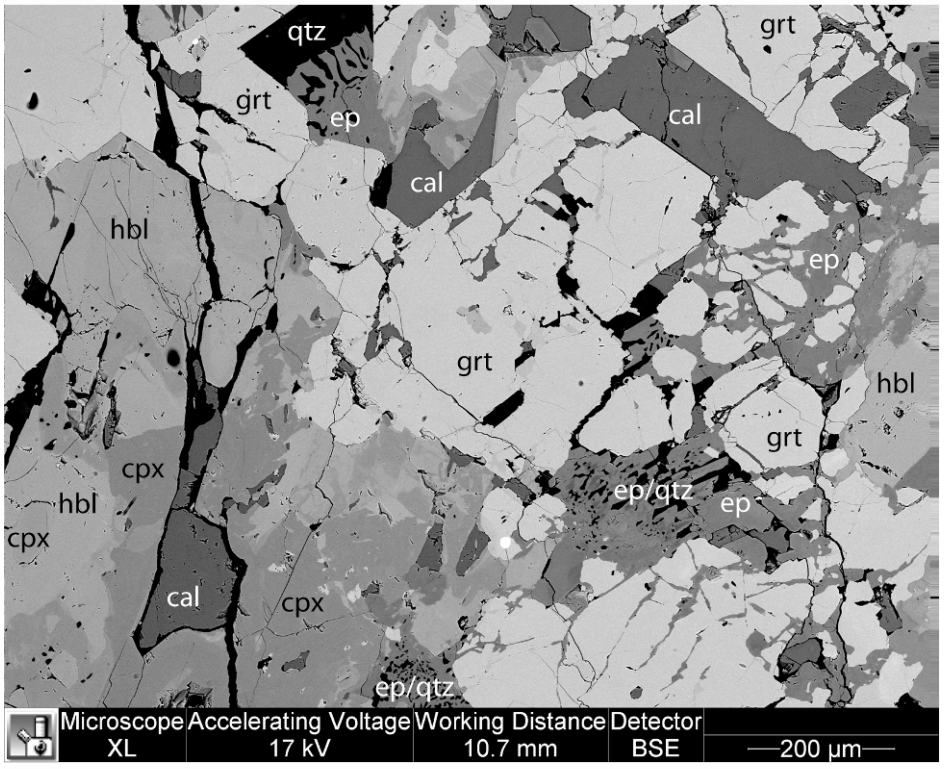

497430 spot 2 Heterogeneous hornblende/clinopyroxene matrix with fragmental garnet and epidote-quartz symplectites. Fractures in the garnet are filled with epidote and calcite.

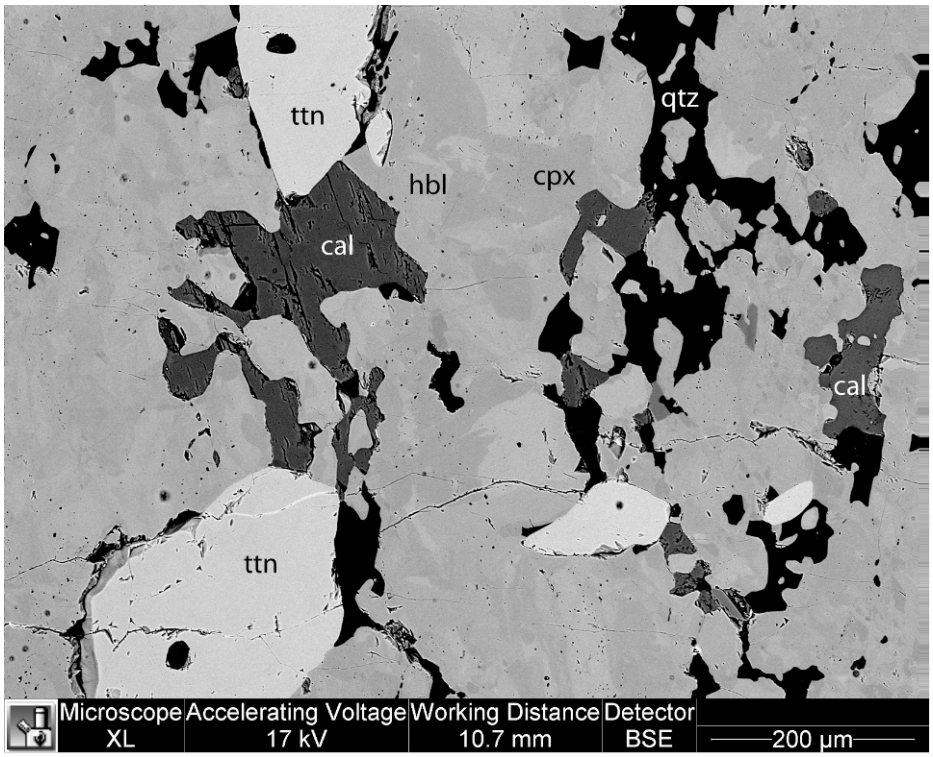

sample 487430 - spot 3 - heterogeneous mixture of hornblende (lighter grey colours) and clinopyroxene (darker grey colours), with titanite grains and interstitial calcite and quartz.

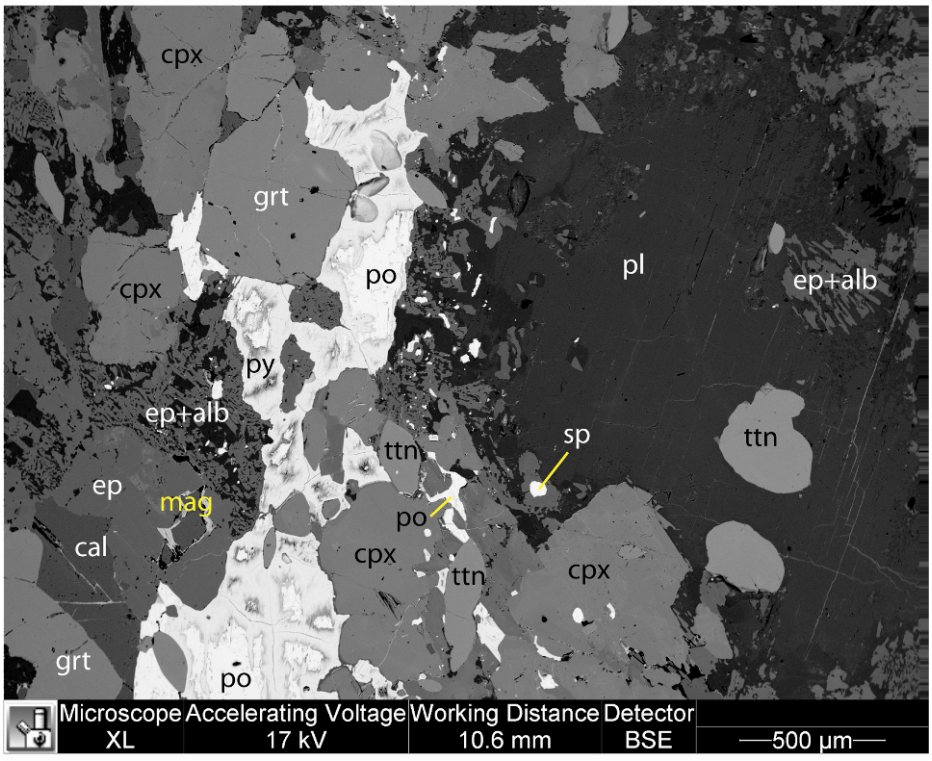

sample 487430 - spot 6 - Large pyrrhotite/pyrite grain, interstitial between other phases. One grain of sphalerite (sp), in mixed hbl-cpx-ttn matrix with epidote-plagioclase symplectites. At mag, a calcite grain is surrounded by magnetite. Epidote occurs as subhedral grains and symplectitic with sodic plagioclase (alb).

Appendix 2: Analytical methods for zircon geochronology

Zircon was separated from the crushed and powdered samples at GEUS through panning in plastic gold pans. Magnetic minerals are removed with a hand-held magnet. The heavy mineral residue is further separated through swirling in ethanol over a strong Nd-magnet, which creates a gradient between zircon, sulphides (mainly pyrite) and phosphates (mainly apatite). Zircon is then hand picked from the final sample and mounted on tape. The mounted zircon grains are cast into epoxy and polished to expose a central cross-section of each grain. The mount is examined in a secondary electron microscope (SEM) using Back Scattered Electron (BSE) imaging to reveal internal structures within each zircon grain.

Gerdes & Zeh (2006) and Frei *et al.* (2006) describe the analytical method in detail, of which a brief summary is given here. The grains are analysed with GEUS' Element2 Laser-Ablation Sector Field Inductively Coupled Plasma Mass Spectrometer (LA-SF-ICP-MS). The laser ablation microprobe uses a focused laser to ablate a small amount of a sample that was mounted together with standards in a low-volume ablation cell. For the spot diameter (20–30 µm) and ablation times (30 s) used in this study, the ablated masses of zircon were approximately 150-300 ng. We use a NewWave Research®/Merchantek® UP213 laser ablation unit that is equipped with a frequency quintupled ND-YAG laser, which emits a beam wavelength of 213 nm. We use a repetition rate of 10 Hz and a nominal energy output of 44 %, corresponding to a laser fluency of 8 J/cm^2.

The ablated material is introduced into the GEUS' Element2 (ThermoFinnigan®, Bremen) single-collector double focusing magnetic sector ICPMS, which is equipped with a fast field regulator for increased scanning speed. The total acquisition time for each analysis is 90 s of which the first 30 s are used to determine the gas blank.

The raw data is corrected for instrumental mass bias and laser-induced U-Pb fractionation through normalisation to the GJ-1 zircon (Jackson *et al.* 2004) using our in-house software ZIRCHRON. Mercury interference at mass 204 is monitored using ^{202}Hg and corrected assuming a natural ^{202}Hg/^{204}Hg ratio. Element fractionation was corrected using linear regression to a common intercept point. All ratios were normalised to the standard GJ-1, which was run in triplicate after each set of ten unknowns. Errors include standard reproducibility errors, which are propagated into each individual data point. Error estimates are quite conservative.

Appendix 3: Tabulated geochronological data

Abbreviations used in the tables: ρ = $^{235}U/^{207}P$ - $^{238}U/^{206}Pb$ error correlation; conc = concordance. Spot numbers refer to spots marked on the SEM-BSE images that were used to find selected grains during analytical runs.

sample	$^{207}Pb/^{206}Pb$	±1σ	$^{207}Pb/^{235}U$	±1σ	$^{206}Pb/^{238}U$	±1σ	ρ	$^{207}Pb/^{235}U$	±2σ	$^{206}Pb/^{238}U$	±2σ	$^{207}Pb/^{206}Pb$	±2σ	Conc
spot		%		%		%		Ma	Ma	Ma	Ma	Ma	Ma	%
484601														
7	0,2890	0,0051	24,859	0,849	0,6238	0,0183	0,86	3303	33	3125	73	3412	27	95
8	0,2101	0,0030	14,289	0,539	0,4932	0,0173	0,93	2769	36	2585	74	2906	23	93
9	0,2012	0,0019	14,130	0,284	0,5094	0,0091	0,89	2758	19	2654	39	2836	15	96
10	0,3286	0,0061	29,601	0,998	0,6534	0,0184	0,83	3474	33	3242	72	3610	29	93
11	0,3100	0,0059	25,968	0,722	0,6075	0,0123	0,73	3345	27	3060	49	3521	29	91
12	0,2300	0,0024	16,329	0,439	0,5149	0,0128	0,92	2896	26	2677	54	3052	17	92
13	0,2180	0,0049	15,224	0,624	0,5066	0,0173	0,83	2829	39	2642	74	2966	36	93
14	0,2483	0,0034	19,720	0,583	0,5760	0,0151	0,89	3078	29	2932	62	3174	22	95
16	0,2028	0,0026	15,927	0,311	0,5697	0,0084	0,76	2872	19	2906	35	2849	21	101
20	0,2121	0,0030	16,541	0,347	0,5657	0,0088	0,74	2909	20	2890	36	2921	23	99
21	0,2017	0,0033	15,186	0,402	0,5462	0,0114	0,79	2827	25	2809	48	2840	26	99
22	0,2057	0,0041	15,909	0,466	0,5609	0,0120	0,73	2871	28	2870	49	2872	33	100
23	0,2302	0,0025	19,395	0,455	0,6111	0,0127	0,89	3062	23	3074	51	3053	17	100
24	0,2019	0,0017	15,550	0,290	0,5587	0,0092	0,89	2850	18	2861	38	2841	14	100
25	0,2027	0,0027	15,382	0,330	0,5504	0,0093	0,79	2839	20	2827	39	2848	21	100
26	0,2936	0,0030	27,938	0,553	0,6901	0,0117	0,86	3417	19	3383	45	3437	16	99
27	0,2914	0,0026	27,280	0,610	0,6789	0,0140	0,92	3394	22	3340	54	3425	14	98
28	0,2038	0,0034	16,851	0,420	0,5996	0,0113	0,75	2926	24	3028	45	2857	27	103
33	0,2094	0,0020	16,673	0,373	0,5774	0,0117	0,90	2916	21	2938	48	2901	16	101
34	0,2103	0,0029	16,391	0,305	0,5652	0,0072	0,68	2900	18	2888	29	2908	22	100
35	0,2394	0,0036	21,746	0,495	0,6587	0,0113	0,75	3172	22	3262	44	3116	24	103
36	0,2250	0,0019	19,556	0,330	0,6303	0,0092	0,87	3070	16	3151	36	3017	13	103
37	0,2392	0,0045	21,862	0,558	0,6629	0,0114	0,67	3178	25	3279	44	3115	30	103
38	0,2003	0,0020	17,164	0,334	0,6216	0,0104	0,86	2944	19	3116	41	2828	16	106
39	0,2372	0,0040	22,489	0,557	0,6876	0,0124	0,73	3205	24	3373	47	3101	27	105
40	0,2080	0,0016	16,203	0,277	0,5651	0,0086	0,89	2889	16	2888	35	2890	12	100
41	0,2028	0,0018	16,587	0,242	0,5931	0,0070	0,80	2911	14	3002	28	2849	14	103
42	0,2029	0,0035	15,911	0,378	0,5688	0,0092	0,68	2871	23	2903	38	2850	28	101

sample spot	$^{207}Pb/^{206}Pb$	±1σ %	$^{207}Pb/^{235}U$	±1σ %	$^{206}Pb/^{238}U$	±1σ %	ρ	$^{207}Pb/^{235}U$ Ma	±2σ Ma	$^{206}Pb/^{238}U$ Ma	±2σ Ma	$^{207}Pb/^{206}Pb$ Ma	±2σ Ma	Conc %
484601 – continued														
46	0,2017	0,0022	15,892	0,331	0,5713	0,0102	0,85	2870	20	2913	42	2840	18	101
47	0,2096	0,0039	16,649	0,461	0,5761	0,0118	0,74	2915	27	2933	48	2903	30	101
48	0,2084	0,0024	16,567	0,356	0,5765	0,0105	0,85	2910	21	2934	43	2893	19	101
49	0,3342	0,0038	34,272	0,828	0,7438	0,0159	0,88	3618	24	3584	59	3636	17	99
50	0,2131	0,0031	17,008	0,576	0,5787	0,0177	0,90	2935	33	2944	72	2930	23	100
51	0,2237	0,0025	16,626	0,332	0,5391	0,0089	0,83	2913	19	2780	37	3007	18	95
52	0,2103	0,0028	16,542	0,566	0,5704	0,0180	0,92	2909	33	2910	74	2908	21	100
54	0,2711	0,0080	25,797	0,958	0,6902	0,0156	0,61	3339	36	3383	60	3312	46	101
55	0,2001	0,0030	15,368	0,440	0,5569	0,0135	0,85	2838	27	2854	56	2827	25	101
59	0,2193	0,0042	18,595	0,527	0,6148	0,0128	0,73	3021	27	3089	51	2976	31	102
60	0,2027	0,0028	15,015	0,412	0,5371	0,0127	0,86	2816	26	2771	53	2848	23	98
61	0,2277	0,0046	18,919	0,755	0,6027	0,0207	0,86	3038	39	3041	83	3036	32	100
62	0,2101	0,0024	16,398	0,417	0,5661	0,0129	0,90	2900	24	2892	53	2906	18	100
64	0,2258	0,0040	18,153	0,469	0,5832	0,0109	0,72	2998	25	2962	44	3022	29	99
65	0,2148	0,0047	16,573	0,536	0,5596	0,0134	0,74	2910	31	2865	55	2942	35	98
66	0,2031	0,0015	15,510	0,307	0,5538	0,0102	0,93	2847	19	2841	42	2851	12	100
67	0,2133	0,0034	16,826	0,436	0,5722	0,0117	0,79	2925	25	2917	48	2931	26	100
484652														
8	0,1770	0,0035	12,292	0,545	0,5037	0,0200	0,89	2627	42	2630	86	2625	33	100
9	0,1771	0,0045	11,500	0,452	0,4711	0,0141	0,76	2565	37	2488	62	2626	42	97
10	0,1803	0,0048	11,609	0,519	0,4671	0,0169	0,81	2573	42	2471	74	2655	44	96
11	0,1772	0,0030	10,586	0,383	0,4332	0,0138	0,88	2487	34	2320	62	2627	28	93
13	0,1756	0,0027	10,998	0,382	0,4543	0,0141	0,90	2523	32	2414	63	2612	26	96
16	0,1787	0,0029	11,950	0,370	0,4851	0,0128	0,85	2600	29	2549	56	2641	27	98
20	0,1793	0,0029	11,210	0,408	0,4535	0,0148	0,90	2541	34	2411	66	2646	27	95
22	0,1775	0,0028	11,783	0,467	0,4816	0,0175	0,92	2587	37	2534	76	2629	26	98
23	0,1771	0,0024	11,525	0,342	0,4719	0,0124	0,89	2567	28	2492	54	2626	23	97

sample spot	$^{207}Pb/^{206}Pb$	±1σ %	$^{207}Pb/^{235}U$	±1σ %	$^{206}Pb/^{238}U$	±1σ %	ρ	$^{207}Pb/^{235}U$ Ma	±2σ Ma	$^{206}Pb/^{238}U$ Ma	±2σ Ma	$^{207}Pb/^{206}Pb$ Ma	±2σ Ma	Conc %
484652 - continued														
25	0,1795	0,0027	11,756	0,342	0,4749	0,0119	0,86	2585	27	2505	52	2649	25	97
26	0,1762	0,0030	12,034	0,404	0,4953	0,0144	0,86	2607	31	2594	62	2618	28	99
27	0,1776	0,0028	11,566	0,331	0,4723	0,0113	0,84	2570	27	2493	49	2631	26	97
28	0,1779	0,0027	11,876	0,349	0,4842	0,0121	0,85	2595	28	2545	53	2633	26	98
29	0,1778	0,0042	11,494	0,375	0,4688	0,0104	0,68	2564	30	2478	46	2633	40	97
33	0,1779	0,0028	11,498	0,380	0,4688	0,0136	0,88	2564	31	2478	60	2633	26	97
34	0,1778	0,0033	11,485	0,368	0,4684	0,0123	0,82	2563	30	2477	54	2633	30	97
35	0,1775	0,0043	11,062	0,447	0,4520	0,0147	0,81	2528	38	2404	65	2630	40	95
36	0,1798	0,0032	12,435	0,387	0,5017	0,0128	0,82	2638	29	2621	55	2651	30	99
37	0,1788	0,0029	12,329	0,399	0,5003	0,0140	0,86	2630	30	2615	60	2641	27	99
38	0,1784	0,0027	11,963	0,383	0,4864	0,0137	0,88	2601	30	2555	60	2638	25	98
40	0,1793	0,0028	12,218	0,412	0,4943	0,0148	0,89	2621	32	2589	64	2646	26	99
42	0,1764	0,0023	12,783	0,389	0,5255	0,0145	0,91	2664	29	2722	61	2620	21	102
46	0,1778	0,0046	12,257	0,486	0,5000	0,0150	0,76	2624	37	2614	64	2632	43	100
47	0,1779	0,0033	12,268	0,370	0,5002	0,0118	0,78	2625	28	2615	51	2633	31	100
48	0,1780	0,0030	12,705	0,510	0,5177	0,0189	0,91	2658	38	2690	80	2634	28	101
49	0,1770	0,0024	12,385	0,347	0,5075	0,0125	0,88	2634	26	2646	53	2625	22	100
487404														
296	0,1715	0,0024	12,576	0,288	0,5319	0,0097	0,80	2648	22	2749	41	2572	23	109
298	0,1750	0,0026	12,037	0,291	0,4989	0,0095	0,79	2607	23	2609	41	2606	25	99
299	0,1706	0,0021	12,415	0,399	0,5277	0,0157	0,92	2636	30	2732	66	2564	21	107
300	0,1708	0,0030	14,719	0,435	0,6249	0,0148	0,80	2797	28	3129	59	2566	29	109
305	0,1713	0,0038	11,082	0,751	0,4692	0,0300	0,94	2530	63	2480	132	2570	37	101
309	0,1696	0,0022	11,643	0,390	0,4978	0,0154	0,92	2576	31	2604	66	2554	21	104
310	0,1718	0,0020	13,338	0,350	0,5631	0,0133	0,90	2704	25	2879	55	2575	19	104
311	0,1666	0,0036	12,361	0,778	0,5380	0,0318	0,94	2632	59	2775	133	2524	37	105
312	0,1745	0,0086	12,159	0,796	0,5052	0,0218	0,66	2617	62	2636	93	2602	82	101

sample spot	$^{207}Pb/^{206}Pb$	±1σ %	$^{207}Pb/^{235}U$	±1σ %	$^{206}Pb/^{238}U$	±1σ %	ρ	$^{207}Pb/^{235}U$ Ma	±2σ Ma	$^{206}Pb/^{238}U$ Ma	±2σ Ma	$^{207}Pb/^{206}Pb$ Ma	±2σ Ma	Conc %
487404 - continued														
313	0,1710	0,0025	12,228	0,354	0,5185	0,0129	0,86	2622	27	2693	55	2568	25	104
317	0,1680	0,0012	12,363	0,222	0,5337	0,0088	0,92	2632	17	2757	37	2538	12	103
326	0,1709	0,0032	11,309	0,565	0,4799	0,0222	0,93	2549	47	2527	97	2567	31	106
330	0,1787	0,0040	12,550	0,564	0,5094	0,0199	0,87	2646	42	2654	85	2641	37	100
331	0,1731	0,0022	14,308	0,471	0,5994	0,0182	0,92	2770	31	3028	73	2588	21	100
337	0,1764	0,0002	14,472	0,450	0,5952	0,0185	1,00	2781	30	3010	75	2619	2	108
339	0,1725	0,0017	14,019	0,353	0,5895	0,0137	0,92	2751	24	2987	56	2582	16	103
341	0,1709	0,0016	13,355	0,340	0,5668	0,0134	0,93	2705	24	2895	55	2566	16	109
342	0,1762	0,0014	13,201	0,355	0,5434	0,0140	0,96	2694	25	2798	58	2617	13	98
344	0,1757	0,0014	12,790	0,318	0,5279	0,0124	0,95	2664	23	2732	52	2613	13	105
348	0,1795	0,0068	12,236	0,610	0,4943	0,0161	0,65	2623	47	2589	69	2649	63	99
349	0,1739	0,0017	14,448	0,183	0,6027	0,0048	0,63	2780	12	3041	19	2595	16	112
350	0,1801	0,0071	15,189	0,728	0,6117	0,0168	0,57	2827	46	3077	67	2654	65	109
487416														
7	0,1769	0,0042	11,198	0,496	0,4591	0,0172	0,85	2540	41	2436	76	2624	39	96
8	0,2009	0,0082	15,275	0,922	0,5514	0,0244	0,73	2833	58	2831	101	2834	67	100
9	0,2017	0,0075	15,019	0,830	0,5402	0,0220	0,74	2816	53	2784	92	2840	61	99
10	0,1773	0,0059	13,592	0,591	0,5559	0,0154	0,64	2722	41	2850	64	2628	56	105
11	0,1776	0,0052	13,162	0,502	0,5375	0,0133	0,65	2691	36	2773	56	2631	48	103
13	0,1769	0,0014	13,592	0,333	0,5573	0,0130	0,95	2722	23	2855	54	2624	13	105
14	0,1786	0,0033	12,763	0,248	0,5183	0,0030	0,30	2662	18	2692	13	2640	31	101
20	0,1781	0,0027	13,512	0,239	0,5503	0,0052	0,54	2716	17	2826	22	2635	25	104
24	0,1822	0,0041	12,366	0,314	0,4921	0,0058	0,46	2633	24	2580	25	2673	37	98
26	0,1762	0,0054	12,859	0,559	0,5294	0,0164	0,71	2669	41	2739	69	2617	51	103
28	0,1825	0,0074	12,299	0,568	0,4887	0,0107	0,47	2627	43	2565	46	2676	67	98
33	0,1788	0,0067	11,698	0,576	0,4746	0,0151	0,65	2581	46	2504	66	2642	62	97

sample	$^{207}Pb/^{206}Pb$	±1σ	$^{207}Pb/^{235}U$	±1σ	$^{206}Pb/^{238}U$	±1σ	ρ	$^{207}Pb/^{235}U$	±2σ	$^{206}Pb/^{238}U$	±2σ	$^{207}Pb/^{206}Pb$	±2σ	Conc
spot		%		%		%		Ma	Ma	Ma	Ma	Ma	Ma	%
487416 - continued														
34	0,1827	0,0088	13,916	0,855	0,5525	0,0212	0,62	2744	58	2835	88	2677	79	103
36	0,1738	0,0058	12,299	0,648	0,5134	0,0208	0,77	2628	49	2671	89	2594	56	102
37	0,2040	0,0052	14,576	0,736	0,5181	0,0225	0,86	2788	48	2691	96	2859	42	97
39	0,1821	0,0057	12,720	0,447	0,5067	0,0083	0,47	2659	33	2642	35	2672	51	99
40	0,1780	0,0061	12,017	0,487	0,4898	0,0107	0,54	2606	38	2570	46	2634	57	99
41	0,2089	0,0073	16,221	0,787	0,5633	0,0189	0,69	2890	46	2880	78	2897	57	100
46	0,2033	0,0076	15,617	0,722	0,5570	0,0151	0,58	2854	44	2854	62	2853	61	100
47	0,1784	0,0044	12,128	0,443	0,4930	0,0133	0,74	2614	34	2583	57	2638	41	99
49	0,2189	0,0114	16,682	1,178	0,5527	0,0263	0,67	2917	68	2837	109	2973	84	97
50	0,2024	0,0083	16,473	0,791	0,5902	0,0145	0,51	2905	46	2990	59	2846	67	103
52	0,1760	0,0042	11,805	0,354	0,4864	0,0089	0,61	2589	28	2555	39	2616	40	99
53	0,1768	0,0052	12,376	0,402	0,5076	0,0071	0,43	2633	30	2646	30	2623	49	100
60	0,1827	0,0097	13,218	0,862	0,5248	0,0200	0,58	2695	62	2719	84	2677	88	101
61	0,1810	0,0027	12,976	0,370	0,5198	0,0126	0,85	2678	27	2698	53	2662	25	101
62	0,1746	0,0038	11,138	0,449	0,4626	0,0157	0,84	2535	38	2451	69	2603	36	97
64	0,1784	0,0015	12,821	0,190	0,5213	0,0063	0,82	2667	14	2705	27	2638	14	101
65	0,2010	0,0059	15,257	0,877	0,5506	0,0272	0,86	2831	55	2828	113	2834	48	100
66	0,1773	0,0038	12,756	0,508	0,5219	0,0176	0,85	2662	38	2707	75	2628	35	102
67	0,1984	0,0047	15,449	0,611	0,5648	0,0180	0,80	2843	38	2887	74	2813	38	102
487467														
244	0,2266	0,0053	20,030	0,794	0,6410	0,0205	0,81	3093	38	3193	81	3028	38	103
245	0,2052	0,0034	8,360	0,380	0,2954	0,0125	0,93	2271	41	1669	62	2868	27	73
247	0,1700	0,0018	12,824	0,461	0,5471	0,0188	0,96	2667	34	2813	78	2558	18	105
248	0,2075	0,0051	15,017	0,507	0,5248	0,0122	0,69	2816	32	2720	52	2886	40	97
249	0,1738	0,0032	12,896	0,412	0,5381	0,0141	0,82	2672	30	2776	59	2595	31	104
250	0,1718	0,0027	12,351	0,529	0,5214	0,0208	0,93	2631	40	2705	88	2575	26	103
251	0,2319	0,0042	19,834	0,680	0,6202	0,0181	0,85	3083	33	3111	72	3065	29	101
252	0,1733	0,0038	13,051	0,681	0,5462	0,0258	0,91	2683	49	2809	108	2590	37	105

sample	$^{207}Pb/^{206}Pb$	±1σ	$^{207}Pb/^{235}U$	±1σ	$^{206}Pb/^{238}U$	±1σ	ρ	$^{207}Pb/^{235}U$	±2σ	$^{206}Pb/^{238}U$	±2σ	$^{207}Pb/^{206}Pb$	±2σ	Conc
spot		%		%		%		Ma	Ma	Ma	Ma	Ma	Ma	%
487467 - continued														
253	0,1721	0,0038	13,068	0,556	0,5506	0,0201	0,86	2685	40	2828	84	2579	36	105
257	0,1743	0,0013	12,409	0,189	0,5165	0,0069	0,88	2636	14	2684	29	2599	12	102
258	0,1751	0,0027	12,918	0,546	0,5350	0,0211	0,93	2674	40	2763	88	2607	25	103
259	0,1751	0,0018	13,110	0,348	0,5429	0,0133	0,92	2688	25	2796	55	2607	17	104
260	0,1728	0,0019	11,115	0,179	0,4665	0,0055	0,73	2533	15	2468	24	2585	18	97
487495														
7	0,2008	0,0023	14,868	0,383	0,5371	0,0125	0,90	2807	25	2771	52	2832	18	99
10	0,2060	0,0035	16,529	0,687	0,5818	0,0220	0,91	2908	40	2956	90	2875	28	102
11	0,3437	0,0044	35,071	1,573	0,7400	0,0318	0,96	3641	44	3571	118	3679	20	98
13	0,1989	0,0015	16,399	0,457	0,5978	0,0160	0,96	2900	27	3021	65	2818	13	104
22	0,2064	0,0041	16,321	0,544	0,5736	0,0153	0,80	2896	32	2923	63	2877	33	101
40	0,2054	0,0019	13,797	0,628	0,4873	0,0217	0,98	2736	43	2559	94	2869	15	94
41	0,2066	0,0041	13,753	0,489	0,4828	0,0143	0,83	2733	34	2539	62	2879	32	93
50	0,2062	0,0018	18,406	0,541	0,6474	0,0182	0,96	3011	28	3218	71	2876	14	107
51	0,2065	0,0026	14,771	0,466	0,5187	0,0150	0,92	2801	30	2694	64	2879	21	96
63	0,2083	0,0037	15,878	0,584	0,5530	0,0178	0,88	2870	35	2837	74	2892	29	99
64	0,1981	0,0028	15,449	0,552	0,5657	0,0186	0,92	2843	34	2890	77	2810	23	102
72a	0,3504	0,0085	36,548	1,304	0,7565	0,0198	0,73	3681	35	3632	73	3709	37	99
74a	0,2034	0,0024	15,346	0,356	0,5472	0,0110	0,86	2837	22	2814	46	2854	19	99
75a	0,2132	0,0035	10,904	0,398	0,3710	0,0121	0,90	2515	34	2034	57	2930	26	81
76a	0,2088	0,0035	14,833	0,499	0,5153	0,0150	0,86	2805	32	2679	64	2896	28	96
77a	0,1768	0,0027	12,096	0,293	0,4962	0,0092	0,77	2612	23	2598	40	2623	26	99
78a	0,2044	0,0042	16,101	0,565	0,5712	0,0162	0,81	2883	34	2913	67	2862	34	101
79a	0,1733	0,0017	12,635	0,195	0,5288	0,0062	0,76	2653	15	2736	26	2590	17	103
80a	0,2039	0,0030	15,337	0,379	0,5456	0,0108	0,80	2836	24	2807	45	2857	24	99
81a	0,1738	0,0015	12,293	0,195	0,5130	0,0068	0,83	2627	15	2669	29	2595	15	102

sample spot	$^{207}Pb/^{206}Pb$	±1σ %	$^{207}Pb/^{235}U$	±1σ %	$^{206}Pb/^{238}U$	±1σ %	ρ	$^{207}Pb/^{235}U$ Ma	±2σ Ma	$^{206}Pb/^{238}U$ Ma	±2σ Ma	$^{207}Pb/^{206}Pb$ Ma	±2σ Ma	Conc %
487495 - continued														
85a	0,2159	0,0040	17,258	0,533	0,5798	0,0143	0,80	2949	30	2948	58	2950	30	100
86a	0,2134	0,0054	21,605	0,740	0,7344	0,0170	0,68	3166	33	3550	63	2931	41	112
87a	0,2133	0,0043	17,016	0,585	0,5786	0,0162	0,81	2936	33	2943	66	2931	32	100
88a	0,1744	0,0020	12,089	0,334	0,5028	0,0126	0,91	2611	26	2626	54	2600	19	101
89a	0,2115	0,0034	16,032	0,486	0,5497	0,0141	0,84	2879	29	2824	58	2917	26	98
90a	0,1755	0,0026	12,213	0,331	0,5046	0,0114	0,84	2621	25	2633	49	2611	25	100
92a	0,2066	0,0067	15,003	0,599	0,5268	0,0124	0,59	2815	38	2728	52	2879	52	97
93a	0,2057	0,0024	15,827	0,378	0,5581	0,0116	0,87	2866	23	2859	48	2872	19	100
94a	0,2010	0,0047	13,824	0,449	0,4987	0,0112	0,69	2738	31	2608	48	2835	38	95
98a	0,1741	0,0034	13,725	0,344	0,5718	0,0089	0,62	2731	24	2915	36	2597	33	107
99a	0,2095	0,0038	15,413	0,412	0,5337	0,0104	0,73	2841	25	2757	44	2901	29	97
100a	0,1743	0,0026	12,425	0,296	0,5169	0,0096	0,78	2637	22	2686	41	2600	25	102
101a	0,2024	0,0039	16,010	0,731	0,5737	0,0238	0,91	2877	44	2923	97	2846	31	102
102a	0,1739	0,0015	12,496	0,258	0,5211	0,0098	0,91	2642	19	2704	41	2596	14	102
103a	0,1738	0,0014	12,955	0,196	0,5406	0,0070	0,85	2676	14	2786	29	2595	13	104
104a	0,2076	0,0026	15,191	0,405	0,5308	0,0125	0,88	2827	25	2745	53	2887	20	97
105a	0,1742	0,0019	12,298	0,225	0,5121	0,0076	0,81	2627	17	2666	32	2598	18	101
106a	0,1978	0,0025	16,026	0,219	0,5876	0,0029	0,35	2878	13	2980	12	2808	21	104
107a	0,1739	0,0014	12,789	0,141	0,5334	0,0040	0,68	2664	10	2756	17	2595	14	103
487918														
72	0,3329	0,0053	36,578	0,735	0,7968	0,0097	0,60	3682	20	3778	35	3631	25	103
81	0,3153	0,0057	23,682	2,247	0,5447	0,0507	0,98	3255	93	2803	212	3547	28	86
85	0,3288	0,0056	32,055	1,631	0,7070	0,0339	0,94	3552	50	3447	128	3612	26	97
86	0,3218	0,0067	34,375	1,016	0,7748	0,0162	0,71	3621	29	3698	59	3578	32	102
87	0,3666	0,0043	40,001	0,938	0,7915	0,0160	0,86	3771	23	3758	58	3777	18	100
91	0,3328	0,0029	32,414	0,734	0,7064	0,0148	0,93	3563	22	3445	56	3630	13	97

sample	$^{207}Pb/^{206}Pb$	±1σ	$^{207}Pb/^{235}U$	±1σ	$^{206}Pb/^{238}U$	±1σ	ρ	$^{207}Pb/^{235}U$	±2σ	$^{206}Pb/^{238}U$	±2σ	$^{207}Pb/^{206}Pb$	±2σ	Conc
spot		%		%		%		Ma	Ma	Ma	Ma	Ma	Ma	%
487918 - continued														
92	0,3387	0,0036	32,614	1,055	0,6984	0,0213	0,94	3569	32	3415	81	3657	16	96
99	0,3416	0,0023	33,102	0,981	0,7029	0,0203	0,97	3584	29	3432	77	3670	10	96
100	0,3235	0,0053	30,784	1,056	0,6901	0,0208	0,88	3512	34	3383	79	3587	25	96
104	0,3257	0,0046	32,888	0,902	0,7323	0,0172	0,86	3577	27	3542	64	3597	22	99
105	0,3333	0,0032	35,308	0,817	0,7684	0,0162	0,91	3647	23	3675	59	3632	15	101
112	0,3401	0,0063	35,129	1,390	0,7491	0,0262	0,88	3642	39	3604	97	3663	28	99
126	0,3374	0,0027	33,430	0,940	0,7186	0,0194	0,96	3593	28	3491	73	3651	12	97
130	0,3390	0,0044	36,181	0,853	0,7742	0,0152	0,83	3671	23	3696	55	3658	20	101
142	0,3548	0,0028	40,002	1,203	0,8177	0,0237	0,97	3771	30	3852	84	3728	12	102
143	0,3350	0,0030	38,679	1,260	0,8373	0,0262	0,96	3737	32	3921	92	3640	14	105
150	0,3419	0,0050	30,377	2,521	0,6443	0,0526	0,98	3499	82	3206	206	3671	23	92
155	0,3171	0,0034	31,343	1,315	0,7170	0,0291	0,97	3530	41	3485	109	3556	17	99
168	0,3094	0,0061	24,976	1,322	0,5856	0,0288	0,93	3307	52	2971	117	3518	30	90
169	0,3350	0,0086	32,287	1,957	0,6991	0,0384	0,91	3559	60	3417	146	3640	39	96
172	0,3559	0,0057	35,938	1,198	0,7323	0,0214	0,88	3665	33	3542	80	3733	24	97
179	0,3183	0,0033	31,840	0,873	0,7256	0,0184	0,92	3545	27	3517	69	3561	16	99
180	0,3381	0,0056	33,299	2,036	0,7143	0,0421	0,96	3589	60	3475	158	3654	25	97
112a	0,3597	0,0078	37,721	1,256	0,7606	0,0192	0,76	3713	33	3646	70	3749	33	98
113a	0,3650	0,0095	37,564	1,472	0,7464	0,0219	0,75	3708	39	3594	81	3771	39	97
115a	0,3304	0,0086	33,822	1,447	0,7423	0,0253	0,80	3605	42	3579	94	3619	40	99
116a	0,3561	0,0070	32,758	1,316	0,6672	0,0234	0,87	3573	40	3295	91	3733	30	92
117a	0,3529	0,0045	39,577	0,736	0,8133	0,0109	0,72	3760	18	3837	39	3720	20	102
118a	0,3335	0,0081	34,411	1,002	0,7483	0,0119	0,55	3622	29	3601	44	3633	37	99
124a	0,3276	0,0046	33,369	0,702	0,7387	0,0116	0,75	3592	21	3566	43	3606	21	99
127a	0,3479	0,0049	39,591	0,697	0,8253	0,0087	0,60	3761	17	3879	31	3698	22	103
132a	0,3321	0,0033	35,254	0,422	0,7699	0,0051	0,55	3646	12	3680	18	3627	15	101
137a	0,3487	0,0040	34,181	0,728	0,7108	0,0127	0,84	3615	21	3462	48	3702	18	96
140a	0,3375	0,0070	31,516	1,116	0,6773	0,0195	0,81	3535	35	3334	75	3651	31	94

sample	$^{207}Pb/^{206}Pb$	±1σ	$^{207}Pb/^{235}U$	±1σ	$^{206}Pb/^{238}U$	±1σ	ρ	$^{207}Pb/^{235}U$	±2σ	$^{206}Pb/^{238}U$	±2σ	$^{207}Pb/^{206}Pb$	±2σ	Conc
spot		%		%		%		Ma	Ma	Ma	Ma	Ma	Ma	%
487921														
261	0,1994	0,0024	17,333	0,295	0,6306	0,0077	0,71	2953	16	3152	30	2821	19	107
262	0,1800	0,0024	14,516	0,419	0,5850	0,0150	0,89	2784	27	2969	61	2653	22	107
263	0,1928	0,0017	15,927	0,360	0,5993	0,0125	0,92	2872	22	3027	50	2766	14	105
264	0,2564	0,0022	26,289	0,607	0,7437	0,0160	0,93	3357	23	3584	59	3225	13	107
270	0,1727	0,0019	11,665	0,358	0,4900	0,0140	0,93	2578	29	2571	61	2584	18	100
271	0,1887	0,0021	17,203	0,487	0,6610	0,0172	0,92	2946	27	3271	67	2731	18	111
272	0,1993	0,0012	15,173	0,236	0,5522	0,0079	0,92	2826	15	2834	33	2821	10	100
274	0,1912	0,0013	15,322	0,185	0,5813	0,0057	0,82	2835	12	2954	23	2752	11	104
275	0,2011	0,0038	16,669	0,594	0,6011	0,0182	0,85	2916	34	3034	73	2835	31	104
276	0,1806	0,0030	13,351	0,758	0,5363	0,0291	0,96	2705	54	2768	122	2658	28	102
277	0,2013	0,0016	17,525	0,556	0,6314	0,0194	0,97	2964	30	3155	77	2837	13	106
278	0,1900	0,0017	15,784	0,684	0,6025	0,0255	0,98	2864	41	3040	103	2742	15	106
279	0,1796	0,0027	12,088	0,604	0,4880	0,0232	0,95	2611	47	2562	101	2650	25	98
283	0,1812	0,0027	13,485	0,654	0,5398	0,0249	0,95	2714	46	2782	104	2664	25	103
284	0,1886	0,0031	14,538	0,589	0,5590	0,0208	0,92	2785	39	2863	86	2730	27	103
285	0,2072	0,0025	15,941	0,798	0,5580	0,0271	0,97	2873	48	2858	112	2884	19	99
286	0,1784	0,0046	12,369	0,534	0,5029	0,0174	0,80	2633	41	2626	75	2638	43	100
287	0,1858	0,0028	14,459	0,530	0,5643	0,0188	0,91	2780	35	2885	78	2706	25	104
288	0,1978	0,0030	15,676	0,792	0,5747	0,0277	0,95	2857	48	2927	113	2809	25	102
289	0,2014	0,0063	16,462	1,091	0,5929	0,0347	0,88	2904	64	3001	140	2837	51	103
290	0,1796	0,0021	14,069	0,315	0,5681	0,0109	0,86	2754	21	2900	45	2649	19	105

sample	$^{207}Pb/^{206}Pb$	±1σ	$^{207}Pb/^{235}U$	±1σ	$^{206}Pb/^{238}U$	±1σ	ρ	$^{207}Pb/^{235}U$	±2σ	$^{206}Pb/^{238}U$	±2σ	$^{207}Pb/^{206}Pb$	±2σ	Conc
spot		%		%		%		Ma	Ma	Ma	Ma	Ma	Ma	%
488110														
193	0,1740	0,0017	11,138	0,478	0,4642	0,0194	0,97	2535	40	2458	85	2597	16	97
194	0,1769	0,0033	11,525	0,371	0,4725	0,0125	0,82	2567	30	2494	55	2624	31	97
196	0,1736	0,0067	11,933	0,836	0,4985	0,0292	0,84	2599	66	2607	126	2593	64	100
197	0,1711	0,0045	11,049	0,867	0,4684	0,0347	0,94	2527	73	2477	152	2568	43	98
198	0,1645	0,0032	11,479	0,726	0,5060	0,0304	0,95	2563	59	2639	130	2503	33	103
199	0,1748	0,0020	13,348	0,552	0,5539	0,0220	0,96	2705	39	2841	91	2604	19	105
200	0,2042	0,0073	12,914	0,930	0,4587	0,0286	0,87	2673	68	2434	126	2860	58	91
205	0,1799	0,0022	12,276	0,401	0,4949	0,0150	0,93	2626	31	2592	65	2652	20	99
206	0,1755	0,0049	12,187	0,692	0,5036	0,0249	0,87	2619	53	2629	107	2611	46	100
208	0,1679	0,0040	12,071	0,469	0,5214	0,0159	0,79	2610	36	2705	67	2537	40	104
209	0,1772	0,0055	16,106	0,975	0,6591	0,0342	0,86	2883	58	3264	133	2627	52	113
210	0,1951	0,0050	13,642	0,754	0,5071	0,0249	0,89	2725	52	2644	106	2786	42	97
213	0,1804	0,0013	11,696	0,620	0,4702	0,0247	0,99	2580	50	2484	108	2657	12	96
214	0,1741	0,0025	12,622	0,247	0,5258	0,0069	0,67	2652	18	2724	29	2598	24	103
218	0,1764	0,0035	11,262	0,461	0,4632	0,0166	0,87	2545	38	2453	73	2619	33	96
219	0,1729	0,0022	13,316	0,321	0,5585	0,0114	0,85	2702	23	2860	47	2586	21	106
220	0,1734	0,0027	12,934	0,288	0,5411	0,0086	0,71	2675	21	2788	36	2590	26	104
221	0,1707	0,0020	12,170	0,311	0,5169	0,0118	0,89	2618	24	2686	50	2565	19	103
222	0,1677	0,0011	10,691	0,282	0,4623	0,0118	0,97	2497	25	2450	52	2535	11	98
223	0,1739	0,0009	11,622	0,286	0,4846	0,0116	0,98	2574	23	2547	51	2596	9	99
224	0,1768	0,0015	13,238	0,259	0,5430	0,0096	0,91	2697	18	2796	40	2623	14	104
225	0,2029	0,0021	14,400	0,396	0,5147	0,0131	0,93	2776	26	2676	56	2850	17	96
226	0,2024	0,0034	14,531	0,428	0,5208	0,0126	0,82	2785	28	2703	53	2845	27	97
231	0,2024	0,0032	14,423	0,548	0,5168	0,0179	0,91	2778	36	2686	76	2846	26	97
232	0,1748	0,0006	11,297	0,137	0,4686	0,0054	0,95	2548	11	2478	24	2605	6	97
232	0,2034	0,0026	14,752	0,648	0,5261	0,0221	0,96	2799	42	2725	93	2854	20	97
233	0,1767	0,0020	12,969	0,320	0,5322	0,0117	0,89	2677	23	2751	49	2623	19	103
234	0,1805	0,0036	9,651	0,265	0,3878	0,0073	0,68	2402	25	2113	34	2657	33	88
237	0,1760	0,0023	12,131	0,362	0,5000	0,0134	0,90	2615	28	2614	58	2615	21	100

Appendix 4: Tabulated geochemical data

Below are the geochemical data from samples collected during 2006 fieldwork. Table 4.1 contains data from Storø (Qingaaq and Aappalaartoq mountains), Table 4.2 contains data from samples collected on Bjørneøen. Figures 4.1 and 4.2 show sample locations on Qingaaq and Aappalaartoq respectively.

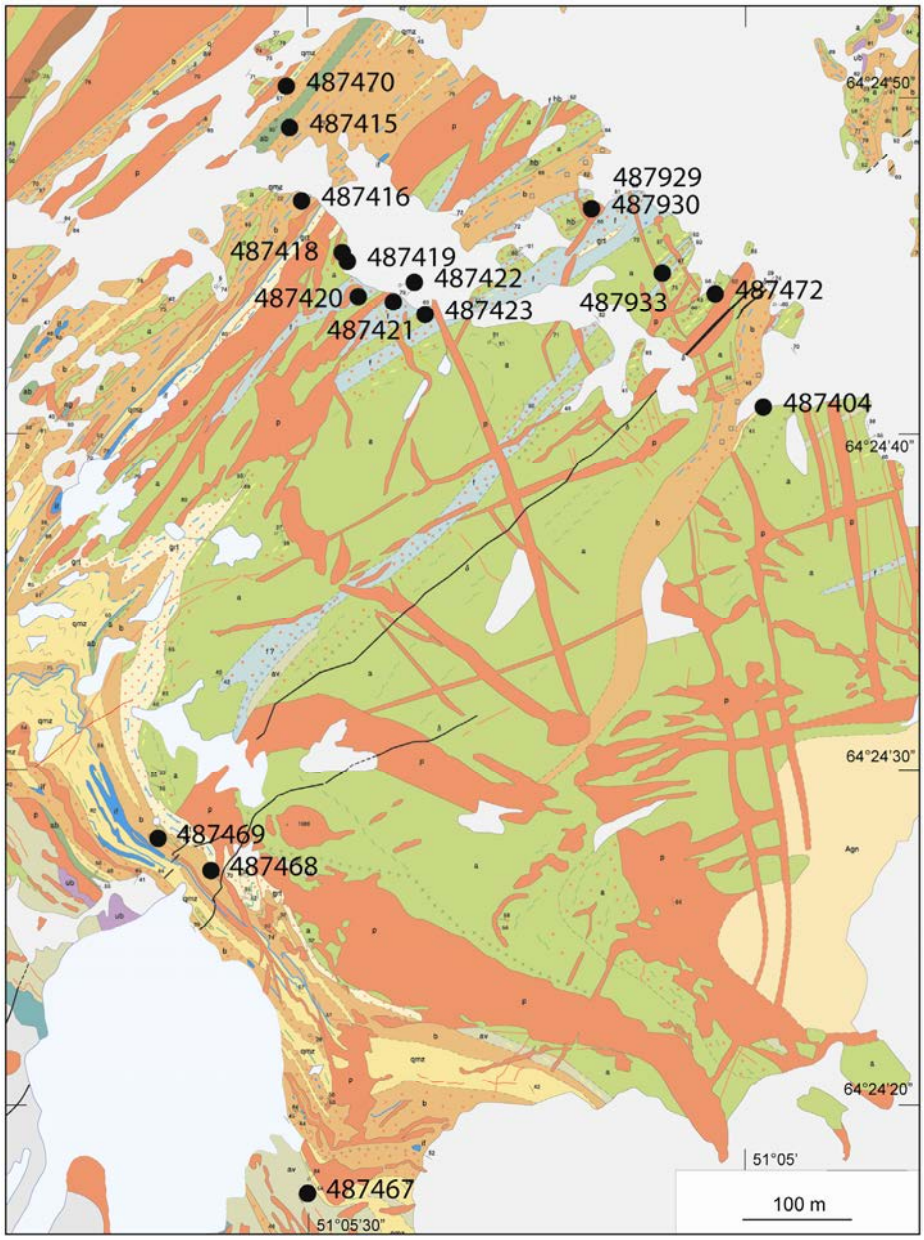

Figure 4.1 *sample location map at Qingaaq mountain, geochemical samples.*

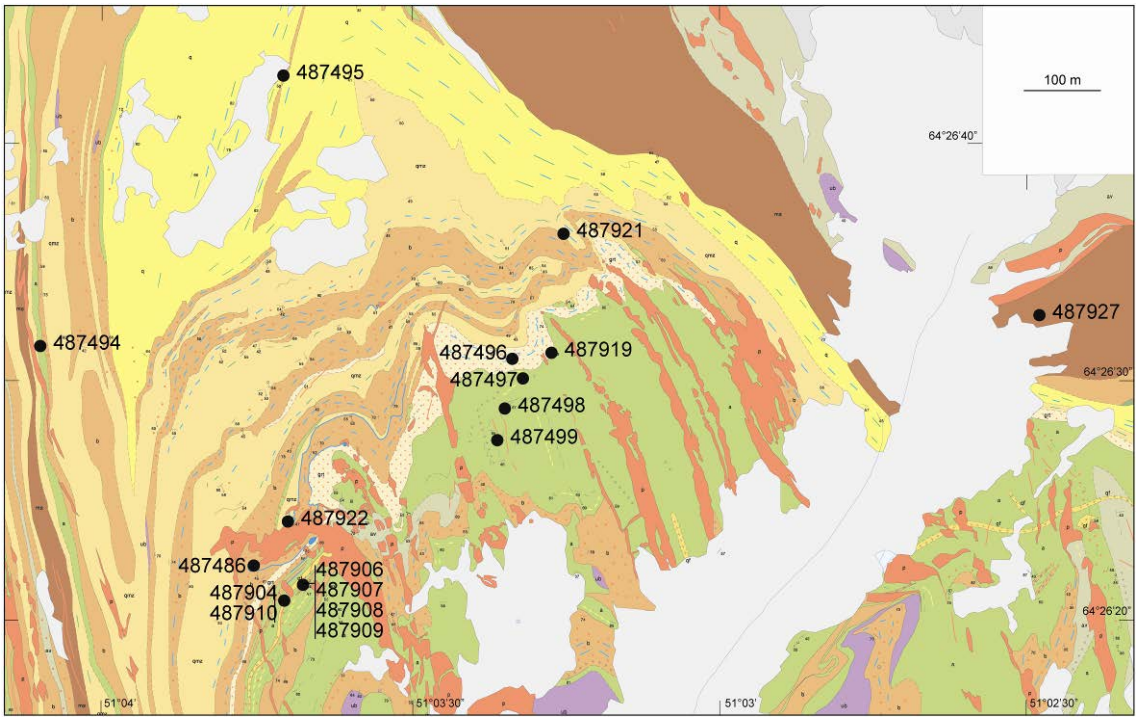

Figure 4.2 *Sample location map at Aappalaartoq mountain, geochemical samples.*

The samples collected and analysed by Polat (2005) that were used in this report were re-classified, based on the sample locations and the sample descriptions. This new classification used in this report is shown in Table 5.3 and compared to that used by Polat (2005).

Table 4.1 *Geochemical data from Storø. Major element oxides in wt%, elements in ppm.*

	amphibolite (HPT)				amphibolite (LPT)			amphibolite	
Sample	**487418**	**487419**	**487497**	**487919**	**487472**	**487494**	**487499**	**465001***	**465007***
SiO2	48,29	48,54	49,55	48,15	48,11	46,72	46,84	49,88	50,74
TiO2	1,62	1,62	1,72	1,69	1,20	1,16	0,92	1,90	1,06
Al2O3	14,45	14,17	13,52	14,96	13,87	16,84	13,87	14,23	12,29
Fe2O3	3,58	1,73	2,69	2,02	1,98	1,92	1,66	15,04	12,71
FeO	10,20	12,19	10,42	10,93	12,45	9,73	8,80		
FeOt	13,42	13,74	12,84	12,75	14,23	11,46	10,29	13,53	11,44
MnO	0,23	0,21	0,20	0,20	0,22	0,17	0,38	0,21	0,27
MgO	4,65	6,56	5,91	6,12	7,93	8,66	5,87	5,60	6,39
CaO	11,80	8,54	9,56	10,55	9,21	9,01	18,28	8,90	12,49
Na2O	2,95	3,45	3,54	2,74	1,97	2,89	1,11	3,15	2,26
K2O	0,33	0,21	0,35	0,13	0,13	0,64	0,21	0,17	0,23
P2O5	0,18	0,20	0,21	0,18	0,09	0,12	0,06	0,21	0,07
LOI	1,26	1,56	1,41	1,44	1,58	1,48	1,34	0,20	0,18
Sum	99,52	98,97	99,08	99,12	98,73	99,35	99,34	99,49	99,35
Sc	35,28	35,90	50,17	37,35	36,01	22,11	44,18	35,03	23,49
Ti	9371	9728	10480	9808	6435	6774	5334	11100	6400
V	317	284	375	365	284	231	343	346	176
Cr	205	170	233	257	64	93	272	145	98
Mn	0,168	0,150	0,152	0,156	0,174	0,132	0,283	0,160	0,220
Co	56,76	45,46	43,25	45,49	66,53	59,24	53,07	43,91	49,22
Ni	121	103	68	87	184	214	89	66	64
Cu	148	183	133	223	151	146	137	45	187
Zn	117	108	87	101	90	78	103	114	223
Ga	18,63	18,95	19,02	19,42	18,00	18,27	17,38	19,14	16,38
Rb	5,91	4,21	7,08	1,80	4,05	32,06	3,85	0,81	3,43
Sr	147	98	107	190	113	277	87	195	213
Y	33,83	35,76	37,12	32,17	31,46	17,62	22,46	36,65	22,41
Zr	114,8	121,3	108,7	101,4	75,4	65,2	49,3	120,5	87,4
Nb	4,897	5,258	4,555	4,279	3,303	3,377	2,433	5,160	6,750
Cs	0,320	0,452	1,935	0,051	0,103	13,758	0,166	0,120	0,370
Ba	31	18	205	17	6	315	25	45	94
Hf	2,931	3,049	2,773	2,519	1,870	1,605	1,408	3,410	2,450
Ta	2,095	0,758	0,848	0,608	1,051	0,496	0,643	0,380	0,450
Pb	7,24	2,97	2,94	2,61	2,06	3,36	5,64	4,69	13,11
Th	0,818	0,876	0,964	0,820	0,369	0,415	0,339	1,030	1,170
U	1,929	0,352	0,247	0,256	0,311	0,248	0,401	0,260	0,650
La	7,32	10,09	8,46	5,29	4,17	4,85	3,05	7,82	10,02
Ce	16,98	22,51	18,50	13,07	10,96	12,11	7,63	19,43	22,23
Pr	2,67	3,28	2,82	2,22	1,83	1,89	1,29	2,91	2,96
Nd	12,86	15,32	12,65	10,50	9,19	8,22	6,37	13,73	12,35
Sm	3,778	4,038	3,867	3,348	2,972	2,253	2,144	4,210	3,050
Eu	1,230	1,251	1,286	1,251	1,058	0,807	0,797	1,410	1,160
Gd	4,754	5,126	4,761	4,199	3,673	2,589	2,749	5,470	3,840
Tb	0,812	0,866	0,850	0,750	0,699	0,434	0,555	0,940	0,600
Dy	5,236	5,493	5,564	5,051	4,459	2,678	3,358	6,170	3,840
Ho	1,193	1,222	1,236	1,163	1,000	0,610	0,800	1,410	0,850
Er	3,301	3,357	3,408	3,111	2,753	1,642	2,142	3,830	2,250
Tm	0,529	0,549	0,557	0,511	0,459	0,274	0,393	0,590	0,350
Yb	3,140	3,420	3,399	3,079	2,898	1,665	2,168	3,790	2,130
Lu	0,489	0,553	0,521	0,489	0,442	0,265	0,375	0,570	0,330

Table 4.1 *continued*

	grt amphibolite								
Sample	**487498**	**487904**	**487907**	**487909**	**487910**	**487930**	**487933**	**465044***	**465051***
SiO2	45,21	51,48	50,50	48,99	52,56	54,50	48,70	39,63	49,16
TiO2	1,86	0,84	1,28	0,95	0,99	1,21	1,54	1,90	1,42
Al2O3	13,37	16,43	14,50	16,16	15,34	18,50	14,89	12,97	13,42
Fe2O3	1,24	2,89	2,69	2,00	3,92	3,16	5,02	35,39	26,65
FeO	15,54	9,32	11,12	9,86	10,00	8,15	13,35		
FeOt	16,65	11,92	13,54	11,66	13,53	10,99	17,86	31,84	23,98
MnO	0,32	0,39	0,24	0,15	0,78	0,37	0,31	0,81	0,60
MgO	3,24	4,90	6,38	7,31	2,02	2,95	4,28	2,65	2,39
CaO	10,36	10,74	8,97	10,61	11,74	3,89	6,95	6,52	5,85
Na2O	2,37	0,98	1,51	1,59	0,30	3,56	2,03	0,39	0,42
K2O	0,68	0,22	0,12	0,14	0,11	1,12	0,64	0,23	0,20
P2O5	0,12	0,09	0,10	0,08	0,09	0,15	0,10	0,27	0,19
LOI	4,02	1,57	1,52	1,54	1,56	1,83	1,35	-1,46	-0,36
Sum	98,32	99,84	98,92	99,35	99,40	99,38	99,17	99,30	99,93
Sc	22,00	45,80	46,34	37,69	62,15	44,29	23,50	35,61	32,00
Ti	12029	5196	7696	5657	5694	7196	9172	11000	8200
V	283	246	317	252	323	366	227	268	287
Cr	-9	90	76	268	112	215	-3	127	63
Mn	0,245	0,305	0,188	0,132	0,565	0,289	0,242	0,630	0,470
Co	60,55	59,25	61,33	60,68	74,00	62,67	58,63	36,72	26,25
Ni	22	187	147	232	121	156	62	89	31
Cu	438	154	176	91	197	182	102	65	53
Zn	160	119	101	90	64	104	155	184	118
Ga	22,50	20,93	18,79	17,65	19,77	20,99	20,32	17,10	17,43
Rb	18,72	7,04	2,03	3,05	4,26	106,49	57,97	2,24	4,05
Sr	240	82	152	151	64	94	169	17	16
Y	38,15	26,15	31,50	20,22	37,59	29,42	26,96	49,38	37,04
Zr	174,8	46,8	78,5	51,7	60,5	69,3	113,9	127,6	105,4
Nb	14,086	2,568	3,873	2,469	2,977	3,373	9,782	4,880	4,280
Cs	1,531	0,667	0,094	0,150	0,321	9,989	17,296	0,160	0,780
Ba	280	36	10	18	17	74	74	5	13
Hf	4,441	1,354	2,189	1,430	1,719	1,963	2,889	3,430	2,850
Ta	1,185	0,577	2,867	0,535	2,282	0,973	0,997	0,340	0,290
Pb	7,43	3,27	2,21	1,58	2,95	6,87	4,27	3,67	2,67
Th	2,508	0,295	0,405	0,302	0,296	0,407	1,500	1,140	0,800
U	0,639	0,329	0,184	0,082	3,223	0,685	0,370	0,550	1,890
La	25,07	3,39	4,11	3,48	3,87	2,85	8,45	6,15	6,25
Ce	53,92	8,21	10,63	8,12	8,73	7,17	22,24	15,30	14,29
Pr	7,52	1,41	1,82	1,43	1,55	1,21	3,60	2,28	1,96
Nd	29,82	6,78	8,90	6,83	7,42	6,04	15,90	11,14	9,47
Sm	6,953	2,560	3,102	2,230	2,582	2,271	4,306	3,800	3,180
Eu	1,873	0,933	1,036	0,778	1,174	0,897	1,332	1,270	1,140
Gd	7,023	3,129	3,800	2,840	3,572	3,318	4,572	5,610	4,670
Tb	1,065	0,608	0,722	0,520	0,679	0,686	0,733	0,980	0,830
Dy	6,486	3,926	4,691	3,239	4,710	4,367	4,507	6,640	5,610
Ho	1,334	0,915	1,090	0,761	1,179	1,021	0,941	1,610	1,310
Er	3,534	2,425	2,893	2,006	3,370	2,779	2,511	4,370	3,630
Tm	0,571	0,415	0,482	0,325	0,595	0,469	0,415	0,670	0,580
Yb	3,472	2,493	2,934	1,983	3,767	2,797	2,468	4,020	3,860
Lu	0,526	0,379	0,473	0,307	0,602	0,434	0,379	0,630	0,610

Table 4.1 *continued*

	grt calc-silicate gneiss				grt rich gneiss			
Sample	**487420**	**487422**	**487423**	**487906**	**487496**	**465003***	**465004***	**465005***
SiO2	54,48	55,16	48,71	53,52	51,67	46,91	53,63	49,77
TiO2	1,01	1,21	2,03	1,53	2,42	1,86	1,81	2,66
Al2O3	17,51	18,07	15,27	14,43	20,62	17,34	16,90	21,15
Fe2O3	4,04	2,65	2,55	2,47	4,89	22,26	15,24	13,77
FeO	8,75	7,87	13,44	11,14	7,84			
FeOt	12,38	10,26	15,73	13,36	12,24	20,03	13,71	12,39
MnO	0,22	0,29	0,27	0,23	0,22	0,33	0,20	0,18
MgO	4,20	3,48	5,41	6,15	2,42	3,36	2,52	2,59
CaO	4,07	4,45	6,31	6,83	3,91	3,65	2,82	5,26
Na2O	2,92	4,15	3,23	1,75	3,09	0,95	2,02	3,03
K2O	0,78	0,82	0,35	0,08	1,02	1,87	1,92	0,89
P2O5	0,06	0,15	0,25	0,13	0,16	0,18	0,13	0,20
LOI	0,90	0,88	1,37	1,22	0,86	0,21	1,65	-0,28
Sum	98,94	99,18	99,16	99,47	99,12	98,90	98,85	99,21
Sc	42,19	43,69	40,33	49,88	48,70	39,05	38,41	45,23
Ti	5591	6968	11906	9013	14478	10700	11000	15800
V	267	292	345	410	507	375	417	534
Cr	254	110	100	101	248	478	451	497
Mn	0,167	0,221	0,202	0,180	0,174	0,260	0,160	0,140
Co	55,83	49,01	51,09	60,55	72,57	36,31	24,89	52,97
Ni	155	139	114	74	137	68	47	95
Cu	123	95	216	93	164	117	164	71
Zn	88	103	148	139	275	218	206	328
Ga	17,96	18,85	21,20	21,12	28,59	25,42	27,57	30,27
Rb	78,76	51,15	22,08	1,25	34,26	58,40	63,85	28,24
Sr	144	133	78	74	108	59	87	115
Y	22,49	26,35	42,70	37,12	45,40	47,15	39,43	39,51
Zr	58,3	66,8	138,7	90,7	179,4	155,1	145,6	171,2
Nb	2,739	3,051	5,995	4,129	9,890	8,070	7,870	8,100
Cs	45,630	9,505	4,143	0,149	2,547	4,730	5,120	2,920
Ba	159	108	38	12	353	271	411	298
Hf	1,714	1,902	3,630	2,509	4,772	4,330	4,120	4,670
Ta	1,009	0,689	1,274	0,678	1,222	0,570	0,530	0,560
Pb	6,17	3,43	4,52	3,85	15,83	10,56	15,78	16,74
Th	0,425	0,335	1,288	0,513	2,627	2,350	2,270	1,760
U	0,768	0,979	1,105	0,267	0,792	0,680	0,660	0,550
La	2,39	3,75	9,07	4,22	15,70	11,06	14,81	12,32
Ce	4,18	9,86	21,12	11,43	35,18	23,78	33,05	28,70
Pr	0,68	1,56	3,28	2,08	5,16	3,04	4,37	4,02
Nd	3,53	7,76	15,73	10,08	21,52	12,74	18,54	17,88
Sm	1,403	2,519	4,588	3,821	6,014	3,810	4,740	5,160
Eu	0,746	0,821	1,463	1,095	1,877	1,390	1,350	1,840
Gd	2,502	3,330	5,732	4,616	6,808	5,140	4,410	5,450
Tb	0,488	0,606	0,999	0,907	1,133	1,120	0,970	1,050
Dy	3,406	4,198	6,588	5,762	7,084	7,430	6,350	6,730
Ho	0,798	0,947	1,484	1,365	1,579	1,750	1,510	1,530
Er	2,192	2,449	4,185	3,637	4,377	4,750	4,010	4,120
Tm	0,352	0,410	0,668	0,659	0,742	0,740	0,630	0,670
Yb	2,118	2,511	4,248	3,728	4,565	4,730	3,990	4,190
Lu	0,341	0,366	0,659	0,596	0,713	0,710	0,620	0,650

Table 4.1 *continued*

	bt gneiss							quartzite	
Sample	**487404**	**487415**	**487416**	**487421**	**487468**	**487921**	**487927**	**487470**	**487495**
SiO2	63,23	61,92	62,23	53,45	64,37	59,34	55,41	81,33	94,44
TiO2	0,64	0,71	1,01	0,71	0,76	0,92	1,25	0,47	0,17
Al2O3	16,39	16,96	18,75	20,44	15,94	19,00	20,88	7,97	3,37
Fe2O3	1,08	0,92	1,48	1,31	1,13	1,74	2,17	0,58	0,24
FeO	4,89	4,90	5,33	5,86	5,48	5,26	7,53	3,09	0,00
FeOt	5,86	5,72	6,66	7,04	6,49	6,82	9,49	3,61	0,21
MnO	0,09	0,08	0,07	0,10	0,06	0,10	0,12	0,03	0,00
MgO	5,07	2,91	3,60	5,94	3,08	3,28	4,56	1,18	0,08
CaO	1,70	2,82	1,47	2,22	1,80	3,06	1,55	0,82	0,00
Na2O	1,95	4,24	2,00	4,17	3,42	2,55	1,53	1,55	0,10
K2O	2,40	2,37	1,87	3,01	3,12	2,43	1,93	1,64	0,93
P2O5	0,07	0,10	0,09	0,08	0,05	0,10	0,07	0,03	0,01
LOI	1,42	1,04	1,32	2,36	1,12	1,13	2,13	0,87	0,53
Sum	98,94	98,95	99,22	99,65	100,32	98,90	99,13	99,56	99,87
Sc	18,28	19,22	27,58	27,34	23,27	24,91	41,27	15,79	9,07
Ti	3571	3965	6048	3944	4163	5341	7569	2758	530
V	127	114	185	173	154	177	288	86	39
Cr	608	113	207	499	243	182	383	179	331
Mn	0,078	0,066	0,058	0,083	0,054	0,094	0,113	0,029	0,002
Co	44,60	33,62	43,89	38,12	39,57	32,75	64,82	40,16	19,73
Ni	159	70	115	259	128	67	186	75	-1
Cu	62	117	104	113	46	86	171	41	21
Zn	111	92	111	113	71	96	137	53	6
Ga	19,84	21,67	23,04	22,86	19,31	22,44	26,92	10,99	5,90
Rb	94,94	117,10	57,80	194,01	260,05	104,18	77,29	194,04	31,99
Sr	85	175	126	77	118	166	94	47	7
Y	20,94	15,79	20,53	19,99	17,77	25,93	29,43	10,05	3,71
Zr	133,1	125,0	154,6	99,7	132,9	170,0	170,9	120,2	154,0
Nb	6,675	6,951	8,018	5,116	5,807	8,321	8,852	5,866	3,088
Cs	11,072	12,772	5,104	47,247	17,391	8,991	3,774	14,134	0,619
Ba	401	480	322	361	404	333	366	336	161
Hf	3,405	3,333	4,096	2,671	3,061	4,443	4,393	2,814	3,977
Ta	4,526	1,234	1,571	1,384	0,729	0,960	1,361	1,699	1,496
Pb	20,83	15,35	10,42	19,94	22,37	19,71	12,17	10,76	1,87
Th	7,839	4,497	4,143	4,688	4,070	5,442	5,051	3,867	7,607
U	1,595	1,761	1,523	2,305	2,077	1,553	1,619	1,836	1,064
La	25,98	21,05	17,75	20,47	19,16	25,56	21,90	18,97	11,45
Ce	48,64	41,69	36,70	38,65	38,20	52,04	44,53	36,38	21,80
Pr	5,76	5,33	4,85	4,96	4,88	6,95	5,76	4,30	2,63
Nd	21,02	20,88	19,14	19,35	17,85	25,77	21,45	15,16	9,26
Sm	3,624	3,883	3,741	3,770	3,529	5,420	4,524	2,669	1,823
Eu	0,844	0,930	0,930	0,845	0,976	1,522	0,890	0,605	0,216
Gd	4,011	4,361	4,302	4,282	3,846	5,534	4,893	2,843	1,810
Tb	0,541	0,555	0,603	0,564	0,543	0,774	0,773	0,346	0,200
Dy	3,385	2,964	3,608	3,281	2,935	4,387	4,766	1,769	0,866
Ho	0,741	0,547	0,733	0,694	0,580	0,905	1,039	0,326	0,125
Er	2,161	1,450	2,018	1,932	1,642	2,440	2,857	0,884	0,324
Tm	0,347	0,221	0,314	0,300	0,252	0,410	0,459	0,125	0,044
Yb	2,193	1,345	2,022	1,755	1,592	2,418	2,796	0,755	0,268
Lu	0,346	0,211	0,318	0,273	0,255	0,382	0,429	0,119	0,050

Table 4.1 *continued*

	garnetite-magnetite rock					felsic band
Sample	**487469**	**487486**	**487908**	**487922**	**487929**	**487467**
SiO2	43,44	42,98	45,54	42,87	43,17	72,61
TiO2	0,23	0,91	2,67	0,23	1,08	0,78
Al2O3	5,12	17,55	16,40	5,02	15,28	11,22
Fe2O3	18,08	14,00	13,54	18,41	6,00	2,27
FeO	27,13	14,92	13,73	26,92	9,86	4,02
FeOt	43,40	27,52	25,91	43,48	15,26	6,06
MnO	0,03	0,12	0,86	0,09	1,75	0,07
MgO	2,07	4,19	2,52	2,39	4,37	1,11
CaO	1,21	1,83	4,06	1,21	14,63	2,66
Na2O	0,01	0,04	0,03	0,04	0,34	3,36
K2O	0,00	1,67	0,07	0,05	0,18	0,83
P2O5	0,09	0,13	0,06	0,09	0,13	0,15
LOI	1,36	1,08	0,14	1,07	2,33	0,64
Sum	98,77	99,43	99,62	98,37	99,11	99,71
Sc	21,98	41,67	75,07	19,95	35,91	13,70
Ti	1192	5054	15638	1059	6151	4030
V	62	198	352	53	245	15
Cr	79	280	37	68	58	2
Mn	0,037	0,098	0,627	0,082	1,314	0,066
Co	20,64	28,76	28,32	14,18	40,79	21,13
Ni	44	124	5	33	69	7
Cu	86	58	57	80	50	41
Zn	53	101	72	29	152	66
Ga	6,77	26,75	14,12	5,82	18,38	27,23
Rb	1,48	104,54	7,68	2,35	9,20	31,00
Sr	2	2	1	8	39	116
Y	11,18	29,34	52,69	11,41	52,98	204,89
Zr	32,6	142,0	169,8	26,6	66,7	489,7
Nb	1,455	22,471	9,513	1,408	10,373	18,167
Cs	0,153	7,936	0,875	0,174	0,418	2,689
Ba	4	345	6	5	40	337
Hf	0,791	3,248	4,558	0,716	1,730	12,775
Ta	1,260	4,133	1,728	1,137	2,481	1,674
Pb	0,62	3,81	0,56	1,34	3,53	6,14
Th	1,135	4,082	1,091	1,028	0,806	5,096
U	0,412	1,353	0,628	0,405	1,803	2,479
La	0,45	20,05	8,45	2,10	3,59	34,97
Ce	1,23	39,88	20,62	4,18	9,19	91,28
Pr	0,23	4,99	3,07	0,53	1,67	14,01
Nd	1,41	18,86	13,19	1,99	8,53	63,18
Sm	1,063	4,248	3,589	0,924	3,327	18,981
Eu	0,432	0,899	0,904	0,392	1,245	3,704
Gd	1,332	5,303	5,476	1,496	4,292	22,170
Tb	0,251	0,850	1,178	0,254	0,902	4,463
Dy	1,525	4,490	8,006	1,640	6,474	29,681
Ho	0,361	0,916	1,855	0,377	1,604	6,955
Er	0,933	2,461	4,901	0,957	4,665	19,844
Tm	0,153	0,394	0,818	0,162	0,812	3,263
Yb	0,975	2,525	5,086	1,007	5,176	20,921
Lu	0,147	0,385	0,789	0,163	0,804	3,196

Table 4.2 *geochemical data from Bjørneøen*

	amphibolites						
Sample	**487438**	**487443**	**487444**	**487447**	**487448**	**487450**	**487453**
SiO2	50,97	56,34	48,47	48,30	48,89	48,76	55,49
TiO2	0,81	0,57	1,19	1,28	1,20	1,44	1,82
Al2O3	18,21	16,91	14,51	14,91	13,08	14,99	13,75
Fe2O3	1,92	1,75	4,29	3,21	2,07	4,30	5,13
FeO	6,33	5,51	7,62	9,19	10,62	12,99	9,30
FeO*	8,05	7,09	11,48	12,08	12,49	16,86	13,92
MnO	0,12	0,14	0,21	0,19	0,24	0,41	0,23
MgO	5,18	4,98	7,73	7,73	7,46	5,10	3,31
CaO	10,38	8,08	10,98	11,26	13,80	8,88	6,01
Na2O	3,18	3,03	1,81	1,34	0,50	0,59	2,04
K2O	0,15	1,28	0,12	0,10	0,19	0,15	0,53
P2O5	0,43	0,12	0,15	0,15	0,08	0,17	0,22
LOI	1,48	1,07	1,91	1,37	1,37	1,44	1,18
Sum	99,13	99,78	98,99	99,03	99,50	99,21	99,02
Sc	26,16	20,60	34,43	37,76	32,14	43,11	44,00
Ti	4725	3174	7550	8034	7582	9232	11581
V	173	139	262	276	296	307	445
Cr	187	259	300	301	238	99	19
Mn	0,092	0,109	0,168	0,156	0,181	0,323	0,181
Co	37,34	37,01	58,38	50,33	49,62	46,15	41,38
Ni	92	112	116	123	119	94	39
Cu	189	127	240	262	92	107	126
Zn	69	79	124	86	113	116	107
Ga	17,06	15,12	16,69	17,22	15,82	18,26	23,24
Rb	1,20	70,29	1,63	1,90	6,84	2,10	21,16
Sr	799	277	156	116	81	53	115
Y	22,73	12,80	20,54	20,72	20,98	27,97	60,22
Zr	138,7	94,6	48,2	50,5	52,0	55,8	149,4
Nb	5,801	4,180	2,096	1,925	2,027	2,293	6,991
Cs	0,076	14,996	0,125	0,225	2,517	0,139	12,040
Ba	33	356	36	12	13	13	216
Hf	3,237	2,362	1,274	1,408	1,388	1,527	4,193
Ta	0,959	1,766	2,596	0,569	1,072	0,804	0,699
Pb	13,20	23,94	5,39	2,28	8,28	5,12	3,93
Th	6,921	4,317	0,264	0,291	0,365	0,379	1,756
U	0,727	0,466	0,114	0,076	0,078	0,112	0,316
La	45,84	18,90	3,39	3,11	3,01	3,50	7,06
Ce	97,62	36,54	8,28	8,05	7,63	9,13	18,98
Pr	13,34	4,55	1,20	1,27	1,26	1,55	2,75
Nd	53,11	18,17	6,13	6,80	6,46	8,13	13,83
Sm	8,671	3,298	1,999	2,124	1,943	2,461	4,442
Eu	1,907	0,883	0,794	0,889	0,764	1,015	1,346
Gd	8,007	3,542	2,580	2,796	2,576	3,391	6,348
Tb	0,876	0,408	0,468	0,479	0,471	0,617	1,263
Dy	4,408	2,251	3,144	3,231	3,058	4,092	8,864
Ho	0,775	0,439	0,702	0,750	0,706	0,948	2,127
Er	2,270	1,224	1,953	2,037	1,954	2,573	5,866
Tm	0,336	0,187	0,302	0,320	0,311	0,419	0,970
Yb	2,066	1,229	1,880	2,010	1,961	2,513	6,206
Lu	0,328	0,196	0,289	0,334	0,302	0,384	0,910

Table 4.2. *continued*

	meta-volcanic rocks							
Sample	**487435**	**487441**	**487449**	**487451**	**487452**	**487455**	**487459**	**487460**
SiO2	47,44	59,84	53,73	53,91	70,38	66,88	65,10	43,31
TiO2	1,43	0,64	1,49	1,74	0,33	0,59	0,72	0,55
Al2O3	14,19	15,85	15,88	18,80	16,35	16,42	18,23	12,44
Fe2O3	2,08	1,01	1,73	1,95	0,96	0,51	0,71	2,03
FeO	11,94	3,77	10,23	7,69	1,48	2,65	2,21	5,84
FeO*	13,81	4,68	11,79	9,44	2,35	3,10	2,85	7,66
MnO	0,18	0,16	0,22	0,15	0,03	0,04	0,05	0,15
MgO	9,53	2,17	5,47	2,88	1,31	1,34	1,04	9,79
CaO	8,75	8,71	7,85	7,82	3,74	4,64	3,47	17,79
Na2O	1,92	2,86	0,79	1,00	3,36	4,28	5,47	0,79
K2O	0,12	1,13	0,24	1,63	1,16	1,02	1,60	0,47
P2O5	0,18	0,18	0,14	0,19	0,09	0,12	0,21	0,25
LOI	1,61	2,95	1,34	1,22	0,46	0,50	0,60	5,45
Sum	99,36	99,28	99,11	98,97	99,64	98,99	99,41	98,85
Sc	37,61	25,14	38,81	50,28	8,76	13,90	21,93	24,76
Ti	8529	3936	9256	11616	1656	3748	3091	3148
V	298	122	413	455	18	72	98	179
Cr	180	565	296	383	5	177	447	526
Mn	0,138	0,132	0,168	0,118	0,032	0,039	0,031	0,119
Co	47,98	35,86	53,22	45,41	14,89	23,43	15,98	50,61
Ni	95	118	132	113	5	70	47	116
Cu	101	62	100	97	12	26	29	69
Zn	103	64	96	76	38	23	15	64
Ga	19,36	14,95	19,81	23,85	19,58	17,47	10,72	13,02
Rb	2,16	48,26	13,66	70,31	36,47	70,80	37,99	15,45
Sr	44	368	71	143	176	188	220	561
Y	36,56	16,89	26,45	22,88	3,51	7,22	12,27	16,64
Zr	82,7	105,6	66,2	68,2	101,1	140,8	77,6	114,0
Nb	3,358	4,827	2,931	2,798	2,616	6,594	3,687	3,788
Cs	0,136	5,548	3,868	18,699	5,414	7,373	1,242	0,804
Ba	34	614	31	341	327	314	862	161
Hf	2,319	2,553	1,738	1,894	2,534	3,408	1,763	2,512
Ta	1,181	1,807	2,854	1,693	1,772	0,830	1,591	0,339
Pb	1,84	12,13	10,58	9,46	7,67	10,01	7,13	7,99
Th	0,617	4,423	0,499	0,466	3,219	4,533	3,502	5,495
U	0,145	1,083	0,120	0,091	0,876	0,884	0,663	1,229
La	7,67	27,82	4,29	34,08	12,57	3,49	24,63	34,38
Ce	17,48	54,52	10,66	69,19	23,91	7,81	43,36	70,72
Pr	2,71	6,64	1,75	6,40	2,64	1,00	6,24	9,71
Nd	13,36	26,13	8,91	22,30	9,33	4,26	24,94	37,12
Sm	3,735	4,496	2,677	2,693	1,510	0,953	4,214	6,305
Eu	1,288	1,092	0,931	1,012	0,495	0,414	0,938	1,444
Gd	4,721	4,820	3,395	4,643	1,600	1,207	4,436	5,701
Tb	0,829	0,540	0,608	0,643	0,160	0,161	0,506	0,641
Dy	5,526	3,060	4,038	3,947	0,731	1,140	2,573	3,022
Ho	1,233	0,570	0,911	0,834	0,122	0,255	0,473	0,540
Er	3,458	1,626	2,471	2,336	0,339	0,764	1,237	1,569
Tm	0,560	0,232	0,402	0,369	0,051	0,146	0,170	0,229
Yb	3,462	1,504	2,524	2,398	0,294	0,978	1,043	1,530
Lu	0,552	0,226	0,377	0,357	0,049	0,154	0,151	0,239

Table 4.2. *continued*

	bt gneiss	tonalite		Ultramafic rock
Sample	**487458**	**487436**	**487457**	**487439**
SiO2	58,75	69,67	67,04	51,39
TiO2	0,54	0,29	0,82	0,21
Al2O3	15,98	15,99	14,94	4,21
Fe2O3	8,09	0,00	3,44	7,05
FeO	5,51	2,05	2,94	2,75
FeO*	12,79	2,05	6,03	9,09
MnO	0,13	0,03	0,12	0,17
MgO	4,82	0,98	1,11	25,79
CaO	0,73	3,22	3,79	3,23
Na2O	0,75	4,61	3,02	0,14
K2O	0,89	1,75	1,46	0,00
P2O5	0,12	0,08	0,25	0,02
LOI	2,79	1,04	0,77	3,67
Sum	99,09	99,69	99,69	98,62
Sc	22,03	5,82	16,04	25,11
Ti	3486	1503	5310	900
V	102	23	20	101
Cr	160	13	2	2980
Mn	0,118	0,025	0,090	0,136
Co	43,74	27,31	28,59	70,30
Ni	113	15	12	634
Cu	386	17	78	79
Zn	187	29	73	61
Ga	17,74	19,06	20,83	4,35
Rb	33,73	68,92	57,61	0,59
Sr	32	418	162	25
Y	12,88	3,02	21,62	4,65
Zr	129,3	96,7	299,5	10,6
Nb	5,327	3,407	15,086	0,515
Cs	17,929	2,534	11,523	0,091
Ba	257	618	535	3
Hf	3,142	2,428	6,696	0,301
Ta	1,322	3,586	4,401	0,746
Pb	9,01	8,51	21,10	0,84
Th	5,990	3,065	6,239	0,100
U	1,283	0,796	1,127	0,085
La	10,06	14,18	10,29	0,72
Ce	20,57	25,40	20,45	1,90
Pr	2,45	2,84	2,19	0,31
Nd	9,47	10,09	6,66	1,61
Sm	2,033	1,571	1,171	0,512
Eu	0,556	0,404	0,514	0,122
Gd	2,232	1,808	1,826	0,616
Tb	0,332	0,143	0,310	0,111
Dy	2,049	0,677	2,598	0,741
Ho	0,435	0,102	0,712	0,161
Er	1,224	0,296	2,250	0,471
Tm	0,195	0,039	0,395	0,069
Yb	1,222	0,253	2,636	0,473
Lu	0,187	0,039	0,399	0,071

Tabel 4.3…*Classification of Polat (2005) samples used in the geochemistry section of this report, compared to the classification used by Polat (2005)*

sample	classification	Polat classification
485489	Amphibolite	amphibolite Group 2
485490	grt amphibolite	amphibolite Group 3
485491	Amphibolite	amphibolite Group 2
485493	grt amphibolite	amphibolite Group 3
485494	grt amphibolite	amphibolite Group 3
485495	grt gneiss	metased
493105	biotite gneiss	metased
493106	biotite gneiss	metased
493107	grt gneiss	metased
493108	Amphibolite	amphibolite Group 2
493109	grt amphibolite	amphibolite Group 1
493110	Amphibolite	amphibolite Group 3
493116	biotite gneiss	metased
493117	biotite gneiss	metased
493118	Amphibolite	amphibolite Group 3
493119	Amphibolite	amphibolite Group 3
493120	Amphibolite	amphibolite Group 3
493121	biotite gneiss	metased
493122	biotite gneiss	metased
493123	biotite gneiss	metased
493125	Amphibolite	amphibolite Group 2

Appendix 5: Bjørneøen geochemistry

The Bjørneøen amphibolites have tholeiitic basalt compositions, while the meta-volcanic rocks range in composition between andesite and dacite. Amphibolites and meta-volcanic rocks are separated into two different units based on field mapping, but as seen in Fig. 5.1 below, these two groups show considerable overlap. One ultramafic rock is characterised by low Al_2O_3, high Cr, Ni and Mg#, and is almost certainly a cumulate phase enriched in olivine and e.g. chromite.

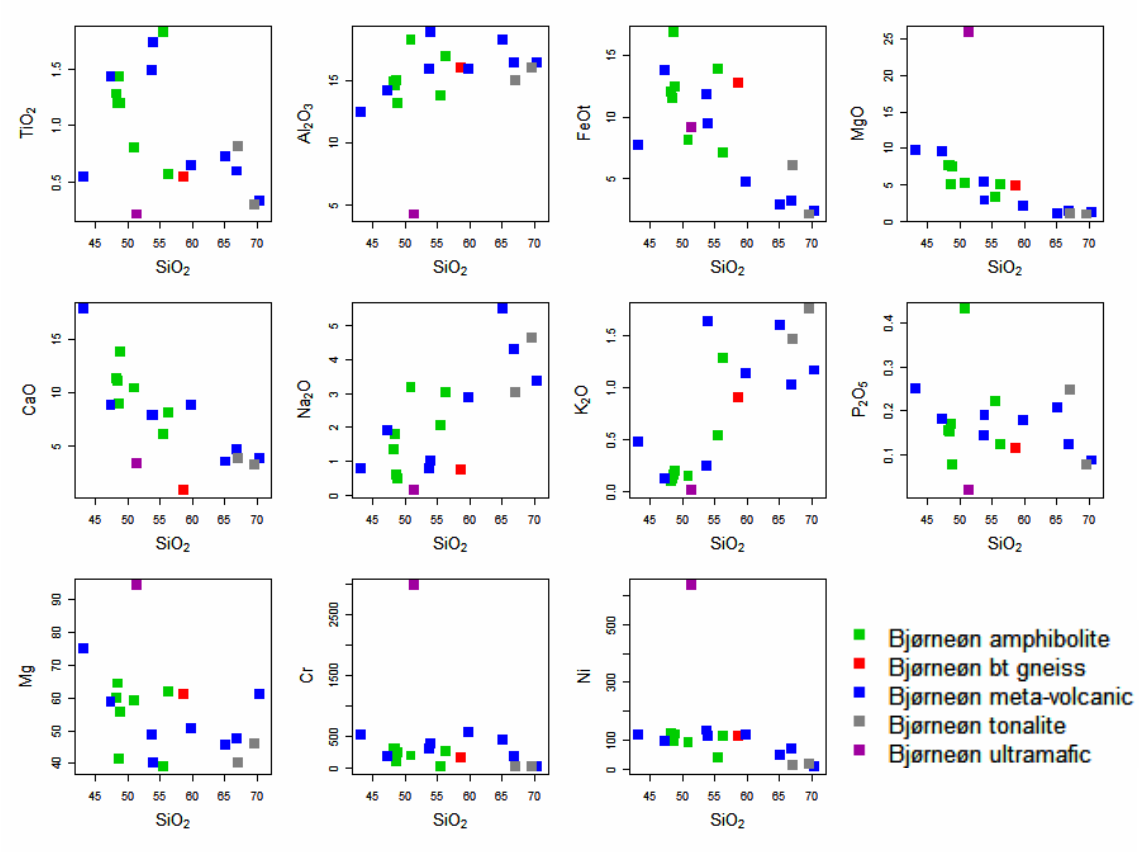

Figure. 5.1. *Harker diagrams for major elements, Mg#, Cr and Ni against SiO2.*

Trace element abundances (Fig. 5.2) show considerable overlap between amphibolites and meta-volcanic rocks, but each rock type display a compositional division, where one is more enriched in incompatible trace elements than the other. The enriched rocks are associated with chondrite normalised La/Yb > 10. These light REE enriched rocks have low Nb/La, Nb/Th, Nb/U, Eu/Eu*, but high Gd/Yb_N, which are positively correlated with Eu/Eu*. Low Nb/La, Nb/Th and Nb/U is typical for rocks forming over subduction zones. The coupled high Gd/Yb_N is indicative of garnet residue during the melting, and a typical feature of Archaean TTG suites. One tonalite has the most extreme La/Yb_N and Gd/Yb_N, where the Gd/Yb_N is higher than the Archaean TTG mean. It is notable that the volcanic rocks lie on a trend towards this end-member, which might imply temporal changes towards increasing melting depth, if these rocks formed an igneous continuum where the tonalite represents a later intrusion as is the case further north in the Akia (Garde 2007). Atypical for this asso-

ciation are the low Eu/Eu*. Archaean usually display insignificant Eu/Eu*, while the one analysed here has a distinct negative anomaly and a Eu/Eu*~0.7. Negative Eu-anomalies seems to be associated with most of the low Nb/La rocks and is associated with the garnet residue signature recorded by the Gd/Yb_N. Residual plagioclase or plagioclase fractionation is usually responsible for the development of Eu-anomalies (Eu^{2+} is preferentially incorporated into plagioclase), but the coupled anomalies in Gd/Yb_N and Eu/Eu* are somewhat unexpected as plagioclase would be consumed during high pressure melting. A possible explanation is a two-stage crust evolution with primary crust formation from melts forming the garnet signature. This protocrust was remelted to form more evolved rocks with an inherited garnet signature and the Eu-anomalies forming from either plagioclase melt residues or early plagioclase rich cumulates.

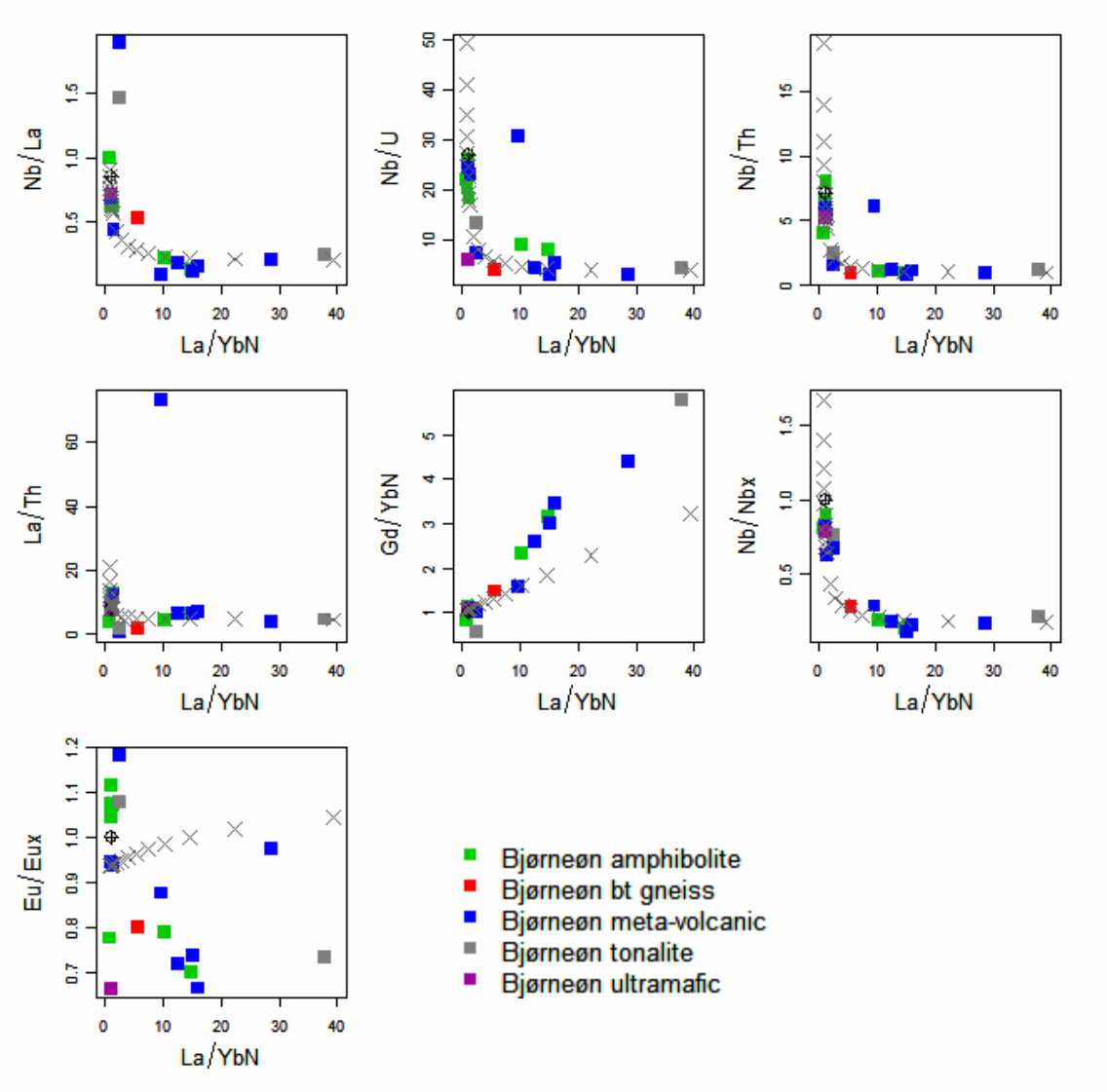

Figure. 5.2. *Trace element ratio plots for the Bjørneøen samples.*